"There is grandeur in this view of life, with its several powers, having been originally breathed into a few forms or into one; and that, whilst this planet has gone cycling on according to the fixed law of gravity, from so simple a beginning endless forms most beautiful and most wonderful have been, and are being, evolved."

Charles Darwin, On the origin of species

Acknowledgments

I would like to thank Professor Mariana Pinho, my thesis supervisor. For the immense impact you had on my scientific life, pushing me to do better, the driving force to always search for improvement and for excellence. I have no doubt that without you this PhD would have been very different. So thank you for all the help, for always meeting me when I had crazy/stupid ideas, and specially for allowing me to experiment on them! I would also like to thank you for all the opportunities to go abroad, expand my horizons, meet so many new and interesting people from different scientific backgrounds, for having so many wonderful collaborations. I truly feel lucky that I could develop my PhD under your supervision. That I could work with your laptop when I did not have one. This and more will never be forgotten.

I thank Professor Sergio Filipe, for all the enthusiastic (and challenging) scientific discussions. Although sometimes it seemed like I was not enjoying the 1000 different questions, deep down I really did. Because that is science. If there is something we wonder about how it could be, we ask. And I got that lesson from you. So thank you.

I would also like to thank to Dr. Abel Oliva and Dr. Adriano Henriques for the helpful discussions.

I would like to thank Professor Dirk-Jan Scheffers, for allowing me to go to his lab in the Netherlands and try FtsZ biochemistry. I had so much fun and so much work in your lab. It was a wonderful experience for me, especially at such an early stage of my PhD. I also thank your lab members, specially Ewa Krol and Ana, whom endured the work after hours, always prepared to feed me and to amuse me with your crazy stories (specially…ANA!!!) and for showing me the Netherlands, inviting me to your houses, to your diners, for making me feel like I belonged

there. I would also like to thank to my Groningen housemates (Lothar, Rik and Timon) for making my stay so welcoming, for showing me all that Groningen had to offer, and to be my home away from home. Really miss you all.

I thank all the members of the Quantitative Imaging and Nanobiophysics group from UCL, specially Professor Ricardo Henriques for allowing me to go to LMCB to experiment on 3D-PALM. I really enjoyed my time in London, it was a stressful but very good time, with helpful discussions and fun science. You guys really know how to work hardcore and have fun at the same time (Legos, Legos everywhere!).

I thank to the members from the Micron Unit facility in Oxford, specially to Andrew and Cvic, who taught me how to use the OMX and were very helpful and patient. I learned a lot from you and hope to meet you again sometime. I also thank Professor David Sherratt and his lab members for giving me a space to work while I was in Oxford. I would also like to thank Dr. Pawel Zawadzki and Dr. Andreas Diepold who helped me understanding some microscopy techniques/sample preparation and whom were really kind and made me feel very welcome in Oxford.

I would like to thank our collaborators Dr. Jen Hsin, Natalie Ng and Professor KC Huang for all the amazing modeling work and for helpful discussions during conferences and overseas skype calls. To Dr. Rut Carballido-Lopez and her lab members Pierre Flores and Dr. Alex Dajkovic for the Bacillus work, and specially for helpful discussions and insightful suggestions. To Dr. Egbert Hoiczyk for your amazing electron microscopy images of my weird cells. To Professors Yves Brun and Michael VanNieuwenhze for the always useful FDDAs. To Dr. Terry Roemer for allowing me to perform experiments on FtsZ mutants isolated in Merck.

I also thank FCT, ERC and EMBO for funding, ITQB-NOVA for providing me a place to perform my experiments, and the MolBios PhD program for spectacular classes and training.

To all the music that made me company during long and after-hours experiments. Everything is easier with a background soundtrack.

I thank all the members of my lab, former and present for making it a fun environment to work in, for all the help you provided, I cannot name all the single important contributions from everyone. Ana Maria, Vania, Trish, Helena, Monireh, Bernardino, Matos, Vanessa, Teresa, Gabriela, Nathalie, João, Pedrinho, Bruno, Moritz, Andreia Tavares, Andreia piquena, Simon, Ambre and Mario. Ana Maria was with me in the beginning of my lab life, giving me lifts to and from work, teaching me the basics, but specially showing me how to really make things properly and accurately. Trish for being my lab coach and for always helping me when I asked, professionally and personally. To Matos, who was always a joy to have around and with whom I grew. To João for putting your work on hold so we could join both of our stories. To Andreia Tavares, who saw me at my best and at my worst and made a collage out of the worst: P maybe someday we finally do the dance train. To Bruno, who made everyone's work easier, and mine possible. For being always helpful and creative and for always going for my crazy overnight requests to build new software. This thesis would not be complete without your input! To "it's me Mario", my nerd counterpart, it was so nice to get to know you and discuss science and why Star Wars ep8 sucks. To Andreia piquena, I think you are very talented and it has been a pleasure seeing you grow in the lab. Pedrinho, my "work husband" and my housemate. You are one of the best people I have ever met, and I have so many funny, good and important moments with you that I would need a whole thesis to describe

them. Maybe someday I publish a book on your crazy vacuum cleaners and lettuces stories (and then we will be rich and have a gigantic house again). Your kindness and special personality made my time here so much more fun and valuable. To Nathalie (aka NATALIA) for being my partner in science, you really pushed me to do better and always allowed me to discuss my ideas with you. It was so fun to mix worktime with friendship and I have nothing but good memories from our time together. I also thank members of Sergio Filipe lab, former and present, for the good environment, friendship and helpful discussions. To my colleagues from the PhD program, it was so nice to share this PhD with you and I will always cherish the work and the fun we had. To my ITQB friends, Inês, Magda, Catarina, Cláudia, Teresa Costa and Mónica. When I joined ITQB you made me feel like I belonged. I really thank you for all the help and for the friendship. An enormous thanks to Magda, who always had a fun story to tell, a good advice to give, or a delicious meal to share. Thanks for making me feel welcome, here or in Oxford.

To all my friends and family. To my friend Catarina. It started as the girl from the lab next door, but it developed to such an awesome friendship. I am so happy to have you in my life and to keep sharing the important moments together. To Katy, from always to ever! My sister from another mother. I hope we can finally share and enjoy this summer in Algarve together. You taught me the kindness and the goodness, we grew up together and I would be a weird and worse person today if you hadn't been by my side. I miss your presence in my life every day!!! To my sister Inês. You don't choose your family members, but if I was given the chance of picking anyone, I would choose you as my sister every time. Facing tough challenges, you always looked to the bright side and you never gave up, never said ok this is it, and that has always been an enormous inspiration for me. I love you more than life and can't wait for

the next chapters in our lives (hopefully living in the same country). To Bruno, who makes me be the best version of myself, who makes my life meaningful and happy, who is my home. You are one of my greatest joys, my forever best friend, and the one person who could (finally) make me enjoy my work-life balance. Thanks for allowing me to be whatever I wake up feeling like, for enabling me to share my life with you. To my cousin Luis, who made my life in Oeiras so much more fun and with a feeling that I could always go to your house and chill, while eating amazing food. I really miss those days. To Sapo who was there chasing me and preventing me from falling even before I can remember. You are a huge inspiration for me, always interested, curious and most importantly, a fantastic human being. This thesis is possible also thanks to you, who lent me books and ensured that I knew how to choose my career for myself. Um enorme obrigada para o meu tio Luiz, que tornou os meus estudos universitários possíveis (e que não gosta nada quando eu escrevo tudo em inglês, portanto cá vai). Entre outras coisas, mas em específico esta tese, não existiriam sem o tio. Por isso e por tudo o resto, um enorme obrigada. Tenho o maior carinho do mundo pelo tio e nunca me esquecerei de tudo o que fez por mim, do quão bem cuidou de mim e da mãe. Um enorme obrigada também ao tio Quim, à minha tia Amália, tia Beta, tia Alzira, e todos os meus priminhos de várias gerações. Sempre me apoiaram e inspiraram para ser o que eu quisesse. Ao meu pai que sempre me incitou o bichinho da curiosidade, sempre me mostrou que o porquê e o como são questões inerentes ao ser humano.

Por fim, à minha mãe, minha fonte de inspiração de toda a vida e que tornou tudo isto e muito mais possível. Que me mostrou que mesmo nas maiores dificuldades, não se questionam as possíbilidades dos nossos sonhos. Que os desafios só fazem com que os queiramos alcançar ainda mais, com que valham mais a pena. São tudo clichés muito bonitos, mas

nós podemos dizer que são mesmo verdade. Obrigada por nunca me fazeres duvidar de mim, por sempre confiares nas minhas capacidades e por me apoiares e amares me incondicionalmente. Tenho imensa sorte em ter a mãe que tenho, e não tenho dúvida nenhuma que sem ti na minha vida não teria chegado até aqui.

Thesis publications

Pereira AR, Hsin J, Krol E, Tavares AC, Flores P, Hoiczyk E, Ng N, Dajkovic A, Brun YV, VanNieuwenhze MS, Roemer T, Carballido-Lopez R, Scheffers DJ, Huang KC, Pinho MG. 2016. FtsZ-Dependent Elongation of a Coccoid Bacterium. MBio 7.

Monteiro JM*, **Pereira AR***, Reichmann N, Saraiva B, Fernandes PB, Veiga H, Tavares AC, Santos M, Ferreira MT, Macario V, VanNieuwenhze M, Pinho MG. 2018. Peptidoglycan synthesis drives an FtsZ-treadmilling-independent step of cytokinesis. Nature, 554, 528-532.

* These authors contributed equally to the work.

CONTENTS

ABBREVIATIONS AND ACRONYMS 11

ABSTRACT 14

RESUMO 17

CHAPTER I - General Introduction 21

CHAPTER II - FtsZ dependent elongation of a coccoid bacterium 83

CHAPTER III - Peptidoglycan synthesis drives FtsZ treadmilling-independent step of cytokinesis 133

CHAPTER IV - Peptidoglycan synthesis inhibition by oxacillin leads to modification of the *S. aureus* Z-ring ultrastructure 179

CHAPTER V - Conclusion and future perspectives 221

ABBREVIATIONS AND ACRONYMS

AFM	Atomic force microscopy
Amp	Ampicillin
ATP	Adenosine triphosphate
BCA	Bicinchoninic acid assay
Bocillin-FL	BODIPY FL bocillin
Cat	Cloramphenicol
CFP	Cyan fluorescent protein
CFU	Colony forming units
CLEM	Correlative light electron microscopy
CTL	C-terminal linker
CTT	C-terminal tail
CTC	conserved C-terminal region
CTV	C-terminus variable
D-Ala-D-Ala	D-alanyl-D-alanine
DMSO	Dimethyl sulfoxide
ECL	Enhanced chemiluminescence
EDTA	Ethylenediaminetetraacetic acid
EGTA	Egtazic acid
EM	Electron microscopy
Ery	Erythromycin
FDDAs	Fluorescent D-amino acids
GFP	Green fluorescent protein
GlcNAc	N-acetylglucosamine
GTP	Guanosine triphosphate
GTPase	Family of enzymes that can hydrolyze GTP
HADA	HCC-amino-D-alanine
HRP	Horseradish peroxidase

IPTG	Isopropyl-β-D-thiogalactopyranoside
Kan	Kanamycin
LB	Luria Bertani
MD	Molecular Dynamics
Mgts	Monofunctional transglycosylases
MIC	Minimum inhibitory concentration
MOPs	Multidrug/ oligosaccharidyl-lipid/polysaccharide
MRSA	Methicillin resistant *S. aureus*
MTS	Membrane targeting sequence
MurNAc	N-acetylmuramic acid
NADA	NBD-amino-D-alanine
Neon	mNeonGreen fluorescent protein
Oxa	Oxacillin
PALM	Photoactivated localization microscopy
PBP	Penicillin-binding protein
PBS	Phosphate buffered saline
PBS-T	PBS plus tween
PG	Peptidoglycan
PVDF	Hybond-P Polyvinylidene fluoride
rbs	Ribossome binding site
SCCmec	Staphylococcal cassette chromosome mec
SDS-PAGE	Sodium dodecyl sulfate polyacrylamide gel electrophoresis
SEDS	sporulation elongation division and synthesis
SEM	Scanning electron microscopy
sGFP	Superfast green fluorescent protein
SIM	Structured illumination microscopy
Spc	Spectinomycin
TDL	TAMRA-D-lysine
TEM	Transmission electron microscopy

TP	Transpeptidase
TSA	Tryptic soy agar
TSB	Tryptic soy broth
Van-FL	BODIPY FL vancomycin
WGA	Wheat germ agglutinin
X-gal	5-bromo-4-chloro-3-indolyl β-D-galactopyranoside

ABSTRACT

The cell shape is such a distinctive characteristic of bacteria that it has been used extensively for their classification. In most bacteria, cell shape is sustained by peptidoglycan, a macromolecular polymer that surrounds the cell conferring mechanical strength and protecting the cell from lysing from high turgor pressure. The ability of bacteria to faithfully maintain morphology in a population and to pass it on to the next generation suggests the existence of molecular mechanisms that control morphogenesis. These mechanisms are usually mediated by cytoskeletal elements that perform the spatial and temporal control of peptidoglycan synthesis and remodeling. Rod-shaped bacteria, such as *Bacillus subtilis* or *Escherichia coli,* acquire and maintain their shape through the action of two peptidoglycan synthesis machineries that incorporate new peptidoglycan at midcell (to divide the cell) and at the lateral wall (to elongate the cell), in processes coordinated by the cytoskeletal proteins FtsZ and MreB, respectively. In contrast, spherical bacteria like *Staphylococcus aureus* possess only one peptidoglycan biosynthetic machinery, coordinated by the tubulin homologue FtsZ. *S. aureus* PG synthesis machinery is diverted from the cell periphery to the septum in preparation for division and inserts new peptidoglycan concentrically, progressively closing the septum. Studying cocci-to-rod and rod-to-cocci cell shape transitions has given great insight into how morphogenesis is controlled. Although several observations of rod-to-cocci transitions had been previously made, the inverse cocci-to-rod transition had not been reported. Here we report for the first time a coccus transition to elongated cells in *S. aureus*. This shape transition was serendipitously observed when studying a FtsZG193D mutant (M5), which was found to have a high frequency of elongated cells in the population. Molecular

dynamics simulations and *in vitro* studies indicated that FtsZG193D filaments were shorter and more twisted than filaments formed by wild-type protein. *In vivo*, these filaments can assemble in arcs or one turn helix structures that lead to cell wall deposition in a helical pattern in the peripheral wall, rather than in a disk at midcell as in wild-type cells. This helical pattern of peptidoglycan insertion leads to elongation, like in rod-shaped cells. Thus, structural flexibility of FtsZ filaments can result in an FtsZ-dependent mechanism for generating elongated cells from cocci.

Although elongation mechanisms vary considerably, cell division is usually mediated through a machinery controlled by FtsZ. This protein polymerizes in filaments that move through treadmilling and form a ring at mid cell (the Z-ring). Z-ring formation is the first step on the assembly of a multiprotein machinery called the divisome. One of the great challenges in cell division is to generate enough force to counteract high turgor pressure. This force could be generated by FtsZ filaments to deform the cellular membrane and pull it to the interior of the cell. Alternatively, peptidoglycan synthesis could provide the force for constriction by pushing the membrane inwards, with FtsZ acting only as a scaffold for peptidoglycan synthesis enzymes. *S. aureus* is an excellent model to study bacterial cell division. This is because of its spherical shape, which allows *S. aureus* division rings to be observed in all orientations under the microscope, enabling the observation of complete cytokinetic rings by 2D-structured illumination microscopy (2D-SIM) in the plane of the microscope slide. We have imaged *S. aureus* dividing cells expressing an FtsZ-sGFP fluorescent fusion and observed that *S. aureus* cytokinesis is biphasic, with a first step of no/slow constriction followed by a second, fast, constriction step. The start of fast Z-ring constriction seems to coincide with septal recruitment of the putative lipid II flippase,

MurJ, which is involved in redirecting peptidoglycan synthesis to midcell. Importantly, the first, slow, step is dependent on FtsZ filament treadmilling, while the second, fast, step is independent of FtsZ dynamics and might be driven by peptidoglycan synthesis instead.

Lastly, we investigated Z-ring localization in *S. aureus* cells with impaired daughter cell separation. In normal conditions, after *S. aureus* produces a septal plate that divides the mother cell in two daughter cells, the closed septum undergoes a period of maturation after which a fast reshaping of the septum into the hemispheres of the daughter cells occurs, originating two fully separated cells. We observed that FtsZ localizes to the next division plane before daughter cells are separated. This results in the formation of FtsZ D-shaped structures instead of rings. Inactivation of *S. aureus* Penicillin-Binding Protein 1 (PBP1) transpeptidase domain resulted in increased frequency of cells that do not quickly separate after septum synthesis and observed a concomitant increase in the number of FtsZ filaments assembled in a D-shaped structure in the daughter cells. Importantly, D-shaped FtsZ structures in cells with inactive PBP1 transpeptidase domain were able to constrict and to recruit late divisome proteins such as MurJ. These results suggest that (i) FtsZ filaments have enough structural plasticity to accommodate other shapes that deviate from a ring and (ii) peptidoglycan rigidity, which controls cellular shape, might impose the ultrastructure that FtsZ filaments adopt in live cells.

RESUMO

A morfologia de células bacterianas é uma propriedade caracteristica de cada espécie bacteriana, pelo que tem sido utilizada extensivamente para classificar estes microrganismos. A forma da maioria das bactérias é mantida pelo peptidoglicano, um polímero que rodeia a célula e exerce força mecânica, protegendo as células de lise devido à pressão osmótica. A capacidade das bactérias de manterem a mesma morfologia em todas as células de uma população, ao longo de várias gerações, sugere que existem mecanismos moleculares que controlam a morfologia. Estes mecanismos dependem geralmente de proteínas do citoesqueleto que controlam onde e quando o novo peptidoglicano é inserido e remodelado. A forma de bastonete, característica por exemplo de *Bacillus subtilis* e *Escherichia coli*, é adquirida através da ação de duas maquinarias de síntese de peptidoglicano: uma que incorpora peptidoglicano a meio da célula formando um septo que divide a célula, coordenada pela proteína do citoesqueleto FtsZ e outra maquinaria que incorpora peptidoglicano na parede lateral, alongando a célula, coordenada pela proteína do citoesqueleto MreB. Bactérias esféricas, tais como *Staphylococcus aureus*, apenas possuem uma maquinaria de síntese de peptidoglicano, regulada pelo homologo da tubulina FtsZ. Durante a divisão celular, esta maquinaria é recrutada para o centro da célula e progressivamente completa o septo através da inserção concêntrica de peptidoglicano. O estudo de transições da forma bacteriana de cocos para bastonete ou vice-versa pode revelar quais os mecanismos que controlam a morfogénese. Apesar de várias transições de bastonetes para cocos terem sido observadas, a transição inversa de cocos para bastonetes nunca foi reportada. Neste trabalho descrevemos um mecanismo pelo qual células

esféricas de *S. aureus* se tornam alongadas. Esta transição de morfologia foi observada enquanto estudávamos o mutante de *S. aureus* FtsZG193D (M5), que observámos ter uma elevada frequência de células alongadas. Através de simulações por dinâmica molecular e de visualização de polímeros de FtsZ por microscopia electrónica mostramos que os polímeros de FtsZG193D são mais curtos e com maior torção do que os formados por FtsZ nativo. *In vivo*, estes filamentos formam estruturas em arcos e helices que levam à deposição de peptidoglicano em padrões helicoidais na parede periférica, em vez de uma inserção num disco no meio da célula. Este padrão de inserção do peptidoglicano em hélice faz com que a célula alongue, semelhante ao que acontece em bastonetes. Os filamentos de FtsZ parecem ter flexibilidade estrutural suficiente para gerar outras estruturas, que não anéis, que resultam na introdução de novo peptidoglicano em vários sítios da célula, de modo a originar células alongadas a partir de coccos.

Apesar dos mecanismos de alongameto bacteriano variarem consideravelmente, a divisão celular é geralmente mediada attravés de uma maquinaria controlada pelo FtsZ. Esta proteína polimeriza em filamentos que se movem através de "treadmilling" e formam, a meio da célula, um anel denominado de anel Z. A formação deste anel Z constitui o primeiro passo na formação de uma maquinaria multiproteica, o divisoma. Um dos grandes desafios durante a divisão celular é a geração de força suficiente para haver constrição da membrana celular contra a elevada pressão de turgor a que as bactérias estão sujeitas. Essa força poderá ser gerada pelos filamentos de FtsZ, que deformariam a membrana celular puxando-a para o interior da célula. Alternativamente, a síntese do peptidoglicano poderá fornecer a força necessária para a constrição ao empurrar a membrana para o interior da célula, e o FtsZ

actuar apenas como um recrutador para as enzimas de síntese de peptidoglicano. *S. aureus* é um excelente modelo para estudar divisão celular, pois a sua forma quase esférica permite a visualização por microscopia dos aneis de divisão em todas as orientações. Isto permite a observação de anéis de citocinese completos no plano do slide de microscopia através de microscopia de iluminação estruturada-2D (SIM-2D). Neste trabalho observamos células de *S. aureus* que expressam o derivado fluorescente FtsZ-sGFP e vimos que a constrição de *S. aureus* é bifásica, possuindo um primeiro passo durante o qual a constrição é muito lenta (ou inexistente), seguido de um segundo passo de constrição rápida. O início do segundo passo de rápida constrição de FtsZ parece coincidir com o momento de recrutamento para o septo da putativa flipase do percussor lipidico para a síntese de peptidoglicano, MurJ, envolvida em redirecionar a síntese do peptidoglicano para o meio da célula. Adicionalmente, mostramos que a capacidade para contrair o anel Z no primeiro passo de citocinese depende da capacidade de "treadmilling" dos filamentos de FtsZ, enquanto que o segundo passo de constrição (rápido) não depende de "treadmilling" de FtsZ, mas sim, provavelmente, de síntese de peptidoglicano.

Por último, investigámos a localização do anel Z em células de *S. aureus* que não conseguem separar-se rápidamente após a divisão celular. Em condições normais, após *S. aureus* sintetizar uma placa septal que divide a célula mãe em duas células filhas, há um período de maturação do septo seguido de um processo de separação extremamente rápido em que o septo adota uma estrutura hemisférica nas células filhas. Durante este processo, os filamentos de FtsZ localizam-se no próximo plano de divisão celular antes das células filhas se separarem. Isto faz com que os filamentos de FtsZ formem uma estrutura em forma de D em vez

de aneis. A inactivação do domínio transpeptidase da proteína de ligação à penicilina 1 (PBP1) resulta num aumento da frequência de células que têm o septo fechado mas que não o remodelam rápidamente. Nestas células observamos um aumento no número de células com estruturas de FtsZ em forma de D, capazes de fazer constrição e de recrutar proteínas tardias do divisoma tais como MurJ. Estes resultados sugerem que (i) os filamentos de FtsZ têm plasticidade estrutural suficiente para acomodar outras formas que não anéis e que (ii) a rigidez do peptidoglicano, que controla a forma celular bacteriana, poderá impôr a ultraestrutura que os filamentos de FtsZ adotam.

CHAPTER I

General Introduction

Chapter I Summary

Bacterial shapes are diverse and have selective value 23
Peptidoglycan, the bacterial shape determinant 25
Distinct growth modes to generate bacterial rod-shapes 26
Ovococci bacteria elongate without MreB 30
Cocci bacteria maintain a spherical shape by dividing without elongating 31
The bacterial divisome 34
Positioning the divisome through control of FtsZ ring formation 34
Pioneering work on divisome discovery 35
Polymerization and attachment of FtsZ to the membrane-Z-ring assembly 37
Recruitment of downstream cell division proteins to midcell completes the bacterial divisome 44
What force drives cell division? 45
The constriction conundrum –going against turgor pressure 45
FtsZ as a force generator protein: the FtsZ-centric model 47
PG synthesis as the force that drives cytokinesis: the PG-centric model 52
Concerted actions of FtsZ and PG synthesis could drive constriction 53
Cell division in the absence of FtsZ 54
Different ways to undergo bacterial daughter cell separation: to invaginate or to not invaginate 56
S. aureus as an antibiotic resistant pathogen 58
References 62

Bacterial shapes are diverse and have selective value

Fascinated by the invention of the first single-lens microscope, Antonie van Leeuwenhoek observed hundreds of specimens, but perhaps his most sensational observation was made in 1683 when he reported that a mouth swab contained several tiny organisms, which he named "animalcules", i.e. little animals (Figure 1). Although the name only appeared 145 years later, this observation marks the discovery of the first bacteria.

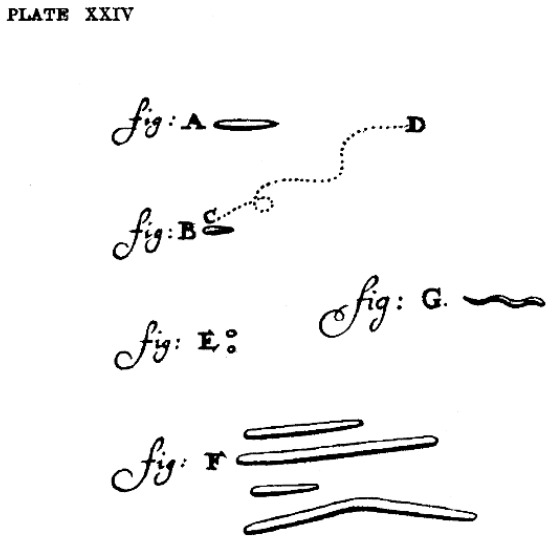

Figure 1: First documented observation of shape diversity in bacteria. In a letter sent to the Royal Society of London, Antonie van Leeuwenhoek documents the constituents of a mouth swab observed with his homemade microscope. This marks one of the first observations of living bacteria ever recorded. At least five different types of "animalcules" were observed: (A) motile bacillus, (B) probably *Selenomonas sputigena* with (C) and (D) representing the path of its motion; (E) Micrococci; (F) probably *Leptothrix buccalis* and (G) a spirochete, probably *Spirochaeta buccalis*. With his simple microscope, van Leeuwenhoek not only discovered bacteria, he also documented that they can differ greatly in shape.

Nowadays we see that bacterial shape diversity extends far beyond the first reports of spheres (cocci); rods (bacilli) and spirals (spirochetes).

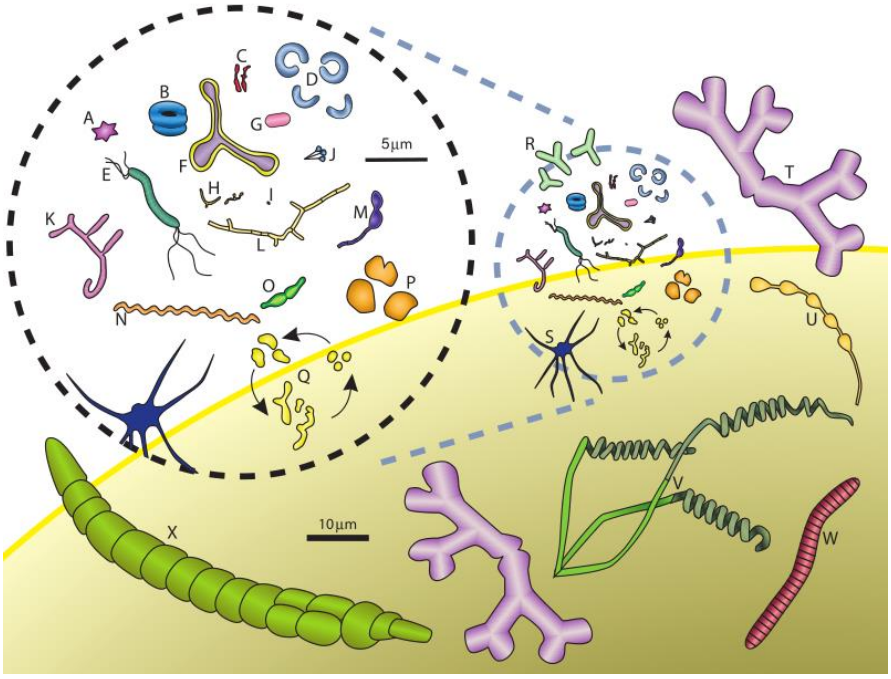

Figure 2: Shape variety in the prokaryotic world. Although most studied species are cocci, rods and ovococci, prokaryotes can adopt several different shapes with some varying shape during different stages of their cell cycle. The represented cells are (A) *Stella strain* IFAM1312; (B) *Ancylobacter flavus*; (C) *Bifidobacterium bifidum*; (D) *Clostridium cocleatum*; (E) *Aquaspirillum autotrophicum*; (F) *Pyroditium abyssi*; (G) *Escherichia coli*; (H) *Bifidobacterium sp.*; (J) *Planctomyces* sp.; (K) *Nocardia opaca*; (M) *Caulobacter* sp.; (N) *Spirochaeta halophila*; (O) *Prosthecobacter fusiformis*; (P) *Methanogenium cariaci*; (Q) *Arthrobacter globiformis* growth cycle; (R) Alphaproteobacteria from marine sponges; (S) *Ancalomicrobium* sp.; (T) *Nevskia ramosa*; (U) *Rhodomicrobium vanniellii*; (V) *Streptomyces* sp.; (W) *Caryophanon latum*; (X) *Calothrix* sp. Reproduced from (Young, 2006).

By looking at different bacteria under the microscope an astounding variety of bizarre morphologies can be discovered (Figure 2). There are star shaped bacteria (Figure 2, A), bean shaped (D), bacteria that look like neurons (S) and others like caterpillars (X). Although there is abundant shape variety, there is also uniformity meaning that, although different shapes can be adopted by different species, a bacterium tends to faithfully transmit morphological traits to the next generation, with shape maintenance within most species.

With a huge variety of possible shapes, morphology selection is likely tailored by fitness, as shape is important for bacterial survival, playing different roles in nutrient diffusion/uptake, predation, motility or immune system evasion (Young, 2006, Young, 2007). This goes in line with observations that some bacteria can modify their shape in response to different niches or stresses (Young, 2006). These morphology shift responses, together with the faithful maintenance of cellular shape, suggest that bacteria have control systems that tightly regulate morphogenesis. However, we cannot fully explain how the most basic shapes arise, let alone complex ones. Therefore, most studies on bacterial shape have been performed in bacteria possessing simple morphologies such as rods, ovococci and cocci (Eswara and Ramamurthi, 2017).

Peptidoglycan, the bacterial shape determinant

In most bacteria, shape is sustained by peptidoglycan (PG), a mesh-like macropolymer of peptide-crosslinked glycan strands that surrounds the cell, protecting bacteria from lysing due to turgor pressure. Results showing that (i) PG depletion leads to loss of cell shape (Gilpin et al., 1973, Allan et al., 2009) and that (ii) isolated PG sacculus retain the original cellular shape (Goodwin and Shedlarski, 1975, Heidrich et al.,

2001, Romaniuk and Cegelski, 2015, Li et al., 2018) suggested PG as the major bacterial shape determinant. However, PG basic chemical structure is fairly conserved in bacteria with different shapes (Vollmer et al., 2008), indicating that the building blocks of PG do not define morphology. Instead, morphology is modulated by controlling when and where new PG is incorporated, a task achieved by cellular cytoskeletal elements which coordinate the sub-cellular localization of PG synthesis enzymes such as penicillin-binding proteins (PBPs), responsible for performing the last stages of polymerizing PG units into a macromolecule.

Distinct growth modes to generate bacterial rod-shapes

A rod shape is essentially a cylindrical tube with two hemispherical poles. Most of the knowledge on how to achieve such shape comes from studies of the two rod bacterial models *Bacillus subtilis* and *Escherichia coli* (Eswara and Ramamurthi, 2017). In these bacteria the poles are generated by the PG synthesis machinery controlled by filaments of the tubulin homologue FtsZ that form the Z-ring at midcell which leads to septation (divisome). The cylindrical shape is generated through the elongation machinery that drives PG insertion along the major axis of the cell (elongasome). Elongation in these organisms is controlled through MreB cytoskeletal elements and, accordingly, depletion/chemical inactivation of MreB or MreB-like proteins leads to widening and rounding of the cell (Jones et al., 2001, Figge et al., 2004, Gitai et al., 2005, Kruse et al., 2005). MreB is structurally related to eukaryotic actins (van den Ent et al., 2001) and undergoes reversible polymerization regulated through binding and hydrolysis of ATP forming antiparallel double-stranded filaments *in vitro* (Salje et al., 2011, van den Ent et al., 2014). In live cells, MreB was initially viewed as a cytoskeletal

helix (Jones et al., 2001). However it was later discovered that MreB binds to the inner side of the membrane (Salje et al., 2011) forming patchy filaments oriented orthogonally (Ouzounov et al., 2016)to the long cell axis , rotating around the rod (Domínguez-Escobar et al., 2011, Garner et al., 2011, Teeffelen et al., 2011) (Figure 3, top panel). By interacting with transmembrane proteins like RodZ and MreCD (Kruse et al., 2005, Shiomi et al., 2008, Alyahya et al., 2009, Bendezu et al., 2009), MreB is indirectly connected to the PG elongation machinery that incorporates PG along the cell (lateral PG synthesis). Importantly, the motion of MreB filaments is dependent on active PG synthesis, suggesting that MreB movement follows PG insertion instead of directing it (Domínguez-Escobar et al., 2011, Garner et al., 2011, Teeffelen et al., 2011). It remains to be determined what is the exact fundamental role of MreB on cellular elongation. MreB filaments could act as a scaffold to help assemble the complex of proteins needed to coordinate the synthesis of PG and other wall associated elements (Domínguez-Escobar et al., 2011, Favini-Stabile et al., 2013) with some reports suggesting that the movement of MreB patches is not fundamental for cellular elongation (Morgenstein et al., 2015). However, a recent report showed that when *B. subtilis* is converted to a sphere it can regenerate into a rod in a process dependent on MreB movement (Hussain et al., 2018). MreB appears to be able to sense differences in membrane bending, re-orient itself along greatest membrane curvature, and through redirection of PG synthesis correct the cellular curvature, generating a rod shape (Hussain et al., 2018). MreB might also be involved in excluding PG incorporation from the cell poles, as MreB tends to avoid anionic phospholipids (Kawazura et al., 2017) which may accumulate at the hemispherical poles (Mukhopadhyay et al., 2008, Renner and Weibel, 2011). Although it was thought that elongation

was exclusively performed by the MreB-regulated elongation machinery, there is evidence which shows that prior to septum synthesis, some PG incorporation occurs at the central region of the cell, leading to slight elongation. In *E. coli* this PG synthesis before septation is FtsZ-dependent (Varma et al., 2007, Varma and Young, 2009, Potluri et al., 2012) and in *Caulobacter crescentus* FtsZ directs the localization of PG precursors to midcell leading to elongation before septation (pre-septal elongation) (Aaron et al., 2007).

Though elongation through insertion of PG along the major cell axis is the best studied example of how to elongate a cell, other organisms have different modes of growth that drive elongation. Some rods from the Actinobacteria phylum (*Corynebacterium glutamicum* and *Mycobacterium tuberculosis*) or *Agrobacterium tumefaciens* elongate by inserting new PG specifically at the pole(s), independently of MreB (Letek et al., 2008, Kuru et al., 2012, Sieger et al., 2013, Kieser and Rubin, 2014, Howell and Brown, 2016) . The more we study non-model species, further exploring the diversity of the bacterial tree of life, the more evident it is that different species found different ways to generate similar shapes.

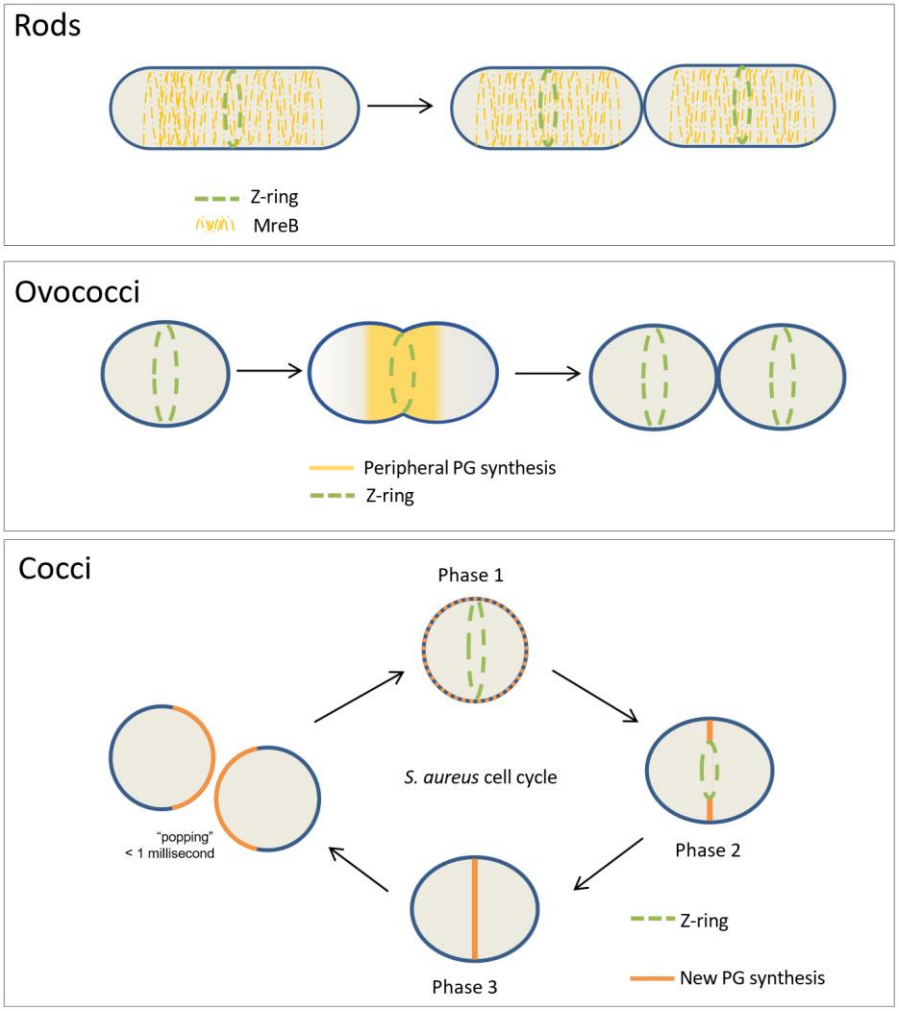

Figure 3: Modes of PG incorporation in rods, ovococci and cocci. Top panel – Rod-shaped cells like *B. subtilis* and *E. coli* have two PG synthesis machineries: the division machinery, coordinated by FtsZ, that incorporates new PG at the septum and generates the cell poles and the elongation machinery, that incorporates PG along the major cell axis. Elongation is coordinated by MreB cytoskeletal elements that form dynamic patches that move circumferentially around the rod. **Middle panel** - Ovococcal species like *Streptococcus pneumoniae* and *Lactococcus lactis* also possess two PG synthesis machineries but the elongation machinery that incorporates PG in a broad band near the septum is dependent on FtsZ (peripheral PG synthesis), slightly elongating the cell. **Bottom panel** - Cocci bacteria like *Staphylococcus aureus* only have one PG synthesis

machinery that is dispersed around the cell periphery before septum synthesis is initiated (Phase 1). The division machinery, coordinated by FtsZ, will then promote diversion of most PG synthesis to midcell upon the recruitment of the putative PG precursor flippase MurJ to the divisome. New septal PG is inserted inwardly (Phase 2) until the septum is closed (Phase 3). The closed septum quickly reshapes (<1 msec) in a "popping-like" motion, forming ~33% of each new daughter cell hemispheres.

Ovococci bacteria elongate without MreB

The slightly elongated ovococcal species like *Streptococcus pneumoniae* or *Lactococcus lactis* possess two modes of PG insertion performed by two PG synthesis machineries: septal and peripheral. Contrasting with rod-shaped bacteria, the machinery that performs PG peripheral insertion does not insert PG along the entire cell length. Instead, PG incorporation is performed in a broad region near the division site (Daniel and Errington, 2003, Kuru et al., 2012, Fleurie et al., 2014b) that is responsible for the slight elongation of the cell (Zapun et al., 2008b) (Figure 3 – middle panel). Comparatively with rod-shape modes of elongation, ovococci peripheral growth is more similar to the FtsZ-dependent pre-septal PG insertion than with MreB-directed elongation. Accordingly, MreB is usually absent in ovococci species like *S. pneumoniae* (Pinho et al., 2013) and so, FtsZ most likely coordinates both septal and peripheral PG machineries. However, other cytoskeletal elements could also be key to direct peripheral PG insertion, as for example MreCD pneumococcal proteins whose deletion leads to cell rounding (Land and Winkler, 2011). Growth performed by two independent PG synthesis machineries (septal and peripheral) implies that inhibition of septal growth results in ovococci conversion to rods, while inhibition of the peripheral PG synthesis machinery results in ovococci conversion to cocci. Accordingly, in *L. lactis* and *S. pneumoniae*,

inhibition of septal PBP2x results in cellular elongation while inactivation of peripheral PBP2b leads to spherical cells (Perez-Nunez et al., 2011, Berg et al., 2013, Land et al., 2013).

Cocci bacteria maintain a spherical shape by dividing without elongating

If shape is defined by the way cells grow, it is tempting to assume that a spherical shape would be the simplest to generate. However, round shapes are not created through random insertion of PG around the cell periphery, as this would only lead to cellular expansion. Instead, cocci bacteria like *Staphylococcus aureus* possess only one PG synthesis machinery which is dispersed around the cell periphery before septation and, in preparation for cell division, is diverted to midcell inserting new PG inwardly to form a division septum that bisects the mother cell in two (Pinho and Errington, 2003, Monteiro et al., 2015). Upon splitting and reshaping of this flat structure, the two new hemispheres of the daughter cells are generated, giving a near-spherical shape (Figure 3, bottom panel) (Zhou et al., 2015, Monteiro et al., 2015). Some cocci bacteria add an extra layer of complexity to this mode of growth as new PG is sequentially inserted in two (neisseriae and deinococci) or even three (staphylococci and micrococci) perpendicular planes (Pinho et al., 2013). The molecular cue that coordinates the selection of the next plane of PG insertion remains elusive.

The full PG synthesis pathway is a multi-enzymatic process that spans three different compartments of the bacterial cell (van Heijenoort, 1998, Scheffers and Pinho, 2005) (Figure 4). PG synthesis starts in the cytoplasm with the synthesis of the UDP-N-acetylmuramyl (UDP-MurNAc)-pentapeptide and UDP-N-acetylglucosamine (UDP-GlcNAc)

nucleotide-sugar-linked precursors. Synthesis of the UDP-MurNAc-pentapeptide is catalyzed by a series of Mur proteins (Lovering et al., 2012) and, once complete, this precursor is attached by MraY to undecaprenyl pyrophosphate at the inner side of the membrane, forming lipid I (Ikeda et al., 1991). Subsequently, MurG adds GlcNAc to lipid I, forming lipid II (Mengin-Lecreulx et al., 1991). In *S. aureus* a peptide bridge of 5 glycines is then added at the third amino acid by Fem proteins forming the lipid II-Gly5 (Kopp et al., 1996). This precursor is then flipped to the external side of the cellular membrane (van Dam et al., 2007) through MurJ or FtsW (Ruiz, 2008, Mohammadi et al., 2011, Sham et al., 2014, Mohammadi et al., 2014) and polymerized by transglycosylation reactions that elongate the glycan chains (performed by PBPs (Sauvage et al., 2008), monofunctional transglycosylases (Mgts) (Wang et al., 2001) and perhaps sporulation elongation division and synthesis (SEDS) proteins (Meeske et al., 2016, Emami et al., 2017) and transpeptidation reactions that crosslink PG, performed by PBPs (Sauvage et al., 2008). In *S. aureus*, localization of PG synthesis proteins has been recently described, showing that during septum synthesis proteins involved in synthesizing UDP-MurNAc-pentapeptide localize in the cytoplasm, MraY and Fem proteins localize to the whole cellular membrane and MurJ, FtsW and PBPs are enriched at midcell (Monteiro et al., 2018). These results indicate that, to synthesize the division septum, *S. aureus* cells redirect the localization only of the enzymes required for the last stages of PG synthesis to midcell, not of all enzymes involved in PG synthesis. Similarly to the formation of polar hemispheres in rod-shape bacteria, *S. aureus* PG incorporation at the septum is dependent on FtsZ polymerizing at midcell as, in its absence, PG insertion is delocalized to the cell periphery (Pinho and Errington, 2003). Despite this, FtsZ has not been shown to directly

recruit the enzymes responsible for the last stages of PG polymerization (PBPs). *S. aureus* only possesses four native PBPs (PBP1-4) with strains resistant to beta-lactams having a fifth PBP - PBP2A - with low affinity to those antibiotics (Graves-Woodward and Pratt, 1998, Lu et al., 1999). The four native PBPs are recruited to midcell through different mechanisms: PBP2 is recruited through substrate-binding (Pinho and Errington, 2005) and PBP4 through an intermediate of wall teichoic acid synthesis (Atilano et al., 2010). PBP1 arrives early at the division site (Monteiro et al., 2018) through an unknown mechanism (perhaps protein-protein interactions with an early divisome protein) and PBP3 recruitment mechanism has not been identified yet.

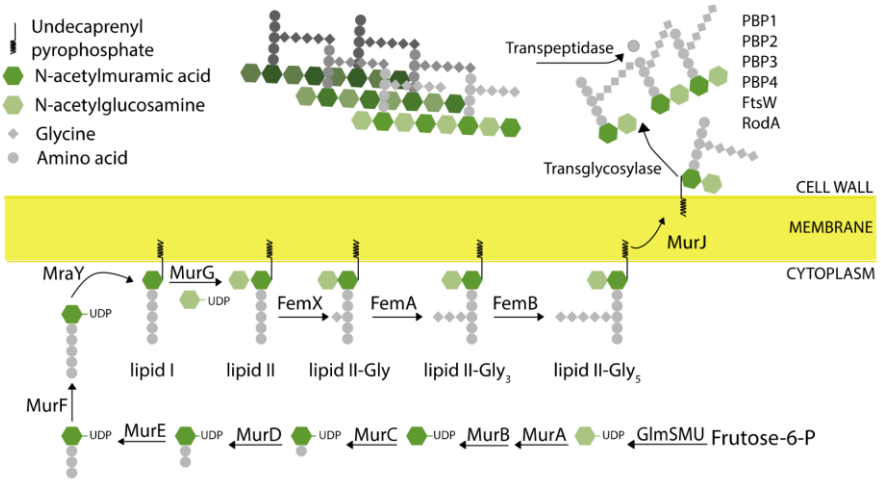

Figure 4: *S. aureus* PG synthesis pathway. Synthesis of PG comprises three stages that occur in distinct cellular places. First, the PG precursor UDP-MurNAc-pentapeptide is synthesized in the cytoplasm by the MurA-F proteins. The second stage takes place at the inner side of the membrane, where MraY attaches the PG precursor to a lipid carrier molecule (undecaprenyl pyrophosphate), forming lipid I. UDP-GlcNAc is then attached to lipid I by MurG, forming lipid II. In the case of *S. aureus*, a peptide crossbridge of five glycine residues is added by FemXAB proteins, forming Lipid II-Gly_5 which is flipped to the external side of the membrane, presumably by MurJ. The third stage of PG synthesis takes place

at the outer side of the cell membrane where new PG is inserted by transglycosylation and transpeptidation reactions. Reproduced from (Monteiro et al., 2018).

For a long time it was thought that *S. aureus* inserted PG exclusively at the septum because (i) *S. aureus* cells would maintain cellular shape prior to cell division (Tzagoloff and Novick, 1977), (ii) new PG labeling by fluorescent vancomycin localized mainly at the septum (Pinho and Errington, 2003) and (iii) FtsZ depletion leads to cell enlargement without elongation, indicating that *S. aureus* does not have an extra, FtsZ-independent PG synthesis machinery (Pinho and Errington, 2003). More recently, using novel super resolution techniques that allow more accurate cellular measurements, it was observed that when *S. aureus* cells are not synthesizing a septum (i.e. when PG synthesis is not diverted to midcell), they incorporate some PG at the cell periphery and slightly elongate through an unknown mechanism (Monteiro et al., 2015).

The bacterial divisome

Positioning the divisome through control of FtsZ ring formation

Bacterial viability is critically dependent on cells ability to properly divide. Most bacteria, regardless of their shape, perform division at midcell along the shorter cell axis, giving rise to two daughter cells with identical size (binary fission). The positioning of the division site is extremely accurate and is defined by positioning filaments of FtsZ as a ring at midcell (Bi and Lutkenhaus, 1991, Guberman et al., 2008, Reshes et al., 2008, Mannik et al., 2012). Z-ring assembly must also be precisely timed with chromosome segregation to avoid bisection of the DNA, a

process controlled by nucleoid occlusion proteins that prevent FtsZ formation on top of the chromosome, through DNA-bound proteins like Noc (Wu and Errington, 2004, Veiga et al., 2011, Adams et al., 2015) or SlmA (Bernhardt and de Boer, 2005). FtsZ positioning at midcell is also determined by other negative regulators that impair formation of FtsZ in determined cellular regions, such as the Min system in *E. coli* and *B. subtilis* (Rowlett and Margolin, 2013) or MipZ in *C. crescentus* (Thanbichler and Shapiro, 2006) or by positive regulators that recruit FtsZ to the correct site, like MapZ in *S. pneumoniae* (Fleurie et al., 2014a) or PomZ in *Myxococcus xanthus* (Treuner-Lange et al., 2013). Interestingly, in *S. aureus*, the only identified FtsZ positioning control mechanism is Noc (Veiga et al., 2011). However, in the absence of Noc, cells are still viable and only a few percentage possess multiple FtsZ rings. Additionally, *E. coli* and *B. subtilis* cells grown in the absence of nucleoid occlusion proteins (SlmA/Noc) and Min can still position FtsZ at midcell and divide (Bailey et al., 2014, Rodrigues and Harry, 2012). These observations indicate that unidentified regulators of FtsZ positioning at the cell center are probably yet to be discovered.

Pioneering work on divisome discovery

Much of what is known about cell division started with studies in the Gram-negative bacteria *E. coli*, done in the 1960s, with an interest in understanding how and why cell filamentation occurred in response to DNA damage. This prompted Piet van de Putte and colleagues to identify cell division mutants that could not pass through a 5 μm filter after growth at high temperatures (filamentous thermosensitive mutants – *fts*) (van De Putte et al., 1964). Because these mutants could still grow at lower temperatures, it was possible to identify several genes such as *ftsZ*

and *ftsA* (Lutkenhaus and Donachie, 1979, Lutkenhaus et al., 1980). After discarding mutations that caused filamentation but were indirectly involved in cell division, these approaches led to the definition of "core cell division genes": genes essential for cellular growth encoding a protein that localizes to the division site. Using this definition there are 12 cell division essential genes identified so far in *E. coli*: *ftsZ*, *ftsA*, *zipA*, *ftsE*, *ftsX*, *ftsK*, *ftsQ*, *ftsL*, *ftsB*, *ftsW*, *ftsI* and *ftsN* (de Boer, 2010, Lutkenhaus et al., 2012). Other proteins are involved in cell division but are not essential (like Zap proteins (Ortiz et al., 2016)) and some PG synthesis proteins are involved in cell division but are also part of the elongation machinery. Actually, out of the 12 PBPs of *E. coli*, only *ftsI* product, PBP3, is exclusively used in cell division (Spratt, 1975, Young, 2001, Lutkenhaus and Du, 2017). A total of at least 30 proteins (Adams and Errington, 2009, Lutkenhaus et al., 2012, Egan and Vollmer, 2013, Haeusser and Margolin, 2016), including the 12 essential ones, are involved in *E. coli* cell division, forming the macromolecular machinery usually called the divisome.

The success of cell division depends on the accurate localization of key cell division components in space and time. Microscopy techniques have been extremely important to understand where, when and how cell division proteins localize to midcell. The first localization of a cell division protein was performed by the Lutkenhaus laboratory using immunogold labelling to image FtsZ localized at *E. coli* midcell (Bi and Lutkenhaus, 1991). Later on, the development of green fluorescent protein (GFP) as a tag for bacterial proteins, prompted the visualization of rings of FtsZ-GFP and FtsA-GFP in live cells (Ma et al., 1996) followed by immunofluorescence imaging of FtsA, FtsQ, FtsI and FtsW that only localized to midcell in the presence of FtsZ (Addinall and Lutkenhaus, 1996, Weiss et al., 1997, Wang et al., 1998, Buddelmeijer et al., 1998).

Importantly, FtsN was shown to localize only if the other cell division genes were intact, indicating that it probably localized later in cell division and it required a preassembled ring (Addinall et al., 1997). This was the first suggestion that divisome assembly is a temporal hierarchical process. Besides a clear hierarchy where recruitment of each protein is required for the assembly of the next one (Egan and Vollmer, 2013), *E. coli* divisome assembly occurs mainly in two temporal steps: FtsZ, FtsA, ZipA, Zap and FtsEX assemble early at the future division site followed by the second set of proteins FtsK, FtsQ, FtsL, FtsB, FtsW, FtsI and FtsN, involved in chromosome segregation and PG remodeling (Aarsman et al., 2005). Similarly, in the Gram-positive bacterial model *B. subtilis*, divisome assembly is a two-step process with a set of early proteins recruited to midcell (FtsZ FtsA, ZapA, and EzrA) followed by a later set of proteins (GpsB, FtsL, DivIB, FtsW, Pbp2B, and DivIVA) (Gamba et al., 2009).

Polymerization and attachment of FtsZ to the membrane - Z-ring assembly

Assembly of a Z-ring at midcell is the first step in bacterial cell division (Rico et al., 2013). The main component of the Z-ring is FtsZ (Bi and Lutkenhaus, 1991), a homologue of eukaryotic tubulin (Nogales et al., 1998) and the first cytoskeletal element to be described in bacteria (Bi and Lutkenhaus, 1991, Ma et al., 1996). Despite the low sequence similarity to tubulin, the two proteins are structurally very similar, with both possessing N- and C-terminal globular domains, separated by a core Helix 7 (Nogales et al., 1998, Lowe and Amos, 1998) (Figure 5a). The C-terminal globular domain is followed by a C-terminal linker (CTL, Figure 5b) that varies in size between different species (Vaughan et al., 2004) and has been shown to influence FtsZ filament dynamics and

ultrastructure (Buske and Levin, 2013, Gardner et al., 2013, Sundararajan and Goley, 2017). After the linker, there is a C-terminal tail (CTT) that mediates interaction with many proteins (Ma and Margolin, 1999, Yan et al., 2000, Haney et al., 2001, Vaughan et al., 2004, Krol et al., 2012, Son and Lee, 2013, Du et al., 2015). This region is comprised of a conserved C-terminal region (CTC) followed by a C-terminus variable (CTV) domain which differs in length and amino acid sequence across various species (Buske and Levin, 2012). While tubulin usually polymerizes as a hollow 13-stranded filament (Tilney et al., 1973, Unger et al., 1990, Chaaban and Brouhard, 2017), FtsZ mostly assembles in linear single-stranded protofilaments that are one subunit thick and about 120-200 nm long (30-50 FtsZ subunits) (Erickson et al., 2010). The head-to-tail linear arrangement of FtsZ monomers sandwiches the nucleotide GTP between its binding site at the N-terminal domain of one monomer and a cation-coordinating loop of the subunit above (T7 loop) (Mukherjee et al., 1993, Oliva et al., 2004). Since this loop mediates GTP hydrolysis, FtsZ acts as a self-activating GTPase, with GTP hydrolysis occurring upon polymerization of the subunits (de Boer et al., 1992, Scheffers et al., 2002, Oliva et al., 2004). FtsZ filaments are highly dynamic, with FtsZ subunits within the Z-ring turning over in within ~10 sec in both *E. coli* and *B. subtilis* (Anderson et al., 2004, Geissler et al., 2007, Buss et al., 2015). Additionally, GTP hydrolysis drives another mode of FtsZ dynamics where FtsZ filaments show apparent movement at the ~100 sec timescale through treadmilling, i.e. one end of the filament grows due to higher rates of polymerization while the other end of the filament shrinks through higher rates of depolymerization (Loose and Mitchison, 2014, Yang et al., 2017, Bisson-Filho et al., 2017). It is not clear how a single-stranded FtsZ filament undergoes polymerization and depolymerization

at different rates on both ends. Recent work using crystal structures of *S. aureus* FtsZ found correlations between different conformational states of FtsZ and the ability to polymerize (Wagstaff et al., 2017). In that study, *S. aureus* FtsZ structures seemed to adopt two distinct conformations: a closed conformation in the monomeric state and an open conformation in FtsZ filaments. The authors proposed that the closed and open forms of FtsZ might result in different "on/off" rates of polymerization with the end with higher "on" rates becoming the growing end of the filament.

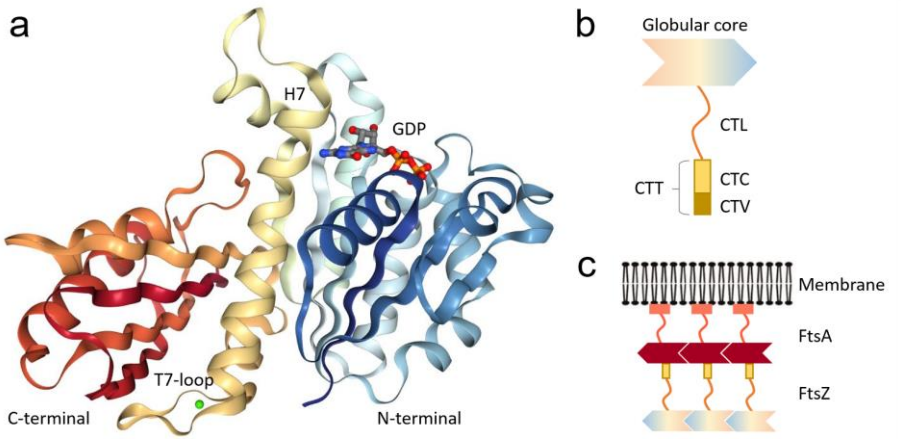

Figure 5: Structural domains of FtsZ. (a) *S. aureus* FtsZ-GDP crystal structure (PDB 3VO8 (Matsui et al., 2012)) showing the globular N-terminal domain in blue, the C-terminal domain in red and Helix 7 (H7) in yellow. A GTP binding site is present in the N-terminal domain and a cation (Ca^{2+}, green dot) coordinated T7-loop is present at the C-terminal portion of H7. **(b)** Cartoon depicting *E. coli* FtsZ domain organization. The globular N- and C-terminal domains (globular core) are followed by a linker (CTL), and a C-terminal tail (CTT) domain comprised of a conserved sequence (CTC) followed by a variable region (CTV). The CTT domain is sometimes described as the FtsZ landing pad because it interacts with several proteins such as FtsA, MinCD and SlmA. **(c)** Representation of FtsA-FtsZ filaments tethered to the membrane through FtsA which interacts with FtsZ CTT region.

In vitro, FtsZ assembles predominantly into single-stranded protofilaments (Erickson et al., 2010) but, depending on the experimental conditions, it can also form helices, mini-rings, sheets, tubules and toroids (Erickson et al., 1996, Bramhill and Thompson, 1994, Popp et al., 2009, Arumugam et al., 2012). However, the organization of FtsZ filaments in live cells is still a matter of debate. An *E. coli* cell has a total of ~6,000 FtsZ molecules (Li et al., 2014), but quantitative fluorescence microscopy data suggests that only 30-40% (~2000 molecules) of total cellular FtsZ is in the Z-ring of *E. coli* (Stricker et al., 2002, Geissler et al., 2007). Considering that one FtsZ subunit is 4.3 nm long (Erickson et al., 1996), one continuous polymer encircling the perimeter of the division site of a 1 μm diameter *E. coli* cell (Nelson and Young, 2000) would require ~700 FtsZ molecules. Therefore, if there are ~2000 molecules in the ring, there is enough FtsZ in filaments to encircle the cell approximately three times, indicating that there is not one single FtsZ filament around the inner side of the membrane.

Two main models have been proposed to explain how FtsZ filaments are organized in the cell: the ribbon model and the scatter model. The ribbon model proposes that FtsZ filaments are parallel and in close contact, annealing in a continuous ring constituted of few filaments, making a ribbon-like structure 10-25 nm wide (2-5 filaments). The scattered model proposes that FtsZ filaments organize into short disorganized polymers that are more spaced, creating a wider structure of ~100 nm. Evidence for the ribbon model comes from cryo Electron Microscopy (cryoEM) images of liposomes containing FtsA and parallel arrays of FtsZ filaments, encircling the cells at constriction sites, in a helical-like loop of 2-4 filaments, one protofilament thick (Szwedziak et

al., 2014). Experimental evidence for the scattered model first came from a cryoEM study of FtsZ from *C. crescentus*, that showed that the filaments were rarely in close contact with each other (Li et al., 2007). This model has gained momentum with the analysis of FtsZ ring dimensions through high resolution microscopy techniques like PALM which showed that FtsZ dimensions were 80–100 nm in axial width and 40–60 nm in radial width (Fu et al., 2010, Holden et al., 2014, Vedyaykin et al., 2016, Jacq et al., 2015, Coltharp et al., 2016). Additionally, structured illumination microscopy (SIM) imaging of FtsZ in live cells from several species revealed that the filaments are patchy and rarely form a continuous ring (Strauss et al., 2012, Rowlett and Margolin, 2014). Together, these results indicate that, in live cells, FtsZ seems to organize in non-continuous structures. However, it is possible that at different times of cell division, or in specific conditions, FtsZ filaments shift from continuous to scattered structures or vice-versa.

For FtsZ filaments to perform their function in cytokinesis, they must bind directly or indirectly to the inner side of the cellular membrane. Since FtsZ is a cytoplasmic protein with no membrane attachment domains, it needs to be tethered to the inner side of the cell membrane by at least one membrane associated protein (Figure 5c). This is a crucial step in divisome assembly and different species perform this through different auxiliary membrane proteins. One of these proteins is FtsA, the second most conserved bacterial division protein and a homologue of eukaryotic actin (Izore and van den Ent, 2017) that associates to the membrane through a membrane targeting sequence (MTS) (Pichoff and Lutkenhaus, 2005) and binds to FtsZ C-terminal tail (CTT), tethering it to the membrane (Din et al., 1998, Yan et al., 2000,

Haney et al., 2001). *In vitro*, *E. coli* FtsA assembled to lipid monolayers forming mini rings, composed of 12 subunits (Krupka et al., 2017) but it remains to be determined if these structures exist in live *E. coli* cells. Importantly, FtsA is also involved in regulating FtsZ dynamics: *in vitro* reconstitutions of FtsZ filaments in planar lipid bilayers using several Z-ring membrane tethering proteins (like FtsA and ZipA), showed association of FtsZ filaments to the membrane (Loose and Mitchison, 2014). However, it was only when FtsA was used as membrane tether that the 1.2 μm diameter, 0.5 μm thick FtsZ-FtsA rings moved directionally through treadmilling, presumably because FtsA destabilizes FtsZ filaments causing detaching of FtsZ from protofilaments. In support of this idea, FtsA from *S. aureus* stimulates the GTPase activity of FtsZ (Fujita et al., 2014), consistent with a role in filament dynamics.

Although *E. coli* FtsA seems to be crucial for FtsZ membrane attachment and treadmilling, in other bacteria additional factors have an important role in FtsZ membrane tethering. Unlike *E. coli*, *ftsA* mutants of *B. subtilis* are viable, although deficient in division (Beall and Lutkenhaus, 1992, Jensen et al., 2005), suggesting that other proteins could partially compensate for the absence of FtsA. Consistent with a role in membrane tethering, SepF overexpression in *B. subtilis* compensates for *ftsA* deletion (Ishikawa et al., 2006) and *sepF* deletion is lethal in the presence of mutations of other *B. subtilis* membrane tethering proteins (Hamoen et al., 2006, Ishikawa et al., 2006). Besides the tethering function (Duman et al., 2013), *in vitro* SepF can assemble in large rings that bundle FtsZ protofilaments, indicating the involvement of the protein in regulating FtsZ (Gundogdu et al., 2011). In species that lack *ftsA* and *ezrA* (like mycobacterium), SepF becomes essential as it may be the sole membrane

tether of FtsZ and, presumably, the one protein bridging FtsZ and PG synthesis proteins (Gola et al., 2015, Gupta et al., 2015).

Another example of an important FtsZ-membrane anchoring protein is a cytoskeletal spectrin-like protein (Cleverley et al., 2014) highly conserved in low G+C Gram-positive bacteria like *S. aureus*, whose deletion in *B. subtilis* makes extra Z-rings (EzrA) (Levin et al., 1999). In the absence of EzrA ~50% of *B. subtilis* cells produce extra Z-rings near the poles, although only 4% of these polar Z-rings are successful in constricting, generating minicells (Levin et al., 1999). Additionally, *ezrA* mutants of *B. subtilis* have a reduced diameter, presumably because the protein is involved in shuttling the PG synthesis protein PBP1 from elongation to division (Claessen et al., 2008). EzrA negatively regulates FtsZ by inhibiting FtsZ polymerization *in vitro* through reduction of FtsZ GTP-binding activity and increased rate of GTP hydrolysis (Chung et al., 2007). In *S. aureus ezrA* deletion leads to a higher proportion of larger cells possessing multiple Z-rings (Jorge et al., 2011). Structurally, EzrA is a membrane protein possessing one transmembrane helix followed by a cytoplasmic domain that contains multiple copies of helical bundle repeats that form a horseshoe shape (Cleverley et al., 2014). This shape has been proposed to act either as a clamp of FtsZ filaments to the membrane or as a divider to separate FtsZ filaments (Cleverley et al., 2014). The mechanisms for how EzrA may control FtsZ dynamics and divisome formation remains to be determined. Although EzrA eukaryotic counterparts (spectrins) have been shown to act as scaffolds to coordinate interactions between membrane proteins (Liem, 2016), the ability of EzrA to perform such role remains elusive.

Recruitment of downstream cell division proteins to midcell completes the bacterial divisome

Once the Z-ring is assembled at the membrane, downstream proteins are recruited to midcell to form a complete divisome. The late divisome has been very well studied in *E. coli* (Lutkenhaus and Du, 2017) and *B. subtilis* (Errington and Wu, 2017) models, and is composed of proteins involved in several processes such as DNA translocation and chromosome dimer resolution (FtsK in *E. coli* and SftA in *B. subtilis*), PG synthesis (FtsW, FtsI and FtsN in *E. coli*; FtsW and PBP2B in *B. subtilis*), structural regulator proteins (FtsQLB complex in *E. coli*; DivIB-FtsL-DivIC complex in *B. subtilis*) and cell division orchestrators (GpsB and DivVIA in *B. subtilis*).

In *S. aureus*, assembly of some cell division components also seems to be a hierarchical process. FtsZ assembly at midcell is followed by recruitment of FtsW, PBP1 and DivIB and, later on, by MurJ and PBP2 (Monteiro et al., 2018). Importantly, MurJ recruitment to midcell requires pre-assembled DivIB-FtsL-DivIC sub-complex (Monteiro et al., 2018). *S. aureus* MurJ (SACOL1804) is a member of the multidrug/ oligosaccharidyl-lipid/polysaccharide (MOPs) exporter superfamily and has been proposed as a functional *E. coli* MurJ orthologue (Huber et al., 2009). Importantly, during *S. aureus* cell division, recruitment of MurJ to midcell coincides with the shift of PG synthesis from the cell periphery to the division site (Monteiro et al., 2018). *E. coli* MurJ (Ruiz, 2008, Inoue et al., 2008) was shown to be a lipid II flippase *in vivo* (Sham et al., 2014) but another cell division protein, FtsW (Boyle et al., 1997, Pastoret et al., 2004), was shown to have lipid II flippase activity *in vitro* (Mohammadi et al., 2014). However, FtsW is a member of sporulation, elongation,

division and synthesis (SEDS) protein family and other proteins of this family (like RodA) have been recently identified as PG transglycosylases that work together with PBPs to polymerize PG in rod-shaped bacteria (Meeske et al., 2016, Emami et al., 2017). Given that in *S. aureus* MurJ, but not FtsW, is responsible for directing PG synthesis to midcell (Monteiro et al., 2018), MurJ is likely to be the main lipid II flippase in this organism, presenting lipid II to the major PG synthesis enzyme (PBP2) which localizes through substrate recognition (Pinho and Errington, 2005). PBP2 would then start massive PG synthesis at the septum (Monteiro et al., 2018). However, it remains to be determined what is the function of FtsW and whether MurJ has lipid II flippase activity in *S. aureus*.

Although the existence of a temporal lag between the assembly of divisome components seems to be conserved in bacteria like *E. coli*, *B. subtilis*, *C. crescentus* and *S. aureus*, the biological relevance for this temporal delay is poorly understood (Aarsman et al., 2005, Gamba et al., 2009, Goley et al., 2011, Monteiro et al., 2018) and the exact signal that triggers the assembly at midcell of the late proteins remains to be discovered.

What force drives cell division?

The constriction conundrum – going against turgor pressure

Cell division through binary fission requires the separation of the cytoplasm of each future daughter cell through inward growth of the membrane and cell wall. This inward progression of the cell envelope (cytokinesis) requires a force-generation mechanism, not only in bacteria but in several kingdoms of life (Balasubramanian et al., 2012). In animal cells this is performed by myosin motors walking on antiparallel actin

filaments (Cheffings et al., 2016). However, equivalent motor proteins have not been identified in bacteria (Balasubramanian et al., 2012).

A major challenge during cytokinesis is to overcome the opposite force of high turgor pressure which bacteria are subjected to (Figure 6). It is estimated that this force ranges from 0.3-3 atm in Gram-negatives like *E. coli* (Cayley et al., 2000) while Gram-positive bacteria like *B. subtilis* and *S. aureus* are subjected to a turgor force of ~20 atm (Whatmore and Reed, 1990, Mitchell and Moyle, 1956) (for comparison, the pressure in a car tire is ~2 atm). Considering the dimensions of the division site (approximately 3 μm in circumference and 60 nm in width) and discarding the rigidity of PG, a force required to constrict the cell envelope at midcell (hereby called constrictive force) of ~50 nN in Gram-negatives or ~ 300 nN in Gram-positives is required to counterbalance turgor pressure (Xiao and Goley, 2016). It was recently proposed that Gram-negatives may perform cytokinesis in an isosmotic space, surpassing the need to constrict against turgor pressure, as the cytoplasm and periplasm have an isotonic composition (Erickson, 2017, Osawa and Erickson, 2018). Because in Gram-positives the existence of a periplasmic space between the membrane and the cell wall is arguable the turgor pressure barrier is most likely at the cellular membrane (Beeby et al., 2013, Osawa and Erickson, 2018). Current evidence therefore favors that in Gram-positives the force(s) that lead to cytokinesis most likely need to overcome the enormous force of turgor (Osawa and Erickson, 2018).

The effects of turgor pressure on cytokinesis are not exclusive of bacteria. Experiments performed in yeast cells show that a decrease in turgor pressure leads to a higher rate of cytokinesis (Proctor et al., 2012).

More work is required to understand how turgor forces play a role in bacterial cytokinesis and growth.

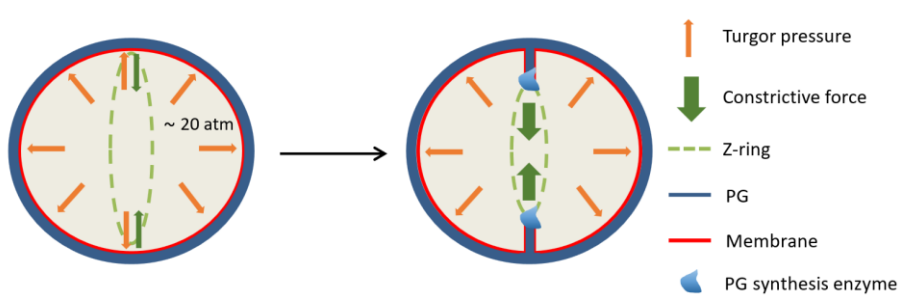

Figure 6: Forces in cytokinesis of Gram-positive bacteria: turgor pressure versus constrictive force. For a cell to start invagination of the cellular envelope (cytokinesis) the outward force generated by turgor pressure (orange arrows) needs to be overcome by a higher force in the opposite direction (constrictive force, green arrow).

FtsZ as a force generator protein: the FtsZ-centric model

As no cognate to eukaryotic motor proteins like myosin that would perform an analogous function in cytokinesis have been identified in bacteria, FtsZ has long been suggested as the constrictive force generator (Erickson et al., 2010). An "FtsZ-centric model" proposes that the force necessary to counteract turgor pressure comes from FtsZ which pulls the cell membrane inwards (Figure 7) (Erickson, 1997, Erickson et al., 2010). Due to FtsZ ability to polymerize/depolymerize and to hydrolyze GTP, several FtsZ-mediated force generator mechanisms have been proposed, where FtsZ could deform membranes through filament bending (Ghosh and Sain, 2008, Osawa et al., 2009, Li et al., 2013); filament condensation (Lan et al., 2009), membrane pinching (Li et al., 2007), lateral bonding between filaments (Horger et al., 2010) and filament polymerization/depolymerization (Allard and Cytrynbaum,

2009). Among the several force generation mechanisms suggested for FtsZ, the two most discussed ones are the "filament bending" and the "condensation" models.

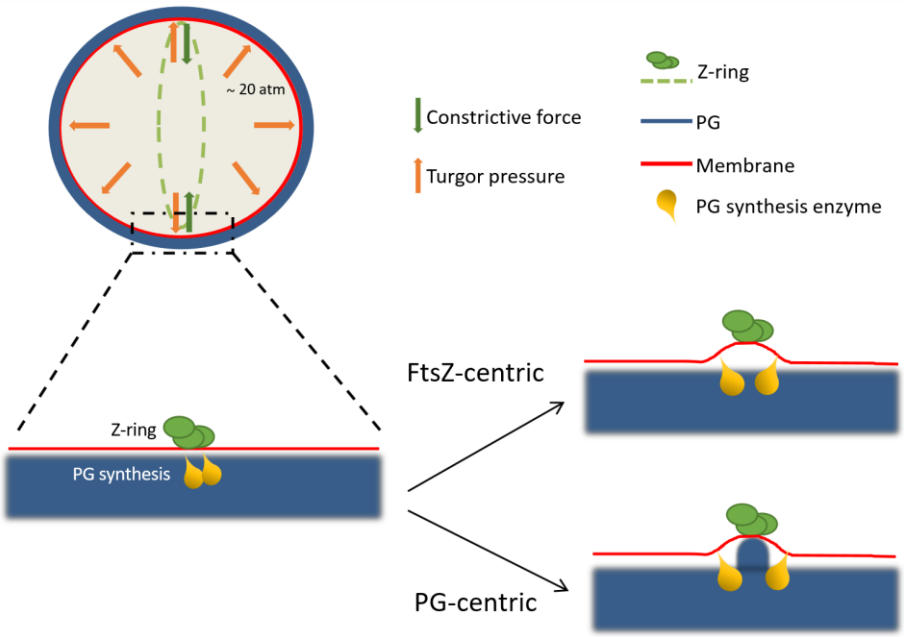

Figure 7: Models for the origin of the force that drives bacterial cytokinesis. Gram-positive bacteria like *S. aureus* probably require a constrictive force that counteracts 20 atm of turgor pressure (total force ~300 nN). The **FtsZ-centric model** proposes that FtsZ filaments tethered to the membrane (Z-ring) might generate a force that **pulls** the cellular membrane inwards while the **PG-centric model** proposes that inward PG deposition at the septum **pushes** the cell membrane, generating the force necessary to constrict.

The FtsZ filament bending model is based on electron microscopy (EM) and Atomic Force Microscopy (AFM) observations that FtsZ-GTP polymers are straight while FtsZ-GDP filaments are curved, indicating that GTP hydrolysis leads to bending of the FtsZ polymer, which could deform the membrane (Lu et al., 2000, Li et al., 2007, Allard and Cytrynbaum, 2009, Li et al., 2013). Most experimental evidence favoring

this model has been obtained *in vitro* from experiments with FtsZ attached to liposomes through a membrane tether, showing that FtsZ rings could deform the membrane (Osawa et al., 2008). Additionally, when FtsZ is tethered to the exterior of a liposome it produces membrane deformations that correlate with the direction of filament curvature, providing strong support for the filament bending model (Osawa et al., 2009). In this model, the role of GTP hydrolysis on bending is debatable because, in the absence of GTP hydrolysis, FtsZ attached to liposomes could still induce membrane deformation (Osawa and Erickson, 2011). Nevertheless, GTP hydrolysis was important to proceed with liposome constriction to smaller diameters, suggesting that GTPase activity might be important for a continuous constrictive force. Alternatively, naturally curved FtsZ filaments, regardless of the nucleotide bound state, could be responsible for membrane bending (Erickson and Osawa, 2017). FtsA may also have a direct or indirect role in membrane constriction, as *in vitro* experiments comparing liposomes with membrane tethered FtsZ versus FtsZ plus FtsA as the membrane tether show that full fission of the membrane is only accomplished in the presence of FtsA (Osawa and Erickson, 2013).

An alternative model for FtsZ as a constrictive force generator of cytokinesis is the condensation model. This model is based on the ability of FtsZ to establish lateral bonds that could lead to sliding between filaments which would constrict the Z-ring and, concomitantly, the membrane (Lan et al., 2009). This model therefore assumes that FtsZ assembles *in vivo* as multiple filaments that form a continuous closed structure (the ribbon model) instead of forming a loose structure where the filaments are not in close contact (scattered model). Recently,

experimental data compatible with the condensation model was observed by cryo-EM imaging of FtsZ and FtsA from *Thermotoga maritima* in liposomes (Szwedziak et al., 2014). In this work, FtsZ assembled as a continuous structure through lateral association between the filaments, deforming the liposome, presumably through filament sliding (Szwedziak et al., 2014). However, *in vivo* observations show that *C. crescentus*, as well as other bacteria, are able to constrict the envelope in the presence of partial FtsZ rings suggesting that a full continuous ring is not required for *in vivo* constriction (Yao et al., 2017).

Another property of FtsZ filaments that could generate a force that leads to envelope constriction is treadmilling. Bent FtsZ filaments that treadmill could create a localized and transient membrane deformation (pinching) that could be crucial for the initiation of constriction (Schoenemann and Margolin, 2017). Recently, the ability of FtsZ filaments to move through treadmilling has been shown to influence septal constriction rates of *B. subtilis*, but not of *E. coli* (Bisson-Filho et al., 2017, Yang et al., 2017). Importantly, FtsZ treadmilling drives the directional motion of PG synthesis proteins in both organisms (PBP3 in *E. coli* (Yang et al., 2017) and PBP2B in *B. subtilis* (Bisson-Filho et al., 2017), so FtsZ treadmilling could drive *B. subtilis* envelope constriction by powering the movement of PG synthesis proteins like PBP2B (discussed below).

Although there is strong evidence showing that FtsZ filaments can generate a constrictive force *in vitro*, some properties of FtsZ and Z-ring assembly are hard to reconcile with an FtsZ-centric constriction model *in vivo*. The two mechanisms of filament bending or condensation that explain how FtsZ could generate a force that drives cytokinesis were

incorporated in several bioinformatic models which show that Z-rings could generate forces up to 100 pN (reviewed in (Coltharp and Xiao, 2017)). Although this force could lead to liposome constriction it does not seem to be sufficient to counteract turgor pressure (50-300 nN) (Coltharp and Xiao, 2017, Osawa and Erickson, 2018). Additionally, in *E. coli*, changes in FtsZ amounts, assembly dynamics or GTP hydrolysis did not influence septal constriction rates, suggesting that a reduction in FtsZ-derived forces does not limit cellular constriction (Coltharp et al., 2016). Also, high resolution imaging through Correlative Light Electron Microscopy (CLEM) indicates that FtsZ presence at *E. coli* midcell does not lead to membrane constriction in the absence of later divisome proteins (Daley et al., 2016). Furthermore, during *E. coli* cell division, FtsZ departs from midcell before the inner membrane has completed constriction, suggesting that perhaps FtsZ is not required for the last stages of cytokinesis (Soderstrom et al., 2014, Coltharp et al., 2016). One of the reasons why bacterial cell cytokinesis likely requires higher forces than liposome constriction is the presence of the cell wall. When *E. coli* cells were deformed using a constant external force, the cells bounced back, suggesting that the cell wall has elastic properties. Furthermore, a sustained cell deformation requires a force applied over many minutes (Amir et al., 2014). Because FtsZ filaments are highly dynamic in live cells, with subunit turnover and treadmilling rates on the second timescale, the Z-ring is unlikely to produce major cell wall deformation through direct mechanical action.

PG synthesis as the force that drives cytokinesis: the PG-centric model

Another source for generating the constrictive force that drives cytokinesis could be PG synthesis. In a "PG-centric model", FtsZ serves only as a scaffold of later divisome proteins, some of which are involved in PG synthesis. Inward synthesis of PG would then push the cell membrane against turgor pressure, driving cytokinesis (Figure 7) (Meier and Goley, 2014). Consistent with a role in constriction, septal PG synthesis is required for cytokinesis, as chemical inhibition/inactivation of divisome PBPs blocks this process (Schwarz et al., 1969, Spratt, 1975, Spratt, 1977, Pogliano et al., 1997, Daniel et al., 2000, Sassine et al., 2017). While alterations in FtsZ properties did not influence *E. coli* rate of constriction, a mutant of the divisome PG synthesis enzyme PBP3 (*ftsI*) had significantly slower constriction rates (Coltharp et al., 2016).

Additionally, late divisome proteins that may be involved in bringing PG synthesis to the division site or that directly contribute to PG polymerization have been shown to modulate constriction rates of *E. coli* and *C. crescentus*. In *E. coli*, mutants of the late divisome complex FtsQLB modulate envelope constriction initiation, with FtsQ mutants showing longer constriction periods (Huls et al., 1999) while point mutations in FtsL and FtsB promote premature constriction initiation (Liu et al., 2015, Tsang and Bernhardt, 2015). In *C. crescentus*, point mutants of the SEDS protein FtsW and point mutants in PBP3 (*ftsI*) lead to a phenotype of hyperactive constriction (Modell et al., 2014). This data indicates that late divisome proteins seem to modulate cytokinesis rates through unknow mechanisms. Supporting the idea that recruitment of late divisome proteins starts envelope constriction, a recent CLEM study in *E. coli*

showed that recruitment of the late divisome protein FtsN to midcell coincides with membrane constriction (Daley et al., 2016). Because FtsN can bind to PG molecules and activate PG synthesis at the division site (Gerding et al., 2009, Yahashiri et al., 2015, Liu et al., 2015, Du and Lutkenhaus, 2017), perhaps the initiation of PG synthesis is the key trigger to start cytokinesis. As FtsN is a poorly conserved protein outside proteobacteria (Moll and Thanbichler, 2009), it seems unlikely that this protein is a common envelope constriction initiator. In S*. aureus* the essential divisome protein DivIB, an FtsQ orthologue, has been shown to bind PG and although the role of the binding in activating the divisome is unknown, DivIB depletion seems to stall septal constriction (Bottomley et al., 2014). Collectively these results suggest that the driving force for cytokinesis is provided by cell wall synthesis and remodeling. However, it is unknown how much force could PG synthesis generate, as there is a lack of knowledge on the orientation and density of the glycan strands.

Concerted actions of FtsZ and PG synthesis could drive constriction

A more inclusive model comprising contributions from both FtsZ and PG synthesis to drive envelope constriction is also plausible. FtsZ could generate a small force that could deform the membrane but the attachment of the membrane to PG would prevent any visible constriction, and so, invagination of the cellular envelope would only start when new PG synthesis caused envelope deformation (Erickson and Osawa, 2017). Additionally, FtsZ dynamics could also contribute for the initiation, efficiency, directionality and/or mechanical regulation of PG synthesis (Coltharp and Xiao, 2017). Evidence for this comes from the analysis of the role of FtsZ treadmilling in *E. coli* and *B. subtilis* cell

division (Yang et al., 2017, Bisson-Filho et al., 2017). In these recent studies, PG synthesis proteins from both organisms were shown to directionally move along the division septum in a manner dependent on FtsZ treadmilling, suggesting that treadmilling could influence PG synthesis dynamics. However, while the rate of treadmilling was directly correlated with PG synthesis and cell division rates in *B. subtilis* (Bisson-Filho et al., 2017), treadmilling impairment had no effect on *E. coli* cell division rate (Yang et al., 2017). Instead of controlling the septal constriction rate, FtsZ treadmilling in *E. coli* influences the shape of the septum by promoting homogeneous PG distribution around the whole circumference of the division septum (Yang et al., 2017). These differences were mainly attributed to differences in the PG thickness of Gram-positive and Gram-negative species (Schoenemann and Margolin, 2017). Further studies in other species are required to fully understand the role of FtsZ treadmilling in controlling PG synthesis *in vivo*. It remains to be determined why impairing FtsZ treadmilling has different consequences on *E. coli* and *B. subtilis* cytokinesis and if treadmilling movement of FtsZ filaments can generate a constrictive force that drives cytokinesis. A unified model of a dynamic FtsZ acting as a signaling hub to regulate PG synthesis enzymes could explain the driving force for envelope constriction in bacteria (Coltharp and Xiao, 2017).

Cell division in the absence of FtsZ

Although FtsZ is essential for cytokinesis in a great number of Bacteria, Euryarchaeota, and some eukaryotic plastids and mitochondria, some bacteria are able to grow in its absence. Streptomyces only needs FtsZ to sporulate but not during vegetative growth (McCormick et al., 1994, Santos-Beneit et al., 2017) while members of the phyla Tenericutes,

Chlamydiae and Planctomycetes do not have *ftsZ* (Adams and Errington, 2009). Chlamydiae evolved an MreB-based mechanism to proliferate (Jacquier et al., 2015, Liechti et al., 2016), and the Planctomycetes *Gemmata obscuriglobus* divides asymmetrically using a budding-like system (Lee et al., 2009, Devos, 2013). Interestingly, *Chlamydia trachomatis* was also shown to divide through asymmetric budding, with an FtsQ orthologue localizing to the site where budding occurs (Abdelrahman et al., 2016). This suggests that other divisome components may take over the function of FtsZ in bacteria that lack this protein. The mechanisms that drive cell division in these less studied bacteria are still largely unknown but show that FtsZ is not the sole protein capable of promoting bacterial cell division.

A remarkable tool to study the principles of cell division are bacteria deprived of PG (L-forms). Several species from different branches of life can adapt to grow without PG in osmoprotective media. Consistent with the role of PG in shape maintenance, cell morphology becomes severely affected in L-forms (Mercier et al., 2014). Strikingly, L-forms have been shown to surpass FtsZ as a requirement to generate progeny, dividing through blebbing or tubulation of the cell membrane due to mutations that lead to overproduction of phospholipids (Leaver et al., 2009, Mercier et al., 2013, Mercier et al., 2014). When *de novo* PG synthesis was induced in *E. coli* L-forms deprived of FtsZ, the bacterial shape was restored, but these walled cells lacking FtsZ were unable to divide (Mercier et al., 2016). Interestingly, some walled *ftsZ* mutants with secondary inactivating mutations in PBP1B could proliferate in the absence of FtsZ but required MreB. This mutants grew by projecting protrusions that developed into branched structures of bulbous

compartments connected through thin bridges of cellular material, in the shape of a cauliflower. The cells divided when the bulbous material separated from the ramified structures through breakage of the connecting bridges (Mercier et al., 2016).

Another interesting experiment showing proliferation in the absence of FtsZ resulted from the construction of a bacterial strain containing a minimal synthetic genome, where three increasingly smaller genomes (syn1.0, syn 2.0 and syn3.0), were synthesized and analyzed (Hutchison et al., 2016). Importantly, from genome 1.0 to genome 3.0 several cell division genes were inactivated, including *ftsZ* and *sepF*, with *ftsA* becoming essential. Although syn3.0 proliferated in the absence of *ftsZ*, cells divided three times slower than syn1.0 cells and lost the original cocci morphology, forming extensive networks of filamentous material.

These experiments show the immense plasticity and adaptability of bacteria to proliferate using alternative modes of growth or cytoskeletal elements and suggest that even bacteria that are adapted to life with FtsZ can surpass the need of this protein by using alternative division strategies.

Different ways to undergo bacterial daughter cell separation: to invaginate or to not invaginate

Cell division in different bacteria comprises a period of no septum synthesis, followed by a stage where septum synthesis starts, with inward growth of PG. However, septum maturation and sister cell separation vary between different bacteria. While *E. coli*, *S. pneumoniae* and *C. crescentus* simultaneously constrict the septum inwards and

invaginate the envelope from the exterior, forming a V-shaped septum (Figure 8a), *S. aureus* and *B. subtilis* first synthesize a septal plate at midcell without external PG invagination and only later PG remodeling leads to splitting of the septum and separation in two daughter cells (Figure 8b) (Uehara and Bernhardt, 2011, Erickson, 2017).

Particularly in *S. aureus* and other Gram-positives like *Actinobacteria*, daughter cells remain fully attached during a considerable time after completion of the septum, until a fast separation (millisecond timescale) with instant reshaping of the flat septum generates the new hemispheres of the daughter cells (Monteiro et al., 2015, Zhou et al., 2015, Zhou et al., 2016). In *S. aureus*, septal reshaping requires turgor pressure and the *sle1* autolysin, as altering their levels leads to some D-shaped cells, unable to perform septal reshaping from a flat to a curved surface (Monteiro et al., 2015). However, in the absence of Sle1, most cells are still able to perform the fast sister cell separation, suggesting alternative players controlling daughter cell separation in *S. aureus*. Some bacterial species that synthesize a septal plate during cell division do not perform the fast daughter cell separation. Instead, once the septum is closed, the cellular envelope slowly invaginates from the exterior, forming a V-shaped intersection between the two daughter cells (Zhou et al., 2016).

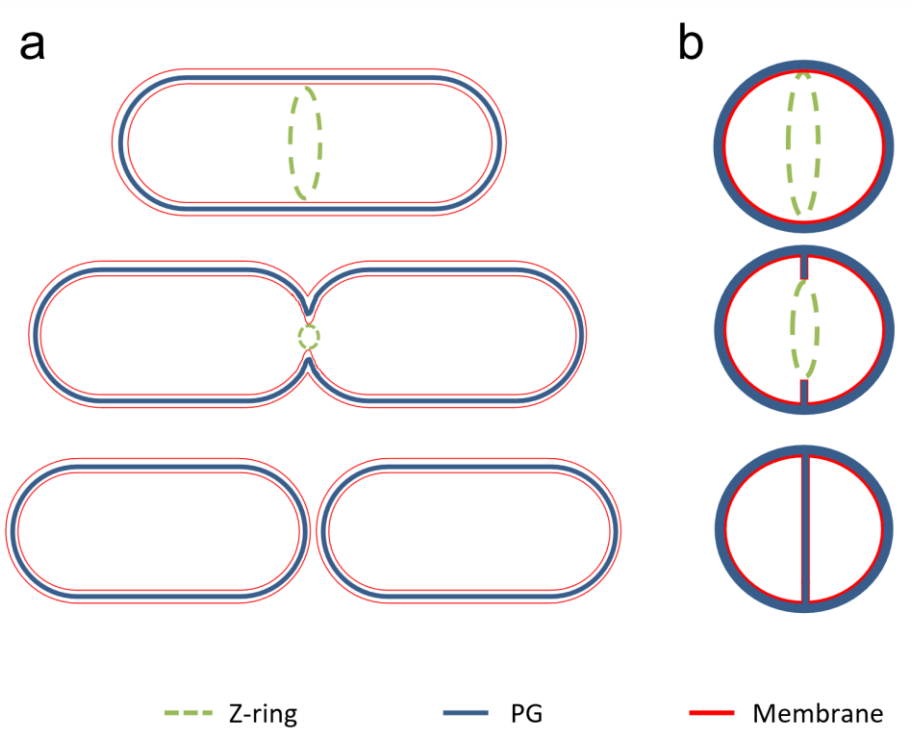

Figure 8: (a) Sister cell separation in bacteria like *E. coli* is concurrent with septum synthesis, as the splitting of the septum occurs during cytokinesis. This mode of division leads to invagination of the cellular envelope from the periphery to the inside. **(b)** Bacteria like *B. subtilis* and *S. aureus* do not invaginate the peripheral envelope during cell division. Instead they first synthesize a septal plate without splitting of the PG material from the outside. Sister cell separation only occurs some time after completion of membrane and septal fusion.

***S. aureus* as an antibiotic resistant pathogen**

S. aureus is both a commensal organism and a pathogen responsible for nosocomial and community-acquired infections. It colonizes around 30% of the human population, preferentially in the skin and nasopharynx (Eriksen et al., 1995, Kluytmans and Wertheim, 2005, Otto, 2010, Edwards et al., 2012). Colonization is often asymptomatic but

if the skin barrier or the mucous membranes are breached, *S. aureus* may establish an invasive infection. Therefore *S. aureus* can cause minor skin lesions or life-threatening diseases, such as bacteremia, endocarditis or pneumonia (Tong et al., 2015). It is also a serious health-care problem due to its remarkable potential to develop antimicrobial resistance (Boucher and Corey, 2008). Beta-lactam antibiotics are amongst the most used drugs to treat bacterial infections caused by several species (Worthington and Melander, 2013). They inhibit PG synthesis through binding to the transpeptidase catalytic site of PBPs, blocking access to their substrates and preventing PG crosslinking (Zapun et al., 2008a). Within a few years after the introduction of the first beta-lactam penicillin, *S. aureus* resistant strains that inactivated the antibiotic were identified in a clinical environment (Barber and Rozwadowska-Dowzenko, 1948). This prompted the development of a penicillin derivative, methicillin, that was not degradable by the bacteria. But soon after, the first methicillin resistant *S. aureus* (MRSA) strains, like COL, were identified in the UK (Jevons et al., 1963). By the 1980s, infections caused by *S. aureus* MRSA strains, an acronym that now identifies strains resistant to virtually all classes of beta-lactam antibiotics, reached global proportions and MRSA strains are currently one of the leading causes of nosocomial infections worldwide (Stefani et al., 2012). Methicillin was then substituted by oxacillin, a more stable and less toxic beta-lactam (Ditlove et al., 1977, McEvoy, 1995), although MRSA strains are still resistant to this antibiotic. The main cause of MRSA resistance is the acquisition of the *mecA* gene, encoded in an exogenous mobile genetic element called staphylococcal cassette chromosome *mec* (SCC*mec*), which codes for an alternative penicillin-binding protein, PBP2A (Hartman and Tomasz, 1984, Reynolds and Brown, 1985). PBP2A has

lower affinity for beta-lactams (Lu et al., 1999, Graves-Woodward and Pratt, 1998) and so it maintains its transpeptidase activity which, in cooperation with the transglycosylase activity of PBP2 (whose transpeptidase domain is inactivated by the presence of the antibiotic), ensures cell wall synthesis in the presence of beta-lactams (Pinho et al., 2001).

Due to its essential role in cell viability, the divisome poses as a new target for antimicrobial therapy. In fact, a compound named PC190723 that targets FtsZ effectively kills MRSA strains (Haydon et al., 2008, Hurley et al., 2016). However, the emergence of PC190723-resistant mutants at high frequency prevented the use of this antibiotic as an alternative to combat *S. aureus* infections (Tan et al., 2012). PC190723 was shown to directly bind to *S. aureus* FtsZ, in a pocket beneath the H7 loop, close to the C-terminal domain (Tan et al., 2012, Matsui et al., 2012). Although its binding site is far from FtsZ GTP-binding domain, it is near the T7 loop which contacts the GTP-binding site of an adjacent FtsZ subunit, forming the catalytic site for GTP hydrolysis (Scheffers et al., 2002). While PC190723 inhibits growth of bacteria like *S. aureus* and *B. subtilis*, the exact mechanism of action remains unclear. Initial studies showed that the compound inhibits FtsZ GTPase activity *in vitro* (Haydon et al., 2008, Andreu et al., 2010), but other recent studies reported that it increases FtsZ GTPase hydrolysis in *S. aureus* leading to an increased polymer formation, presumably through reduction of the lag phase of polymer assembly. (Elsen et al., 2012, Anderson et al., 2012), Importantly, *in vivo* studies showed that PC190723 compound inhibits *B. subtilis* FtsZ treadmilling (Bisson-Filho et al., 2017).

Detailed studies on how current antibiotics may affect cell division, together with understanding the fundamental roles of this fundamental process, might lead to the discovery of new antimicrobial targets that impair cell proliferation.

REFERENCES

Aaron, M., Charbon, G., Lam, H., Schwarz, H., Vollmer, W. and Jacobs-Wagner, C. (2007). The tubulin homologue FtsZ contributes to cell elongation by guiding cell wall precursor synthesis in *Caulobacter crescentus*. Mol Microbiol*, 64***,** 938-52.

Aarsman, M. E., Piette, A., Fraipont, C., Vinkenvleugel, T. M., Nguyen-Disteche, M. and den Blaauwen, T. (2005). Maturation of the *Escherichia coli* divisome occurs in two steps. Mol Microbiol*, 55***,** 1631-45.

Abdelrahman, Y., Ouellette, S. P., Belland, R. J. and Cox, J. V. (2016). Polarized Cell Division of *Chlamydia trachomatis*. PLoS Pathog*, 12***,** e1005822.

Adams, D. W. and Errington, J. (2009). Bacterial cell division: assembly, maintenance and disassembly of the Z ring. Nat Rev Microbiol*, 7***,** 642-53.

Adams, D. W., Wu, L. J. and Errington, J. (2015). Nucleoid occlusion protein Noc recruits DNA to the bacterial cell membrane. Embo j*, 34***,** 491-501.

Addinall, S. G., Cao, C. and Lutkenhaus, J. (1997). FtsN, a late recruit to the septum in *Escherichia coli*. Mol Microbiol*, 25***,** 303-9.

Addinall, S. G. and Lutkenhaus, J. (1996). FtsA is localized to the septum in an FtsZ-dependent manner. J Bacteriol*, 178***,** 7167-72.

Allan, E. J., Hoischen, C. and Gumpert, J. (2009). Bacterial L-forms. Adv Appl Microbiol*, 68***,** 1-39.

Allard, J. F. and Cytrynbaum, E. N. (2009). Force generation by a dynamic Z-ring in *Escherichia coli* cell division. Proc Natl Acad Sci U S A*, 106***,** 145-50.

Alyahya, S. A., Alexander, R., Costa, T., Henriques, A. O., Emonet, T. and Jacobs-Wagner, C. (2009). RodZ, a component of the bacterial core morphogenic apparatus. Proc Natl Acad Sci U S A*, 106***,** 1239-44.

Amir, A., Babaeipour, F., McIntosh, D. B., Nelson, D. R. and Jun, S. (2014). Bending forces plastically deform growing bacterial cell walls. Proc Natl Acad Sci U S A*, 111***,** 5778-83.

Anderson, D. E., Gueiros-Filho, F. J. and Erickson, H. P. (2004). Assembly dynamics of FtsZ rings in *Bacillus subtilis* and *Escherichia coli* and effects of FtsZ-regulating proteins. J Bacteriol*, 186***,** 5775-81.

Anderson, D. E., Kim, M. B., Moore, J. T., O'Brien, T. E., Sorto, N. A., Grove, C. I., Lackner, L. L., Ames, J. B. and Shaw, J. T. (2012). Comparison of small molecule inhibitors of the bacterial cell division protein FtsZ and identification of a reliable cross-species inhibitor. ACS Chem Biol*, 7***,** 1918-28.

Andreu, J. M., Schaffner-Barbero, C., Huecas, S., Alonso, D., Lopez-Rodriguez, M. L., Ruiz-Avila, L. B., Nunez-Ramirez, R., Llorca, O. and Martin-Galiano, A. J. (2010). The antibacterial cell division inhibitor PC190723 is an FtsZ polymer-stabilizing agent that induces filament assembly and condensation. J Biol Chem*, 285***,** 14239-46.

Arumugam, S., Chwastek, G., Fischer-Friedrich, E., Ehrig, C., Monch, I. and Schwille, P. (2012). Surface topology engineering of membranes for the mechanical investigation of the tubulin homologue FtsZ. Angew Chem Int Ed Engl*, 51***,** 11858-62.

Atilano, M. L., Pereira, P. M., Yates, J., Reed, P., Veiga, H., Pinho, M. G. and Filipe, S. R. (2010). Teichoic acids are temporal and spatial regulators of peptidoglycan cross-linking in *Staphylococcus aureus*. Proc Natl Acad Sci U S A*, 107***,** 18991-6.

Bailey, M. W., Bisicchia, P., Warren, B. T., Sherratt, D. J. and Mannik, J. (2014). Evidence for divisome localization mechanisms independent of the Min system and SlmA in *Escherichia coli*. PLoS Genet*, 10***,** e1004504.

Balasubramanian, M. K., Srinivasan, R., Huang, Y. and Ng, K. H. (2012). Comparing contractile apparatus-driven cytokinesis mechanisms across kingdoms. Cytoskeleton (Hoboken)*, 69***,** 942-56.

Barber, M. and Rozwadowska-Dowzenko, M. (1948). Infection by penicillin-resistant staphylococci. Lancet*, 2***,** 641-4.

Beall, B. and Lutkenhaus, J. (1992). Impaired cell division and sporulation of a *Bacillus subtilis* strain with the *ftsA* gene deleted. J Bacteriol*, 174***,** 2398-403.

Beeby, M., Gumbart, J. C., Roux, B. and Jensen, G. J. (2013). Architecture and assembly of the Gram-positive cell wall. Mol Microbiol*, 88***,** 664-72.

Bendezu, F. O., Hale, C. A., Bernhardt, T. G. and de Boer, P. A. (2009). RodZ (YfgA) is required for proper assembly of the MreB actin cytoskeleton and cell shape in *E. coli*. Embo j*, 28***,** 193-204.

Berg, K. H., Stamsas, G. A., Straume, D. and Havarstein, L. S. (2013). Effects of low PBP2b levels on cell morphology and peptidoglycan composition in *Streptococcus pneumoniae* R6. J Bacteriol*, 195***,** 4342-54.

Bernhardt, T. G. and de Boer, P. A. (2005). SlmA, a nucleoid-associated, FtsZ binding protein required for blocking septal ring assembly over Chromosomes in *E. coli*. Mol Cell*, 18***,** 555-64.

Bi, E. F. and Lutkenhaus, J. (1991). FtsZ ring structure associated with division in *Escherichia coli*. Nature*, 354***,** 161-4.

Bisson-Filho, A. W., Hsu, Y. P., Squyres, G. R., Kuru, E., Wu, F., Jukes, C., Sun, Y., Dekker, C., Holden, S., VanNieuwenhze, M. S.*, et al.* (2017). Treadmilling

by FtsZ filaments drives peptidoglycan synthesis and bacterial cell division. Science*, 355*, 739-743.

Bottomley, A. L., Kabli, A. F., Hurd, A. F., Turner, R. D., Garcia-Lara, J. and Foster, S. J. (2014). *Staphylococcus aureus* DivIB is a peptidoglycan-binding protein that is required for a morphological checkpoint in cell division. Mol Microbiol.

Boucher, H. W. and Corey, G. R. (2008). Epidemiology of methicillin-resistant *Staphylococcus aureus*. Clin Infect Dis*, 46 Suppl 5*, S344-9.

Boyle, D. S., Khattar, M. M., Addinall, S. G., Lutkenhaus, J. and Donachie, W. D. (1997). *ftsW* is an essential cell-division gene in *Escherichia coli*. Mol Microbiol*, 24*, 1263-73.

Bramhill, D. and Thompson, C. M. (1994). GTP-dependent polymerization of *Escherichia coli* FtsZ protein to form tubules. Proc Natl Acad Sci U S A*, 91*, 5813-7.

Buddelmeijer, N., Aarsman, M. E., Kolk, A. H., Vicente, M. and Nanninga, N. (1998). Localization of cell division protein FtsQ by immunofluorescence microscopy in dividing and nondividing cells of *Escherichia coli*. J Bacteriol*, 180*, 6107-16.

Buske, P. J. and Levin, P. A. (2012). Extreme C terminus of bacterial cytoskeletal protein FtsZ plays fundamental role in assembly independent of modulatory proteins. J Biol Chem*, 287*, 10945-57.

Buske, P. J. and Levin, P. A. (2013). A flexible C-terminal linker is required for proper FtsZ assembly in vitro and cytokinetic ring formation in vivo. Mol Microbiol*, 89*, 249-63.

Buss, J., Coltharp, C., Shtengel, G., Yang, X., Hess, H. and Xiao, J. (2015). A multi-layered protein network stabilizes the *Escherichia coli* FtsZ-ring and modulates constriction dynamics. PLoS Genet*, 11*, e1005128.

Cayley, D. S., Guttman, H. J. and Record, M. T., Jr. (2000). Biophysical characterization of changes in amounts and activity of *Escherichia coli* cell and compartment water and turgor pressure in response to osmotic stress. Biophys J*, 78*, 1748-64.

Chaaban, S. and Brouhard, G. J. (2017). A microtubule bestiary: structural diversity in tubulin polymers. Mol Biol Cell*, 28*, 2924-2931.

Cheffings, T. H., Burroughs, N. J. and Balasubramanian, M. K. (2016). Actomyosin Ring Formation and Tension Generation in Eukaryotic Cytokinesis. Curr Biol*, 26*, R719-r737.

Chung, K. M., Hsu, H. H., Yeh, H. Y. and Chang, B. Y. (2007). Mechanism of regulation of prokaryotic tubulin-like GTPase FtsZ by membrane protein EzrA. J Biol Chem*, 282*, 14891-7.

Claessen, D., Emmins, R., Hamoen, L. W., Daniel, R. A., Errington, J. and Edwards, D. H. (2008). Control of the cell elongation-division cycle by shuttling of PBP1 protein in *Bacillus subtilis*. Mol Microbiol*, 68***,** 1029-46.

Cleverley, R. M., Barrett, J. R., Basle, A., Bui, N. K., Hewitt, L., Solovyova, A., Xu, Z. Q., Daniel, R. A., Dixon, N. E., Harry, E. J.*, et al.* (2014). Structure and function of a spectrin-like regulator of bacterial cytokinesis. Nat Commun*, 5***,** 5421.

Coltharp, C., Buss, J., Plumer, T. M. and Xiao, J. (2016). Defining the rate-limiting processes of bacterial cytokinesis. Proc Natl Acad Sci U S A*, 113***,** E1044-53.

Coltharp, C. and Xiao, J. (2017). Beyond force generation: Why is a dynamic ring of FtsZ polymers essential for bacterial cytokinesis? Bioessays*, 39***,** 1-11.

Daley, D. O., Skoglund, U. and Soderstrom, B. (2016). FtsZ does not initiate membrane constriction at the onset of division. Sci Rep*, 6***,** 33138.

Daniel, R. A. and Errington, J. (2003). Control of cell morphogenesis in bacteria: two distinct ways to make a rod-shaped cell. Cell*, 113***,** 767-76.

Daniel, R. A., Harry, E. J. and Errington, J. (2000). Role of penicillin-binding protein PBP 2B in assembly and functioning of the division machinery of *Bacillus subtilis*. Mol Microbiol*, 35***,** 299-311.

de Boer, P., Crossley, R. and Rothfield, L. (1992). The essential bacterial cell-division protein FtsZ is a GTPase. Nature*, 359***,** 254-6.

de Boer, P. A. (2010). Advances in understanding *E. coli* cell fission. Curr Opin Microbiol*, 13***,** 730-7.

Devos, D. P. (2013). *Gemmata obscuriglobus*. Curr Biol*, 23***,** R705-7.

Din, N., Quardokus, E. M., Sackett, M. J. and Brun, Y. V. (1998). Dominant C-terminal deletions of FtsZ that affect its ability to localize in Caulobacter and its interaction with FtsA. Mol Microbiol*, 27***,** 1051-63.

Ditlove, J., Weidmann, P., Bernstein, M. and Massry, S. G. (1977). Methicillin nephritis. Medicine (Baltimore)*, 56***,** 483-91.

Domínguez-Escobar, J., Chastanet, A., Crevenna, A. H., Fromion, V., Wedlich-Söldner, R. and Carballido-López, R. (2011). Processive movement of MreB-associated cell wall biosynthetic complexes in bacteria. Science*, 333***,** 225-228.

Du, S. and Lutkenhaus, J. (2017). Assembly and activation of the *Escherichia coli* divisome. Mol Microbiol*, 105***,** 177-187.

Du, S., Park, K. T. and Lutkenhaus, J. (2015). Oligomerization of FtsZ converts the FtsZ tail motif (conserved carboxy-terminal peptide) into a multivalent ligand with high avidity for partners ZipA and SlmA. Mol Microbiol*, 95***,** 173-88.

Duman, R., Ishikawa, S., Celik, I., Strahl, H., Ogasawara, N., Troc, P., Lowe, J. and Hamoen, L. W. (2013). Structural and genetic analyses reveal the protein SepF as a new membrane anchor for the Z ring. Proc Natl Acad Sci U S A*, 110*, E4601-10.

Edwards, A. M., Massey, R. C. and Clarke, S. R. (2012). Molecular mechanisms of *Staphylococcus aureus* nasopharyngeal colonization. Mol Oral Microbiol*, 27*, 1-10.

Egan, A. J. and Vollmer, W. (2013). The physiology of bacterial cell division. Ann N Y Acad Sci*, 1277*, 8-28.

Elsen, N. L., Lu, J., Parthasarathy, G., Reid, J. C., Sharma, S., Soisson, S. M. and Lumb, K. J. (2012). Mechanism of action of the cell-division inhibitor PC190723: modulation of FtsZ assembly cooperativity. J Am Chem Soc*, 134*, 12342-5.

Emami, K., Guyet, A., Kawai, Y., Devi, J., Wu, L. J., Allenby, N., Daniel, R. A. and Errington, J. (2017). RodA as the missing glycosyltransferase in *Bacillus subtilis* and antibiotic discovery for the peptidoglycan polymerase pathway. Nat Microbiol*, 2*, 16253.

Erickson, H. P. (1997). FtsZ, a tubulin homologue in prokaryote cell division. Trends Cell Biol*, 7*, 362-7.

Erickson, H. P. (2017). How bacterial cell division might cheat turgor pressure - a unified mechanism of septal division in Gram-positive and Gram-negative bacteria. Bioessays*, 39*.

Erickson, H. P., Anderson, D. E. and Osawa, M. (2010). FtsZ in bacterial cytokinesis: cytoskeleton and force generator all in one. Microbiol Mol Biol Rev*, 74*, 504-28.

Erickson, H. P. and Osawa, M. (2017). FtsZ Constriction Force - Curved Protofilaments Bending Membranes. Subcell Biochem*, 84*, 139-160.

Erickson, H. P., Taylor, D. W., Taylor, K. A. and Bramhill, D. (1996). Bacterial cell division protein FtsZ assembles into protofilament sheets and minirings, structural homologs of tubulin polymers. Proc Natl Acad Sci U S A*, 93*, 519-23.

Eriksen, N. H., Espersen, F., Rosdahl, V. T. and Jensen, K. (1995). Carriage of *Staphylococcus aureus* among 104 healthy persons during a 19-month period. Epidemiol Infect*, 115*, 51-60.

Errington, J. and Wu, L. J. (2017). Cell Cycle Machinery in *Bacillus subtilis*. Subcell Biochem*, 84*, 67-101.

Eswara, P. J. and Ramamurthi, K. S. (2017). Bacterial Cell Division: Nonmodels Poised to Take the Spotlight. Annu Rev Microbiol*, 71*, 393-411.

Favini-Stabile, S., Contreras-Martel, C., Thielens, N. and Dessen, A. (2013). MreB and MurG as scaffolds for the cytoplasmic steps of peptidoglycan biosynthesis. Environ Microbiol*, 15*, 3218-28.

Figge, R. M., Divakaruni, A. V. and Gober, J. W. (2004). MreB, the cell shape-determining bacterial actin homologue, co-ordinates cell wall morphogenesis in *Caulobacter crescentus*. Mol Microbiol*, 51*, 1321-32.

Fleurie, A., Lesterlin, C., Manuse, S., Zhao, C., Cluzel, C., Lavergne, J. P., Franz-Wachtel, M., Macek, B., Combet, C., Kuru, E.*, et al.* (2014a). MapZ marks the division sites and positions FtsZ rings in *Streptococcus pneumoniae*. Nature*, 516*, 259-262.

Fleurie, A., Manuse, S., Zhao, C., Campo, N., Cluzel, C., Lavergne, J. P., Freton, C., Combet, C., Guiral, S., Soufi, B.*, et al.* (2014b). Interplay of the serine/threonine-kinase StkP and the paralogs DivIVA and GpsB in pneumococcal cell elongation and division. PLoS Genet*, 10*, e1004275.

Fu, G., Huang, T., Buss, J., Coltharp, C., Hensel, Z. and Xiao, J. (2010). *In vivo* structure of the *E. coli* FtsZ-ring revealed by photoactivated localization microscopy (PALM). PLoS One*, 5*, e12682.

Fujita, J., Maeda, Y., Nagao, C., Tsuchiya, Y., Miyazaki, Y., Hirose, M., Mizohata, E., Matsumoto, Y., Inoue, T., Mizuguchi, K.*, et al.* (2014). Crystal structure of FtsA from *Staphylococcus aureus*. FEBS Lett*, 588*, 1879-85.

Gamba, P., Veening, J. W., Saunders, N. J., Hamoen, L. W. and Daniel, R. A. (2009). Two-step assembly dynamics of the *Bacillus subtilis* divisome. J Bacteriol*, 191*, 4186-94.

Gardner, K. A., Moore, D. A. and Erickson, H. P. (2013). The C-terminal linker of *Escherichia coli* FtsZ functions as an intrinsically disordered peptide. Mol Microbiol*, 89*, 264-75.

Garner, E. C., Bernard, R., Wang, W., Zhuang, X., Rudner, D. Z. and Mitchison, T. (2011). Coupled, circumferential motions of the cell wall synthesis machinery and MreB filaments in *B. subtilis*. Science*, 333*, 222-225.

Geissler, B., Shiomi, D. and Margolin, W. (2007). The *ftsA** gain-of-function allele of *Escherichia coli* and its effects on the stability and dynamics of the Z ring. Microbiology*, 153*, 814-25.

Gerding, M. A., Liu, B., Bendezu, F. O., Hale, C. A., Bernhardt, T. G. and de Boer, P. A. (2009). Self-enhanced accumulation of FtsN at Division Sites and Roles for Other Proteins with a SPOR domain (DamX, DedD, and RlpA) in *Escherichia coli* cell constriction. J Bacteriol*, 191*, 7383-401.

Ghosh, B. and Sain, A. (2008). Origin of contractile force during cell division of bacteria. Phys Rev Lett*, 101*, 178101.

Gilpin, R. W., Young, F. E. and Chatterjee, A. N. (1973). Characterization of a stable L-form of *Bacillus subtilis* 168. J Bacteriol*, 113*, 486-99.

Gitai, Z., Dye, N. A., Reisenauer, A., Wachi, M. and Shapiro, L. (2005). MreB actin-mediated segregation of a specific region of a bacterial chromosome. Cell*, 120*, 329-41.

Gola, S., Munder, T., Casonato, S., Manganelli, R. and Vicente, M. (2015). The essential role of SepF in mycobacterial division. Mol Microbiol*, 97*, 560-76.

Goley, E. D., Yeh, Y. C., Hong, S. H., Fero, M. J., Abeliuk, E., McAdams, H. H. and Shapiro, L. (2011). Assembly of the Caulobacter cell division machine. Mol Microbiol*, 80*, 1680-98.

Goodwin, S. D. and Shedlarski, J. G., Jr. (1975). Purification of cell wall peptidoglycan of the dimorphic bacterium *Caulobacter crescentus*. Arch Biochem Biophys*, 170*, 23-36.

Graves-Woodward, K. and Pratt, R. F. (1998). Reaction of soluble penicillin-binding protein 2a of methicillin-resistant *Staphylococcus aureus* with beta-lactams and acyclic substrates: kinetics in homogeneous solution. Biochem J*, 332 (Pt 3)*, 755-61.

Guberman, J. M., Fay, A., Dworkin, J., Wingreen, N. S. and Gitai, Z. (2008). PSICIC: noise and asymmetry in bacterial division revealed by computational image analysis at sub-pixel resolution. PLoS Comput Biol*, 4*, e1000233.

Gundogdu, M. E., Kawai, Y., Pavlendova, N., Ogasawara, N., Errington, J., Scheffers, D. J. and Hamoen, L. W. (2011). Large ring polymers align FtsZ polymers for normal septum formation. Embo j*, 30*, 617-26.

Gupta, S., Banerjee, S. K., Chatterjee, A., Sharma, A. K., Kundu, M. and Basu, J. (2015). Essential protein SepF of mycobacteria interacts with FtsZ and MurG to regulate cell growth and division. Microbiology*, 161*, 1627-1638.

Haeusser, D. P. and Margolin, W. (2016). Splitsville: structural and functional insights into the dynamic bacterial Z ring. Nat Rev Microbiol*, 14*, 305-19.

Hamoen, L. W., Meile, J. C., de Jong, W., Noirot, P. and Errington, J. (2006). SepF, a novel FtsZ-interacting protein required for a late step in cell division. Mol Microbiol*, 59*, 989-99.

Haney, S. A., Glasfeld, E., Hale, C., Keeney, D., He, Z. and de Boer, P. (2001). Genetic analysis of the *Escherichia coli* FtsZ.ZipA interaction in the yeast two-hybrid system. Characterization of FtsZ residues essential for the interactions with ZipA and with FtsA. J Biol Chem*, 276*, 11980-7.

Hartman, B. J. and Tomasz, A. (1984). Low-affinity penicillin-binding protein associated with beta-lactam resistance in *Staphylococcus aureus*. J Bacteriol*, 158*, 513-6.

Haydon, D. J., Stokes, N. R., Ure, R., Galbraith, G., Bennett, J. M., Brown, D. R., Baker, P. J., Barynin, V. V., Rice, D. W., Sedelnikova, S. E.*, et al.* (2008). An

inhibitor of FtsZ with potent and selective anti-staphylococcal activity. Science*, 321*, 1673-5.

Heidrich, C., Templin, M. F., Ursinus, A., Merdanovic, M., Berger, J., Schwarz, H., de Pedro, M. A. and Holtje, J. V. (2001). Involvement of N-acetylmuramyl-L-alanine amidases in cell separation and antibiotic-induced autolysis of *Escherichia coli*. Mol Microbiol*, 41*, 167-78.

Holden, S. J., Pengo, T., Meibom, K. L., Fernandez Fernandez, C., Collier, J. and Manley, S. (2014). High throughput 3D super-resolution microscopy reveals *Caulobacter crescentus* in vivo Z-ring organization. Proc Natl Acad Sci U S A*, 111*, 4566-71.

Horger, I., Campelo, F., Hernandez-Machado, A. and Tarazona, P. (2010). Constricting force of filamentary protein rings evaluated from experimental results. Phys Rev E Stat Nonlin Soft Matter Phys*, 81*, 031922.

Howell, M. and Brown, P. J. (2016). Building the bacterial cell wall at the pole. Curr Opin Microbiol*, 34*, 53-59.

Huber, J., Donald, R. G., Lee, S. H., Jarantow, L. W., Salvatore, M. J., Meng, X., Painter, R., Onishi, R. H., Occi, J., Dorso, K.*, et al.* (2009). Chemical genetic identification of peptidoglycan inhibitors potentiating carbapenem activity against methicillin-resistant *Staphylococcus aureus*. Chem Biol*, 16*, 837-48.

Huls, P. G., Vischer, N. O. and Woldringh, C. L. (1999). Delayed nucleoid segregation in *Escherichia coli*. Mol Microbiol*, 33*, 959-70.

Hurley, K. A., Santos, T. M., Nepomuceno, G. M., Huynh, V., Shaw, J. T. and Weibel, D. B. (2016). Targeting the Bacterial Division Protein FtsZ. J Med Chem*, 59*, 6975-98.

Hussain, S., Wivagg, C. N., Szwedziak, P., Wong, F., Schaefer, K., Izore, T., Renner, L. D., Holmes, M. J., Sun, Y., Bisson-Filho, A. W.*, et al.* (2018). MreB filaments align along greatest principal membrane curvature to orient cell wall synthesis. Elife*, 7*.

Hutchison, C. A., 3rd, Chuang, R. Y., Noskov, V. N., Assad-Garcia, N., Deerinck, T. J., Ellisman, M. H., Gill, J., Kannan, K., Karas, B. J., Ma, L.*, et al.* (2016). Design and synthesis of a minimal bacterial genome. Science*, 351*, aad6253.

Ikeda, M., Wachi, M., Jung, H. K., Ishino, F. and Matsuhashi, M. (1991). The *Escherichia coli mraY* gene encoding UDP-N-acetylmuramoyl-pentapeptide: undecaprenyl-phosphate phospho-N-acetylmuramoyl-pentapeptide transferase. J Bacteriol*, 173*, 1021-6.

Inoue, A., Murata, Y., Takahashi, H., Tsuji, N., Fujisaki, S. and Kato, J. (2008). Involvement of an essential gene, *mviN*, in murein synthesis in *Escherichia coli*. J Bacteriol*, 190*, 7298-301.

Ishikawa, S., Kawai, Y., Hiramatsu, K., Kuwano, M. and Ogasawara, N. (2006). A new FtsZ-interacting protein, YlmF, complements the activity of FtsA during progression of cell division in *Bacillus subtilis*. Mol Microbiol*, 60***,** 1364-80.

Izore, T. and van den Ent, F. (2017). Bacterial Actins. Subcell Biochem*, 84***,** 245-266.

Jacq, M., Adam, V., Bourgeois, D., Moriscot, C., Di Guilmi, A. M., Vernet, T. and Morlot, C. (2015). Remodeling of the Z-Ring Nanostructure during the *Streptococcus pneumoniae* Cell Cycle Revealed by Photoactivated Localization Microscopy. MBio*, 6*.

Jacquier, N., Viollier, P. H. and Greub, G. (2015). The role of peptidoglycan in chlamydial cell division: towards resolving the chlamydial anomaly. FEMS Microbiol Rev*, 39***,** 262-75.

Jensen, S. O., Thompson, L. S. and Harry, E. J. (2005). Cell division in *Bacillus subtilis*: FtsZ and FtsA association is Z-ring independent, and FtsA is required for efficient midcell Z-Ring assembly. J Bacteriol*, 187***,** 6536-44.

Jevons, M. P., Coe, A. W. and Parker, M. T. (1963). Methicillin resistance in staphylococci. Lancet*, 1***,** 904-7.

Jones, L. J., Carballido-Lopez, R. and Errington, J. (2001). Control of cell shape in bacteria: helical, actin-like filaments in *Bacillus subtilis*. Cell*, 104***,** 913-22.

Jorge, A. M., Hoiczyk, E., Gomes, J. P. and Pinho, M. G. (2011). EzrA contributes to the regulation of cell size in *Staphylococcus aureus*. PLoS One*, 6***,** e27542.

Kawazura, T., Matsumoto, K., Kojima, K., Kato, F., Kanai, T., Niki, H. and Shiomi, D. (2017). Exclusion of assembled MreB by anionic phospholipids at cell poles confers cell polarity for bidirectional growth. Mol Microbiol*, 104***,** 472-486.

Kieser, K. J. and Rubin, E. J. (2014). How sisters grow apart: mycobacterial growth and division. Nat Rev Microbiol*, 12***,** 550-62.

Kluytmans, J. A. and Wertheim, H. F. (2005). Nasal carriage of *Staphylococcus aureus* and prevention of nosocomial infections. Infection*, 33***,** 3-8.

Kopp, U., Roos, M., Wecke, J. and Labischinski, H. (1996). Staphylococcal peptidoglycan interpeptide bridge biosynthesis: a novel antistaphylococcal target? Microb Drug Resist*, 2***,** 29-41.

Krol, E., van Kessel, S. P., van Bezouwen, L. S., Kumar, N., Boekema, E. J. and Scheffers, D. J. (2012). *Bacillus subtilis* SepF binds to the C-terminus of FtsZ. PLoS One*, 7***,** e43293.

Krupka, M., Rowlett, V. W., Morado, D., Vitrac, H., Schoenemann, K., Liu, J. and Margolin, W. (2017). *Escherichia coli* FtsA forms lipid-bound minirings

that antagonize lateral interactions between FtsZ protofilaments. Nat Commun*, 8*, 15957.

Kruse, T., Bork-Jensen, J. and Gerdes, K. (2005). The morphogenetic MreBCD proteins of *Escherichia coli* form an essential membrane-bound complex. Mol. Microbiol*., 55*, 78-89.

Kuru, E., Hughes, H. V., Brown, P. J., Hall, E., Tekkam, S., Cava, F., de Pedro, M. A., Brun, Y. V. and VanNieuwenhze, M. S. (2012). In Situ probing of newly synthesized peptidoglycan in live bacteria with fluorescent D-amino acids. Angew Chem Int Ed Engl*, 51*, 12519-23.

Lan, G., Daniels, B. R., Dobrowsky, T. M., Wirtz, D. and Sun, S. X. (2009). Condensation of FtsZ filaments can drive bacterial cell division. Proc Natl Acad Sci U S A*, 106*, 121-6.

Land, A. D., Tsui, H. C., Kocaoglu, O., Vella, S. A., Shaw, S. L., Keen, S. K., Sham, L. T., Carlson, E. E. and Winkler, M. E. (2013). Requirement of essential Pbp2x and GpsB for septal ring closure in *Streptococcus pneumoniae* D39. Mol Microbiol*, 90*, 939-55.

Land, A. D. and Winkler, M. E. (2011). The requirement for pneumococcal MreC and MreD is relieved by inactivation of the gene encoding PBP1a. J Bacteriol*, 193*, 4166-79.

Leaver, M., Dominguez-Cuevas, P., Coxhead, J. M., Daniel, R. A. and Errington, J. (2009). Life without a wall or division machine in *Bacillus subtilis*. Nature*, 457*, 849-53.

Lee, K. C., Webb, R. I. and Fuerst, J. A. (2009). The cell cycle of the planctomycete *Gemmata obscuriglobus* with respect to cell compartmentalization. BMC Cell Biol*, 10*, 4.

Letek, M., Fiuza, M., Ordonez, E., Villadangos, A. F., Ramos, A., Mateos, L. M. and Gil, J. A. (2008). Cell growth and cell division in the rod-shaped actinomycete *Corynebacterium glutamicum*. Antonie Van Leeuwenhoek*, 94*, 99-109.

Levin, P. A., Kurtser, I. G. and Grossman, A. D. (1999). Identification and characterization of a negative regulator of FtsZ ring formation in *Bacillus subtilis*. Proc Natl Acad Sci U S A*, 96*, 9642-7.

Li, G. W., Burkhardt, D., Gross, C. and Weissman, J. S. (2014). Quantifying absolute protein synthesis rates reveals principles underlying allocation of cellular resources. Cell*, 157*, 624-35.

Li, K., Yuan, X. X., Sun, H. M., Zhao, L. S., Tang, R., Chen, Z. H., Qin, Q. L., Chen, X. L., Zhang, Y. Z. and Su, H. N. (2018). Atomic Force Microscopy of Side Wall and Septa Peptidoglycan From *Bacillus subtilis* Reveals an Architectural Remodeling During Growth. Front Microbiol*, 9*, 620.

Li, Y., Hsin, J., Zhao, L., Cheng, Y., Shang, W., Huang, K. C., Wang, H. W. and Ye, S. (2013). FtsZ protofilaments use a hinge-opening mechanism for constrictive force generation. Science*, 341*, 392-5.

Li, Z., Trimble, M. J., Brun, Y. V. and Jensen, G. J. (2007). The structure of FtsZ filaments in vivo suggests a force-generating role in cell division. EMBO J*, 26*, 4694-4708.

Liechti, G., Kuru, E., Packiam, M., Hsu, Y. P., Tekkam, S., Hall, E., Rittichier, J. T., VanNieuwenhze, M., Brun, Y. V. and Maurelli, A. T. (2016). Pathogenic Chlamydia Lack a Classical Sacculus but Synthesize a Narrow, Mid-cell Peptidoglycan Ring, Regulated by MreB, for Cell Division. PLoS Pathog*, 12*, e1005590.

Liem, R. K. (2016). Cytoskeletal Integrators: The Spectrin Superfamily. Cold Spring Harb Perspect Biol*, 8*.

Liu, B., Persons, L., Lee, L. and de Boer, P. A. (2015). Roles for both FtsA and the FtsBLQ subcomplex in FtsN-stimulated cell constriction in *Escherichia coli*. Mol Microbiol*, 95*, 945-70.

Loose, M. and Mitchison, T. J. (2014). The bacterial cell division proteins FtsA and FtsZ self-organize into dynamic cytoskeletal patterns. Nat Cell Biol*, 16*, 38-46.

Lovering, A. L., Safadi, S. S. and Strynadka, N. C. (2012). Structural perspective of peptidoglycan biosynthesis and assembly. Annu Rev Biochem*, 81*, 451-78.

Lowe, J. and Amos, L. A. (1998). Crystal structure of the bacterial cell-division protein FtsZ. Nature*, 391*, 203-6.

Lu, C., Reedy, M. and Erickson, H. P. (2000). Straight and curved conformations of FtsZ are regulated by GTP hydrolysis. J Bacteriol*, 182*, 164-70.

Lu, W. P., Sun, Y., Bauer, M. D., Paule, S., Koenigs, P. M. and Kraft, W. G. (1999). Penicillin-binding protein 2a from methicillin-resistant *Staphylococcus aureus*: kinetic characterization of its interactions with beta-lactams using electrospray mass spectrometry. Biochemistry*, 38*, 6537-46.

Lutkenhaus, J. and Du, S. (2017). *E. coli* Cell Cycle Machinery. Subcell Biochem*, 84*, 27-65.

Lutkenhaus, J., Pichoff, S. and Du, S. (2012). Bacterial cytokinesis: From Z ring to divisome. Cytoskeleton (Hoboken)*, 69*, 778-90.

Lutkenhaus, J. F. and Donachie, W. D. (1979). Identification of the *ftsA* gene product. J Bacteriol*, 137*, 1088-94.

Lutkenhaus, J. F., Wolf-Watz, H. and Donachie, W. D. (1980). Organization of genes in the *ftsA-envA* region of the *Escherichia coli* genetic map and identification of a new *fts* locus (*ftsZ*). J Bacteriol*, 142*, 615-20.

Ma, X., Ehrhardt, D. W. and Margolin, W. (1996). Colocalization of cell division proteins FtsZ and FtsA to cytoskeletal structures in living *Escherichia coli* cells by using green fluorescent protein. Proc Natl Acad Sci U S A*, 93***,** 12998-3003.

Ma, X. and Margolin, W. (1999). Genetic and functional analyses of the conserved C-terminal core domain of *Escherichia coli* FtsZ. J Bacteriol*, 181***,** 7531-44.

Mannik, J., Wu, F., Hol, F. J., Bisicchia, P., Sherratt, D. J., Keymer, J. E. and Dekker, C. (2012). Robustness and accuracy of cell division in *Escherichia coli* in diverse cell shapes. Proc Natl Acad Sci U S A*, 109***,** 6957-62.

Matsui, T., Yamane, J., Mogi, N., Yamaguchi, H., Takemoto, H., Yao, M. and Tanaka, I. (2012). Structural reorganization of the bacterial cell-division protein FtsZ from *Staphylococcus aureus*. Acta Crystallogr. D. Biol. Crystallogr.*, 68***,** 1175-88.

McCormick, J. R., Su, E. P., Driks, A. and Losick, R. (1994). Growth and viability of *Streptomyces coelicolor* mutant for the cell division gene *ftsZ*. Mol Microbiol*, 14***,** 243-54.

McEvoy, G. K. (1995). American Hospital Formulary Service - Drug Information 95. American Society of Hospital Pharmacists, Inc.*, , (Plus Supplements 1995)***,** 268.

Meeske, A. J., Riley, E. P., Robins, W. P., Uehara, T., Mekalanos, J. J., Kahne, D., Walker, S., Kruse, A. C., Bernhardt, T. G. and Rudner, D. Z. (2016). SEDS proteins are a widespread family of bacterial cell wall polymerases. Nature**,** 634–638.

Meier, E. L. and Goley, E. D. (2014). Form and function of the bacterial cytokinetic ring. Curr Opin Cell Biol*, 26***,** 19-27.

Mengin-Lecreulx, D., Texier, L., Rousseau, M. and van Heijenoort, J. (1991). The *murG* gene of *Escherichia coli* codes for the UDP-N-acetylglucosamine: N-acetylmuramyl-(pentapeptide) pyrophosphoryl-undecaprenol N-acetylglucosamine transferase involved in the membrane steps of peptidoglycan synthesis. J Bacteriol*, 173***,** 4625-36.

Mercier, R., Kawai, Y. and Errington, J. (2013). Excess membrane synthesis drives a primitive mode of cell proliferation. Cell*, 152***,** 997-1007.

Mercier, R., Kawai, Y. and Errington, J. (2014). General principles for the formation and proliferation of a wall-free (L-form) state in bacteria. Elife*, 3*.

Mercier, R., Kawai, Y. and Errington, J. (2016). Wall proficient E. coli capable of sustained growth in the absence of the Z-ring division machine. Nat Microbiol*, 1***,** 16091.

Mitchell, P. and Moyle, J. (1956). Osmotic structure and function in bacteria. Bacterial Anatomy*, 6th Symposium of the Society for General Microbiology, Cambridge University Press*.

Modell, J. W., Kambara, T. K., Perchuk, B. S. and Laub, M. T. (2014). A DNA damage-induced, SOS-independent checkpoint regulates cell division in *Caulobacter crescentus*. PLoS Biol*, 12***,** e1001977.

Mohammadi, T., Sijbrandi, R., Lutters, M., Verheul, J., Martin, N. I., den Blaauwen, T., de Kruijff, B. and Breukink, E. (2014). Specificity of the transport of lipid II by FtsW in *Escherichia coli*. J Biol Chem*, 289***,** 14707-18.

Mohammadi, T., van Dam, V., Sijbrandi, R., Vernet, T., Zapun, A., Bouhss, A., Diepeveen-de Bruin, M., Nguyen-Distèche, M., de Kruijff, B. and Breukink, E. (2011). Identification of FtsW as a transporter of lipid-linked cell wall precursors across the membrane. EMBO J*, 30***,** 1425-32.

Moll, A. and Thanbichler, M. (2009). FtsN-like proteins are conserved components of the cell division machinery in proteobacteria. Mol Microbiol*, 72***,** 1037-53.

Monteiro, J. M., Fernandes, P. B., Vaz, F., Pereira, A. R., Tavares, A. C., Ferreira, M. T., Pereira, P. M., Veiga, H., Kuru, E., VanNieuwenhze, M. S*., et al.* (2015). Cell shape dynamics during the staphylococcal cell cycle. Nat Commun*, 6***,** 8055.

Monteiro, J. M., Pereira, A. R., Reichmann, N. T., Saraiva, B. M., Fernandes, P. B., Veiga, H., Tavares, A. C., Santos, M., Ferreira, M. T., Macario, V*., et al.* (2018). Peptidoglycan synthesis drives an FtsZ-treadmilling-independent step of cytokinesis. Nature*, 554***,** 528-532.

Morgenstein, R. M., Bratton, B. P., Nguyen, J. P., Ouzounov, N., Shaevitz, J. W. and Gitai, Z. (2015). RodZ links MreB to cell wall synthesis to mediate MreB rotation and robust morphogenesis. Proc Natl Acad Sci U S A*, 112***,** 12510-5.

Mukherjee, A., Dai, K. and Lutkenhaus, J. (1993). *Escherichia coli* cell division protein FtsZ is a guanine nucleotide binding protein. Proc Natl Acad Sci U S A*, 90***,** 1053-7.

Mukhopadhyay, R., Huang, K. C. and Wingreen, N. S. (2008). Lipid localization in bacterial cells through curvature-mediated microphase separation. Biophys J*, 95***,** 1034-49.

Nelson, D. E. and Young, K. D. (2000). Penicillin binding protein 5 affects cell diameter, contour, and morphology of *Escherichia coli*. J Bacteriol*, 182***,** 1714-21.

Nogales, E., Downing, K. H., Amos, L. A. and Lowe, J. (1998). Tubulin and FtsZ form a distinct family of GTPases. Nat Struct Biol*, 5***,** 451-8.

Oliva, M. A., Cordell, S. C. and Lowe, J. (2004). Structural insights into FtsZ protofilament formation. Nat Struct Mol Biol*, 11*, 1243-50.

Ortiz, C., Natale, P., Cueto, L. and Vicente, M. (2016). The keepers of the ring: regulators of FtsZ assembly. FEMS Microbiol Rev*, 40*, 57-67.

Osawa, M., Anderson, D. E. and Erickson, H. P. (2008). Reconstitution of contractile FtsZ rings in liposomes. Science*, 320*, 792-4.

Osawa, M., Anderson, D. E. and Erickson, H. P. (2009). Curved FtsZ protofilaments generate bending forces on liposome membranes. Embo j*, 28*, 3476-84.

Osawa, M. and Erickson, H. P. (2011). Inside-out Z rings--constriction with and without GTP hydrolysis. Mol Microbiol*, 81*, 571-9.

Osawa, M. and Erickson, H. P. (2013). Liposome division by a simple bacterial division machinery. Proc Natl Acad Sci U S A*, 110*, 11000-4.

Osawa, M. and Erickson, H. P. (2018). Turgor Pressure and Possible Constriction Mechanisms in Bacterial Division. Front Microbiol*, 9*, 111.

Otto, M. (2010). Staphylococcus colonization of the skin and antimicrobial peptides. Expert Rev Dermatol*, 5*, 183-195.

Ouzounov, N., Nguyen, J. P., Bratton, B. P., Jacobowitz, D., Gitai, Z. and Shaevitz, J. W. (2016). MreB Orientation Correlates with Cell Diameter in *Escherichia coli*. Biophys J*, 111*, 1035-43.

Pastoret, S., Fraipont, C., den Blaauwen, T., Wolf, B., Aarsman, M. E., Piette, A., Thomas, A., Brasseur, R. and Nguyen-Disteche, M. (2004). Functional analysis of the cell division protein FtsW of *Escherichia coli*. J Bacteriol*, 186*, 8370-9.

Perez-Nunez, D., Briandet, R., David, B., Gautier, C., Renault, P., Hallet, B., Hols, P., Carballido-Lopez, R. and Guedon, E. (2011). A new morphogenesis pathway in bacteria: unbalanced activity of cell wall synthesis machineries leads to coccus-to-rod transition and filamentation in ovococci. Mol. Microbiol.*, 79*, 759-71.

Pichoff, S. and Lutkenhaus, J. (2005). Tethering the Z ring to the membrane through a conserved membrane targeting sequence in FtsA. Mol Microbiol*, 55*, 1722-34.

Pinho, M. G., de Lencastre, H. and Tomasz, A. (2001). An acquired and a native penicillin-binding protein cooperate in building the cell wall of drug-resistant staphylococci. Proc Natl Acad Sci U S A*, 98*, 10886-91.

Pinho, M. G. and Errington, J. (2003). Dispersed mode of *Staphylococcus aureus* cell wall synthesis in the absence of the division machinery. Mol. Microbiol.*, 50*, 871-81.

Pinho, M. G. and Errington, J. (2005). Recruitment of penicillin-binding protein PBP2 to the division site of *Staphylococcus aureus* is dependent on its transpeptidation substrates. Mol. Microbiol.*, 55*, 799-807.

Pinho, M. G., Kjos, M. and Veening, J.-W. (2013). How to get (a)round: mechanisms controlling growth and division of coccoid bacteria. Nat. Rev. Microbiol*., 11*, 601-614.

Pogliano, J., Pogliano, K., Weiss, D. S., Losick, R. and Beckwith, J. (1997). Inactivation of FtsI inhibits constriction of the FtsZ cytokinetic ring and delays the assembly of FtsZ rings at potential division sites. Proc Natl Acad Sci U S A*, 94*, 559-64.

Popp, D., Iwasa, M., Narita, A., Erickson, H. P. and Maeda, Y. (2009). FtsZ condensates: an in vitro electron microscopy study. Biopolymers*, 91*, 340-50.

Potluri, L. P., Kannan, S. and Young, K. D. (2012). ZipA is required for FtsZ-dependent preseptal peptidoglycan synthesis prior to invagination during cell division. J Bacteriol*, 194*, 5334-42.

Proctor, S. A., Minc, N., Boudaoud, A. and Chang, F. (2012). Contributions of turgor pressure, the contractile ring, and septum assembly to forces in cytokinesis in fission yeast. Curr Biol*, 22*, 1601-8.

Renner, L. D. and Weibel, D. B. (2011). Cardiolipin microdomains localize to negatively curved regions of *Escherichia coli* membranes. Proc Natl Acad Sci U S A*, 108*, 6264-9.

Reshes, G., Vanounou, S., Fishov, I. and Feingold, M. (2008). Cell shape dynamics in *Escherichia coli*. Biophys J*, 94*, 251-64.

Reynolds, P. E. and Brown, D. F. (1985). Penicillin-binding proteins of beta-lactam-resistant strains of *Staphylococcus aureus*. Effect of growth conditions. FEBS Lett*, 192*, 28-32.

Rico, A. I., Krupka, M. and Vicente, M. (2013). In the beginning, *Escherichia coli* assembled the proto-ring: an initial phase of division. J Biol Chem*, 288*, 20830-6.

Rodrigues, C. D. and Harry, E. J. (2012). The Min system and nucleoid occlusion are not required for identifying the division site in *Bacillus subtilis* but ensure its efficient utilization. PLoS Genet*, 8*, e1002561.

Romaniuk, J. A. and Cegelski, L. (2015). Bacterial cell wall composition and the influence of antibiotics by cell-wall and whole-cell NMR. Philos Trans R Soc Lond B Biol Sci*, 370*.

Rowlett, V. W. and Margolin, W. (2013). The bacterial Min system. Curr Biol*, 23*, R553-6.

Rowlett, V. W. and Margolin, W. (2014). 3D-SIM super-resolution of FtsZ and its membrane tethers in *Escherichia coli* cells. Biophys J*, 107*, L17-20.

Ruiz, N. (2008). Bioinformatics identification of MurJ (MviN) as the peptidoglycan lipid II flippase in *Escherichia coli*. Proc Natl Acad Sci U S A*, 105*, 15553-7.

Salje, J., van den Ent, F., de Boer, P. and Lowe, J. (2011). Direct membrane binding by bacterial actin MreB. Mol Cell*, 43***,** 478-87.

Santos-Beneit, F., Roberts, D. M., Cantlay, S., McCormick, J. R. and Errington, J. (2017). A mechanism for FtsZ-independent proliferation in Streptomyces. Nat Commun*, 8***,** 1378.

Sassine, J., Xu, M., Sidiq, K. R., Emmins, R., Errington, J. and Daniel, R. A. (2017). Functional redundancy of division specific penicillin-binding proteins in *Bacillus subtilis*. Mol Microbiol*, 106***,** 304-318.

Sauvage, E., Kerff, F., Terrak, M., Ayala, J. A. and Charlier, P. (2008). The penicillin-binding proteins: structure and role in peptidoglycan biosynthesis. FEMS Microbiol Rev*, 32***,** 234-58.

Scheffers, D. J., de Wit, J. G., den Blaauwen, T. and Driessen, A. J. (2002). GTP hydrolysis of cell division protein FtsZ: evidence that the active site is formed by the association of monomers. Biochemistry*, 41***,** 521-9.

Scheffers, D. J. and Pinho, M. G. (2005). Bacterial cell wall synthesis: new insights from localization studies. Microbiol Mol Biol Rev*, 69***,** 585-607.

Schoenemann, K. M. and Margolin, W. (2017). Bacterial Division: FtsZ Treadmills to Build a Beautiful Wall. Curr Biol*, 27***,** R301-r303.

Schwarz, U., Asmus, A. and Frank, H. (1969). Autolytic enzymes and cell division of *Escherichia coli*. J Mol Biol*, 41***,** 419-29.

Sham, L. T., Butler, E. K., Lebar, M. D., Kahne, D., Bernhardt, T. G. and Ruiz, N. (2014). Bacterial cell wall. MurJ is the flippase of lipid-linked precursors for peptidoglycan biogenesis. Science*, 345***,** 220-2.

Shiomi, D., Sakai, M. and Niki, H. (2008). Determination of bacterial rod shape by a novel cytoskeletal membrane protein. Embo j*, 27***,** 3081-91.

Sieger, B., Schubert, K., Donovan, C. and Bramkamp, M. (2013). The lipid II flippase RodA determines morphology and growth in *Corynebacterium glutamicum*. Mol Microbiol*, 90***,** 966-82.

Soderstrom, B., Skoog, K., Blom, H., Weiss, D. S., von Heijne, G. and Daley, D. O. (2014). Disassembly of the divisome in *Escherichia coli*: evidence that FtsZ dissociates before compartmentalization. Mol Microbiol*, 92***,** 1-9.

Son, S. H. and Lee, H. H. (2013). The N-terminal domain of EzrA binds to the C terminus of FtsZ to inhibit *Staphylococcus aureus* FtsZ polymerization. Biochem Biophys Res Commun*, 433***,** 108-14.

Spratt, B. G. (1975). Distinct penicillin binding proteins involved in the division, elongation, and shape of *Escherichia coli* K12. Proc Natl Acad Sci U S A*, 72***,** 2999-3003.

Spratt, B. G. (1977). Properties of the penicillin-binding proteins of *Escherichia coli* K12. Eur J Biochem*, 72***,** 341-52.

Stefani, S., Chung, D. R., Lindsay, J. A., Friedrich, A. W., Kearns, A. M., Westh, H. and Mackenzie, F. M. (2012). Meticillin-resistant *Staphylococcus aureus* (MRSA): global epidemiology and harmonisation of typing methods. Int J Antimicrob Agents*, 39*, 273-82.

Strauss, M. P., Liew, A. T., Turnbull, L., Whitchurch, C. B., Monahan, L. G. and Harry, E. J. (2012). 3D-SIM super resolution microscopy reveals a bead-like arrangement for FtsZ and the division machinery: implications for triggering cytokinesis. PLoS Biol*, 10*, e1001389.

Stricker, J., Maddox, P., Salmon, E. D. and Erickson, H. P. (2002). Rapid assembly dynamics of the *Escherichia coli* FtsZ-ring demonstrated by fluorescence recovery after photobleaching. Proc Natl Acad Sci U S A*, 99*, 3171-5.

Sundararajan, K. and Goley, E. D. (2017). The intrinsically disordered C-terminal linker of FtsZ regulates protofilament dynamics and superstructure in vitro. J Biol Chem*, 292*, 20509-20527.

Szwedziak, P., Wang, Q., Bharat, T. A., Tsim, M. and Lowe, J. (2014). Architecture of the ring formed by the tubulin homologue FtsZ in bacterial cell division. Elife*, 3*, e04601.

Tan, C. M., Therien, A. G., Lu, J., Lee, S. H., Caron, A., Gill, C. J., Lebeau-Jacob, C., Benton-Perdomo, L., Monteiro, J. M., Pereira, P. M., *et al.* (2012). Restoring methicillin-resistant *Staphylococcus aureus* susceptibility to beta-lactam antibiotics. Sci. Transl. Med*., 4*, 126-135.

Teeffelen, S. v., Wang, S., Furchtgott, L., Huang, K. C., Wingreen, N. S., Shaevitz, J. W. and Gitai, Z. (2011). The bacterial actin MreB rotates and rotation depends on cell-wall assembly. Proc. Natl. Acad. Sci. U S A*, 108*, 15822-7.

Thanbichler, M. and Shapiro, L. (2006). MipZ, a spatial regulator coordinating chromosome segregation with cell division in Caulobacter. Cell*, 126*, 147-62.

Tilney, L. G., Bryan, J., Bush, D. J., Fujiwara, K., Mooseker, M. S., Murphy, D. B. and Snyder, D. H. (1973). Microtubules: evidence for 13 protofilaments. J Cell Biol*, 59*, 267-75.

Tong, S. Y., Davis, J. S., Eichenberger, E., Holland, T. L. and Fowler, V. G., Jr. (2015). *Staphylococcus aureus* infections: epidemiology, pathophysiology, clinical manifestations, and management. Clin Microbiol Rev*, 28*, 603-61.

Treuner-Lange, A., Aguiluz, K., van der Does, C., Gomez-Santos, N., Harms, A., Schumacher, D., Lenz, P., Hoppert, M., Kahnt, J., Munoz-Dorado, J*., et al.* (2013). PomZ, a ParA-like protein, regulates Z-ring formation and cell division in *Myxococcus xanthus*. Mol Microbiol*, 87*, 235-53.

Tsang, M. J. and Bernhardt, T. G. (2015). A role for the FtsQLB complex in cytokinetic ring activation revealed by an *ftsL* allele that accelerates division. Mol Microbiol*, 95*, 925-44.

Tzagoloff, H. and Novick, R. (1977). Geometry of cell division in *Staphylococcus aureus*. J Bacteriol*, 129*, 343-50.

Uehara, T. and Bernhardt, T. G. (2011). More than just lysins: peptidoglycan hydrolases tailor the cell wall. Curr Opin Microbiol*, 14*, 698-703.

Unger, E., Bohm, K. J. and Vater, W. (1990). Structural diversity and dynamics of microtubules and polymorphic tubulin assemblies. Electron Microsc Rev*, 3*, 355-95.

van Dam, V., Sijbrandi, R., Kol, M., Swiezewska, E., de Kruijff, B. and Breukink, E. (2007). Transmembrane transport of peptidoglycan precursors across model and bacterial membranes. Mol Microbiol*, 64*, 1105-14.

van De Putte, P., van, D. and Roersch, A. (1964). The selection of mutants of *Escherichia coli* with impaired cell division at elevated temperature. Mutat Res*, 106*, 121-8.

van den Ent, F., Amos, L. A. and Lowe, J. (2001). Prokaryotic origin of the actin cytoskeleton. Nature*, 413*, 39-44.

van den Ent, F., Izore, T., Bharat, T. A., Johnson, C. M. and Lowe, J. (2014). Bacterial actin MreB forms antiparallel double filaments. Elife*, 3*, e02634.

van Heijenoort, J. (1998). Assembly of the monomer unit of bacterial peptidoglycan. Cell Mol Life Sci*, 54*, 300-4.

Varma, A., de Pedro, M. A. and Young, K. D. (2007). FtsZ directs a second mode of peptidoglycan synthesis in *Escherichia coli*. J Bacteriol*, 189*, 5692-704.

Varma, A. and Young, K. D. (2009). In *Escherichia coli*, MreB and FtsZ direct the synthesis of lateral cell wall via independent pathways that require PBP 2. J Bacteriol*, 191*, 3526-33.

Vaughan, S., Wickstead, B., Gull, K. and Addinall, S. G. (2004). Molecular evolution of FtsZ protein sequences encoded within the genomes of archaea, bacteria, and eukaryota. J Mol Evol*, 58*, 19-29.

Vedyaykin, A. D., Vishnyakov, I. E., Polinovskaya, V. S., Khodorkovskii, M. A. and Sabantsev, A. V. (2016). New insights into FtsZ rearrangements during the cell division of *Escherichia coli* from single-molecule localization microscopy of fixed cells. Microbiologyopen*, 5*, 378-86.

Veiga, H., Jorge, A. M. and Pinho, M. G. (2011). Absence of nucleoid occlusion effector Noc impairs formation of orthogonal FtsZ rings during *Staphylococcus aureus* cell division. Mol. Microbiol.*, 80*, 1366-80.

Vollmer, W., Blanot, D. and de Pedro, M. A. (2008). Peptidoglycan structure and architecture. FEMS Microbiol Rev*, 32*, 149-67.

Wagstaff, J. M., Tsim, M., Oliva, M. A., Garcia-Sanchez, A., Kureisaite-Ciziene, D., Andreu, J. M. and Lowe, J. (2017). A Polymerization-Associated Structural Switch in FtsZ That Enables Treadmilling of Model Filaments. MBio*, 8*.

Wang, L., Khattar, M. K., Donachie, W. D. and Lutkenhaus, J. (1998). FtsI and FtsW are localized to the septum in *Escherichia coli*. J Bacteriol*, 180***,** 2810-6.

Wang, Q. M., Peery, R. B., Johnson, R. B., Alborn, W. E., Yeh, W. K. and Skatrud, P. L. (2001). Identification and characterization of a monofunctional glycosyltransferase from *Staphylococcus aureus*. J Bacteriol*, 183***,** 4779-85.

Weiss, D. S., Pogliano, K., Carson, M., Guzman, L. M., Fraipont, C., Nguyen-Disteche, M., Losick, R. and Beckwith, J. (1997). Localization of the *Escherichia coli* cell division protein Ftsl (PBP3) to the division site and cell pole. Mol Microbiol*, 25***,** 671-81.

Whatmore, A. M. and Reed, R. H. (1990). Determination of turgor pressure in *Bacillus subtilis*: a possible role for K+ in turgor regulation. J Gen Microbiol*, 136***,** 2521-6.

Worthington, R. J. and Melander, C. (2013). Overcoming resistance to beta-lactam antibiotics. J Org Chem*, 78***,** 4207-13.

Wu, L. J. and Errington, J. (2004). Coordination of cell division and chromosome segregation by a nucleoid occlusion protein in *Bacillus subtilis*. Cell*, 117***,** 915-25.

Xiao, J. and Goley, E. D. (2016). Redefining the roles of the FtsZ-ring in bacterial cytokinesis. Curr Opin Microbiol*, 34***,** 90-96.

Yahashiri, A., Jorgenson, M. A. and Weiss, D. S. (2015). Bacterial SPOR domains are recruited to septal peptidoglycan by binding to glycan strands that lack stem peptides. Proc Natl Acad Sci U S A*, 112***,** 11347-52.

Yan, K., Pearce, K. H. and Payne, D. J. (2000). A conserved residue at the extreme C-terminus of FtsZ is critical for the FtsA-FtsZ interaction in *Staphylococcus aureus*. Biochem Biophys Res Commun*, 270***,** 387-92.

Yang, X., Lyu, Z., Miguel, A., McQuillen, R., Huang, K. C. and Xiao, J. (2017). GTPase activity-coupled treadmilling of the bacterial tubulin FtsZ organizes septal cell wall synthesis. Science*, 355***,** 744-747.

Yao, Q., Jewett, A. I., Chang, Y. W., Oikonomou, C. M., Beeby, M., Iancu, C. V., Briegel, A., Ghosal, D. and Jensen, G. J. (2017). Short FtsZ filaments can drive asymmetric cell envelope constriction at the onset of bacterial cytokinesis. Embo j*, 36***,** 1577-1589.

Young, K. D. (2001). Approaching the physiological functions of penicillin-binding proteins in *Escherichia coli*. Biochimie*, 83***,** 99-102.

Young, K. D. (2006). The selective value of bacterial shape. Microbiol. Mol. Biol. Rev*., 70*, 660-703.

Young, K. D. (2007). Bacterial morphology: why have different shapes? Curr Opin Microbiol*, 10*, 596-600.

Zapun, A., Contreras-Martel, C. and Vernet, T. (2008a). Penicillin-binding proteins and beta-lactam resistance. FEMS Microbiol Rev*, 32*, 361-85.

Zapun, A., Vernet, T. and Pinho, M. G. (2008b). The different shapes of cocci. FEMS Microbiol Rev*, 32*, 345-60.

Zhou, X., Halladin, D. K., Rojas, E. R., Koslover, E. F., Lee, T. K., Huang, K. C. and Theriot, J. A. (2015). Bacterial division. Mechanical crack propagation drives millisecond daughter cell separation in *Staphylococcus aureus*. Science*, 348*, 574-8.

Zhou, X., Halladin, D. K. and Theriot, J. A. (2016). Fast Mechanically Driven Daughter Cell Separation Is Widespread in Actinobacteria. MBio*, 7*.

CHAPTER II

FtsZ-dependent elongation of a coccoid bacterium

Chapter II Summary

ABSTRACT....87
INTRODUCTION....88
EXPERIMENTAL PROCEDURES....91
Bacterial strains and growth conditions....91
Super-resolution structured illumination microscopy (SIM)....93
Preparation of *S. aureus* cells for transmission electron microscopy (TEM) .94
Preparation of *S. aureus* cells for scanning electron microscopy (SEM)....95
Measurements of cellular aspect ratios....95
Western blot analysis....96
Construction of *Bacillus subtilis ftsZ* mutants....97
Lethality analysis of the FtsZ^{G193D} mutation in *B. subtilis*....98
Localization of FtsZ^{G193D}-GFP in *B. subtilis*....98
Molecular dynamics simulations....98
Protein purification....99
Transmission electron microscopy (TEM) of FtsZ polymers....100
GTP hydrolysis assays....101
Construction of *S. aureus* mutants....101
Epifluorescence Microscopy....103
EzrA-mCherry localization by SIM....103
Immunofluorescence microscopy....104
3D reconstructions using super resolution structured illumination microscopy....105
Cell wall staining with FDDAs....105
SIM time-lapse imaging....106
RESULTS....107
FtsZ^{G193D} mutation leads to elongated cells in *S. aureus*....107
The G193D mutation leads to shorter, twisted FtsZ polymers....112
Z-rings are misplaced in *S. aureus* FtsZ^{G193D} mutant cells....116
FtsZ^{G193D} structures recruit PG synthesis enzymes....119

FtsZ^{G193D} leads to a new mode of cell division for *S. aureus* 123
DISCUSSION 125
REFERENCES 127

Pereira AR contribution:

Pereira, A.R., performed all experiments, except *S. aureus* TEM and SEM preparation and acquisition (TEM performed by Hoiczyk, E., and SEM performed by Tavares A.C.,), MD simulations (performed by Hsin, J., Ng, N., and Huang, K.C.,) and *B. subtilis* strain construction and lethality assessment (performed by Flores, P., from Carballido-Lopez, R., laboratory).

Acknowledgements:

We thank E. Harry (University of Technology, Sydney) for the generous gift of the anti-FtsZ antibody.

Data contained in this chapter was published in:

Pereira AR, Hsin J, Krol E, Tavares AC, Flores P, Hoiczyk E, Ng N, Dajkovic A, Brun YV, VanNieuwenhze MS, Roemer T, Carballido-Lopez R, Scheffers DJ, Huang KC, Pinho MG. 2016. "FtsZ-Dependent Elongation of a Coccoid Bacterium." MBio 7.

ABSTRACT

A mechanistic understanding of the determination and maintenance of the simplest bacterial cell shape, a sphere, remains elusive compared with that of more complex shapes. Cocci seem to lack a dedicated elongation machinery, and a spherical shape has been considered an evolutionary dead-end morphology, as a transition from a spherical to a rod-like shape has never been observed in bacteria.

Here we show that a *Staphylococcus aureus* mutant (M5) expressing the *ftsZG193D* allele exhibits elongated cells. Molecular dynamics simulations and *in vitro* studies indicate that FtsZG193D filaments are more twisted and shorter than wild-type filaments. *In vivo*, M5 cell wall deposition is initiated asymmetrically, only on one side of the cell, and progresses into a helical pattern rather than into a constricting ring as in wild-type cells. This helical pattern of wall insertion leads to elongation, as in rod-shaped cells. Thus, structural flexibility of FtsZ filaments can result in an FtsZ-dependent mechanism for generating elongated cells from cocci.

INTRODUCTION

Cell morphology is a distinctive characteristic of bacterial species and has been used extensively for their classification (Young, 2006). In most bacteria, cell shape is maintained by the peptidoglycan (PG), a macromolecular polymer that surrounds the cell, confers mechanical strength and resists expansion due to turgor pressure. Spatial and temporal control of PG synthesis and remodeling is critical for defining and maintaining a particular shape (Typas et al., 2012, Pinho et al., 2013). Nevertheless, the mechanisms by which cell shape diversity is generated remain largely elusive.

Although a myriad of shapes within the bacterial kingdom has been described, most of the well-studied species are rods, ovococci, or cocci. These shapes result from different mechanisms of cell wall growth and from the presence of various cytoskeletal elements. The best studied rod-shaped bacteria maintain their characteristic shape through two PG synthesis modes coordinated by major cytoskeletal elements: elongation of the sidewall, coordinated mainly by the actin homologue MreB, and placement of a crosswall (septum) during division, coordinated by the tubulin homologue FtsZ (Cava et al., 2013). FtsZ is a self-activating GTPase that forms a ring (the Z-ring) at the future site of division, which recruits several other cell division and PG synthesis proteins that drive septum formation (Adams and Errington, 2009). While the division mechanism is conserved in most bacteria, elongation modes are variable. In rod-shaped species that express MreB homologues, such as *Bacillus subtilis* (Garner et al., 2011, Domínguez-Escobar et al., 2011) and *Escherichia coli* (Teeffelen et al., 2011), MreB-associated PG-synthesizing

complexes assemble in dynamic patches underneath the cell membrane and promote the coordinated insertion of PG throughout the cell periphery to result in cell elongation. Ovococcoid bacteria do not possess MreB homologues, but they also elongate, albeit slightly, by the so-called peripheral PG synthesis that occurs in close proximity to the division site, coordinated by the Z-ring (Pinho et al., 2013, Tsui et al., 2014). Spherical cocci lack dedicated elongation machinery and divide using an FtsZ-dependent system, placing new cell wall mostly at the mid-cell division septum (Monteiro et al., 2015).

Interestingly, phylogenetic analyses suggest that modern cocci evolved from rod-shaped bacteria, possibly through the loss of dedicated elongation machinery (Siefert and Fox, 1998). An example of this rod to coccus transition by loss of specific genes was recently reported for *Neisseria meningitidis* and *Moraxella catarrhalis* during adaption to the nasopharynx niche (Veyrier et al., 2015). Accordingly, rod-shaped bacteria can acquire a spherical shape upon inactivation of elongation-specific cytoskeletal proteins or PG synthesis enzymes (Ogura et al., 1989, Murray et al., 1997, Jones et al., 2001, Wei et al., 2003, Kruse et al., 2005, Muchova et al., 2013). As for the opposite coccus-to-rod transition, ovococci can generate more elongated cells upon the inhibition of septation, despite the absence of MreB (Lleo et al., 1997, Perez-Nunez et al., 2011). However, to the best of our knowledge, there are no reports of elongation in otherwise spherical bacteria. Spherical morphology is therefore viewed as an evolutionary dead-end from the perspective of cell shape (Siefert and Fox, 1998).

In this report, we describe the first mechanism to convert spherical *Staphylococcus aureus* cells into elongated cells. This behavior

was observed in a mutant previously isolated during the screening of methicillin-resistant *S. aureus* strain COL strain for resistance to PC190723, an antibiotic that inhibits cell division by targeting FtsZ (Haydon et al., 2008, Tan et al., 2012). Genome sequencing of the mutant revealed a single point mutation (G193D) in FtsZ (Tan et al., 2012). On the basis of our findings obtained with a combination of super resolution microscopy, electron microscopy, molecular dynamics (MD), and biochemical analyses of the FtsZ mutant protein, we propose an FtsZ-dependent mechanism for the morphogenesis of elongated *S. aureus* cells.

EXPERIMENTAL PROCEDURES

Bacterial strains and growth conditions

All of the strains and plasmids used in this study are listed in Table II.1. The sequences of the primers used are listed in Table II.2. *E. coli* and *B. subtilis* strains were grown on Luria Bertani agar (LB agar, Difco) or in Luria Bertani broth (LB broth, Difco). *S. aureus* strains were grown on tryptic soy agar (TSA, Difco) or in tryptic soy broth (TSB, Difco) at 37°C with aeration. The medium was supplemented, when required, with appropriate antibiotics (ampicillin 100 µg/ml; erythromycin 10 µg/ml; kanamycin 50 µg/ml; Sigma), with 5-bromo-4-chloro-3-indolyl β-D-galactopyranoside 100 µg/ml (X-Gal; Apollo Scientific) or with isopropyl-β-D-thiogalactopyranoside 0.5 mM (IPTG; Apollo Scientific). For *B. subtilis* strains, the medium was supplemented when required with antibiotics (spectinomycin 100 µg/ml, chloramphenicol 10 µg/ml and erythromycin 5 µg m^{-1}), 0.1 mM IPTG (VWR) and 0.2 % (w/v) xylose (Sigma).

Table II.1 – Strains and plasmids used in this study.

Plasmids and strains	Relevant characteristics	Source or reference
Plasmids		
$pCXZ_{BS}$	pJF118HE plasmid that contains P_{tac}-*ftsZ* from *B. subtilis*; Amp^r	(Wang and Lutkenhaus, 1993)
$pCXZ_{SA}$	pJF118HE plasmid that contains *bla* P_{tac}-*ftsZ* from *S. aureus*; Amp^r	This study
pCXZ-*g578a*	pJF118HE plasmid that contains *bla* P_{tac}-*ftsZg578a* from *S. aureus*; Amp^r	This study
pMAD	*E. coli – S. aureus* shuttle vector with the *bgaB* gene encoding a ß-galactosidase and thermosensitive origin of replication for Gram-positive bacteria, Amp^r Ery^r	(Arnaud et al., 2004)

pMAD*ftsZg578a*	pMAD derivative used for replacement of *ftsZ* for *ftsZg578a,* Amp^r Ery^r	This study
pMUTINCFPKan	Integrative vector for C-terminal CFP fusions; Amp^r, Kan^r	(Veiga et al., 2011)
pBCBRP001	pMUTINKan derivative containing *ftsZg578a-cfp*; Amp^R Kan^r	This study
pBCB13	pMAD derivative with P_{spac} *lacI* between up- and downstream regions of the *spa* gene, Amp^r Ery^r	(Pereira et al., 2010)
pBCB13-*ftsZg578a-cfp*	pBCB13 derivative containing P_{spac}-*ftsZg578a-5aa-cfp lacI;* Amp^r Ery^r	This study
E. coli		
DC10B	Δ*dcm* in the DH10B background; Dam methylation only	(Monk et al., 2012)
BL21(DE3)	*E. coli* B F^- *dcm ompT hsdS*(r_B^- m_B^-) *gal* λ (DE3)	Stratagene
BL21(DE3)pCXZ$_{SA}$	BL21DE3 transformed with pCXZ$_{SA}$; Amp^r	This study
BL21(DE3)pCXZ-*g578a*	BL21DE3 transformed with pCXZ-*g578a*; Amp^r	This study
B. subtilis		
168	Wild-type strain	Lab collection
BW121	*ftsZ::spc^r, thrC::P_{xyl}-ftsZ ery^r*	(Weart and Levin, 2003)
PL950	*amyE::P_{spachy}-ftsZ cat^r*	(Weart and Levin, 2003)
PAL1114	*amyE::P_{spac}-ftsZ-gfp cat^r*	(Weart and Levin, 2003)
BDA950	168 *amyE::P_{spachy}-ftsZ cat^r*	This study
PF17	168 *amyE::P_{spachy}-ftsZ^{G193D} cat^r*	This study
PF19	BW121 *amyE::P_{spachy}-ftsZ cat^r*	This study
PF20	BW121 *amyE::P_{spachy}-ftsZ^{G193D} cat^r*	This study
PF21	BW121 *amyE::P_{spac}-ftsZ-gfp cat^r*	This study
PF22	BW121 *amyE::P_{spac}-ftsZ^{G193D}-gfp cat^r*	This study
S. aureus		
RN4220	MSSA strain. Mutagenized strain derived from NCTC8325-4 that accepts foreign DNA	R. Novick
COL	MRSA strain	(Gill et al., 2005)
M5	COL with *ftsZg578a* mutation encoding FtsZG193D	(Tan et al., 2012)

BCBPM073	COL*pbpB::sgfp-pbpB*	(Tan et al., 2012)
BCBRP003	COL*ftsZg578a pbpB::sgfp-pbpB*	This study
BCBAJ020	COLΔ*spa*::P_{spac}-*ftsZ-5aa-cfp lacI*	(Tan et al., 2012)
BCBRP004	COLΔ*spa*::P_{spac}-*ftsZg578a-5aa-cfp lacI*	This study
BCBRP005	COL*ftsZg578a*Δ*spa*::P_{spac}-*ftsZg578a-5aa-cfp lacI*	This study
BCBAJ012	COL*ezrA::ezrA-mCherry*	(Jorge et al., 2011)
BCBRP006	COL*ftsZg578a ezrA::ezrA-mCherry*	This study

Table II.2 – Primers used in this study. Underlined sequences correspond to restriction sites.

Primer Name	Sequence (5'-3')
ftsZP1	TACTCCCCGGGGGCCAATAAAACTAGGAGG
ftsZP2	TGCACAGATCTATTAACCGATTAACGTCTTG
ftsZP3	ATCGTGGGATCCTCTATTTGAATGATTATTG
ftsZP4	ATCGTGGAATTCAATAACTTTGAAAAACTTAAATG
ftsZP5	GCTGCGGTACCGGCCAATAAAACTAGGAGG
ftsZP6	GCTGCGGTACCGGAGGCGCCGCAGGAACGTCTTGTTCTTCTTGAACG
ftsZP7	TACTCCCCGGGGGCCAATAAAACTAGGAGG
ftsZP8	GCTGCCTCGAGTTACTTGTACAGCTCGTCCATGCCGAG
AC1257	AAACCTCTTTACTGCCGTTATTCG
AC1258	TCCCGTCTAGCCTTGCCCTCAATGG
PF37	ACTTCGCCAAGATGTTCAAGGTATTTCTGACTTGA
PF38	AGAAATACCTTGAACATCTTGGCGAAGTACGTTA

Super-resolution structured illumination microscopy (SIM)

SIM imaging was performed using a Plan-Apochromat 63x/1.4NA oil DIC M27 objective, in an Elyra PS.1 microscope (Zeiss). Images were acquired using five phase shifts, either three or five grid rotations, with a

34-µm grating period for the 561-nm laser (100 mW), 28-µm period for the 488-nm laser (100 mW), and 23-µm period for the 405-nm laser (50 mW). Images were acquired using a sCMOS Pco.edge 5.5 camera and reconstructed using the ZEN software (black edition, 2012, version 8.1.0.484) based on a structured illumination algorithm (Heintzmann and Cremer, 1999) using synthetic and channel-specific optical transfer functions. ZEN software algorithms were used for channel alignment.

Preparation of *S. aureus* cells for transmission electron microscopy (TEM)

Embedding and thin sectioning of *S. aureus* cells was performed as described previously (Jorge et al., 2011). Briefly, cells were harvested in exponential phase ($OD_{600\ nm}$ = 0.6) and washed with 0.1 M of sodium cacodylate buffer pH 7.4. Cell fixation was performed using 2.5% of glutaraldehyde in 0.1 M of sodium cacodylate buffer pH 7.4 followed by 1% osmium tetroxide. The fixed cells were rinsed to remove fixative and then dehydrated using increasing concentrations of acetone. After two final washes with 100% acetone, the cells were infiltrated with Spurr's resin, transferred to 60 °C for polymerization, and the resulting blocks were thin-sectioned using an ultramicrotome (Reichert). Thin sections, ca. 80 nm thick, were picked up on un-coated 200 mesh copper grids and stained using uranyl acetate and lead nitrate (Reynolds, 1963). Thin sections were viewed in a Philips CM120 electron microscope and images were taken using an AMT ER50 5 megapixel CCD camera (Advanced Microscopy Techniques Corp., Danvers, MA) at magnifications ranging from 5,000 to 52,000x.

Preparation of *S. aureus* cells for scanning electron microscopy (SEM)

Cells were harvested in exponential phase, resuspended in fixative solution (2.5% glutaraldehyde in 0.2 M sodium cacodylate buffer, pH 7.4), deposited on glass discs (Marienfeld) and kept for one week at 4°C. The fixative solution was subsequently removed and the cells were washed three times with the sodium cacodylate solution. The sample was progressively dehydrated by immersion in a graded series of ethanol (50% - 100%) and then mounted on aluminium stubs with carbon adhesive discs (Agarscientific). The sample was critical-point dried under CO_2 and sputter coated with gold-palladium (Polaron SC7640) for 200 s at 10 mA. SEM observations were performed using secondary electron images (2 kV) with a Hitachi S4500 instrument at the Microscopy and Imaging Platform (Micalis, B2HM, Massy, France) of the INRA research centre of Jouy-en-Josas (France).

Measurements of cellular aspect ratios

S. aureus overnight cultures were diluted 1/200 in fresh medium and incubated at 37 ºC. One milliliter of each culture in exponential phase ($OD_{600\ nm}$ = 0.6) was incubated with the membrane dye Nile red (10 µg/ml), at 37ºC for 5 min with shaking. Cells were harvested, resuspended and 1 µl was placed on a pad of 1.2% agarose in TSB mounted on a microscope slide. Epifluorescence images were recorded every 5 min with a Zeiss Axio Observer.Z1 microscope equipped with a Photometrics CoolSNAP HQ2 camera (Roper Scientific) using ZEN blue software. Fifty round cells of each strain were chosen and the longer (length) and shorter (width) axes were measured at the beginning of the experiment and at the stage of maximum elongation (end of the cell cycle,

just prior to cell splitting). The length to width ratios at both time points were then calculated. Statistical analyses were performed in GraphPad Prism 5 by using the Mann-Whitney test for non-normal distributions.

Western blot analysis

Expression levels of FtsZ were analysed by Western blotting, using a polyclonal anti-FtsZ specific antibody produced against *B. subtilis* FtsZ. A polyclonal anti-PBP2 antibody was used as an internal control (Reed et al., 2011). Samples were taken from cultures of COL and M5 grown until an $OD_{600\,nm}$ of 0.8. Cells were broken with glass beads in a Fast Prep FP120 (Thermo Electron Corporation) and debris was removed by centrifugation. The total protein content of the extracts was quantified by the Bradford method, using bovine serum albumin as a standard (BCA protein assay kit, Pierce). 10 µg and 20 µg of total protein from each sample were loaded onto an 10% SDS-PAGE gel and separated at 120 V. Proteins were then transferred to a Hybond-P Polyvinylidene fluoride (PVDF) membrane (GE Healthcare) using a semidry transfer cell (Bio-Rad). The membranes were cut to separate the region containing PBP2 and FtsZ. Each half of the membrane was blocked with blocking buffer (PBS; 5% milk; 0.5% Tween 20) for 1 h and incubated with either a polyclonal anti-PBP2 antibody (Reed et al., 2011) or with an anti-FtsZ antibody for 16 h at 4 °C. Membranes were washed three times with PBS-T (PBS containing 0.5% Tween 20) and incubated with secondary antibodies (HRP anti-rabbit diluted 1/100,000 for PBP2 detection, GE Healthcare; HRP anti-sheep diluted 1/50,000 for FtsZ detection, Pierce). The detection was performed using an ECL Plus Western blotting detection system (Amersham) according to the manufacturer's guidelines.

Construction of *Bacillus subtilis ftsZ* mutants

To construct *B. subtilis* strains expressing the *ftsZg578a,g579t* allele, we used strain PL950 (Weart et al., 2007), which contains an additional copy of the wild-type *ftsZ* allele at the ectopic *amyE* locus under control of the IPTG-inducible promoter P_{spachy}, and strain BW121 (Weart et al., 2007), which has its native *ftsZ* gene deleted and expresses FtsZ only from an ectopic *ftsZ* copy placed in the *thrC* locus under the control of a xylose-inducible promoter (P_{xyl}). Similarly, we used strain PAL1114 (Weart and Levin, 2003) which contains a copy of a functional wild-type *ftsZ-gfp* fusion at the *amyE* locus, under control of the IPTG-inducible promoter P_{spac}. We amplified the *amyE* locus from PL950 and PAL1114 chromosomal DNA, using primer pairs AC1257, PF38 and AC1258, PF37 (Table II.2), generating, in each case, two fragments with a 28-bp overlap that included the *g578a,g579t* mutation in either *ftsZ* or *ftsZ-gfp*. In each case, the overlapping fragments were ligated following a standard Gibson assembly protocol (Gibson et al., 2009). Strains PF17 and PF20 were obtained by directly transforming wild-type strain 168 and strain BW121, respectively, with the resulting PCR products, and strains BDA950 and PF19 were obtained by transforming strains 168 and BW121, respectively, with a control PCR fragment that did not contain the mutation. Likewise, strains PF22 and PF21 were obtained by transforming strain BW121 with a PCR product containing either the *ftsZg578a,g579-gfp* or *ftsZ-gfp* allele, respectively. Transformations were performed using a standard *B. subtilis* transformation protocol for linear DNA fragments (Albano et al., 1987).

Lethality analysis of the FtsZ^{G193D} mutation in *B. subtilis*

To assess the lethality of the FtsZ^{G193D} mutation, we examined the growth phenotypes of strains PF19 (*ftsZ::spc, thrC::P$_{xyl}$-ftsZ erm, amyE::P$_{spachy}$-ftsZ cat*) and PF20 (*ftsZ::spc, thrC::Pxyl-ftsZ erm, amyE::P$_{spachy}$-ftsZ^{G193D} cat*). Strains PF19 and PF20 were streaked out on LB-agar plates supplemented with either 0.5% xylose (w/v) or 10 mM IPTG to induce expression of the *ftsZ* genes controlled by the respective inducible promoters. To determine growth rates, overnight PF19 and PF20 cultures in LB + 0.2% xylose were diluted to an $OD_{600\ nm}$ of 0.005 in the same medium and grown to an $OD_{600\ nm}$ of 0.1. Culture samples were then washed and diluted ten-fold in either LB + xylose (0.2% w/v) or LB + IPTG (100 µM), and $OD_{600\ nm}$ was followed for 3 h.

Localization of FtsZ^{G193D}-GFP in *B. subtilis*

Cells from overnight liquid cultures in LB supplemented with xylose (0.2% w/v) of merodiploid strains PF21 and PF22 were diluted in fresh LB supplemented with xylose (0.2% w/v) until $OD_{600\ nm}$ = 0.1, then washed and diluted ten-fold in LB + 100 µM IPTG. 2h after this dilution, cells were mounted on an agarose pad and imaged by epifluorescence microscopy on an inverted microscope (Nikon Ti-E) using a 488-nm laser and an exposure time of 100 msec.

Molecular dynamics simulations

All simulations were performed with the molecular dynamics package NAMD (Phillips et al., 2005) with the CHARMM27 force field (MacKerell et al., 1998, Foloppe and MacKerell Jr, 2000), including CMAP corrections (Mackerell et al., 2004). Water molecules were described with the TIP3P model (Jorgensen et al., 1983). Long-range electrostatic forces were evaluated by means of the particle-mesh Ewald summation

approach with a grid spacing of <1 Å. An integration time step of 2 fs was used (Tuckerman et al., 1992). Bonded terms and short-range, nonbonded terms were evaluated at every time step, and long-range electrostatics were evaluated at every other time step. A constant temperature (T = 310 K) was maintained by using Langevin dynamics (Brünger et al., 1984), with a damping coefficient of 1.0 ps^{-1}. A constant pressure of 1 atm was enforced using the Langevin piston algorithm (Feller et al., 1995) with a decay period of 200 fs and a time constant of 50 fs. Simulations were initialized from the *S. aureus* GDP-bound FtsZ dimer structure (Protein Data Bank [PDB] code: 3VO8) (Matsui et al., 2012). Water and neutralizing ions were added around the FtsZ dimer. Force field parameters for GTP and GDP molecules were taken from reference (Hsin et al., 2012). All simulations with FtsZ dimers contained approximately 211,000 atoms. Setup, analysis, and rendering of the simulation systems were performed with the software VMD (Humphrey et al., 1996).

Protein purification

To produce *S. aureus* $FtsZ^{WT}$ and $FtsZ^{G193D}$ untagged proteins in *E. coli* BL21(DE3), DNA fragments containing the *ftsZ* and *ftsZg578a* alleles were amplified from the COL and M5 genomes, respectively, using primers ftsZP3 and ftsZP4. These PCR fragments were digested with BamHI and EcoRI and cloned into the $pCXZ_{BS}$ expression plasmid (Wang and Lutkenhaus, 1993) previously digested with BamHI/EcoRI to remove the *B. subtilis ftsZ* allele. The resulting plasmids ($pCXZ_{SA}$ and pCXZ-*g578a*) were sequenced and transformed into competent BL21(DE3) cells to generate strains BL21(DE3)$pCXZ_{SA}$ and BL21(DE3)pCXZ-*g578a*, respectively.

S. aureus $FtsZ^{WT}$ protein was purified from strain BL21(DE3)$pCXZ_{SA}$ as previously described, with minor modifications (Mukherjee and Lutkenhaus, 1998, Scheffers, 2008). Briefly, FtsZ was precipitated from a membrane-free cell extract with a 50% ammonium sulphate cut, resuspended in a solution of 50 mM Tris/HCl, 1 mM EDTA, and 10% (v/v) glycerol (pH 8.5), and loaded onto a Source 30Q anion exchange column (GE Life Sciences). Elution of the protein was performed with a 50-500 mM KCl gradient. Purified FtsZ was dialyzed against storage buffer (20 mM Tris/HCl, 1 mM EGTA, 2.5 mM magnesium acetate, 10% (v/v) glycerol, and 50 mM KCl, pH 7.9), frozen in liquid nitrogen, and stored at -80 °C.

S. aureus $FtsZ^{G193D}$ protein was purified from strain BL21(DE3)pCXZ-*g578a* as described above with the addition of an extra gel-filtration step after the anion-exchange chromatography using a Superdex 200 HiLoad 16/60 column equilibrated and eluted with storage buffer. Purified $FtsZ^{G193D}$ aliquots were frozen in liquid nitrogen and stored at -80 °C. FtsZ protein concentrations were determined using the BCA protein assay kit (Pierce, Life Technologies).

Transmission electron microscopy (TEM) of FtsZ polymers

TEM of $FtsZ^{WT}$ and $FtsZ^{G193D}$ polymers was performed as previously described (Krol and Scheffers, 2013). Briefly, 5 µM $FtsZ^{WT}$ or $FtsZ^{G193D}$ protein were individually incubated in polymerization buffer (50 mM HEPES-NaOH pH 7.5, 300 mM KCl, 10 mM $MgCl_2$) for 5 min at 30 ºC. Polymerization was initiated by adding GTP to a final concentration of 2 mM, after which the samples were incubated at 30 ºC for 10 min. Per reaction, two microliters were placed on individual glow-discharged 400-mesh carbon-coated copper grids and immediately blotted dry with filter

paper. Samples were negatively stained with 2 µL of 2% uranyl acetate. Grids were viewed using a Philips CM120 electron microscope equipped with a LaB_6 filament operating at 120 kV. Images were recorded with a Gatan 4000 SP 4K slow-scan CCD camera. The lengths of more than 70 polymers were measured using ImageJ (Schindelin et al., 2012). Statistical analyses of length differences between $FtsZ^{WT}$ and $FtsZ^{G193D}$ polymers were analyzed with GraphPad Prism 5 using the Mann-Whitney test for non-normal distributions.

GTP hydrolysis assays

GTP hydrolysis was measured as previously described (Krol and Scheffers, 2013), using the malachite green phosphate assay kit (Bioassays) to measure phosphate release over time. Either $FtsZ^{WT}$ or $FtsZ^{G193D}$ proteins (10 µM) were incubated in polymerization buffer supplemented with 2 mM GTP at 30 ºC (final reaction volume of 40 µL). At different time points, 20 µL of each reaction were mixed with 20 µL of malachite green working reagent (Bioassays) to stop the reaction. After incubation for 30 min at room temperature, the $OD_{630\ nm}$ was recorded using a PowerWave HT microplate spectrophotometer (BioTek). Released phosphate was calculated using an internal phosphate standard. Phosphate release over time, from four experiments, was plotted using GraphPad Prism 5.

Construction of *S. aureus* mutants

To replace wild-type *ftsZ* with an *ftsZ* gene containing the *g578a* mutation encoding $FtsZ^{G193D}$ in the background of *S. aureus* strains encoding fluorescent fusions of sGFP-PBP2 (strain BCBPM073 (Tan et al., 2012)) or EzrA-mCherry (strain BCBAJ012 (Jorge et al., 2011)), we first amplified an 1172-kb DNA fragment, using the M5 genome DNA as a

template and primers ftsZP1 and ftsZP2. This DNA fragment contains a G to A point mutation in *ftsZ*, at nucleotide position 578 (*ftsZg578a*). This DNA fragment was then cloned into the pMAD plasmid (Arnaud et al., 2004), giving rise to pMAD*ftsZg578a* which was confirmed by sequencing. This plasmid was electroporated into RN4220 (Veiga and Pinho, 2009) and subsequently transduced into strains BCBPM073 and BCBAJ012 using phage 80α (Oshida and Tomasz, 1992). Integration and excision of pMAD*ftsZg578a* from the genome was performed as previously described (Arnaud et al., 2004) and colonies in which native *ftsZ* was replaced by the *ftsZg578a* allele were selected by replica plating on TSA supplemented or not with 25 μg/ml of oxacillin as the M5 mutant is susceptible to this antibiotic (Tan et al., 2012). Strains that did not grow in the presence of oxacillin were sequenced to confirm *ftsZ* replacement by the *ftsZg578a* allele. Strains derived from BCBPM073 and BCBAJ012 that contained the *ftsZg578a* allele were named BCBRP003 and BCBRP006, respectively.

For the construction of a strain expressing an FtsZ^{G193D}-CFP fusion from the ectopic *spa* locus, a PCR fragment encompassing the *ftsZg578a* mutation was amplified from M5 genomic DNA using primers ftsZP5 and ftsZP6 (which encodes a 5 amino acid linker), cloned into pMUTINCFPKan (Veiga et al., 2011) and sequenced, generating the pBCBRP001 plasmid. The full *ftsZg578a-5aa-cfp* construct was then amplified from the pBCBRP001 plasmid using primers ftsZP7 and ftsZP8 and cloned into the pBCB13 plasmid (Pereira et al., 2010), downstream of the IPTG-inducible P_{spac} promoter. The resulting plasmid (pBCB13-*ftsZg578a-cfp*) was confirmed by sequencing. This plasmid was then electroporated into RN4220 (Veiga and Pinho, 2009), grown at 30 ºC with

erythromycin selection, and subsequently transduced into COL strain using phage 80α (Oshida and Tomasz, 1992). The replacement of the *spa* gene with the P_{spac}-*ftsZg578a-cfp* construct was performed as previously described (Pereira et al., 2010) and confirmed by PCR. The resulting COL strain expressing *ftsZg578a-cfp* from the *spa* locus was named BCBRP004. Since this strain still has a wild-type *ftsZ* copy at the native locus, we transduced the pMAD*ftsZg578a* construct into BCBRP004 and substituted the native *ftsZ* gene by the *ftsZg578a* allele, as described above, giving rise to strain BCBRP005.

Epifluorescence Microscopy

BCBPM073, BCBRP003, BCBAJ020 and BCBRP005 strains were grown overnight in TSB and diluted 1/500 in either TSB (BCBPM073 and BCBRP003 strains) or TSB supplemented with 0.1 mM of IPTG (BCBAJ020 and BCBRP005 strains) and incubated at 37 ºC. At mid-exponential phase ($OD_{600\ nm}$ of 0.6), cells (1 ml of each culture) were pelleted by centrifugation, re-suspended in 20 µL of phosphate-buffered saline (PBS) and 1 µL was placed on microscopy slide covered with a thin layer of 1.2% agarose in PBS. Images were obtained using a Zeiss Axio Observer.Z1 microscope equipped with a photometrics CoolSNAP HQ2 camera (Roper Scientific) using Metamorph software (Molecular Devices).

EzrA-mCherry localization by SIM

Exponentially growing cultures of strains BCBAJ012 and BCBRP006 ($OD_{600\ nm}$ = 0.6) were labelled with a 1:1 (vol/vol) mixture of the cell-wall dye Van-FL (1 µg/ml, Invitrogen) with nonfluorescent vancomycin (1 µg/ml, Sigma) for 5 min at room temperature with shaking. Cultures were pelleted, resuspended in 20 µl phosphate-buffered saline (PBS), and placed on top of a thin layer of 1.2% agarose in

PBS mounted on a microscope slide. Imaging was performed by SIM with the 561 nm laser at maximal power for mCherry observation and the 488 nm laser at 20% maximal power for Van-FL.

Immunofluorescence microscopy

Immunofluorescence labelling of FtsZ was performed as previously described (Pinho and Errington, 2003). Briefly, *S. aureus* COL and M5 strains were grown to an $OD_{600\ nm}$ of 0.6, culture samples (10 ml) were centrifuged and the pellet was fixed with 1 ml of Histochoice (Amresco). Cells were washed three times with PBS and re-suspended in 500 µl of GTE buffer (50 mM glucose, 20 mM Tris-HCl, pH 7.5, 10 mM EDTA). A gentle lysis was performed using lysostaphin (Sigma) at a final concentration of 10 µg/ml for 1 minute. During the incubation with lysostaphin, 25 µL of each culture were placed on top of polylysine-treated slide wells. After the incubation period with lysostaphin, cells were washed three times with GTE, air dried, rehydrated with PBS, and blocked with 2% bovine serum albumin (BSA, Sigma) in PBS for 15 min. Cells were then incubated overnight at 4 °C with anti-FtsZ primary antibody, which was added in consecutive two-fold dilutions from 1/800 to 1/3600. The following day, cells were washed eight times with PBS and incubated with secondary antibody (Alexa Fluor 488 donkey anti-sheep IgG, Invitrogen diluted 1/500 in 2% BSA/PBS) in the dark for 1 h. Cells were again washed eight times with PBS and 1.5 µL of Vectashield mounting medium (Vector Laboratories) was added. Cells were visualized by epifluorescence microscopy.

3D reconstructions using super resolution structured illumination microscopy

S. aureus overnight M5 cultures were diluted 1/200 in fresh media and incubated at 37ºC. One milliliter of each culture in exponential phase ($OD_{600\ nm}$ = 0.6) was incubated with the membrane dye Nile Red (10 µg/ml, Invitrogen) and with the cell-wall dye Van-FL (1 µg/ml, Invitrogen) mixed in a 1:1 (v:v) proportion with non-fluorescent vancomycin (1 µg/ml, Sigma). Cells were harvested by centrifugation, resuspended in 20 µl of PBS and placed on top of a thin layer of 1.2% agarose in PBS mounted on a microscope slide. 3D reconstruction of SIM images was performed with a Zeiss Elyra PS.1 microscope, by acquiring z-stacks with 0.15 µm increments. 3D reconstruction of SIM images was performed using the Zen software and a point spread function (PSF) based on theoretical models.

Cell wall staining with FDDAs

Pulse-labeling experiments were performed essentially as previously described (Kuru et al., 2012). In brief, the COL and M5 strains were incubated overnight at 37 ºC in TSB, diluted 1/200 in fresh medium and incubated at 37 ºC. At $OD_{600\ nm}$ = 0.8, 500 µl of each culture was harvested by centrifugation, resuspended in 150 µl of supernatant, and labelled with 250 µM NADA (Kuru et al., 2012, Kuru et al., 2015). Labelling was performed for 10 min at 37 ºC with shaking. Unbound NADA was removed by washing with 200 µl of PBS, and NADA-labelled cultures were resuspended in 150 µl of spent medium. Then, a second labelling step was performed using 250 µM of red TDL (Kuru et al., 2012, Kuru et al., 2015) for 10 min at 37 ºC with shaking. Unbound TDL was removed by washing with 200 µl of PBS and NADA-TDL-labelled cultures were

resuspended in 150 µl of spent medium. A third labelling step was performed using 250 µM HADA for 10 min at 37 ºC with shaking. Cultures were then washed with 200 µl PBS and resuspended in 50 µl of PBS, and 1 µl was placed on a microscopy slide covered with a thin layer of 1.2% agarose in PBS. NADA, TDL, and HADA fluorescence was imaged by SIM with 50% of the maximal 488-nm laser power, 50% of 561 nm, and 50% of 405 nm, respectively, with an exposure time of 30 msec.

SIM time-lapse imaging

To observe individual cell division events, exponentially growing cultures ($OD_{600\ nm}$ = 0.8) of *S. aureus* wild-type COL or M5 were first stained with the peripheral cell-wall dye (WGA-Alexa488, Invitrogen) at a final concentration of 2 µg/ml for 5 min at 37 °C with shaking. Unbound dye was removed by washing cells with TSB. Cells were then placed on an agarose pad mounted on a microscope slide containing 50% TSB in PBS and the membrane dye Nile red (10 µg/ml). Cell growth was tracked by SIM from images acquired every 20 min with 20 msec exposures at 10% of the maximal 488-nm laser power and 20% of the maximal 561-nm laser power.

RESULTS

FtsZ^{G193D} mutation leads to elongated cells in *S. aureus*

S. aureus cells are approximately spherical and there are no previous reports of a sphere-to-rod transition in cocci. Putative mechanisms to generate elongated cells of *S. aureus* include expressing an actin-like cytoskeleton or inhibiting cell division or septal cell wall synthesis. However, expression of *B. subtilis* MreB (Yepes et al., 2014) or Mbl (our unpublished observations) does not result in elongated *S. aureus* cells. Similarly, mutations that reduce FtsZ function can produce enlarged spherical cells (Pinho and Errington, 2003, Adams et al., 2015), showing that the peripheral PG synthesis that occurs in *S. aureus* does not support elongation (Monteiro et al., 2015). Serendipitously, while characterizing PC190723-resistant *S. aureus* mutant M5 (Tan et al., 2012), which carries a G to D substitution at the 193rd residue of FtsZ, within helix 7, we noticed the presence of cells that were not spherical. In order to examine the shape alterations of this mutant in more detail, we labelled the COL wild-type and M5 mutant strains with fluorescently-modified vancomycin (Van-FL, which labels the entire cell wall in *S. aureus*) and the DNA dye Hoechst 33342. Super resolution imaging of the labelled cells by structured illumination microscopy (SIM) confirmed the presence of cells with altered morphology, including curved elongated cells (Figure 1a). To quantitatively evaluate elongation, COL and M5 cells were stained with the membrane dye Nile red and cell shape alterations were monitored over the cell cycle by time-lapse microscopy. Measurements of the longer (cell length) and shorter (cell width) axes of both M5 and COL cells (n > 50 cells) showed that the length-to-width ratio is significantly increased in M5 mutant cells (Figure 1b). Elongation of *S. aureus* M5 cells was

further confirmed by transmission electron microscopy and scanning electron microscopy (Figure 1 c and d).

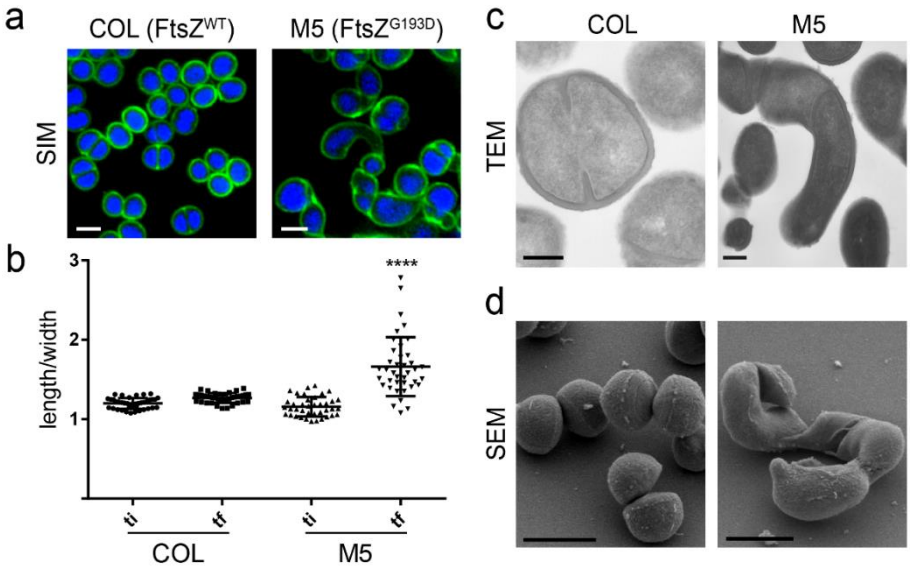

Figure 1: The FtsZ^{G193D} mutation leads to *S. aureus* cell elongation. (a) SIM images of wild-type COL (left) and FtsZ^{G193D} mutant M5 (right) cells labelled with the cell-wall dye Vancomycin-FL (green) and the DNA dye Hoechst 33342 (blue). Scale bar: 1 µm. **(b)** The ratio of the longer to shorter axis was calculated in two time-points during the cell cycle: initial time point (ti), when cells had a round shape and final time point (tf) when cells were most elongated, prior to the splitting of the mother cell. M5 cells elongate significantly more during the cell cycle when compared to COL wild-type cells (p<0.001). **(c)** Transmission electron micrographs of thin sections of COL and M5 cells. Scale bar: 200 nm. **(d)** Scanning electron microscopy images of COL and M5 cells. Scale bar: 1 µm.

Membrane labelling also confirmed that cells underwent true elongation, not division without cell separation, as long cells were devoid of septa (Figure 2).

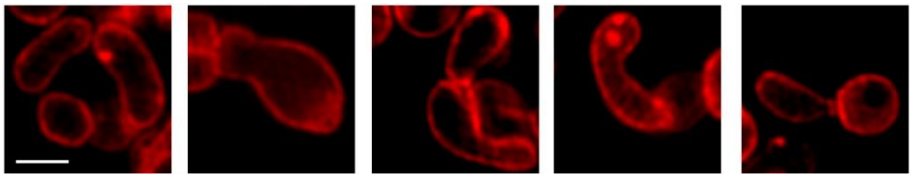

Figure 2 M5 mutant cell elongation observed by SIM. Examples of elongated M5 cells without a septum stained with the membrane dye Nile red and observed by SIM. Scale bar: 1 µm.

Despite the substantial morphological changes, M5 mutant cells were able to grow reasonably well, albeit more slowly than parental strain COL grown in batch culture (25 versus 47 min, respectively, Figure 3).

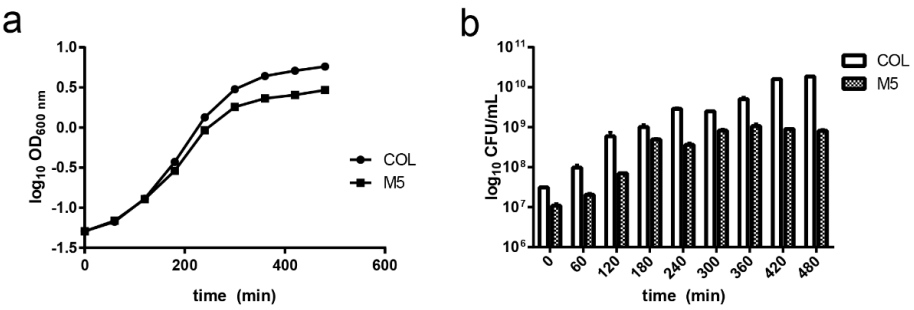

Figure 3: Analysis of COL wild-type and M5 mutant culture growth at 37°C. **(a)** Growth of COL and M5 cultures in TSB medium was monitored by recording the OD_{600} every hour. **(b)** The number of CFUs was also determined throughout the growth curve by plating appropriate dilutions of the growing COL and M5 cultures on solid tryptic soy agar. The graph shows the $\log_{10}$ number of CFU/ml versus time.

Changes in morphology were not due to altered FtsZ expression levels, as the total amounts of $FtsZ^{G193D}$ and $FtsZ^{WT}$ in M5 and COL cells, respectively, were similar, as determined by Western blotting (Figure 4).

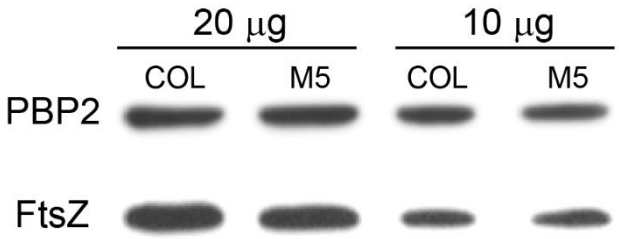

Figure 4: FtsZ^{G193D} levels in M5 cells are similar to FtsZ^{WT} levels in COL cells. Western blot analysis shows similar levels of FtsZ protein in COL and M5 cells. Twenty micrograms (first two lanes) or 10 μg (last two lanes) of total protein in crude cell extracts was loaded into the gel. PBP2 was used as an internal control.

Since G193 is well conserved across FtsZ proteins, we wondered if introduction of the FtsZ^{G193D} mutation into a rod-shaped bacterium would also have an effect on cell shape, generating longer or curved cells. We attempted to replace the native *ftsZ* allele in *B. subtilis* with the allele encoding the G193D mutation. However, in agreement with a recent report (Adams et al., 2015), we were unable to obtain viable *B. subtilis* colonies expressing *ftsZ^{G193D}* as the sole copy of *ftsZ* on the chromosome, suggesting that the mutation is lethal in *B. subtilis*. We then constructed *B. subtilis* strain PF20 with both *ftsZ^{WT}* and *ftsZ^{G193D}* alleles under the control of two different inducible promoters (Figure 5a). This strain failed to form colonies when *ftsZ^{G193D}* was the only allele expressed, confirming that the mutation is lethal in *B. subtilis* (Figure 5b and c). Consistently, FtsZ^{G193D} was delocalized and did not form Z-rings, indicating that it is unable to promote cell division (Figure 5d).

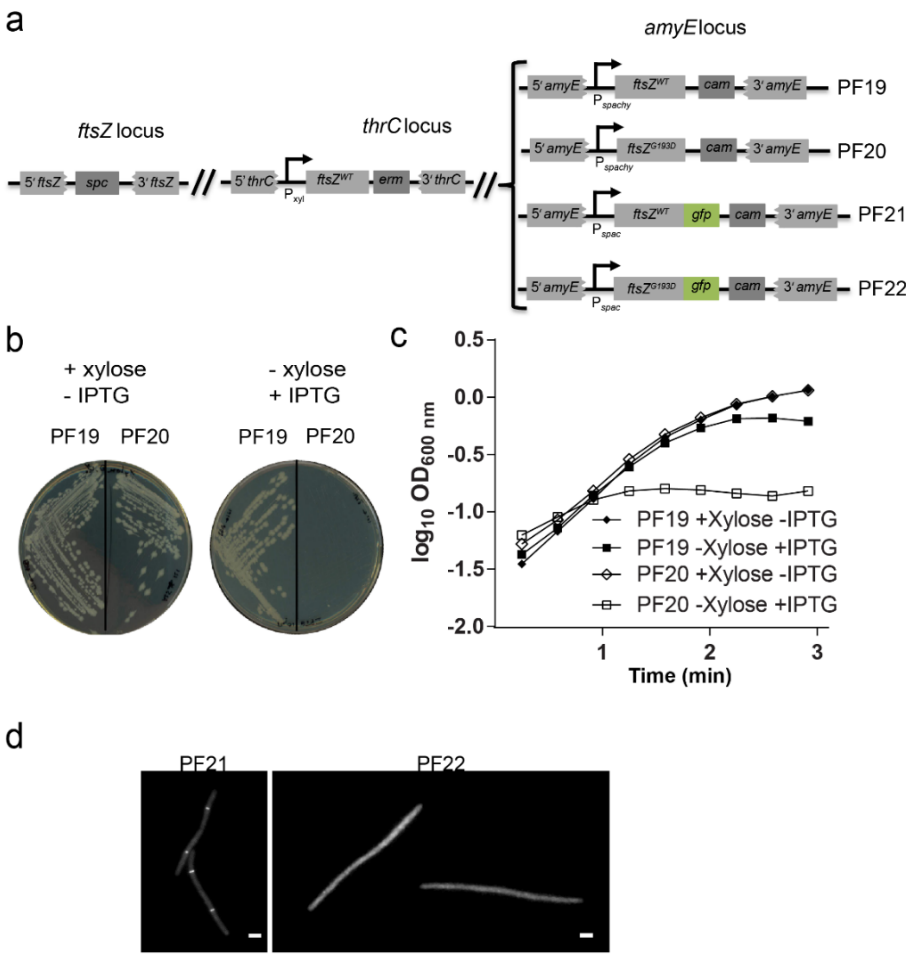

Figure 5: The FtsZ^{G193D} mutation renders FtsZ nonfunctional in *B. subtilis*. **(a)** Schematic representation of the genotypes of strains PF19, PF20, PF21, and PF22 used in this study. **(b)** Strains PF19 and PF20 were streaked onto plates supplemented with either 0.5% (wt/vol) xylose (left) or 10 µM isopropyl-β-D-thiogalactopyranoside (IPTG) (right) to induce the expression of the *ftsZ* alleles controlled by the respective promoters, as indicated in panel a. No differences in growth between strains PF20 and PF19 expressing only FtsZ^{WT} (in the presence only of xylose) were observed. However, strain PF20 was not viable when expressing FtsZ^{G193D} as the only source of FtsZ in the cell (in the presence only of IPTG). **(c)** Growth of PF20 and PF19 was measured in either LB plus xylose (0.2% [wt/vol], diamonds) or LB plus IPTG (100 µM, squares), confirming that cells expressing only FtsZ^{G193D} are not viable. **(d)** FtsZ^{G193D}-GFP localizes as a diffuse cytoplasmic signal in *B. subtilis* and cannot form Z-rings. Cells of strains PF21

(left) and PF22 (right) were grown in LB plus IPTG (100 μM) to express $FtsZ^{WT}$ or $FtsZ^{G193D}$, respectively, mounted on an agarose pad, and imaged by epifluorescence microscopy. Scale bars: 2 μm.

The G193D mutation leads to shorter, twisted FtsZ polymers

The FtsZ filament binding interface has been shown to have the capacity to rearrange itself to accommodate different degrees of bending (Li et al., 2013, Hsin et al., 2012). We wondered whether the G193D mutation might cause major structural rearrangements in FtsZ, resulting in misassembled and/or mislocalized FtsZ rings that could produce the morphological phenotypes of M5 cells. We carried out all-atom MD simulations of *S. aureus* $FtsZ^{WT}$ and $FtsZ^{G193D}$ dimers to assay whether the structure of the subunits and/or the polymers would likely be affected by the mutation (Figure 6a). Simulations were initiated from a straight, untwisted state, as shown by repeating the dimer interface to create a long polymer (Figure 6a and b). However, $FtsZ^{G193D}$ homodimers reproducibly adopted a twist of >15° between the two monomers within the first 50 ns of simulation, while the $FtsZ^{WT}$ dimer remained untwisted for >100 ns (Figure 6a-6c). This predicted twist could have two effects *in vivo*: (i) the spatial pattern of membrane binding could be more likely to follow a helix rather than the normal Z-ring, and (ii) such twisting could impair the formation or stability of FtsZ polymers.

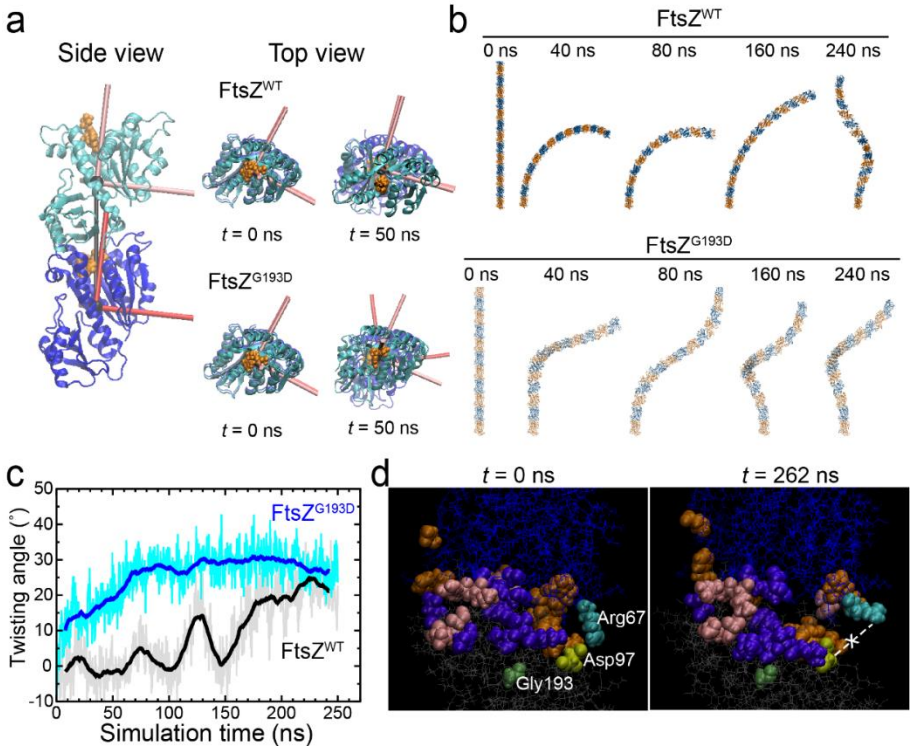

Figure 6: FtsZ^{G193D} produces twisted polymers. (a) Molecular dynamics (MD) simulations of dimers of *S. aureus* FtsZ^{WT} (PDB: 3VO8) and FtsZ^{G193D} reveal a propensity for twist in FtsZ^{G193D} dimers. Simulations were initialized as straight dimers at $t = 0$ (side view). Top view highlights the development of twist between the principal axes of the two FtsZ^{G193D} subunits at t = 50 ns. **(b)** Shown are filaments of 14 subunits constructed by extrapolating the dimer interface from time points during the MD simulations. The FtsZ^{WT} dimer bent, but remained straight for the first ~100 ns. **(c)** The FtsZ^{G193D} dimer rapidly adopts a substantial degree of twist, while the FtsZ^{WT} dimer acquires this twist much later in the simulation. **(d)** Snapshots at the beginning and end of the FtsZ^{WT} dimer simulation, in which residues are colored if they interact (defined as being within 5 Å of another residue) with the opposite subunit at any point during the simulation. Orange: specific to the non-twisted state of wild-type, with an interaction in the first 100 ns, and no interaction after 150 ns (and no interaction throughout the FtsZ^{G193D} simulation); purple: generally present in twisted states (always interacting in FtsZ^{G193D} and after 150 ns for FtsZ^{WT}); pink: specific to FtsZ^{G193D}. The salt bridge between Asp97 (light green) and Arg67 (cyan) is broken at t = 262 ns. Gly193 is shown in dark green.

To examine how the binding interface between the subunits reorganized upon twisting, we identified all of the pairs of amino acids that spanned both subunits and whose closest atoms lay within 5 Å. The number of such pairs ranged between 13 and 24 and between 14 and 26 during the simulation of the $FtsZ^{WT}$ and $FtsZ^{G193D}$ dimers, respectively. Such interactions could be classified into three groups: those that are present early in the $FtsZ^{WT}$ dimer simulation and never in $FtsZ^{G193D}$ (representing a non-twisted state), those that are always present in $FtsZ^{G193D}$ and only later in $FtsZ^{WT}$ (general to twisted states), and those that are present only in $FtsZ^{G193D}$ (specific to the twisted state of the mutant) (Figure 6d and 7a). The residues in each of these groups were spatially clustered (Figure 6d), indicating that it is not merely fluctuations of the interface that generate the interactions, and that there are binding interfaces specific to $FtsZ^{WT}$ and $FtsZ^{G193D}$, with $FtsZ^{G193D}$ having interactions that do not exist in the $FtsZ^{WT}$ twisted state. There was also a single interaction, between the arginine at position 67 on the top FtsZ subunit and the aspartic acid at position 97 on the bottom subunit, that followed dynamics similar to those of the twist angle in the $FtsZ^{WT}$ dimer (Figure 6d). This salt bridge was connected for the first 100 ns, broke, reformed briefly and then was broken for the remainder of the simulation (Figure 7b). Upon closer examination, the arginine appeared to form a swinging lever that was initially bound to the aspartic acid but swung upward during the periods of twisting. Glycine 193 is part of a helix on the bottom subunit that connects to residues 202 to 204 and Asp97, suggesting that the mutation to aspartic acid (G193D) allosterically disrupts the salt bridge and potentially destabilizes the interface.

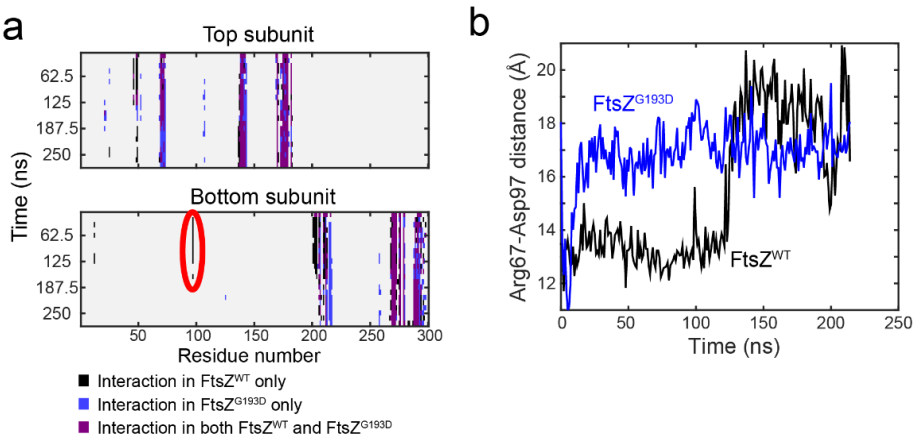

Figure 7: Interfacial interactions differ in FtsZ^{WT} and FtsZ^{G193D} and between the nontwisted and twisted states. (a) All of the residues that interact with the opposite subunit (defined as being within 5 Å of another residue) were identified in each frame of the simulations. Shown are the interactions in 12.5-ns blocks. Black, specific to the nontwisted state of the wild type, with an interaction in the first 100 ns and no interaction after 150 ns (and no interaction throughout the FtsZ^{G193D} simulation); purple, generally present in twisted states (always interacting in FtsZ^{G193D} and after 150 ns for FtsZ^{WT}); blue, specific to FtsZ^{G193D}. Red oval highlights Asp97. **(b)** Shown is the distance between the centers of mass of Arg67 and Asp97 spanning the dimer interface. The salt bridge was rapidly broken in the FtsZ^{G193D} dimer simulation. In the FtsZ^{WT} dimer simulation, the salt bridge briefly destabilized at t =~100 ns and then broke for the remainder of the simulation at around t = 120 ns, mimicking the trajectory of polymer twist (Fig. 6b).

We next purified *S. aureus* FtsZ^{WT} and FtsZ^{G193D} and studied *in vitro* polymer formation by transmission electron microscopy. Although FtsZ^{G193D} was capable of polymerization, the resulting polymers were significantly shorter than those made by FtsZ^{WT} under the same conditions (Figure 8a and b), suggesting that FtsZ^{G193D} polymers could potentially be less stable, as predicted by the MD simulations. Changes in FtsZ polymer stability, especially those mediated by regulatory proteins, are often linked to changes in the GTP hydrolysis activity of FtsZ (Huang

et al., 2013). However, there was no significant difference between the GTP hydrolysis rates of FtsZ^{WT} and FtsZ^{G193D} (0.14 ± 0.02 and 0.15 ± 0.03 mol of phosphate released per mol of FtsZ per min, respectively; Figure 8c).

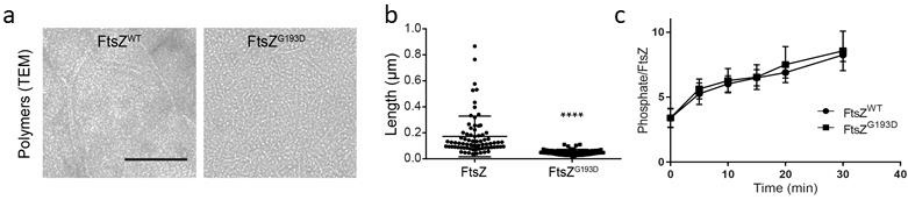

Figure 8: FtsZ^{G193D} produces twisted polymers without affecting GTP hydrolysis. (a) Polymers of *S. aureus* FtsZ^{WT} (left) and FtsZ^{G193D} (right) imaged by transmission electron microscopy. Scale bar: 100 nm. **(b)** Length of FtsZ^{WT} and FtsZ^{G193D} polymers (n>70) as measured from the transmission electron microscopy images, show that FtsZ^{G193D} polymers are significantly shorter than FtsZ^{WT} polymers (p<0.0001). **(c)** Shown is the average number of phosphate molecules released per FtsZ^{WT} (circles) or FtsZ^{G193D} (squares) molecule. Average values are from four independent assays, and error bars represent standard deviations.

Z-rings are misplaced in *S. aureus* FtsZ^{G193D} mutant cells

Our simulations predict a propensity for twisting in FtsZ^{G193D} homodimers (Figure 6a and b) that could result in polymers that assemble into extended helical structures instead of a ring. Interestingly, helical FtsZ structures have been observed both in *E. coli* and in *B. subtilis* (Addinall and Lutkenhaus, 1996, Ben-Yehuda and Losick, 2002, Peters et al., 2007, Fu et al., 2010). Therefore, we determined the localization of a fluorescent protein-fusion of FtsZ^{G193D} in live *S. aureus* cells. Given that available fusions with *S. aureus* FtsZ are not fully functional (Veiga et al., 2011), we expressed FtsZ^{G193D} tagged with cyan-fluorescent protein (CFP) at the C-terminus from the ectopic *spa* locus, under control of the P$_{spac}$ promoter (Veiga et al., 2011). We then replaced the wild-type *ftsZ*

gene at the native chromosomal locus with an allele containing the *ftsZ g578a* mutation that encodes the FtsZ^{G193D} protein, thereby generating strain BCBRP005, which recapitulates the morphological phenotypes of M5. While FtsZ^{WT}-CFP localized as a ring at mid-cell (Figure 9a, top panel) as previously described (Veiga et al., 2011), FtsZ^{G193D}-CFP localized in structures that extend along the cell in different orientations (Figure 9a, bottom panel). These localization patterns were confirmed by immunofluorescence microscopy in the original COL and M5 strains (Figure 9b).

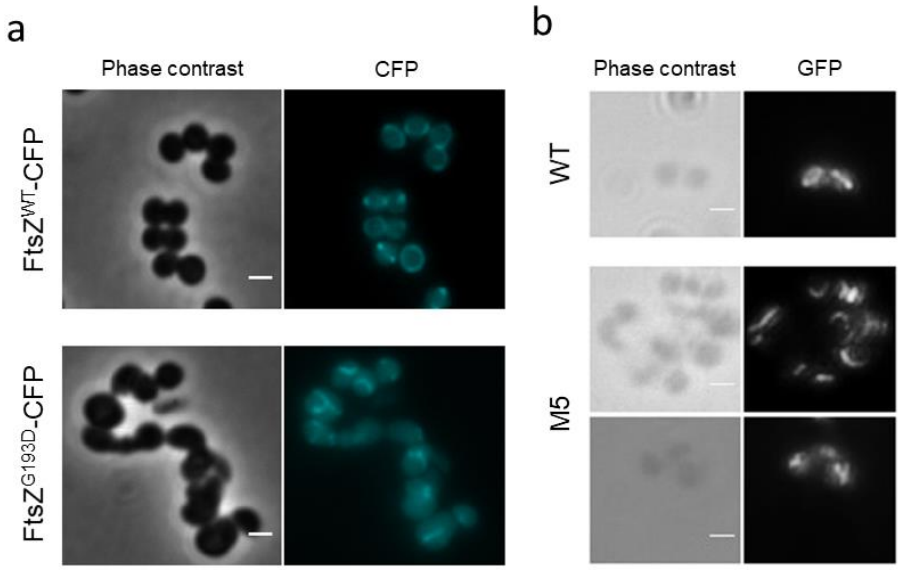

Figure 9: FtsZ^{G193D} does not form a mid-cell ring in *S. aureus*. (a) Localization of FtsZ^{WT}-CFP in BCBAJ020 cells (top) or FtsZ^{G193D}-CFP in BCBRP005 cells (bottom) **(b)** Phase contrast (left) and immunofluorescence (right) images of either COL, expressing FtsZ^{WT} or M5, expressing FtsZ^{G193D}, using an anti-FtsZ primary antibody. Scale bars: 1 µm.

As fluorescent protein fusions with FtsZ are not fully functional and the weak FtsZ-CFP fluorescence is incompatible with SIM, we used EzrA-mCherry as a proxy for Z-ring localization. EzrA, an early

component of the divisome, is a regulator of FtsZ polymerization and directly interacts with FtsZ (Haeusser et al., 2004, Singh et al., 2007, Chung et al., 2007, Jorge et al., 2011, Steele et al., 2011). We replaced the native *ftsZ* gene with the *ftsZ*^{G193D} allele in strain BCBAJ012, which expresses EzrA-mCherry as the sole copy of EzrA (Jorge et al., 2011), to create strain BCBRP006. These cells had a morphological phenotype similar to that of M5 cells (Figure 10), confirming that FtsZ^{G193D} is sufficient to cause cell elongation. In the presence of the FtsZ^{G193D} mutation, EzrA-mCherry no longer localized only as a mid-cell ring, but instead frequently assembled at only one side of cells that were beginning to elongate (white box inset in Figure 10) or in a Y shape in cells that were partially elongated (asterisk in Figure 10). As FtsZ^{G193D} mutant cells elongated further, EzrA structures became localized toward the "poles" of the cells (white arrow in Figure 10).

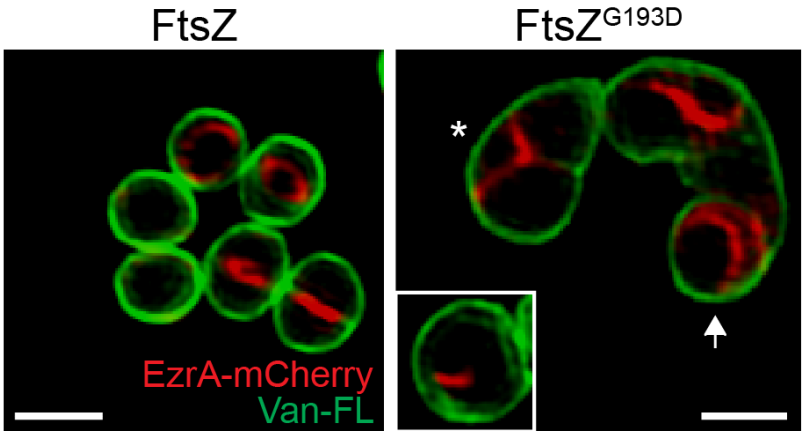

Figure 10: Fluorescent fusions to EzrA lose mid-cell localization in M5 cells. SIM images of EzrA-mCherry (red) and cell wall labelled with Van-FL (green), in BCBAJ012 cells expressing FtsZ^{WT} (left) and in BCBRP006 cells expressing FtsZ^{G193D} (right). In the presence of FtsZ^{G193D}, EzrA-mCherry fails to localize as a mid-cell ring. Instead, structures assemble on only one side of the cell (white box) or in Y patterns compatible with one-turn helical structures (asterisk). More elongated BCBRP006 cells show EzrA-mCherry localized towards the poles of the cell (white arrow). Scale bars: 1 µm.

One-turn helical structures would appear as such Y shapes in two-dimensional microscopy images (Figure 10, asterisk). Because of photobleaching, we were unable to visualize the EzrA-mCherry Y shapes in three dimensions by SIM. We therefore acquired Z-stacks of SIM images of M5 cells labelled with Van-FL, which labels the cell wall, including the nascent septum, confirming that Y shapes along the membrane corresponded to one-turn helical structures (Figure 11).

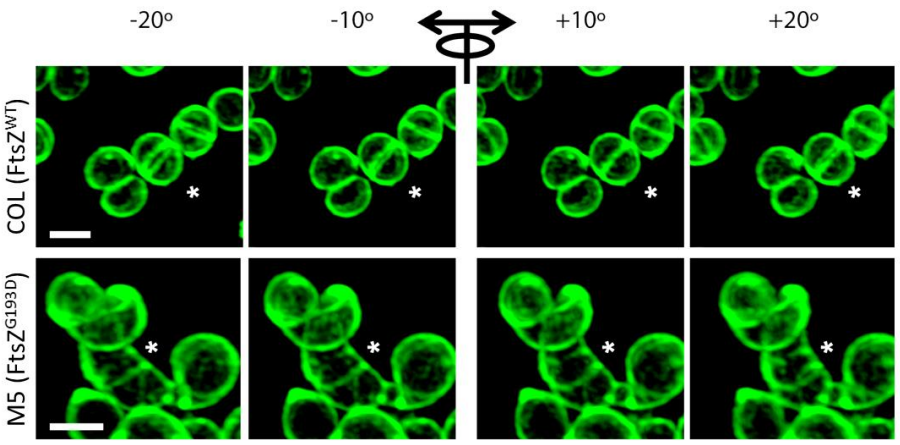

Figure 11: *S. aureus* M5 mutant cells exhibit a one-turn helical septum. *S. aureus* wild-type COL (top) or mutant M5 (bottom) were labelled with the cell wall dye Vancomycin-FL and imaged by SIM (Z-stack). Snapshots of -10° and +10° rotation angle increments are shown. In wild-type *S. aureus* cells the division septa is placed as a midcell ring. Bottom panel shows a M5 mutant cell where a helical division septum can be observed. Asterisks indicate the same cell observed at different angles. Scale bars 1µm.

FtsZ^{G193D} structures recruit PG synthesis enzymes

Wild-type FtsZ rings recruit PG synthesis proteins, namely penicillin-binding proteins (PBPs), that catalyze the synthesis of glycan strands (transglycosylation) and their cross-linking via peptide bridges (transpeptidation). These activities are required for the formation of the

division septum, which is perpendicular to the cell surface and extends inward, across the mother cell. If misplaced FtsZ^{G193D} structures also recruit PBPs, then spatially misplaced incorporation of septal PG could follow, which could explain cell elongation.

S. aureus has four native PBPs, of which PBP2 is the only bifunctional enzyme, capable of catalyzing both transpeptidation and transglycosylation reactions (Murakami et al., 1994, Massova and Mobashery, 1998, van Heijenoort, 2001). PBP2 localizes to the septum in an FtsZ-dependent manner and, in the absence of FtsZ, PBP2 becomes dispersed over the entire cell surface (Pinho and Errington, 2003). To localize PBP2 in the presence of FtsZ^{G193D}, wild-type *ftsZ* was replaced with the *ftsZ^{G193D}* allele in the background of strain BCBPM073 (Tan et al., 2012), which expresses superfast green fluorescent protein (sGFP) PBP2 as the sole copy of PBP2. In FtsZ^{G193D} mutant cells, sGFP-PBP2 no longer formed septal rings at mid-cell, but, rather than becoming dispersed, it had a localization pattern similar to that of FtsZ^{G193D} structures (Figure 12). On the basis of this, we infer that FtsZ^{G193D} filaments are still capable of recruiting PBP2 and possibly other PG synthesis proteins, indicating that FtsZ^{G193D} filaments are competent to promote cell wall synthesis.

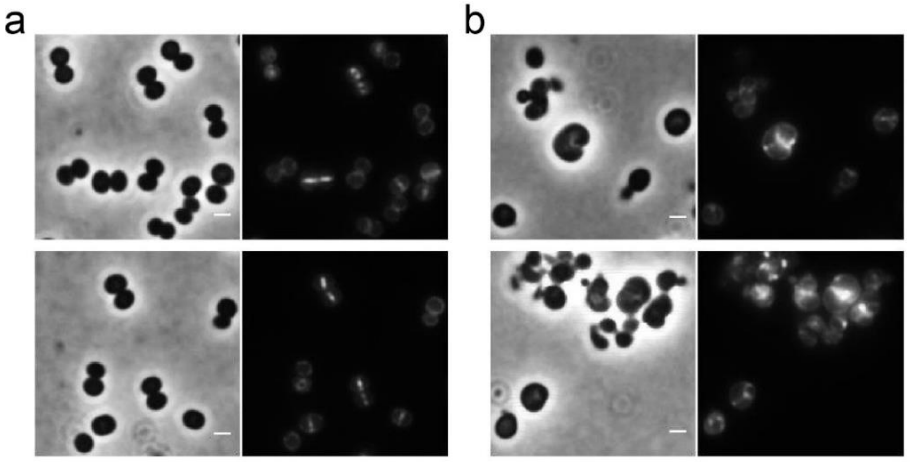

Figure 12: PBP2 does not form mid-cell rings in an FtsZ^{G193D} background. Phase contrast (left) and fluorescence images (right) showing the localization of sGFP-PBP2 in **(a)** BCBPM073 (expressing FtsZ^{WT}) and **(b)** BCBRP003 (expressing FtsZ^{G193D}). Scale bars: 1µm.

We therefore examined PG incorporation over the cell cycle, by sequentially labelling COL and M5 cells with fluorescent D-amino acids (FDAAs) derivatized with fluorophores of different colours, which are incorporated at sites of active PG synthesis (Kuru et al., 2012), thereby creating a virtual time-lapse image of PG synthesis locations.COL and M5 cells were labelled with green NADA for a short 10-min pulse, followed by a 10-min pulse with the red TDL, and finally by a 10-min pulse with the blue HADA. We then imaged the subcellular localization of PG synthesis by SIM (Figure 13). As expected, septal PG synthesis progression in wild-type COL cells occurred in continuous mid-cell rings that constricted over time and finally split, giving rise to the new daughter cells (Figure 13b). Note that *S. aureus* divides into three perpendicular planes over successive division cycles and therefore sequential division planes are orthogonal (Pinho et al., 2013, Veiga et al., 2011). By contrast, in M5 cells PG was first incorporated only on one side of the cell (asterisk

in Figure 13c), and then progressed along the periphery of the cell, in a pattern compatible with a helical structure (blue fluorescence, white arrows in Figure 13c).

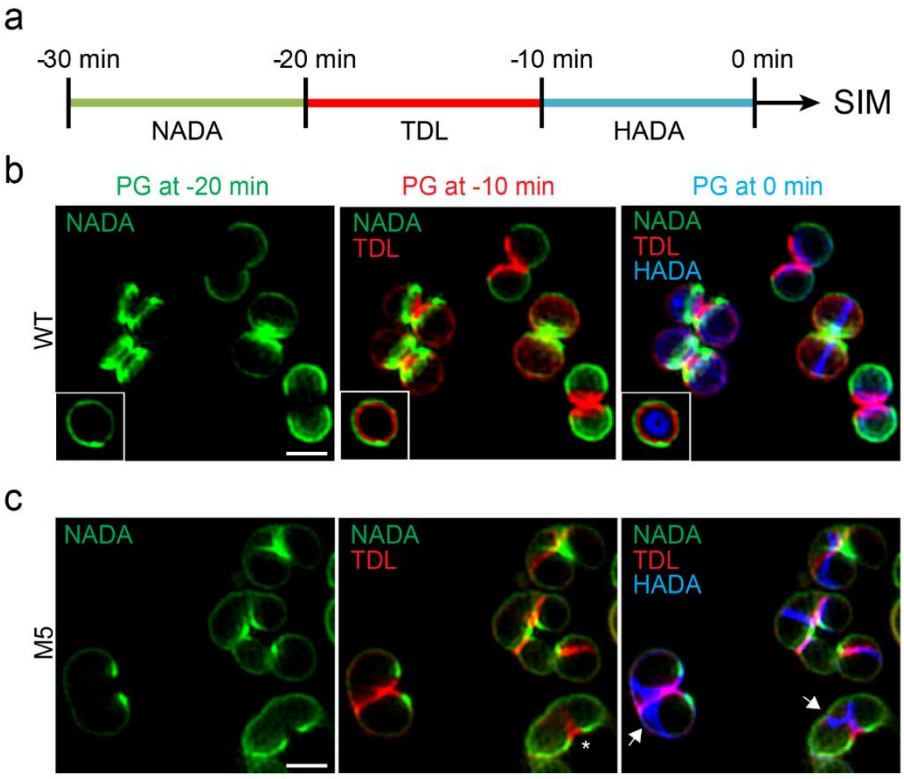

Figure 13: PG incorporation dynamics suggest a new mode of cell growth in *S. aureus* FtsZ^{G193D} cells. (a) Schematic representation of pulse labelling with fluorescent D-amino acids. Cells were labelled with three sequential 10-min pulses of NADA (green), TDL (red), and HADA (blue) and observed by SIM. The same cell imaged in three different channels therefore shows the PG synthesized 30-20 min (green), 20-10 min (red) and 10-0 min (blue) prior to imaging. **(b)** In COL cells, septum synthesis initiates as a symmetric ring at mid-cell that constricts over time, concomitant with concentric PG synthesis (white box). **(c)** In M5 cells, PG synthesis occurs in two steps: first, PG is asymmetrically incorporated on only one side of a cell, eventually leading to a local splitting (asterisks). Second, PG is inserted along a "Y" pattern compatible with one-turn helical path (blue fluorescence, white arrows). Scale bar: 1 µm.

FtsZ^{G193D} leads to a new mode of cell division for *S. aureus*

To observe the fate of cells with different modes of PG insertion, COL or M5 cells were labelled with the dye wheat germ agglutinin-Alexa Fluor 488 conjugate dye (WGA-Alexa488), which labels nonseptal cell-wall. Labelled cells were then placed on an agarose pad containing growth medium and the membrane dye Nile red and imaged in time-lapse mode by SIM (Figure 14). As previously observed, wild-type COL cells displayed a mid-cell septum that constricted and split to generate approximately one third of the surface of each new daughter cell (Monteiro et al., 2015) (Figure 14a, white arrow). In M5 mutant cells, septum synthesis did not initiate as a homogeneous ring encircling the cell. Instead, during early stages of division, septum formation progressed from only one side of the cell (Figure 14b, asterisk 1). The region where the asymmetric septum first formed proceeded into local splitting of the cell, increasing the cell surface in a manner similar to wild-type *S. aureus* cells upon splitting of the division septum (compare the bottom cell labelled with an asterisk in the left and middle panel of Figure 14b). At a later stage the asymmetric septum extended, forming a structure compatible with a one-turn helix (Figure 14b, asterisk 2). Regions where PG was inserted along this pattern resulted in cell elongation without splitting, via increase of the surface area of the peripheral wall (see also blue dye indicated by white arrows of Figure 13c), reminiscent of elongation in rod-shaped bacteria.

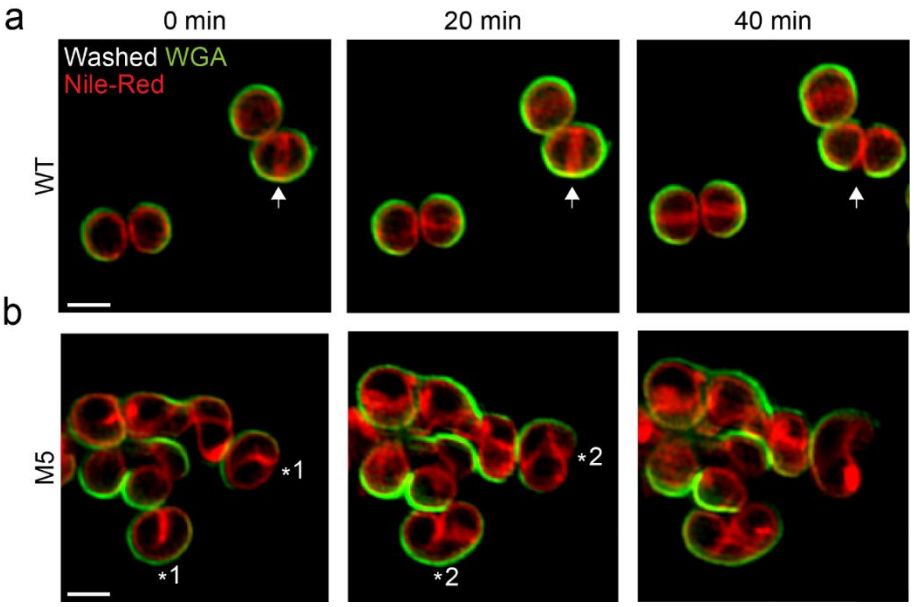

Figure 14: SIM time-lapse imaging reveals the mode of elongation of M5 cells. *S. aureus* COL ($FtsZ^{WT}$) and M5 ($FtsZ^{G193D}$) cells were stained with the peripheral cell-wall dye WGA-488 (green). Unbound dye was washed away, labelled cells were stained with the membrane dye Nile red, and growth was followed by SIM. **(a)** COL wild-type cells synthesized a ring-like septum at mid-cell (white arrow at 0 min) that constricts and eventually splits, giving rise to two daughter cells (arrow at 40 min). **(b)** M5 mutant cells initially synthesized an asymmetric septum on only one side of the cell (asterisk 1), which later developed into a pattern compatible with a one-turn helical structure (asterisk 2) and led to elongation. Scale bars: 1 μm.

DISCUSSION

In this work, we provide the first report of elongation in spherical bacteria, i.e., true cocci, which have no dedicated PG-synthesis elongation machinery. Wild-type *S. aureus* cells synthesize cell wall mostly at the septum, which, upon splitting, generates approximately one third of the cell surface of the new daughter cells and thereby constitutes the largest cell surface increase event in the staphylococcal cell cycle (Monteiro et al., 2015). The FtsZ^{G193D} mutation in M5 cells results in shorter and twisted FtsZ polymers that fail to localize as a ring at mid-cell. As a consequence, the typical mid-cell localization of PG synthesis is lost and during cell division, septum synthesis is initiated in a helical pattern. We propose that helical FtsZ^{G193D} structures direct PG synthesis, initially localized asymmetrically to only one side of the cell (Figure 15, division stage I). This mode of synthesis is similar to septal synthesis in wild-type *S. aureus* cells (Figure 15, top panel division stage I and II), and is followed by local splitting, generating an increase in surface area as the septal wall is converted into peripheral wall and exposed to the external milieu (Figure 15, bottom panel, from stage II to stage III, orange arrows). PG incorporation then occurs in a partial helical pattern (Figure 15, division stage III) around the cell periphery, leading to cell elongation (Figure 15, division stage IV). This elongation is not equivalent to the dispersed PG synthesis all over the cell surface that we recently described for wild-type cells (Monteiro et al., 2015), which is not dependent on a cytoskeletal element. Instead, it is reminiscent of MreB-dependent sidewall elongation in rod-shaped bacteria, since this elongation is localized and directed by a cytoskeletal element, namely FtsZ filaments.

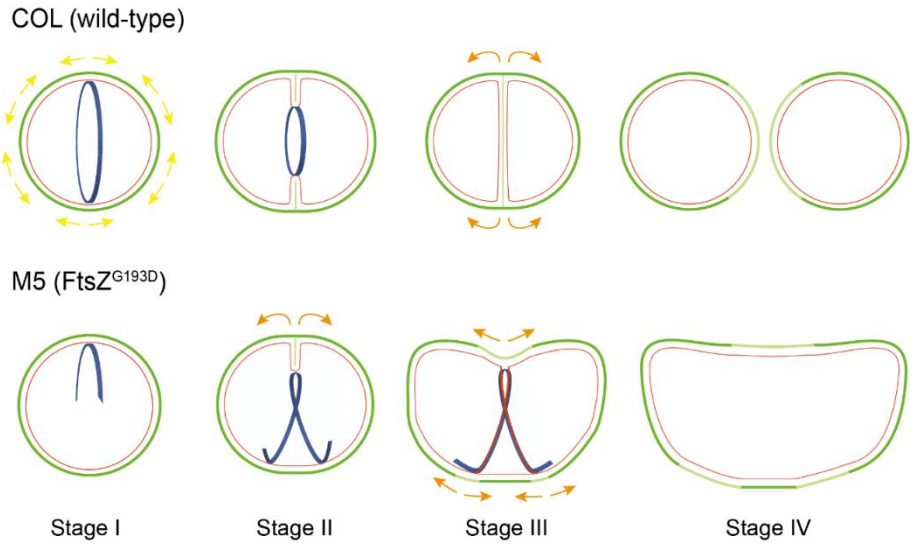

Figure 15: Model for cell elongation in *S. aureus* M5 cells. Schematic of cell division events in wild-type COL (top) and M5 cells (bottom). The images show old cell wall (dark green), new cell wall (light green), membrane (red) and FtsZ structures (blue). Yellow/orange arrows correspond to surface expansion. In wild-type cells (top), FtsZ assembles as a ring at mid-cell and recruits PG synthesis enzymes, leading to incorporation of new PG at mid-cell. New PG is also inserted along the cell periphery, leading to cell surface expansion (yellow arrows). Splitting of the septum generates ~1/3 of the cell surface of each of the new daughter cells, thereby increasing the total surface area exposed to the external milieu. M5 cells (bottom), expressing FtsZ^{G193D} rather than FtsZ^{WT}, incorporate PG in two steps: first, PG deposition occurs on only one side of the cell (asymmetric septum, division stage I), which will initiate local splitting due to septal constriction (stage II) that leads to surface area expansion only on that side of the cell (orange arrows). Second, PG deposition is directed by FtsZ along a partial helical path, leading to further surface expansion resembling elongation of rod-shaped cells (stage III). Thus, M5 cells combine a coccus-like (septal) mode of PG incorporation (stage II) with a rod-like elongation mode (stage III and IV), both of which are coordinated by FtsZ.

REFERENCES

Adams, D. W. and Errington, J. (2009). Bacterial cell division: assembly, maintenance and disassembly of the Z ring. Nat Rev Microbiol*, 7*, 642-53.

Adams, D. W., Wu, L. J. and Errington, J. (2015). A benzamide-dependent *ftsZ* mutant reveals residues crucial for Z-ring assembly. Mol Microbiol.

Addinall, S. G. and Lutkenhaus, J. (1996). FtsZ-spirals and -arcs determine the shape of the invaginating septa in some mutants of *Escherichia coli*. Mol Microbiol*, 22*, 231-7.

Albano, M., Hahn, J. and Dubnau, D. (1987). Expression of competence genes in *Bacillus subtilis*. J. Bacteriol*., 169*, 3110-7.

Arnaud, M., Chastanet, A. and Debarbouille, M. (2004). New vector for efficient allelic replacement in naturally nontransformable, low-GC-content, gram-positive bacteria. Appl. Environ. Microbiol*., 70*, 6887-6891.

Ben-Yehuda, S. and Losick, R. (2002). Asymmetric cell division in *B. subtilis* involves a spiral-like intermediate of the cytokinetic protein FtsZ. Cell*, 109*, 257-66.

Brünger, A., Brooks, C. L. and Karplus, M. (1984). Stochastic boundary conditions for molecular dynamics simulations of ST2 water. Chem Phys Lett*, 105*, 495-500.

Cava, F., Kuru, E., Brun, Y. V. and de Pedro, M. A. (2013). Modes of cell wall growth differentiation in rod-shaped bacteria. Curr Opin Microbiol*, 16*, 731-7.

Chung, K. M., Hsu, H. H., Yeh, H. Y. and Chang, B. Y. (2007). Mechanism of regulation of prokaryotic tubulin-like GTPase FtsZ by membrane protein EzrA. J Biol Chem*, 282*, 14891-7.

Domínguez-Escobar, J., Chastanet, A., Crevenna, A. H., Fromion, V., Wedlich-Söldner, R. and Carballido-López, R. (2011). Processive movement of MreB-associated cell wall biosynthetic complexes in bacteria. Science*, 333*, 225-228.

Feller, S. E., Zhang, Y., Pastor, R. W. and Brooks, B. R. (1995). Constant pressure molecular dynamics simulation: the Langevin piston method. J. Chem. Phys*., 103*, 4613-4621.

Foloppe, N. and MacKerell Jr, A. D. (2000). All‐atom empirical force field for nucleic acids: I. Parameter optimization based on small molecule and condensed phase macromolecular target data. J. Comput. Chem*., 21*, 86-104.

Fu, G., Huang, T., Buss, J., Coltharp, C., Hensel, Z. and Xiao, J. (2010). *In vivo* structure of the *E. coli* FtsZ-ring revealed by photoactivated localization microscopy (PALM). PLoS One*, 5***,** e12682.

Garner, E. C., Bernard, R., Wang, W., Zhuang, X., Rudner, D. Z. and Mitchison, T. (2011). Coupled, circumferential motions of the cell wall synthesis machinery and MreB filaments in *B. subtilis*. Science*, 333***,** 222-225.

Gibson, D. G., Young, L., Chuang, R. Y., Venter, J. C., Hutchison, C. A. and Smith, H. O. (2009). Enzymatic assembly of DNA molecules up to several hundred kilobases. Nat. Methods*, 6***,** 343-5.

Gill, S. R., Fouts, D. E., Archer, G. L., Mongodin, E. F., Deboy, R. T., Ravel, J., Paulsen, I. T., Kolonay, J. F., Brinkac, L., Beanan, M.*, et al.* (2005). Insights on evolution of virulence and resistance from the complete genome analysis of an early methicillin-resistant *Staphylococcus aureus* strain and a biofilm-producing methicillin-resistant *Staphylococcus epidermidis* strain. J. Bacteriol.*, 187***,** 2426-2438.

Haeusser, D. P., Schwartz, R. L., Smith, A. M., Oates, M. E. and Levin, P. A. (2004). EzrA prevents aberrant cell division by modulating assembly of the cytoskeletal protein FtsZ. Mol. Microbiol.*, 52***,** 801-14.

Haydon, D. J., Stokes, N. R., Ure, R., Galbraith, G., Bennett, J. M., Brown, D. R., Baker, P. J., Barynin, V. V., Rice, D. W., Sedelnikova, S. E.*, et al.* (2008). An inhibitor of FtsZ with potent and selective anti-staphylococcal activity. Science*, 321***,** 1673-5.

Heintzmann, R. and Cremer, C. G. (1999). Laterally modulated excitation microscopy: improvement of resolution by using a diffraction grating. Proceedings of the SPIE3568 (Optical Biopsies and Microscopic Techniques III). 185–196

Hsin, J., Gopinathan, A. and Huang, K. C. (2012). Nucleotide-dependent conformations of FtsZ dimers and force generation observed through molecular dynamics simulations. Proc. Natl. Acad. Sci. U S A*, 109***,** 9432-7.

Huang, K. H., Durand-Heredia, J. and Janakiraman, A. (2013). FtsZ ring stability: of bundles, tubules, crosslinks, and curves. J. Bacteriol.*, 195***,** 1859-68.

Humphrey, W., Dalke, A. and Schulten, K. (1996). VMD: visual molecular dynamics. J. Mol. Graph.*, 14***,** 33-38, 27-28.

Jones, L. J., Carballido-Lopez, R. and Errington, J. (2001). Control of cell shape in bacteria: helical, actin-like filaments in *Bacillus subtilis*. Cell*, 104***,** 913-22.

Jorge, A. M., Hoiczyk, E., Gomes, J. P. and Pinho, M. G. (2011). EzrA contributes to the regulation of cell size in *Staphylococcus aureus*. PLoS One*, 6***,** e27542.

Jorgensen, J. H., Johnson, J. E., Alexander, G. A., Paxson, R. and Alderson, G. L. (1983). Comparison of automated and rapid manual methods for the same-day identification of Enterobacteriaceae. Am. J. Clin. Pathol*., 79*, 683-7.

Krol, E. and Scheffers, D. J. (2013). FtsZ polymerization assays: simple protocols and considerations. J. Vis. Exp*., 81*, e50844.

Kruse, T., Bork-Jensen, J. and Gerdes, K. (2005). The morphogenetic MreBCD proteins of *Escherichia coli* form an essential membrane-bound complex. Mol. Microbiol*., 55*, 78-89.

Kuru, E., Hughes, H. V., Brown, P. J., Hall, E., Tekkam, S., Cava, F., de Pedro, M. A., Brun, Y. V. and VanNieuwenhze, M. S. (2012). *In situ* probing of newly synthesized peptidoglycan in live bacteria with fluorescent D-amino acids. Angew. Chem. Int. Ed. Engl*., 51*, 12519-23.

Kuru, E., Tekkam, S., Hall, E., Brun, Y. V. and Van Nieuwenhze, M. S. (2015). Synthesis of fluorescent D-amino acids and their use for probing peptidoglycan synthesis and bacterial growth in situ. Nat. Protoc*., 10*, 33-52.

Li, Y., Hsin, J., Zhao, L., Cheng, Y., Shang, W., Huang, K. C., Wang, H. W. and Ye, S. (2013). FtsZ protofilaments use a hinge-opening mechanism for constrictive force generation. Science*, 341*, 392-5.

Lleo, M. M., Canepari, P., Fontana, R. and Satta, G. (1997). Inhibition of bacterial cell surface extension by various means causes blocking of macromolecular synthesis. Res. Microbiol*., 148*, 11-20.

MacKerell, A. D., Bashford, D., Bellott, M., Dunbrack, R. L., Evanseck, J. D., Field, M. J., Fischer, S., Gao, J., Guo, H., Ha, S*., et al.* (1998). All-atom empirical potential for molecular modeling and dynamics studies of proteins. J. Phys. Chem. B*., 102*, 3586-616.

Mackerell, A. D., Jr., Feig, M. and Brooks, C. L., 3rd (2004). Extending the treatment of backbone energetics in protein force fields: limitations of gas-phase quantum mechanics in reproducing protein conformational distributions in molecular dynamics simulations. J. Comput. Chem*., 25*, 1400-15.

Massova, I. and Mobashery, S. (1998). Kinship and diversification of bacterial penicillin-binding proteins and beta-lactamases. Antimicrob. Agents Chemother*., 42*, 1-17.

Matsui, T., Yamane, J., Mogi, N., Yamaguchi, H., Takemoto, H., Yao, M. and Tanaka, I. (2012). Structural reorganization of the bacterial cell-division protein FtsZ from *Staphylococcus aureus*. Acta Crystallogr. D. Biol. Crystallogr*., 68*, 1175-88.

Monk, I. R., Shah, I. M., Xu, M., Tan, M. W. and Foster, T. J. (2012). Transforming the untransformable: application of direct transformation to manipulate genetically *Staphylococcus aureus* and *Staphylococcus epidermidis*. MBio*, 3*.

Monteiro, J. M., Fernandes, P. B., Vaz, F., Pereira, A. R., Tavares, A. C., Ferreira, M. T., Pereira, P. M., Veiga, H., Kuru, E., VanNieuwenhze, M. S.*, et al.* (2015). Cell shape dynamics during the staphylococcal cell cycle. Nat. Commun.*, 6*, 8055.

Muchova, K., Chromikova, Z. and Barak, I. (2013). Control of *Bacillus subtilis* cell shape by RodZ. Environ. Microbiol.*, 15*, 3259-71.

Mukherjee, A. and Lutkenhaus, J. (1998). Dynamic assembly of FtsZ regulated by GTP hydrolysis. EMBO j.*, 17*, 462-9.

Murakami, K., Fujimura, T. and Doi, M. (1994). Nucleotide sequence of the structural gene for the penicillin-binding protein 2 of *Staphylococcus aureus* and the presence of a homologous gene in other staphylococci. FEMS Microbiol. Lett.*, 117*, 131-6.

Murray, T., Popham, D. L. and Setlow, P. (1997). Identification and characterization of *pbpA* encoding *Bacillus subtilis* penicillin-binding protein 2A. J. Bacteriol.*, 179*, 3021-9.

Ogura, T., Bouloc, P., Niki, H., D'Ari, R., Hiraga, S. and Jaffe, A. (1989). Penicillin-binding protein 2 is essential in wild-type *Escherichia coli* but not in *lov* or *cya* mutants. J. Bacteriol.*, 171*, 3025-30.

Oshida, T. and Tomasz, A. (1992). Isolation and characterization of a Tn551-autolysis mutant of *Staphylococcus aureus*. J. Bacteriol.*, 174*, 4952-9.

Pereira, P. M., Veiga, H., Jorge, A. M. and Pinho, M. G. (2010). Fluorescent reporters for studies of cellular localization of proteins in *Staphylococcus aureus*. Appl. Environ. Microbiol.*, 76*, 4346-53.

Perez-Nunez, D., Briandet, R., David, B., Gautier, C., Renault, P., Hallet, B., Hols, P., Carballido-Lopez, R. and Guedon, E. (2011). A new morphogenesis pathway in bacteria: unbalanced activity of cell wall synthesis machineries leads to coccus-to-rod transition and filamentation in ovococci. Mol. Microbiol.*, 79*, 759-71.

Peters, P. C., Migocki, M. D., Thoni, C. and Harry, E. J. (2007). A new assembly pathway for the cytokinetic Z ring from a dynamic helical structure in vegetatively growing cells of *Bacillus subtilis*. Mol. Microbiol.*, 64*, 487-99.

Phillips, J. C., Braun, R., Wang, W., Gumbart, J., Tajkhorshid, E., Villa, E., Chipot, C., Skeel, R. D., Kale, L. and Schulten, K. (2005). Scalable molecular dynamics with NAMD. J. Comput. Chem.*, 26*, 1781-802.

Pinho, M. G. and Errington, J. (2003). Dispersed mode of *Staphylococcus aureus* cell wall synthesis in the absence of the division machinery. Mol. Microbiol*., 50*, 871-81.

Pinho, M. G., Kjos, M. and Veening, J. W. (2013). How to get (a)round: mechanisms controlling growth and division of coccoid bacteria. Nat. Rev. Microbiol*., 11*, 601-14.

Reed, P., Veiga, H., Jorge, A. M., Terrak, M. and Pinho, M. G. (2011). Monofunctional transglycosylases are not essential for *Staphylococcus aureus* cell wall synthesis. J. Bacteriol*., 193*, 2549-56.

Reynolds, E. S. (1963). The use of lead citrate at high pH as an electron-opaque stain in electron microscopy. J Cell Biol*, 17*, 208-12.

Scheffers, D. J. (2008). The effect of MinC on FtsZ polymerization is pH dependent and can be counteracted by ZapA. FEBS Lett*, 582*, 2601-8.

Schindelin, J., Arganda-Carreras, I., Frise, E., Kaynig, V., Longair, M., Pietzsch, T., Preibisch, S., Rueden, C., Saalfeld, S., Schmid, B*., et al.* (2012). Fiji: an open-source platform for biological-image analysis. Nat Methods*, 9*, 676-682.

Siefert, J. L. and Fox, G. E. (1998). Phylogenetic mapping of bacterial morphology. Microbiology*, 144 (Pt 10)*, 2803-8.

Singh, J. K., Makde, R. D., Kumar, V. and Panda, D. (2007). A membrane protein, EzrA, regulates assembly dynamics of FtsZ by interacting with the C-terminal tail of FtsZ. Biochemistry*, 46*, 11013-22.

Steele, V. R., Bottomley, A. L., Garcia-Lara, J., Kasturiarachchi, J. and Foster, S. J. (2011). Multiple essential roles for EzrA in cell division of *Staphylococcus aureus*. Mol. Microbiol*., 80*, 542-55.

Tan, C. M., Therien, A. G., Lu, J., Lee, S. H., Caron, A., Gill, C. J., Lebeau-Jacob, C., Benton-Perdomo, L., Monteiro, J. M., Pereira, P. M*., et al.* (2012). Restoring methicillin-resistant *Staphylococcus aureus* susceptibility to beta-lactam antibiotics. Sci. Transl. Med*., 4*, 126-135.

Teeffelen, S. v., Wang, S., Furchtgott, L., Huang, K. C., Wingreen, N. S., Shaevitz, J. W. and Gitai, Z. (2011). The bacterial actin MreB rotates and rotation depends on cell-wall assembly. Proc. Natl. Acad. Sci. U S A*, 108*, 15822-7.

Tsui, H. C., Boersma, M. J., Vella, S. A., Kocaoglu, O., Kuru, E., Peceny, J. K., Carlson, E. E., VanNieuwenhze, M. S., Brun, Y. V., Shaw, S. L*., et al.* (2014). Pbp2x localizes separately from Pbp2b and other peptidoglycan synthesis proteins during later stages of cell division of *Streptococcus pneumoniae* D39. Mol Microbiol*, 94*, 21-40.

Tuckerman, M., Berne, B. J. and Martyna, G. J. (1992). Reversible multiple time scale molecular dynamics. J. Chem. Phys*., 97*, 1990-2001.

Typas, A., Banzhaf, M., Gross, C. A. and Vollmer, W. (2012). From the regulation of peptidoglycan synthesis to bacterial growth and morphology. Nat. Rev. Microbiol*., 10*, 123-36.

van Heijenoort, J. (2001). Formation of the glycan chains in the synthesis of bacterial peptidoglycan. Glycobiology*, 11*, 25r-36r.

Veiga, H., Jorge, A. M. and Pinho, M. G. (2011). Absence of nucleoid occlusion effector Noc impairs formation of orthogonal FtsZ rings during *Staphylococcus aureus* cell division. Mol. Microbiol*., 80*, 1366-80.

Veiga, H. and Pinho, M. G. (2009). Inactivation of the SauI type I restriction-modification system is not sufficient to generate *Staphylococcus aureus* strains capable of efficiently accepting foreign DNA. Appl. Environ. Microbiol*., 75*, 3034-8.

Veyrier, F. J., Biais, N., Morales, P., Belkacem, N., Guilhen, C., Ranjeva, S., Sismeiro, O., Pehau-Arnaudet, G., Rocha, E. P., Werts, C*., et al.* (2015). Common Cell Shape Evolution of Two Nasopharyngeal Pathogens. PLoS Genet*, 11*, e1005338.

Wang, X. and Lutkenhaus, J. (1993). The FtsZ protein of *Bacillus subtilis* is localized at the division site and has GTPase activity that is dependent upon FtsZ concentration. Mol. Microbiol*., 9*, 435-42.

Weart, R. B., Lee, A. H., Chien, A. C., Haeusser, D. P., Hill, N. S. and Levin, P. A. (2007). A metabolic sensor governing cell size in bacteria. Cell*, 130*, 335-47.

Weart, R. B. and Levin, P. A. (2003). Growth rate-dependent regulation of medial FtsZ ring formation. J. Bacteriol*., 185*, 2826-34.

Wei, Y., Havasy, T., McPherson, D. C. and Popham, D. L. (2003). Rod shape determination by the *Bacillus subtilis* class B penicillin-binding proteins encoded by *pbpA* and *pbpH*. J. Bacteriol*., 185*, 4717-26.

Yepes, A., Koch, G., Waldvogel, A., Garcia-Betancur, J. C. and Lopez, D. (2014). Reconstruction of *mreB* expression in *Staphylococcus aureus* via a collection of new integrative plasmids. Appl Environ Microbiol*, 80*, 3868-78.

Young, K. D. (2006). The selective value of bacterial shape. Microbiol. Mol. Biol. Rev*., 70*, 660-703.

CHAPTER III

Peptidoglycan synthesis drives FtsZ treadmilling-independent step of cytokinesis

Chapter III Summary

ABSTRACT 136
INTRODUCTION 137
EXPERIMENTAL PROCEDURES 140
Bacterial strains and growth conditions 140
Strain construction 143
Functionality test for FtsZ fluorescent constructs 146
Cell cycle distribution in the presence of cell division inhibitors 146
Protein analysis by Western blot and fluorescence 147
S. aureus imaging by Structured Illumination Microscopy (SIM) 148
Sample mounting procedure for time lapse microscopy 148
Imaging of $FtsZ^{55-56}$-sGFP treadmilling by SIM 149
Visualisation of divisome ring constriction by SIM 149
Functionality test for EzrA-GFP construct 151
RESULTS 153
FtsZ filaments move bidirectionally in *S. aureus* 158
Z-ring constriction is biphasic in *S. aureus* and the second step of cytokinesis is independent of FtsZ movement 161
S. aureus fast step of cytokinesis might be driven by PG synthesis 165
DISCUSSION 171
ANNEX 1 174
REFERENCES 175

A.R. Pereira contribution:

Pereira, A. R., performed all experiments, except construction of plasmids pMUTIN4kan (performed by Pereira, P.M.,) pBCB33 (performed by Reichmann, N.,) and pSGEzrA-GFP (performed by Jorge, A.,). Experiments on cell cycle distribution in the presence of cell division inhibitors were performed by Fernandes, P.B. Software development of eHooke, image aligner and kymographs was performed by Saraiva, B.M.

Acknowledgements:

We thank E. Harry (University of Technology, Sydney) for the generous gift of the anti-FtsZ antibody and to T. Roemer (Merck) for kindly providing the DMPI compound.

Data in this chapter is included in:

Monteiro, J. M*., **A. R. Pereira***, N. T. Reichmann, B. M. Saraiva, P. B. Fernandes, H. Veiga, A. C. Tavares, M. Santos, M. T. Ferreira, V. Macário, M. S. VanNieuwenhze, S. R. Filipe and M. G. Pinho (2018). "Peptidoglycan synthesis drives an FtsZ-treadmilling-independent step of cytokinesis." Nature 554: 528."

* equal contribution to the work; data obtained by Monteiro J.M. is not included in this chapter.

ABSTRACT

In most bacteria, the tubulin homologue FtsZ is the key component to assemble the divisome, a multi-molecular machinery that carries out cytokinesis. This conserved GTPase polymerizes at the future division site forming a highly dynamic ring-like structure (the Z-ring) that recruits later divisome proteins including peptidoglycan synthesis proteins, which synthesize the division septum. Although the divisome performs cellular constriction, the origin of the force that drives the cytokinetic event has remained elusive. Here we studied *Staphylococcus aureus* Z-ring dynamics during cell division and showed that like in *Escherichia coli* and B*acillus subtilis*, Z-ring filaments are able to move, presumably through treadmilling. Additionally, we found that cytokinesis is biphasic and starts with an initial slow step, dependent on FtsZ treadmilling, followed by a second faster step, independent of FtsZ treadmilling. Recruitment of the putative lipid II flippase to midcell (MurJ) corresponds to the turning point in cytokinesis between these two steps, with peptidoglycan synthesis providing additional force for the late stages of cell envelope constriction.

INTRODUCTION

Cell division is paramount for successful duplication of a mother cell into two daughter cells. In bacteria that divide through binary fission, cytokinesis comprises the inward constriction of the cellular envelope at midcell, through membrane invagination and peptidoglycan (PG) synthesis. The formation of the division septum is achieved through the activity of a dynamic macromolecular protein complex called the "divisome". In most walled bacteria, cell division is orchestrated by FtsZ, a tubulin homologue that, through GTP hydrolysis, assembles and disassembles in dynamic filaments in a head-to-tail fashion. During early stages of cell division, this cytoplasmic protein is attached to the inner side of the cellular membrane through membrane anchoring proteins, forming a Z-ring at midcell. The Z-ring then recruits several downstream proteins, many of them involved in PG synthesis, that promote inward incorporation of PG to divide the cellular compartment in two. As cell division likely occurs in a high turgor pressure environment (Osawa and Erickson, 2018), there is a need to exert an opposite, larger, force that counteracts turgor pressure. But despite many efforts, the origin of the force that drives cytokinesis is still a matter of debate. In the absence of cognate eukaryotic motor proteins, the observation that liposomes with membrane-anchored FtsZ are able to constrict powered the hypothesis that this protein can, when anchored to the membrane, pull the membrane inwards, presumably through bending (Osawa et al., 2008, Osawa and Erickson, 2011). Although the estimated force that FtsZ filaments could generate seems sufficient to constrict a membrane (Osawa and Erickson, 2018), in live cells this force needs to counteract a high turgor pressure (Xiao and Goley, 2016), which in Gram-positive

bacteria like *Staphylococcus aureus* is around 20 atm (Mitchell and Moyle, 1956, Whatmore and Reed, 1990). Another function of the Z-ring is to serve as a scaffold that recruits later divisome proteins like PG synthesis enzymes. Septal PG synthesis is also essential for cell division, as inhibition of divisome-specific penicillin-binding proteins (PBPs) leads to cell division impairment in several species (Pogliano et al., 1997, Daniel et al., 2000, Perez-Nunez et al., 2011, Coltharp et al., 2016). PG directional ingrowth could perhaps push the cellular membrane inwards, against turgor pressure, acting as the force that drives cytokinesis.

Recent reports in both Gram-negative and Gram-positive rod-shaped bacteria show that FtsZ GTPase activity is required for filament movement through treadmilling of Z-ring filaments (i.e. dynamic depolymerization through one end of the filament and polymerization through the other end) (Yang et al., 2017, Bisson-Filho et al., 2017). Importantly, in the Gram-positive *Bacillus subtilis*, the rate of treadmilling controls the rate of PG synthesis and cell division (Bisson-Filho et al., 2017), while in the Gram-negative bacteria *Escherichia coli* the rate of constriction does not change with lower treadmilling rates (Yang et al., 2017). Instead, FtsZ GTPase activity and treadmilling, are involved in the correct spatial organization of PG synthesis complexes along the cell circumference, important to achieve a homogeneous septum (Yang et al., 2017).

In this work we used *S. aureus* as a model to study the process of cytokinesis in bacteria using super-resolution structured illumination microscopy (SIM). *E. coli* and *B. subtilis* are rod-shaped cells that always place the division ring perpendicularly to the coverslip. Therefore, the full divisome ring can be only observed through 3D imaging or using complex

microscopy preparations to place the cell itself perpendicular to the slide. Unlike rod-shaped bacteria, the cocci *S. aureus* divides in three orthogonal planes and due to its near-spherical shape, *S. aureus* division rings can be observed in all orientations by 2D microscopy, enabling the easy observation of complete cytokinetic rings with higher resolution. We took advantage of this to study the dynamics of cytokinesis in Gram-positive bacteria.

EXPERIMENTAL PROCEDURES

Bacterial strains and growth conditions

All the strains and plasmids used in this study are listed in Table III.1. The sequences of the primers used are listed in Table III.2. *S. aureus* strains were grown in tryptic soy broth (TSB, Difco) at 200 r.p.m with aeration at 37 °C or on tryptic soy agar (TSA, Difco) at 30 or 37°C. *E. coli* strains were grown in Luria–Bertani broth (Difco) with aeration, or Luria–Bertani agar (Difco) at 37 or 30°C. When necessary, antibiotics ampicillin (100 μg/ml), erythromycin (10 μg/ml), kanamycin (150 μg/ml or 50 μg/ml when combined with neomycin) and neomycin (50 μg/ml) were added to the media. 5-bromo-4-chloro-3-indolyl β-D-galactopyranoside (X-gal, Apollo Scientific) was used at 100 μg/ml. Unless stated otherwise, isopropyl β-D-1-thiogalactopyranoside (IPTG, Apollo Scientific) was used at 0.5 mM to induce expression of constructs under the control of the P_{spac} promoter and cadmium chloride ($CdCl_2$, Sigma-Aldrich) was used at 0.1 μM when required to induce expression of constructs under the control of the P_{cad} promoter.

Table III.1 – Strains and plasmids used in this study.

Plasmids and strains	Relevant characteristics	Source or reference
Plasmids		
pNFtsZ-1	pMUTIN4 shuttle vector with P_{spac}-*rbs*-*ftsZ*truncated, Amp^r Ery^r	(Pinho and Errington, 2003)
pMUTIN4	pMUTIN4-P_{spac} shuttle vector that allows integrations in *S. aureus* genome by single crossover, Amp^r Ery^r	(Vagner et al., 1998)
pMutinYFPKan	pMUTIN4- plasmid with *yfp* downstream of P_{spac} and kan^r cassette, Amp^r Kan^r	(Atilano et al., 2010)
pMUTIN4kan	pMUTIN4 plasmid where ery^r cassette was substituted for kan^r, Amp^r Kan^r	(Pereira and Pinho, unpublished)

pNFtsZ-1KAN	pMUTIN4 plasmid with P_{spac}-*rbs*-*ftsZ*truncated, Amp^r Kan^r	This work
pBCB13	pMAD derivative with up- and downstream regions of the *spa* locus and P*spac-lacI*, Amp^r Ery^r *lacZ*	(Pereira et al., 2010)
pCN51	Replicative vector containing a cadmium inducible P*cad* promoter; Amp^r Ery^r	(Charpentier et al., 2004)
pBCB33	pBCB13-P_{cad} plasmid, Amp^r Ery^r	(Reichmann and Pinho, unpublished)
pBCB33-FtsZ	pBCB13-P_{cad}-FtsZ, Amp^r Ery^r	This work
pBCB33-Neon-Z	pBCB13-P_{cad}-mNeonGreen-15aaBS-FtsZ, Amp^r Ery^r	This work
pTRC99a-P7	Vector containing *sgfp-p7*; Amp^r	(Fisher and DeLisa, 2008)
pCNX	Replicative vector containing the cadmium inducible P*cad* promoter; Amp^r Kan^r	(Monteiro et al., 2015)
pCN-FtsZ$^{55\text{-}56}$sGFP	pCNX derivative with P_{cad}- FtsZ$^{55\text{-}56}$-sGFP sandwich fusion; Amp^r Kan^r	This work
pSG5082	*S. aureus* integrative vector that allows for C-terminal *gfpmut*P2 fusions; Amp^r Ery^r	(Pinho and Errington, 2004)
pSG-ezrA	pSG5082 derivative containing a 3´fragment of *ezrA*; Amp^r Ery^r	This work
S. aureus		
COL	HA-Methicillin Resistant *Staphylococcus aureus* (MRSA) strain	(Gill et al., 2005)
RN4220	Restriction-deficient derivative of NCTC8325-4	(Nair et al., 2011)
COLΔEzrA	COL with *ezrA* gene deleted	(Jorge et al., 2011)
ColpSGEzrA-GFP	COL*ezrA-gfp*; pSG-ezrA integrated by single crossover; Ery^r	This work
RNpFtsZ-1	RN4220 *ftsZ*::P_{spac}-*ftsZ*, pNFtsZ-1 integrated by single crossover; Ery^r	(Pinho and Errington, 2003)
RN4220 P_{spac}-FtsZkan	RN4220 *ftsZ*::P_{spac}-*ftsZ*, pNFtsZ-1KAN integrated by single crossover; Kan^r	This work
RN4220 P_{spac}-FtsZ + Z	RN4220 *ftsZ*::P_{spac}-*ftsZ* pBCB33-FtsZ. pNFtsZ-1Kan integrated by single crossover and replicative pBCB33-FtsZ; Ery^r Kan^r IPTG	This work

RN4220Δ*spa*::P$_{cad}$-*neon-ftsZ*	RN4220 with mNeonGreen-15aaBS-FtsZ expressed from spa locus, under the control of the P$_{cad}$ promoter	This work
ColFtsZ$^{55\text{-}56}$-sGFP	COL pCN-ftsZ$^{55\text{-}56}$sGFP, sandwich *ftsZ* fusion expressed from P$_{cad}$ inducible replicative plasmid	This work
RN4220 P$_{spac}$-FtsZ + Z$^{55\text{-}56}$sGFP	RN4220 *ftsZ*::P$_{spac}$-*ftsZ* pBCB33-FtsZ; pNFtsZ-1 integrated by single crossover and replicative pBCB33-FtsZ$^{55\text{-}56}$-sGFP; Ery^{r} Kan^{r} IPTG	This work
ColFtsW-sGFP	COL *ftsW*::*ftsW-sgfp*	(Monteiro et al., 2018)
ColMurJ-sGFP	COL *murJ*::*murJ-sgfp*	(Monteiro et al., 2018)
ColWgZm	COL *ftsW*::*ftsW-sgfp*, Δ*spa*::P*spac-ftsZ-mcherry*	(Monteiro et al., 2018)
ColJgZm	COL *murJ*::*murJ-sgfp*, Δ*spa*::P*spac-ftsZ-mcherry*	(Monteiro et al., 2018)

Table III.2 – Primers used in this study. Underlined sequences correspond to restriction sites. Bold highlighting corresponds to *rbs* sequences.

Primer Name	Sequence (5'-3')
IVP25	GACTACGCCATGGGTTCATGTAATCACTCCTTC
IVP26	GCGAGATCTGGAAATAATTCTATGAGTCGC
P1_pBCB33	GCCGAATTCGCATGCGCACTTATTCAAGTG
P2_pBCB33	GCCGCTAGCTACTCGAGTACCCGGGTGCAGGTTCAGACATTGAC
P1_Z	GCTTTTCCCGGG**AGGAGG**TACCTTATGTTAGAATTTGAACAAG
P2_Z	GCTGCCTCGAGTTAACGTCTTGTTCTTCTTGAACG
ftsZswgfp_pCNX_P1	TCTAGAGGATCC**AGGAGG**TACCTTATGTTAGAATTTGAACAAGG
ftsZswgfp_pCNX_P2	ACCTCCGCCAGAACCGCCTCCACCAGCTTTAGATAAGTTTAAAGC
ftsZswgfp_pCNX_P3	TGGAGGCGGTTCTGGCGGAGGTGGCTCTAGTAAAGGAGAAGAAC TTTT
ftsZswgfp_pCNX_P4	CCGCCGCCACCAGACCCACCACCGCCGTCGACTTTGTATAGTTCAT
ftsZswgfp_pCNX_P5	TGGTGGGTCTGGTGGCGGCGGATCTGAATCTAAAATCCAAATCGG
ftsZswgfp_pCNX_P6	GCGCCTGAATTCTTAACGTCTTGTTCTTCTTGAAC
ezrAP8Kpn	CGGGTACCCGATATAGCGAGGTTCAGG
ezrAP9Xho	CGCTCGAGTTGCTTAATAACTTCTTCTTC

Strain construction

Strain ColFtsZ$^{55-56}$-sGFP was constructed using the pCNX replicative plasmid (Monteiro et al., 2015) to express an FtsZ-sGFP sandwich fusion. In brief, three DNA fragments (F1, F2 and F3) with overhangs were amplified in order to construct a *sgfp* fusion inserted within the *ftsZ* coding sequence between codons 55 and 56 (Moore et al., 2017), flanked by 10 amino acid linkers on each side (GGGGSx2). F1, containing a *rbs* and the first 165 bp of *ftsZ*, was amplified from COL DNA using primers ftsZswgfp_pCNX_P1 and ftsZswgfp_pCNX_P2; F2, containing *sgfp* flanked by linker sequences, was amplified from pTRC99a-P7 using primers ftsZswgfp_pCNX_P3 and ftsZswgfp_pCNX_P4; F3, containing the remaining 1008 bp of *ftsZ* (from nucleotide 166 onwards), was amplified from COL DNA using primers ftsZswgfp_pCNX_P5 and ftsZswgfp_pCNX_P6. The three fragments were joined by overlap PCR, digested with BamHI/EcoRI and ligated into pCNX digested with the same enzymes. The ligation mix was used to transform competent DC10B *E. coli* cells and the correct insert was confirmed by sequencing, giving pCN-FtsZ$^{55-56}$sGFP plasmid. Electroporation of the pCN-FtsZ$^{55-56}$sGFP plasmid to electrocompetent RN4220 cells was performed as previously described (Veiga and Pinho, 2009) and the plasmid was then transduced into COL using phage 80α (Oshida and Tomasz, 1992), resulting in strain ColFtsZ$^{55-56}$-sGFP.

To test functionality of the sandwich FtsZ$^{55-56}$-sGFP construct, plasmid pCN-FtsZ$^{55-56}$sGFP was transduced into *ftsZ* inducible strain RNpFtsZ-1 (Pinho and Errington, 2003), generating strain RN4220 Pspac-FtsZ+Z$^{55-56}$sGFP, selected with erythromycin, kanamycin/neomycin and IPTG 0.5 mM at 30°C.

Construction of RN4220 Pspac-FtsZ + Z was perfomed as follows. First we constructed pBCB33-FtsZ, a plasmid expressing *ftsZ* ectopically from a cadmium inducible promoter. This was performed by amplifying a nucleotide sequence comprising a *rbs* and a full length *ftsZ* from *S. aureus* strain COL using primers P1_Z and P2_Z. This product was then digested with SmaI and XhoI restriction enzymes and cloned in pBCB33 plasmid (see below) generating plasmid pBCB33-Z. pBCB33 plasmid is a derivative of the thermosensitive pMAD based pBCB13 plasmid (Pereira et al., 2010), replicative at 30°C, where the P_{spac} promoter and regulatory regions were substituted for the cadmium inducible P_{cad} promoter from pCN51 (Charpentier et al., 2004). To construct pBCB33, the P_{cad} promoter and regulatory regions were amplified using primers P1_pBCB33 and P2_pBCB33 and the pCN51 DNA as template. Then P_{spac} and its regulatory sequences were removed from pBCB13 plasmid by digestion with EcoRI and NheI, followed by purification through gel excision. Then the purified pBCB13 without P_{spac} was ligated to the P_{cad} insert generating the pBCB33 (pBCB13-P_{cad}) plasmid (Reichmann, N. and Pinho, MG., unpublished). Because the pBCB33-FtsZ plasmid harbors an erythromycin resistance marker, the pMutin4 erythromycin resistance marker was substituted by a kanamycin resistance marker. pMUTIN4kan plasmid was constructed by Pereira, P.M. and Pinho, M.G., (unpublished), where the pMUTIN4 (Vagner et al., 1998) erythromycin-resistance cassette was substituted for the kanamycin-resistance cassette from pMutinYFPKan plasmid (Atilano et al., 2010). For that purpose primers IVP25 and IVP26 were used to amplify by PCR the entire pMutin4 plasmid, excluding the erythromycin marker, and the resulting product was digested with NcoI and BglII. Plasmid pMutin4YFPKan was also digested with NcoI and BglII in order to extract the 1.5 kb kanamycin cassette, which was separated

by agarose gel electrophoresis and purified by gel extraction. The kanamycin marker was then ligated to pMutin4 deprived of the erythromycin cassette, originating plasmid pMUTIN4Kan. To construct pNFtsZ-1KAN, the 480 bps insert of pNFtsZ-1, which contain the *rbs* and a truncated *ftsZ* was obtained by digesting the plasmid with BamHI and EcoRI, followed by purification of the insert by gel extraction. The insert was then ligated to pMUTIN4kan plasmid, giving rise to plasmid pNFtsZ-1KAN. The plasmid was electroporated into RN4220 giving rise to strain RN4220 P_{spac}-FtsZkan. Finally, to construct strain RN4220 Pspac-FtsZ + Z, plasmid pBCB33-FtsZ was transduced (Oshida and Tomasz, 1992) to RN4220 P_{spac}-FtsZkan strain using erythromycin; kanamycin/neomycin and IPTG 0.5 mM selection at 30°C.

The *S. aureus* N-terminal Neon-FtsZ derivative was constructed using the same linker and fluorescent protein amino acid sequence as the *B. subtilis* Neon-FtsZ described by Bisson-Filho and colleagues (Bisson-Filho et al., 2017). The *mNeonGreen* nucleotide sequence (Shaner et al., 2013) was codon optimized for *S. aureus* by the ATUM company® (California, USA) and the new nucleotide sequence can be consulted in Annex 1. In more detail, to construct an *S. aureus* Neon-FtsZ fusion, the insert DNA sequence comprising SmaI-*rbs*-*mNeonGreen*-15aaBS-*ftsZ*-XhoI was synthesized by NZYtech. The insert was then digested with SmaI and XhoI and cloned in pBCB33 plasmid originating pBCB33-Neon-Z plasmid. The sequence of the pBCB33-Neon-Z insert was confirmed by sequencing and the plasmid was electroporated to RN4220, where through integration and excision of the plasmid at the *spa* locus, it originated strain RN4220Δ*spa*::P_{cad}-*neon-ftsZ*. To test functionality of the Neon-FtsZ fluorescent construct the pBCB33-Neon-Z plasmid was

transduced into strain RN4220 P_{spac}-FtsZkan generating strain RN4220 P_{spac}-FtsZ + Neon-Z, selected using erythromycin, kanamycin/neomycin and IPTG 0.5 mM at 30°C.

To construct ColpSGEzrA-GFP, the last 564bps of *ezrA* without the stop codon were amplified from *S. aureus* COL genome using primers ezrAP8Kpn and ezrAP9Xho, digested with KpnI and XhoI and cloned in the pSG5082 vector (Pinho and Errington, 2004) originating plasmid pSG-ezrA which was sequenced, electroporated to RN4220 and transduced to COL.

Functionality test for FtsZ fluorescent constructs

Strains RN4220 P_{spac}-FtsZ + Z; RN4220 Pspac-FtsZ + Neon-Z and RN4220 P_{spac}-FtsZ + Z $^{55\text{-}56}$-sGFP were grown overnight in TSB plus erythromycin 10 µg/ml, kanamycin 150 µg/ml and IPTG 0.5 mM. Cultures were diluted 1/200 into fresh TSB supplemented with IPTG 0.5 mM and $CdCl_2$ 0.1 µM and incubated at 30 °C with aeration. When cultures reached an OD_{600nm}~0.4, ten microliters of 10^0, 10^{-2}, 10^{-4} and 10^{-6} dilutions were spotted on TSA containing erythromycin 10 µg/ml; kanamycin 150 µg/ml and either no inducers (no *ftsZ* is induced), IPTG 0.5 mM (native *ftsZ* induced) or $CdCl_2$ (ectopic *ftsZ* allele induced using either 0.1; 0.5; 1; 2; 3; 4; and 5 µM of cadmium). Plates were incubated for two days at 30 °C.

Cell cycle analysis in the presence of cell division inhibitors

An overnight culture of *S. aureus* strain COL was back-diluted 1/200 and grown until OD_{600nm} ~ 0.4 at which point either DMPI (3 µg/ml, gift from Merck), PC190723 (2.5 µg/ml, Merck Millipore), oxacillin (1000 µg/ml, Sigma-Aldrich), or DMSO (0.2 %, Sigma) were added to the medium. Cells were then grown for 30 minutes with each inhibitor,

harvested and labelled with Nile Red, as described above, before being imaged by SIM. Cells were classified into each phase of the cell cycle, as previously described (Monteiro et al., 2015).

Protein analysis by Western blot and fluorescence

S. aureus strains COL and ColFtsZ$^{55\text{-}56}$-sGFP were grown overnight in TSB and TSB containing kanamycin 150 µg/ml. Both cultures were then back-diluted 1/200 in fresh TSB or TSB supplemented with 0.05 µM or 0.1 µM of $CdCl_2$. Cultures were incubated at 37°C until an OD_{600nm} of approximately 0.8 and cells were collected and broken with glass beads in a FastPrep FP120 cell disrupter (Thermo Electron Corporation). Samples were centrifuged to remove unbroken cells and debris and total protein content of the clarified lysates was determined using the Bradford method and bovine serum albumin as a standard (BCA Protein Assay Kit, Pierce). Twenty micrograms of nonboiled total protein from each sample were loaded on one 8% SDS-PAGE gel and another 20 µg from each sample were boiled and loaded on another 8% SDS-PAGE. Proteins were separated at 80V until the methylene blue was near the end of the gel. The gel containing the nonboiled samples was used to observe sGFP protein fluorescence, detected by a Fuji FLA-5100 reader, using a 473 nm laser. The gel containing boiled protein samples was used for Western blot detection of FtsZ. For this purpose, the gel was transferred to a Hybond-P PVDF membrane (GE Healthcare) using a Semi-dry transfer cell (Biorad), at 10 V for 1 hour. The membrane was then blocked with blocking buffer (PBS; 5% milk; 0.5% Tween 20) for 1 h and incubated with an anti-FtsZ antibody diluted 1/5000 in blocking buffer for 16 h at 4 °C. The membrane was washed three times with PBS-T (PBS containing 0.5% Tween 20) and incubated with secondary antibody (HRP

anti-sheep diluted 1/50,000 for FtsZ detection, Pierce). The detection was performed using an ECL Plus Western blotting detection system (Amersham) according to the manufacturer's guidelines. FtsZ protein band densities were calculated using Quantity One free version (BioRad).

S. aureus imaging by structured illumination microscopy (SIM)

Super-resolution SIM imaging was performed using an Elyra PS.1 microscope (Zeiss) with a Plan-Apochromat 63x/1.4 oil DIC M27 objective. Images were acquired using five phase shifts, either three or five grid rotations, with 34 µm grating period for the 561 nm laser (100 mW), 28 µm period for 488 nm laser (100 mW) and 23 µm period for 405 nm laser (50 mW). Images were captured using a Pco.edge 5.5 camera and reconstructed using ZEN software (black edition, 2012, version 8.1.0.484) based on a structured illumination algorithm, using synthetic, channel specific optical transfer functions and noise filter settings ranging from −6 to −8.

Sample mounting procedure for time lapse microscopy

For time-lapse experiments, all cultures were grown overnight in TSB. For ColFtsZ$^{55\text{-}56}$-sGFP the media was supplemented with kanamycin 150 µg/ml and for strain ColpSGEzrA-GFP with erythromycin 10 µg/ml. Overnight cultures were diluted 1/200 in fresh TSB media without antibiotic but supplemented with appropriate inducers ($CdCl_2$ 0.1 µM for ColFtsZ$^{55\text{-}56}$-sGFP and RN4220Δ*spa*::P_{cad}-*neon-ftsZ*; IPTG 0.5mM for ColWgZm and ColJgZm). After being harvested, cells were re-suspended in M9 microscopy media (KH_2PO_4 3.4 g/l, VWR; K_2HPO_4 2.9 g/l, VWR; di-ammonium citrate 0.7 g/l, Sigma-Aldrich; sodium acetate 0.26 g/l, Merck; Glucose 1 %, Merck; $MgSO_4$ 0.7 mg/l, Sigma-Aldrich; $CaCl_2$ 7 mg/l, Sigma-

Aldrich; casaminoacids 1 %, Difco; MEM amino acids 1X, Thermo Scientific; MEM vitamins, 1X Thermo Scientific). The media was supplemented when required with IPTG (0.5 mM), $CdCl_2$ (0.1 µM), DMPI (8 µg/ml) or PC190723 (5 µg/ml). Cultures were then spotted on a pad of 1.5 % agarose in the same supplemented media and mounted in a geneframe (Thermo Scientific) on a microscope slide. The time it took between the cells contacting the pad and the start of acquisition was 5 min in all conditions.

Imaging of FtsZ$^{55\text{-}56}$-sGFP treadmilling by SIM

To visualise FtsZ$^{55\text{-}56}$-sGFP movement in strain ColFtsZ$^{55\text{-}56}$-sGFP, and EzrA-GFP movement in strain ColpSGEzrA-GFP, 50 frames of SIM images were acquired with 5 second intervals (total time of acquisition of 250 seconds) using the 488 nm laser at 50% and a 50 msec exposure time. Following this acquisition, for FtsZ, a short timelapse of 3 images taken 15 minutes apart was acquired to check if the corresponding rings were constricting. These experiments were performed with and without PC190723 at 5 µg/ml. To analyse FtsZ or EzrA movement, the 50 frames were aligned and 1 pixel lines were manually drawn over the rings and then plotted in a kymograph.

Visualisation of divisome ring constriction by SIM

In order to follow FtsZ$^{55\text{-}56}$-sGFP or EzrA-GFP ring constriction over time, ColFtsZ$^{55\text{-}56}$-sGFP or ColpSGEzrA-GFP dividing cells were imaged by SIM every 5 minutes for 1 hour using the 488 nm laser at 50% power and a 50 msec exposure time. These experiments were performed with and without PC190723 (5 µg/ml; laser power 50%) and with DMPI for FtsZ only (8 µg/ml; laser power 100%). Following SIM image reconstruction, cropped stacks containing individual cells were used to

plot Z-ring constriction kymographs over the 1 hour period by drawing a 3 pixel line across the diameter of the cell, crossing the fluorescent signal, using Fiji software (Schindelin et al., 2012). The percentage of cells for which the FtsZ ring did not constrict, constricted with defects or constricted in relation to their initial ring size, in the presence of PC190723, was plotted using GraphPad Prism 6.

In order to follow constriction of FtsW-sGFP and MurJ-sGFP rings in strains ColFtsW-sGFP and ColMurJ-sGFP respectively, cultures were spotted on an M9 microscopy medium pad, with and without PC190723, and imaged by SIM. The 488 nm laser was used at 100% intensity, with an exposure time of 50 msec. To decrease photodamage due to high laser power, images were acquired every 10 min (instead of 5 min) during 1 hour. These settings were also applied for ColFtsZ$^{55\text{-}56}$-sGFP for comparison. For MurJ-sGFP, timelapses were also performed with a 5 min interval to confirm the absence of biphasic behaviour of the constricting ring. Only cells with MurJ-sGFP signal absent in the first frame but present in the second frame were analysed to ensure that the entire constriction process was observed. Following SIM image reconstruction, cropped stacks containing individual cells were used to plot constriction kymographs as described above.

Timelapse stacks obtained from imaging ColFtsZ$^{55\text{-}56}$-sGFP, ColFtsW-sGFP and ColMurJ-sGFP in the presence of PC190723 were used to count the number of cells that had the fluorescently labelled protein at midcell in the first frame and determine the percentage of those cells that constricted, constricted with defects or did not constrict in the presence of PC190723 for 60 min. Data was plotted using GraphPad Prism 6.

To observe constriction of FtsW-sGFP and MurJ-sGFP rings in cells expressing FtsZ-mCherry, strains ColWgZm and ColJgZm were grown overnight in TSB and then diluted 1/200 into TSB plus IPTG 0.1mM at 37°C. Once the OD_{600nm} reached ~0.6, cells were pelleted and resuspended in M9 supplemented with IPTG 0.1mM. Cells were then imaged by SIM every 10 min for 1 h, using the 488 nm laser and the 561 nm laser (100% laser power, 50 msec and 50% laser power, 50 msec respectively). Cells of ColWgZm where FtsZ-mCherry showed biphasic constriction behaviour, and cells of ColJgZm where MurJ-sGFP signal appeared on the third frame, were used to measure the ring diameter for each protein in all frames.

Functionality test for EzrA-GFP construct

Strains COL and COLΔEzrA were grown overnight in TSB and strain ColpSGEzrA-GFP was grown in TSB plus erythromycin at 37°C with aeration. Overnight cultures were diluted 1/200 in fresh TSB and incubated at 37°C with aeration. Once the OD_{600nm} reached ~0.6, cells were pelleted, resuspended in PBS and spotted on a thin layer of 1.2% agarose in PBS. Cultures were imaged by phase-contrast, single cells were identified and cell area measured using eHooke (see below), as lack of EzrA results in the appearance of larger cells (Jorge et al., 2011).

The eHooke software (Monteiro et al., 2018) performs automatic cell segmentation by using the phase-contrast images and applies the isodata algorithm (Velasco, 1980) for automatic thresholding to find a pixel intensity value that separates the pixels corresponding to the background from those corresponding to cells. Using this threshold, the software then creates a binary mask which is used to compute the Euclidean distances (Falcão et al., 2004) of each pixel in order to find the

centres of individual regions inside the mask. The software then expands those centres to define individual cell regions using the watershed algorithm (Roerdink and Meijster, 2000). In order to measure cell areas, eHooke first defines each individual cell region and computes the area by counting the number of pixels inside the region.

RESULTS

S. aureus cell division cycle can be divided in three phases, relative to the progression of the division septum: newborn cells which have not initiated septum synthesis (Phase 1); cells undergoing septum synthesis (Phase 2), and cells with a closed septum (Phase 3) which then quickly split into two daughter cells (Monteiro et al., 2015). We envisioned that if we inhibit either FtsZ treadmilling or PG synthesis we could pinpoint the importance of these processes in cell cycle progression. To stop FtsZ treadmilling we incubated *S. aureus* strain COL cells with PC190723 (Haydon et al., 2008), shown to inhibit treadmilling of FtsZ in *B. subtilis* (Bisson-Filho et al., 2017). To inhibit PG synthesis redirection to midcell (Monteiro et al., 2018) we incubated COL cells with the MurJ inhibitor DMPI (Huber et al., 2009). To block the final stages of PG polymerization we incubated COL cells with oxacillin, an inhibitor of PG transpeptidation, performed by penicillin-binding proteins (PBPs). To assess the distribution of cells in each cell cycle phase, *S. aureus* strain COL was incubated with each antibiotic for the duration of one cell cycle and the distribution of cells in the three phases of the cell cycle was analyzed. Consistent with previous data (Monteiro et al., 2015) in the absence of inhibitors, approximately half (58% ± 2.4) of the cells were in Phase 1, with the other half split evenly between Phase 2 (21% ± 4.1) and Phase 3 (21% ± 2) (Figure 1). In the presence of DMPI, we observed a striking accumulation of cells without a septum (Phase 1, 70% ± 1.5), showing that MurJ is crucial to start septum synthesis and enter in Phase 2. Additionally, incubation with DMPI did not change the frequency of Phase 2 cells (26% ± 2.2), indicating that PG synthesis is required to complete septum synthesis. The late PG synthesis inhibitor oxacillin led to an

increase of the proportion of cells in Phase 2 (37% ± 4.6) and Phase 3 (27% ± 4.6), concomitant with a decrease in the proportion of cells in Phase 1 (36% ± 2.5), showing that PBP activity is mostly required for septum synthesis during Phase 2, but not for Phase 1 entry (Figure 1). When *S. aureus* cells were incubated with the FtsZ inhibitor PC190723, there was an increase in the number of cells in Phase 1 (94% ± 2), a result in agreement with FtsZ importance to start cell division. However, PC190723 incubation led to an almost complete absence of Phase 2 cells (3.5% ± 1) (undergoing septum synthesis), in contrast with the PG synthesis inhibitor DMPI. As this compound inhibits FtsZ treadmilling in *B. subtilis* and FtsZ treadmilling rate was shown to control the rate of cell division of this organism (Bisson-Filho et al., 2017), one would expect that addition of PC190723 would prevent cells that were halfway through the process of septum synthesis from completing this process. As this was not the case, we wondered if either *S. aureus* FtsZ filaments did not undergo treadmilling, if PC190723 compound did not inhibit FtsZ treadmilling in *S. aureus* or if FtsZ treadmilling in this organism was not essential for septum synthesis progression.

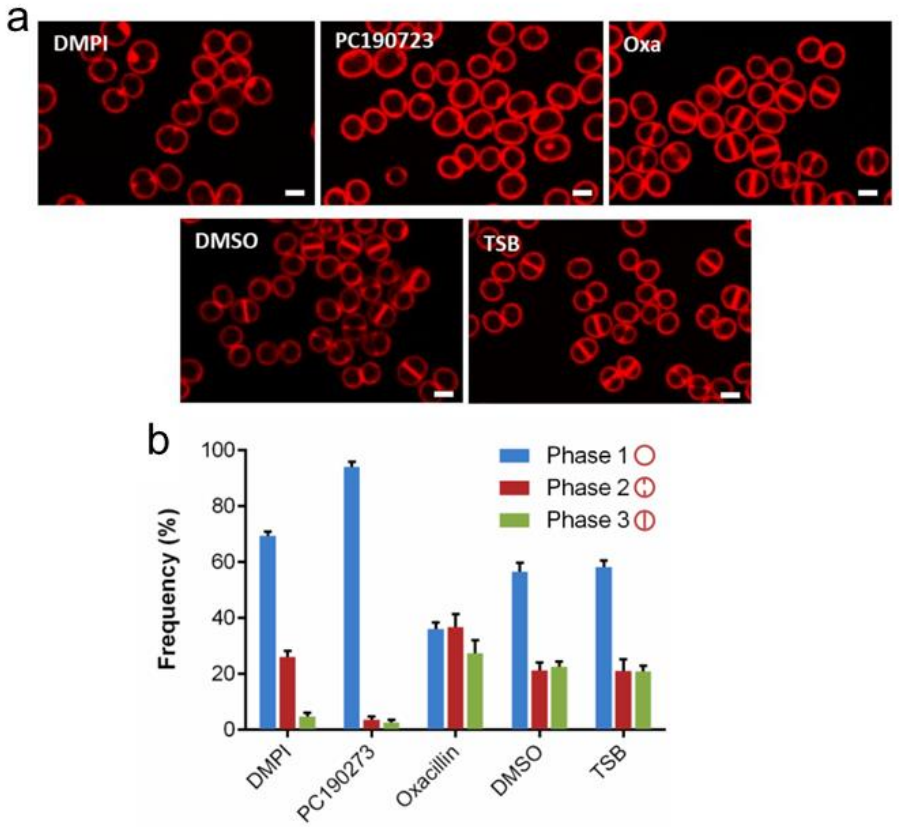

Figure 1: Effect of cell division inhibitors on *S. aureus* COL cell cycle. (a) COL cells treated with DMPI (MurJ inhibitor), PC190723 (FtsZ inhibitor), oxacillin (cell wall synthesis inhibitor), DMSO or TSB (mock controls) for the duration of a cell cycle (30 min) were stained with the membrane dye Nile Red and imaged by SIM. **(b)** Cells in the different conditions were classed by cell cycle Phase and are represented as a percentage of the total population (N> 500). The height of the graph column represents the mean and the whiskers are the standard deviation. Scale bars 1 μm.

Construction of FtsZ fluorescent derivatives

To test if FtsZ filaments treadmill in live *S. aureus*, we aimed to construct a functional fluorescent derivative of this protein. For that we constructed two fluorescent FtsZ derivatives, a N-terminal mNeonGreen fusion to FtsZ (Neon-Z), equivalent to a fusion shown to be functional in

B. subtilis (Bisson-Filho et al., 2017), and an sGFP sandwich fusion FtsZ$^{55-56}$-sGFP, equivalent to a fusion functional in *E. coli* where sGFP is placed between FtsZ amino acids 55 and 56, flanked by linkers (Moore et al., 2017). To test the functionality of these fluorescent derivatives we designed an expression system in *S. aureus* where expression of native FtsZ is under the control of an IPTG inducible P_{spac} promoter at the native locus and a fluorescent derivative or a second copy of native FtsZ, is expressed from a multicopy plasmid, under the control of the cadmium inducible P_{cad} promoter. By analysing growth in solid agar of the strain RN4220 P_{spac}-FtsZ + Z (which has two copies of native FtsZ) in the absence of IPTG (to prevent expression of *ftsZ* from the native locus) but in the presence of cadmium (to induce the expression of plasmid-encoded *ftsZ*), we confirmed that cellular growth was restored when FtsZ was ectopically produced, but only at $CdCl_2$ concentrations above 5 μM (Figure 2). We then tested growth on solid media of strains expressing either the N-terminal Neon-Z or the sandwich FtsZ$^{55-56}$-sGFP fluorescent derivatives (strains RN4220 P_{spac}-FtsZ + Neon-Z and RN4220 P_{spac}-FtsZ + Z$^{55-56}$-sGFP, respectively). Only FtsZ$^{55-56}$-sGFP was marginally functional (Figure 2). We therefore chose to proceed with the FtsZ$^{55-56}$-sGFP derivative and transduced the plasmid that harbors the FtsZ sandwich fusion into *S. aureus* strain COL, creating the merodiploid strain ColFtsZ$^{55-56}$-sGFP.

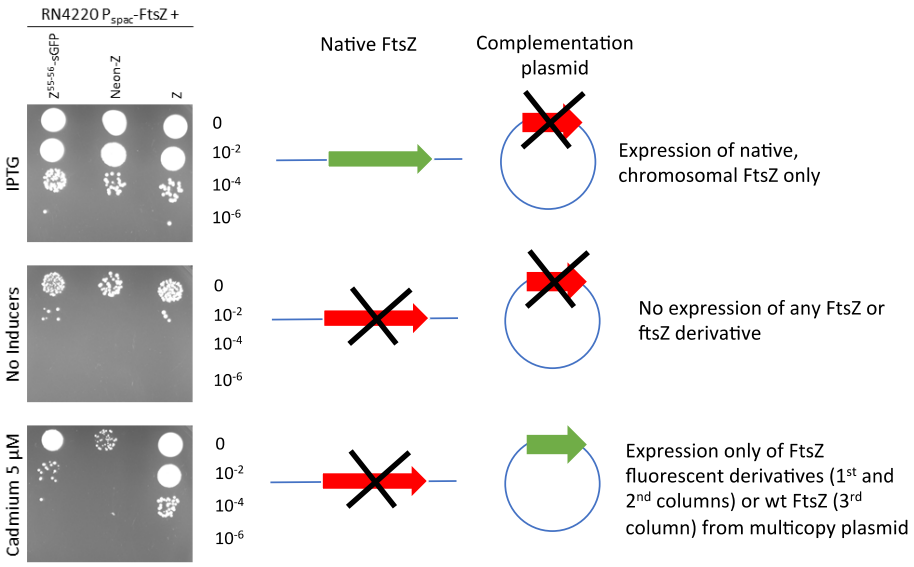

Figure 2: Test of functionality of FtsZ fluorescent derivatives. All strains tested have *ftsZ* under the control of the IPTG inducible P_{spac} promoter at the native chromosomal locus. Strain RN4220 P_{spac}-FtsZ + Z^{55-56}-sGFP (left), RN4220 P_{spac}-FtsZ + Neon-Z (middle) and RN4220 P_{spac}-FtsZ + Z (right), expressed the sandwich fluorescent derivative $FtsZ^{55-56}$-sGFP, the Neon-FtsZ N-terminal fusion or the FtsZ WT protein, respectively, from a multicopy plasmid under the control of the cadmium inducible P_{cad} promoter. In the presence of cadmium alone, only FtsZ WT could fully complement growth. However, the FtsZ sandwich fusion $FtsZ^{55-56}$-sGFP enables slightly more growth on the cadmium plate than the Neon-Z fusion, indicating that it may be partially functional.

We confirmed that ColFtsZ$^{55-56}$-sGFP strain produced a FtsZ$^{55-56}$-sGFP fluorescent derivative that was not cleaved when protein expression was induced by cadmium (Figure 3a). Western blot analysis indicated that the fluorescently tagged FtsZ$^{55-56}$-sGFP protein is produced at approximately the same amount as the native protein FtsZ when induced with 0.1 µM of cadmium (Figure 3b, lane 4).

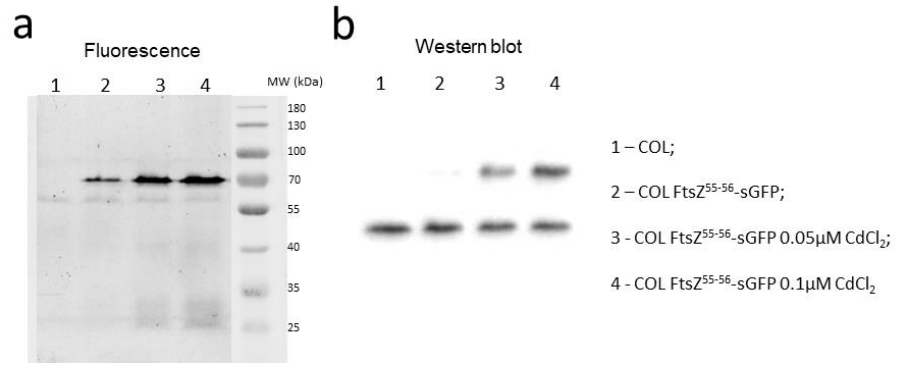

Figure 3: Protein fluorescence detection and expression levels of FtsZ$^{55-56}$-sGFP in strain ColFtsZ$^{55-56}$-sGFP. (a) FtsZ$^{55-56}$-sGFP protein fluorescence detected by imaging protein extracts separated by SDS-PAGE. Unboiled protein extracts of COL (lane 1); ColFtsZ$^{55-56}$-sGFP strain grown without cadmium (lane 2), with 0.05 μM of $CdCl_2$ (lane 3) and with 0.1 μM of $CdCl_2$ (lane 4) showed increased expression of the fluorescent protein derivative (band appearing at 70 kDa). FtsZ$^{55-56}$-sGFP predicted molecular weight is 70 kDa and sGFP runs as a 35 kDa protein in nonboiled samples. In all conditions only one band with the expected molecular weight of FtsZ$^{55-56}$-sGFP and no band corresponding to sGFP alone was observed, confirming the integrity of the fluorescent derivative**. (b)** Western blot against FtsZ of boiled protein extracts where native FtsZ is detected in all samples (lower bands) and sGFP-FtsZ$^{55-56}$-sGFP (upper bands) is detected when the culture was induced with 0.05 μM of $CdCl_2$ (lane 3) and with 0.1 μM of $CdCl_2$ (lane 4). Induction with 0.1 μM of $CdCl_2$ (lane 4) results in approximately the same amounts of FtsZ$^{55-56}$-sGFP and native FtsZ proteins.

FtsZ filaments move bidirectionally in *S. aureus*

Movement of FtsZ filaments through treadmilling has been recently reported in *E. coli* (Yang et al., 2017) and *B. subtilis* (Bisson-Filho et al., 2017). Importantly, in *B. subtilis* incubation with the PC190723 compound (Haydon et al., 2008) caused FtsZ movement to stop (Bisson-Filho et al., 2017). To determine if FtsZ filament movement also occurred in *S. aureus*, we imaged strain ColFtsZ$^{55-56}$-sGFP every 5 seconds by structured illumination microscopy (SIM) for a total of 250 seconds, followed by imaging of the cells every 15 min to evaluate Z-ring constriction. These experiments were performed in the absence and in

the presence of PC190723. Drawing a line over the fluorescence signal and plotting the fluorescence intensity distribution of those pixels over the course of the experiment generates a kymograph that facilitates the identification of the presence (when diagonal lines are observed) or absence (if vertical lines are observed) of movement of FtsZ filaments. Indeed, we observed FtsZ$^{55\text{-}56}$-sGFP filaments moving bidirectionally in the absence of PC190723 (Figure 3a, kymographs showing diagonal lines in both directions). This movement was especially evident in the next plane of cell division (diagonal lines in Figure 4a, lower kymograph). FtsZ filament motion was stopped by addition of the FtsZ GTPase inhibitor PC190723 (vertical lines in Figure 4b). The most surprising result was that rings where the FtsZ filament movement was stopped by PC190723 were still able to constrict (Figure 4b, time-lapse snapshots).

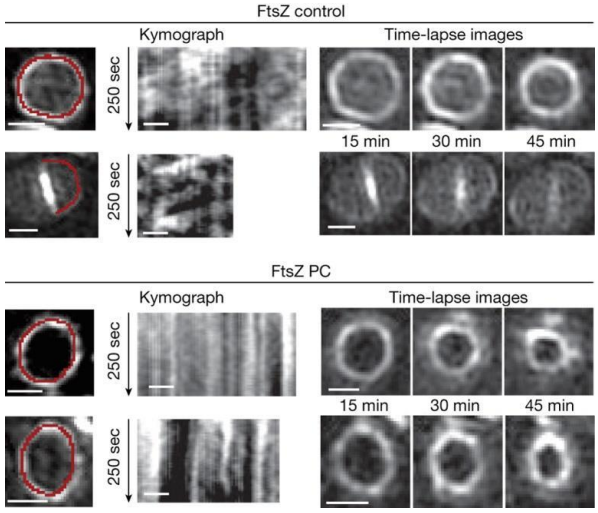

Figure 4: PC190723 impairs FtsZ$^{55\text{-}56}$-sGFP treadmilling in *S. aureus*. ColFtsZ$^{55\text{-}56}$-sGFP cells were imaged by SIM every 5 sec for 250 sec, followed by three images taken 15 minutes apart. Kymographs were obtained by extracting fluorescence intensity values along the red line indicated in cells in left panels, with each horizontal line of the kymograph corresponding to one time point. **(a)** In the absence of PC190723, FtsZ movement is observed, leading to diagonal

lines in the kymograph. **(b)** Addition of PC190723 (5 µg/ml) abolished FtsZ movement, resulting in vertical lines in the kymograph that correspond to maintenance of signal at fixed locations, but did not impair Z-ring constriction (timelapse on the right). Scale bars, 0.5 µm.

We also tested FtsZ treadmilling using the mNeonGreen N-terminal fusion (Neon-Z), expressed ectopically from the *spa* locus in RN4220Δ*spa*::P_{cad}-*neon-ftsZ* strain. Neon-Z filament motion was also observed in the absence, but not in the presence of PC190723 (Figure 5).

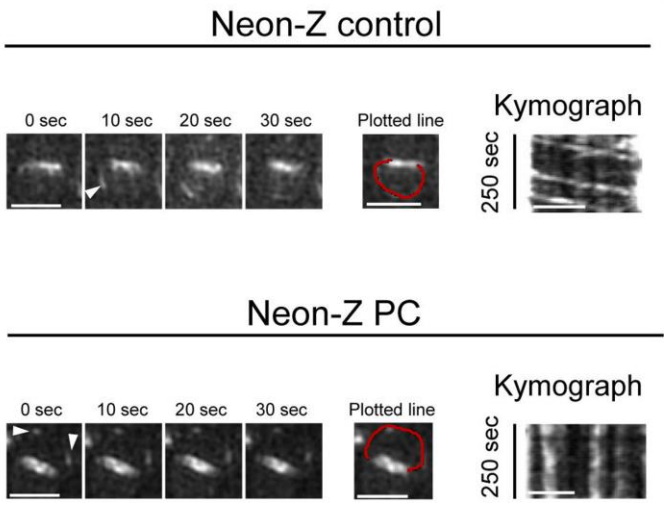

Figure 5: N-terminal fusion of Neon-FtsZ shows bidirectional movement, stopped by PC190723 in *S. aureus*. RN4220Δ*spa*::P_{cad}-*neon-ftsZ* cells were imaged by SIM every 5 sec, in the absence (Neon-Z control) or presence (Neon-Z PC) of 5 µg/ml of PC190723. Examples of 10 sec interval snapshots show Neon-FtsZ moving around the cells next division plane in control conditions (arrowhead in Neon-Z control). The protein stopped moving when PC190723 was added (arrowheads in Neon-Z PC). Kymographs were obtained by extracting fluorescence intensity values along the red line indicated in middle panels (Plotted line). Similarly to what was observed for $FtsZ^{55-56}$-sGFP, addition of PC190723 abolished Neon-FtsZ movement (vertical lines in the Neon-Z PC kymographs). Scale bars 1 µm.

Z-ring constriction is biphasic in *S. aureus* and the second step of cytokinesis is independent of FtsZ movement

To better understand how Z-rings constrict during *S. aureus* cell division, exponentially growing cells of ColFtsZ$^{55\text{-}56}$-sGFP strain were spotted on agarose pads containing M9 microscopy media and imaged every 5 min by SIM (Figure 6). Once septation was complete (Figure 6, 0 min) FtsZ$^{55\text{-}56}$-sGFP was already seen localizing to the next division plane of the daughter cells, prior to cell splitting. Additionally, the new FtsZ rings did not immediately start to constrict, but did so after some time (Figure 6, from 30-40 min).

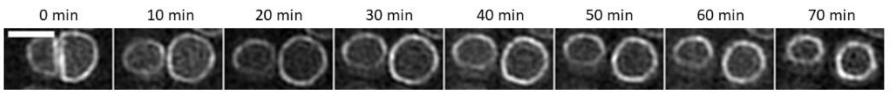

Figure 6: FtsZ$^{55\text{-}56}$-sGFP rings visualized by SIM time-lapse microscopy. The first frame shows a cell with FtsZ localizing in the next division plane prior to splitting. The cell then splits to generate two daughter cells (10 min). Interestingly, FtsZ rings do not immediately start to constrict but only do so after 30-40 min. Snapshots were taken every 5 min; frames depicted in the image are 10 min apart. Scale bar 1 μm.

To analyze dynamics of Z-ring constriction in *S. aureus* in more detail, we used time-lapse stacks from individual cells (Figure 7a, top) and drew a line across the cell for each time point (red line in Figure7a). Extraction of fluorescence intensity values along the red line generated a constriction kymograph, where each horizontal line corresponds to one timepoint (Figure 7a, bottom). By analyzing these constriction kymographs from several FtsZ$^{55\text{-}56}$-sGFP rings we observed two patterns: cells with a larger diameter, at the start of the experiment, showed a biphasic cytokinesis where the Z-ring barely constricts in a first step, which is followed by a second step of rapid Z-ring constriction (Figure 7a

control, left panel, bellow the arrowheads). Cells with smaller Z-rings, that had already initiated the process of constriction at the start of the experiment, showed only the second, fast, constriction step (Figure 7a, control right panel). Another striking observation was that in the presence of the PC190723 inhibitor some Z-rings were still able to continue constricting while others were impaired in that process. Furthermore, in the presence of PC190723, all constricting rings were at the second, fast, stage of cytokinesis (Figure 7a and b, +PC). Analysis of Z-ring constriction in the presence of PC190723 suggested that cells that had already started cytokinesis (i.e. cells with smaller Z-rings) and were going through the second, fast, cytokinesis step when PC190723 was added, were able to complete cell division. To confirm if there was a relationship between the Z-ring size upon PC190723 addition and the ability to constrict, we measured the Z-ring diameter at the beginning of the time-lapse and classed the cells as constricting; constricting with defects or non constricting (Figure 8). We observed that addition of PC190723 blocked constriction of large FtsZ rings, presumably in the first step of cytokinesis, but not of smaller FtsZ rings which are further ahead in the process, indicating that cytokinesis is only dependent on FtsZ treadmilling during the first, slow, step of cytokinesis.

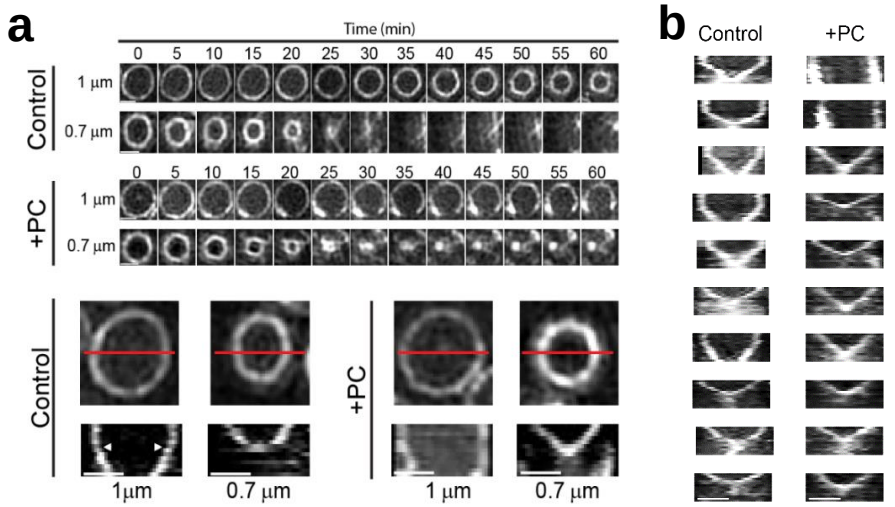

Figure 7: Z-rings show biphasic constriction and the second stage of fast constriction is not inhibited by PC190723. (a) Top panels show timelapse SIM snapshots of FtsZ$^{55\text{-}56}$-sGFP rings with 2 different starting diameters (1 μm or 0.7 μm) in the absence (Control) or presence (+PC) of FtsZ inhibitor PC190723. Bottom panels were obtained by drawing a line (exemplified in red) across the cell for each time point. Arrowheads in the control kymograph on the left point to the transition from first (no/slow constriction) to second (fast constriction) step of cytokinesis. **(b)** Additional kymographs showing constriction of FtsZ$^{55\text{-}56}$-sGFP. Kymographs of different cells are ordered by ring diameter from larger (top) to smaller (bottom). Since *S. aureus* cells are not synchronized, cells at all stages of cytokinesis can be observed. Therefore, during the control experiment, larger FtsZ$^{55\text{-}56}$-sGFP rings had a biphasic behavior (no/slow constriction followed by fast constriction) while smaller rings, further ahead in the cell cycle, were only observed undergoing the fast constriction step. Addition of PC190723 inhibited constriction of larger rings (see top two kymographs), but not of smaller rings, which were in the second (fast) stage of constriction and completed cytokinesis. Scale bars 0.5 μm.

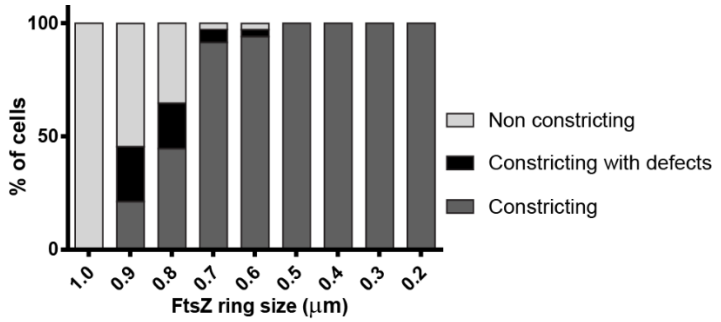

Figure 8: Addition of PC190723 only blocks cytokinesis of large Z-rings. Percentage of FtsZ$^{55\text{-}56}$-sGFP rings of different diameters that constricted in the presence of 5 μg/ml of PC190723 during 60 min.

Since the experiments described above were performed using a partially functional FtsZ fluorescent fusion (FtsZ$^{55\text{-}56}$-sGFP, see Figure 2) we repeated these experiments using the fluorescent derivative EzrA-GFP, expressed from the native locus, as a proxy for FtsZ localization (Figure 9). EzrA is a cell division protein that interacts directly with FtsZ and has been described as part of the divisome of some Gram-positive species (Son and Lee, 2013, Haeusser et al., 2004, Levin et al., 1999). Importantly, since the absence of EzrA leads to enlarged *S. aureus* cells (Jorge et al., 2011) we confirmed that the strain expressing EzrA-GFP (ColpSGEzrA-GFP) has a size distribution similar to wild-type COL, indicating that the fusion is functional (Figure 9a). Like FtsZ, EzrA showed movement that was inhibited by PC190723 and EzrA rings underwent biphasic constriction where the second, faster, step was insensitive to PC190723 (Figure 9b and c).

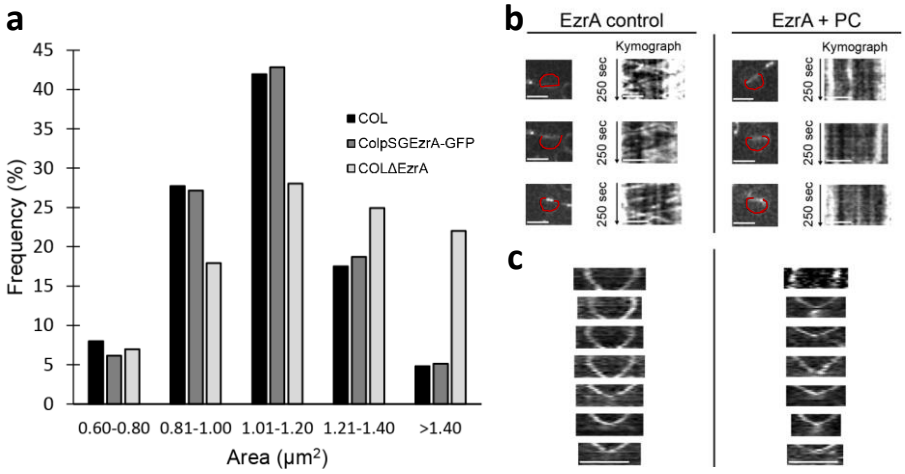

Figure 9: Z-ring protein EzrA shows impaired treadmilling in the presence of PC190723 and biphasic ring constriction. (a) To test the functionality of the EzrA-GFP construct, strains COL, ColpSGEzrA-GFP and COLΔEzrA (lacking *ezrA*) were grown in TSB, imaged by phase contrast and cell area was measured. The lack of EzrA in COLΔEzrA resulted in cell enlargement, while the size distribution of ColpSGEzrA-GFP cells mimicked that of parental strain COL, indicating that the EzrA fluorescent fusion is functional (N>850). **(b)** ColpSGEzrA-GFP cells, expressing a functional EzrA fusion to GFP, were imaged by SIM every 5 sec in the absence (EzrA control) or presence (EzrA + PC) of PC190723. Kymographs were obtained by extracting fluorescence intensity values along the red line indicated in cells in the left panels. Similarly to what was observed for $FtsZ^{55-56}$-sGFP, addition of PC190723 abolished EzrA movement (vertical lines in the kymographs). Scale bars, 1 µm. **(c)** ColpSGEzrA-GFP cells were imaged by SIM every 5 min in the absence (left) or presence (right) of PC190723 and kymographs showing constriction of EzrA-GFP rings were plotted. In control conditions the larger EzrA rings showed biphasic constriction behavior while in the presence of PC190723 only the rings in the second stage of cytokinesis were able to constrict. Scale bars, 1 µm.

S. aureus fast step of cytokinesis might be driven by PG synthesis

Two cell division processes have been shown to influence constriction rates: FtsZ treadmilling and PG synthesis (Bisson-Filho et al., 2017, Coltharp et al., 2016). Because in *S. aureus* FtsZ treadmilling is not

responsible for the fast constriction of the division septum we tested whether PG synthesis was required for the second cytokinesis step. In *S. aureus* the substantial PG synthesis at the division septum is initiated after recruitment of MurJ, the putative lipid II flippase to midcell (Monteiro et al., 2018). We therefore tested whether MurJ arrival coincided with the transition between the first and the second step of Z-ring constriction. As a control we used FtsW, a cell division protein that like MurJ exclusively localizes at midcell but whose recruitment to the divisome does not coincide with initiation of septal PG synthesis (Monteiro et al., 2018). By imaging $FtsZ^{55\text{-}56}$-sGFP; FtsW-sGFP and MurJ-sGFP fluorescent fusions every 10 min by SIM we observed that FtsW rings paralleled the biphasic behavior of the FtsZ ring (Figure 10, FtsZ and FtsW controls). However, MurJ rings did not display the first step of slow/no constriction (Figure 10, MurJ control). Imaging MurJ rings with increased time resolution (snapshots taken every 5 min instead of 10 min) did not reveal a biphasic constriction behavior (Figure 11). Furthermore, constriction of rings containing MurJ was insensitive to PC190723 (Figure 10, MurJ + PC and Figure 12), while constriction of large rings containing FtsW was impaired in 33% of the cells that had the protein at midcell in the beginning of the timelapse (presumably, cells in the first slow step of cytokinesis) (Figure 10, FtsW + PC and Figure 12).

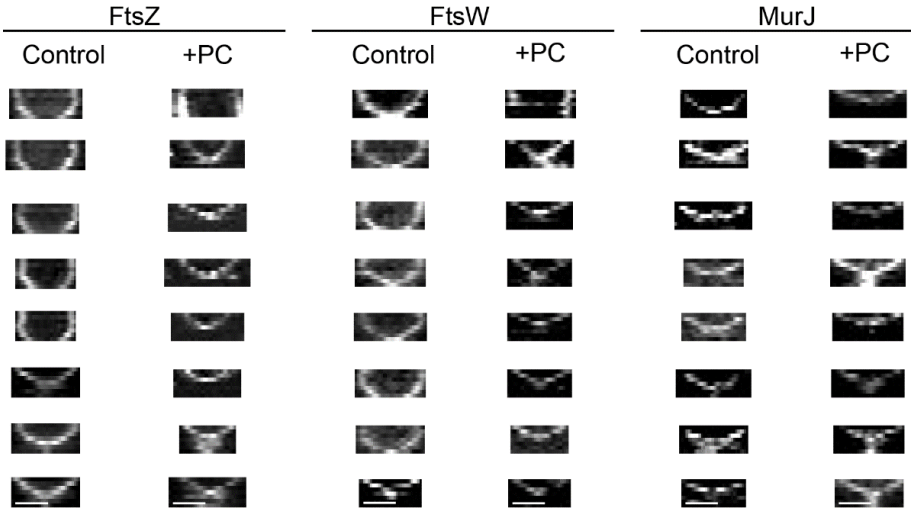

Figure 10: Kymographs showing constriction of FtsZ$^{55\text{-}56}$-sGFP, FtsW-sGFP and MurJ-sGFP rings during cell division. Strains ColFtsZ$^{55\text{-}56}$-sGFP, ColFtsW-sGFP and ColMurJ-sGFP were imaged every 10 min in the absence (control) or presence (+PC) of PC190723 for a total of 60 min. MurJ-sGFP control kymographs were performed on cells where MurJ-sGFP signal appears on the second frame, to ensure that the entire constriction process was observed (i.e. that the absence of a biphasic behavior did not result from only imaging cells in later stages of cell division). FtsZ$^{55\text{-}56}$-sGFP and FtsW-sGFP rings showed a biphasic constriction behavior (no/slow constriction followed by fast constriction). Addition of PC190723 inhibited constriction of larger FtsZ$^{55\text{-}56}$-sGFP and FtsW-sGFP rings (see top kymographs), but not of smaller rings which were undergoing fast constriction. MurJ-sGFP rings only displayed fast constriction and therefore were always able to constrict in the presence of PC190723. Scale bars 0.5 µm.

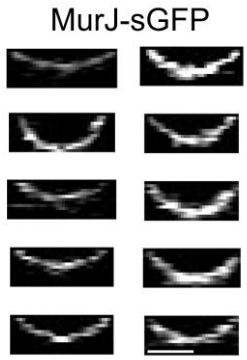

Figure 11: MurJ rings only display fast cytokinesis. Kymographs showing constriction of MurJ-sGFP rings in ColMurJ-sGFP cells imaged every 5 min for a total of 60 min (laser power 100%). Cells where MurJ-sGFP signal appears on the second frame were chosen for analysis to ensure that the entire constriction process was imaged. Fast constriction started immediately upon MurJ-sGFP arrival to the division septum and therefore rings did not show biphasic behavior. Scale bar 0.5 μm.

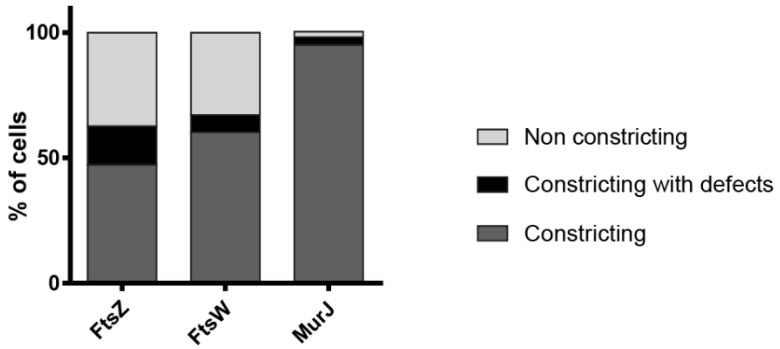

Figure 12: MurJ rings constrict in the presence of PC190723. Strains ColFtsZ$^{55\text{-}56}$-sGFP, ColFtsW-sGFP and ColMurJ-sGFP were imaged every 10 min for a total of 60 min in the presence of 5 μg/ml PC190723. Percentage of FtsZ$^{55\text{-}56}$-sGFP, FtsW-sGFP and MurJ-sGFP rings that constricted with PC190723.

To consolidate the observation that MurJ recruitment to the divisome, and presumably PG synthesis redirection to midcell, coincides with the start of fast cytokinesis we analyzed cytokinesis of individual cells that expressed both FtsZ-mCherry and MurJ-GFP (Figure 13a) or the

FtsZ-mCherry and FtsW-GFP (Figure 13b). By measuring the ring diameter for each protein over time we observed that recruitment of MurJ coincided with the start of fast constriction while FtsW recruitment to midcell recapitulated the two-step cytokinetic behavior of Z-rings.

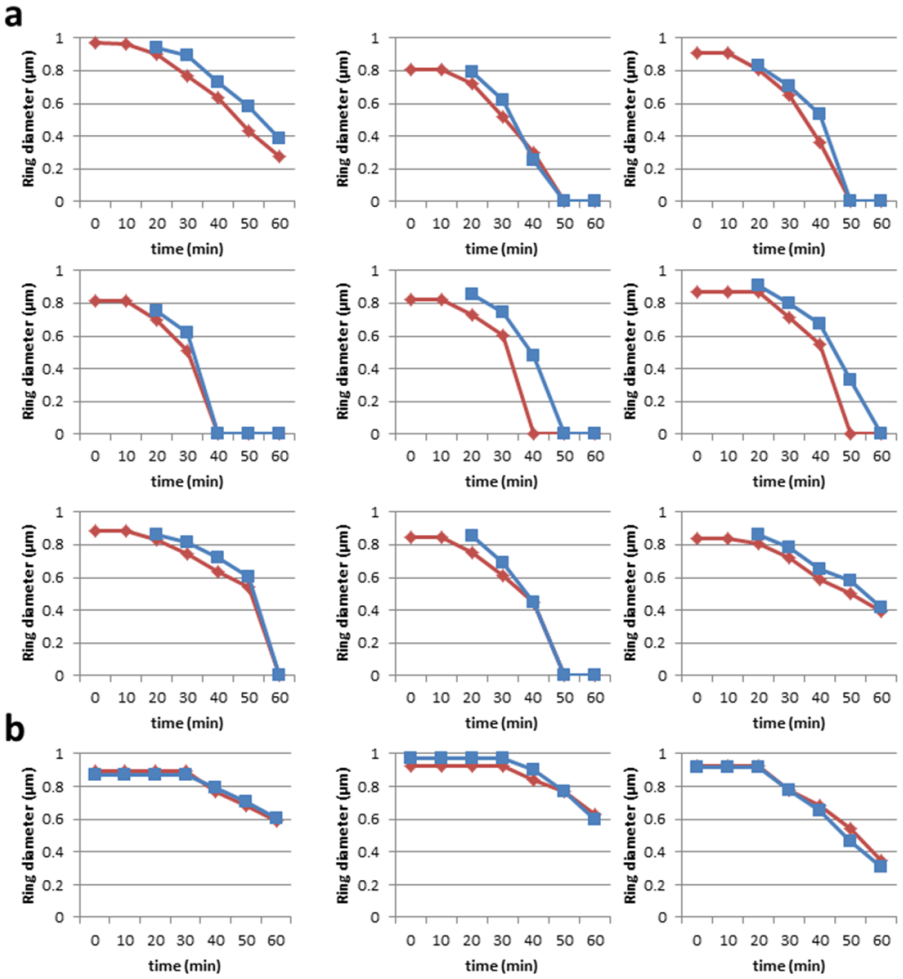

Figure 13: MurJ and FtsW ring diameter relative to FtsZ during constriction of single cells. (a) Graphs of ring diameters of FtsZ-mCherry (red lines) and MurJ-sGFP (blue lines) in strain ColJgZm. SIM images were taken every 10 min and measurements of ring aperture of FtsZ-mCherry and MurJ-sGFP were performed in cells where MurJ-sGFP signal first appeared after 20 minutes. **(b)**

Graphs of ring diameters of FtsZ-mCherry (red lines) and FtsW-sGFP (blue lines) in strain ColWgZm. SIM images were taken every 10 min and measurements of ring diameter of FtsZ-mCherry and FtsW-sGFP were performed in cells where FtsZ-mCherry ring diameter was constant for the first 20 minutes.

If MurJ recruitment to midcell was responsible for driving the fast cytokinetic step of cell division, inhibition of MurJ activity should stop cytokinesis at any point of the cell cycle. This was indeed the case as in the presence of DMPI (Huber et al., 2009), an antibiotic which specifically inhibits MurJ without delocalizing the protein (Monteiro et al., 2018), we observed that all FtsZ$^{55\text{-}56}$-sGFP rings, large or small were unable to constrict (Figure 14).

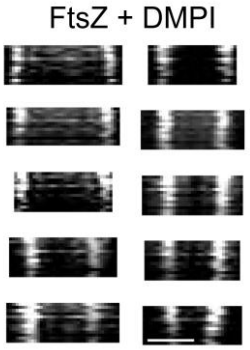

Figure 14: Addition of MurJ inhibitor DMPI blocks FtsZ$^{55\text{-}56}$-sGFP rings of all sizes. Kymographs of ten FtsZ$^{55\text{-}56}$-sGFP rings obtained by imaging cells every 5 min for a total of 60 min in the presence of DMPI. The MurJ inhibitor completely blocked constriction of all FtsZ$^{55\text{-}56}$-sGFP rings analyzed. Scale bar 0.5 μm.

These findings suggest that septum synthesis in *S. aureus* starts with a step dependent on FtsZ treadmilling, which may be responsible for the very initial invagination of the cell membrane. This is followed by recruitment of the lipid II flippase MurJ, which brings PG synthesis activity to the division septum, providing the force for cytokinesis, which becomes independent of FtsZ treadmilling activity.

DISCUSSION

S. aureus is an excellent model to study cytokinesis as we can easily visualize the entire Z-ring, parallel to the microscope slide. This allowed us to follow the cytokinesis process over time and determine that Z-ring assembly at midcell did not initiate major Z-ring constriction. In fact, cytokinesis was biphasic, with an initial, slow step followed by a fast constriction step. Time-lapse imaging of FtsZ in *E. coli* and *Streptococcus pneumoniae* shows that the Z-ring assembly is followed by a period where no invagination is observed, suggesting that biphasic constriction could be a common feature of cytokinesis in bacteria (Coltharp et al., 2016, Berge et al., 2017). Our data allowed us to propose a model for *S. aureus* cytokinesis (Figure 15), where after a round of cell division, when the septum is closed in the mother cell, but before its splitting into two daughter cells, FtsZ is already localizing at the next cell division plane. After cell splitting, and presumably during Phase 1, the cells do not immediately initiate Z- ring constriction and septum synthesis. Following Z-ring assembly, MurJ is recruited to the divisome, which ensures that translocation of lipid II occurs exclusively at midcell. Substrate affinity then diverts the major PG synthase, PBP2 (Pinho and Errington, 2005), from the periphery to midcell where, together with other PG synthesis enzymes, it incorporates lipid II into the growing PG network, starting massive PG synthesis at the leading edge of the constricting septum. Once this process is initiated, the FtsZ inhibitor PC190723, which inhibits FtsZ treadmilling, no longer prevents cytokinesis. Nevertheless, FtsZ treadmilling is likely to have a role in the organisation of septum synthesis, since ~24% of the Z-rings that were able to constrict in the presence of PC190723, did so defectively, similarly to *E. coli* FtsZ mutants

impaired in GTPase activity which stopped treadmilling (Yang et al., 2017).

Our data may reconcile two models proposed in the literature for the origin of the force required for cytokinesis to occur. In one model, this force derives from FtsZ, either from the chemical energy of GTP hydrolysis which could promote bending of the FtsZ polymers or from the affinity of FtsZ filaments to bundle, which could result in condensation of the Z-ring (Ghosh and Sain, 2008, Lan et al., 2009, Li et al., 2013). Alternatively, cell wall synthesis has been suggested to generate the force for cytokinesis (Coltharp et al., 2016, Coltharp and Xiao, 2017). We propose that cytokinesis occurs in two steps: an initial, slow one, dependent on FtsZ treadmilling, for which FtsZ may be the driving force and that may be responsible for the initial invagination of the cell membrane, followed by a second, faster step, for which PG synthesis might provide the driving force.

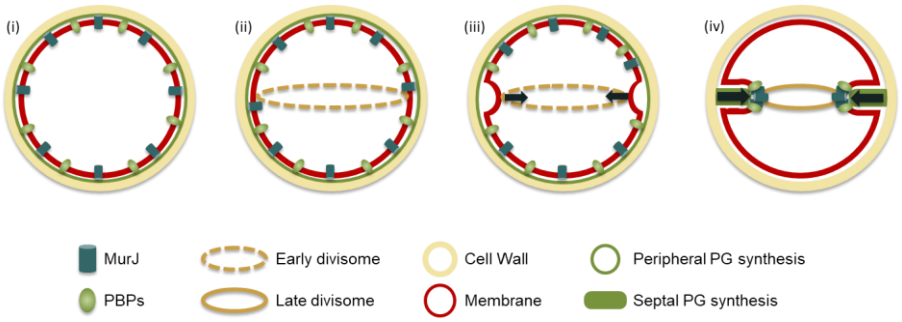

Figure 15: Model for cytokinesis in *S. aureus*. (i) Cells in Phase 1 of the cell cycle (before septum synthesis is initiated) synthesize peptidoglycan at the cell periphery. **(ii)** In preparation for division, FtsZ and early components of the divisome assemble at midcell. **(iii)** At this stage, cells initiate the first, slow step of cytokinesis, which is dependent on FtsZ treadmilling. FtsZ may be the driving force for the initial invagination of the membrane. **(iv)** MurJ then arrives to the

divisome, bringing the PG precursor (lipid II) flippase activity to midcell. The major *S. aureus* PG synthase, PBP2, is recruited to midcell through substrate (translocated lipid II) recognition, and massive PG synthesis is initiated to synthesize the septum. From this point onwards, cytokinesis no longer depends on FtsZ treadmilling and is probably driven by PG synthesis.

ANNEX 1

mNeonGreen nucleotide sequence (5'-3'), was codon optimized for *Staphylococcus aureus* by ATUM. ATUM company:

ATGGTATCAAAAGGTGAAGAAGATAATATGGCAAGCTTACCAGCAACACACGAATT
ACATATTTTCGGTTCTATAAACGGAGTGGATTTTGATATGGTTGGTCAAGGCACAG
GTAACCCAAATGATGGTTATGAAGAACTTAATCTTAAAAGTACGAAAGGTGACTTA
CAATTTAGTCCTTGGATTTTAGTTCCGCATATTGGTTATGGGTTTCATCAATACTT
GCCATATCCAGATGGTATGTCTCCTTTTCAAGCAGCGATGGTTGACGGATCGGGAT
ACCAAGTACATAGAACGATGCAGTTTGAAGATGGCGCGTCATTAACAGTCAATTAC
AGATATACTTATGAAGGGTCACATATTAAAGGTGAAGCTCAAGTTAAAGGTACTGG
CTTCCCAGCTGATGGACCAGTGATGACAAATAGTTTAACTGCAGCCGACTGGTGTC
GATCAAAGAAAACATATCCTAATGATAAAACAATAATCTCTACGTTTAAGTGGTCA
TATACTACGGGAAATGGTAAAAGATATCGTAGCACAGCTCGCACAACATATACATT
TGCAAAACCTATGGCAGCAAATTATTTAAAGAATCAACCGATGTATGTTTTTCGTA
AAACAGAATTGAAACATAGTAAAACTGAGCTAAACTTTAAAGAATGGCAAAAAGC
TTTCACTGATGTAATGGGCATGGATGAGTTATACAAATAA

REFERENCES

Atilano, M. L., Pereira, P. M., Yates, J., Reed, P., Veiga, H., Pinho, M. G. and Filipe, S. R. (2010). Teichoic acids are temporal and spatial regulators of peptidoglycan cross-linking in *Staphylococcus aureus*. Proc Natl Acad Sci U S A*, 107***,** 18991-6.

Berge, M. J., Mercy, C., Mortier-Barriere, I., VanNieuwenhze, M. S., Brun, Y. V., Grangeasse, C., Polard, P. and Campo, N. (2017). A programmed cell division delay preserves genome integrity during natural genetic transformation in *Streptococcus pneumoniae*. Nat Commun*, 8***,** 1621.

Bisson-Filho, A. W., Hsu, Y. P., Squyres, G. R., Kuru, E., Wu, F., Jukes, C., Sun, Y., Dekker, C., Holden, S., VanNieuwenhze, M. S.*, et al.* (2017). Treadmilling by FtsZ filaments drives peptidoglycan synthesis and bacterial cell division. Science*, 355***,** 739-743.

Charpentier, E., Anton, A. I., Barry, P., Alfonso, B., Fang, Y. and Novick, R. P. (2004). Novel cassette-based shuttle vector system for gram-positive bacteria. Appl. Environ. Microbiol.*, 70***,** 6076-6085.

Coltharp, C., Buss, J., Plumer, T. M. and Xiao, J. (2016). Defining the rate-limiting processes of bacterial cytokinesis. Proc Natl Acad Sci U S A*, 113***,** E1044-53.

Coltharp, C. and Xiao, J. (2017). Beyond force generation: Why is a dynamic ring of FtsZ polymers essential for bacterial cytokinesis? Bioessays*, 39***,** 1-11.

Daniel, R. A., Harry, E. J. and Errington, J. (2000). Role of penicillin-binding protein PBP 2B in assembly and functioning of the division machinery of *Bacillus subtilis*. Mol Microbiol*, 35***,** 299-311.

Falcão, A. X., Stolfi, J. and de Alencar Lotufo, R. (2004). The image foresting transform: theory, algorithms, and applications. IEEE Trans Pattern Anal Mach Intell*, 26***,** 19-29.

Fisher, A. C. and DeLisa, M. P. (2008). Laboratory evolution of fast-folding green fluorescent protein using secretory pathway quality control. PLoS One*, 3***,** e2351.

Ghosh, B. and Sain, A. (2008). Origin of contractile force during cell division of bacteria. Phys Rev Lett*, 101***,** 178101.

Gill, S. R., Fouts, D. E., Archer, G. L., Mongodin, E. F., Deboy, R. T., Ravel, J., Paulsen, I. T., Kolonay, J. F., Brinkac, L., Beanan, M.*, et al.* (2005). Insights on evolution of virulence and resistance from the complete genome analysis of an early methicillin-resistant *Staphylococcus aureus* strain and a biofilm-producing methicillin-resistant *Staphylococcus epidermidis* strain. J. Bacteriol.*, 187***,** 2426-2438.

Haeusser, D. P., Schwartz, R. L., Smith, A. M., Oates, M. E. and Levin, P. A. (2004). EzrA prevents aberrant cell division by modulating assembly of the cytoskeletal protein FtsZ. Mol Microbiol*, 52***,** 801-814.

Haydon, D. J., Stokes, N. R., Ure, R., Galbraith, G., Bennett, J. M., Brown, D. R., Baker, P. J., Barynin, V. V., Rice, D. W., Sedelnikova, S. E.*, et al.* (2008). An inhibitor of FtsZ with potent and selective anti-staphylococcal activity. Science*, 321***,** 1673-5.

Huber, J., Donald, R. G., Lee, S. H., Jarantow, L. W., Salvatore, M. J., Meng, X., Painter, R., Onishi, R. H., Occi, J., Dorso, K.*, et al.* (2009). Chemical genetic identification of peptidoglycan inhibitors potentiating carbapenem activity against methicillin-resistant *Staphylococcus aureus*. Chem Biol*, 16***,** 837-48.

Jorge, A. M., Hoiczyk, E., Gomes, J. P. and Pinho, M. G. (2011). EzrA Contributes to the Regulation of Cell Size in *Staphylococcus aureus*. Plos One*, 6***,** e27542.

Lan, G., Daniels, B. R., Dobrowsky, T. M., Wirtz, D. and Sun, S. X. (2009). Condensation of FtsZ filaments can drive bacterial cell division. Proc Natl Acad Sci U S A*, 106***,** 121-6.

Levin, P. A., Kurtser, I. G. and Grossman, A. D. (1999). Identification and characterization of a negative regulator of FtsZ ring formation in *Bacillus subtilis*. Proc Natl Acad Sci U S A*, 96***,** 9642-7.

Li, Y., Hsin, J., Zhao, L., Cheng, Y., Shang, W., Huang, K. C., Wang, H. W. and Ye, S. (2013). FtsZ protofilaments use a hinge-opening mechanism for constrictive force generation. Science*, 341***,** 392-5.

Mitchell, P. and Moyle, J. (1956). Osmotic structure and function in bacteria. Bacterial Anatomy*, 6th Symposium of the Society for General Microbiology, Cambridge University Press*.

Monteiro, J. M., Fernandes, P. B., Vaz, F., Pereira, A. R., Tavares, A. C., Ferreira, M. T., Pereira, P. M., Veiga, H., Kuru, E., VanNieuwenhze, M. S.*, et al.* (2015). Cell shape dynamics during the staphylococcal cell cycle. Nat Commun*, 6***,** 8055.

Monteiro, J. M., Pereira, A. R., Reichmann, N. T., Saraiva, B. M., Fernandes, P. B., Veiga, H., Tavares, A. C., Santos, M., Ferreira, M. T., Macario, V.*, et al.* (2018). Peptidoglycan synthesis drives an FtsZ-treadmilling-independent step of cytokinesis. Nature*, 554***,** 528-532.

Moore, D. A., Whatley, Z. N., Joshi, C. P., Osawa, M. and Erickson, H. P. (2017). Probing for binding regions of the FtsZ protein surface through site-directed insertions: discovery of fully functional FtsZ-fluorescent proteins. J Bacteriol*, 199***,** e00553-16.

Nair, D., Memmi, G., Hernandez, D., Bard, J., Beaume, M., Gill, S., Francois, P. and Cheung, A. L. (2011). Whole-genome sequencing of *Staphylococcus*

aureus strain RN4220, a key laboratory strain used in virulence research, identifies mutations that affect not only virulence factors but also the fitness of the strain. J Bacteriol*, 193***,** 2332-2335.

Osawa, M., Anderson, D. E. and Erickson, H. P. (2008). Reconstitution of contractile FtsZ rings in liposomes. Science*, 320***,** 792-4.

Osawa, M. and Erickson, H. P. (2011). Inside-out Z rings--constriction with and without GTP hydrolysis. Mol Microbiol*, 81***,** 571-9.

Osawa, M. and Erickson, H. P. (2018). Turgor Pressure and Possible Constriction Mechanisms in Bacterial Division. Front Microbiol*, 9***,** 111.

Oshida, T. and Tomasz, A. (1992). Isolation and characterization of a Tn*551*-autolysis mutant of *Staphylococcus aureus*. J Bacteriol*, 174***,** 4952-4959.

Pereira, P., Veiga, H., Jorge, A. and Pinho, M. (2010). Fluorescent reporters for studies of cellular localization of proteins in *Staphylococcus aureus*. Appl. Environ. Microbiol*., 76***,** 4346-4353.

Perez-Nunez, D., Briandet, R., David, B., Gautier, C., Renault, P., Hallet, B., Hols, P., Carballido-Lopez, R. and Guedon, E. (2011). A new morphogenesis pathway in bacteria: unbalanced activity of cell wall synthesis machineries leads to coccus-to-rod transition and filamentation in ovococci. Mol. Microbiol*., 79***,** 759-71.

Pinho, M. and Errington, J. (2003). Dispersed mode of *Staphylococcus aureus* cell wall synthesis in the absence of the division machinery. Mol Microbiol*, 50***,** 871-881.

Pinho, M. G. and Errington, J. (2004). A *divIVA* null mutant of *Staphylococcus aureus* undergoes normal cell division. FEMS Microbiology Letters*, 240***,** 145-149.

Pinho, M. G. and Errington, J. (2005). Recruitment of penicillin-binding protein PBP2 to the division site of *Staphylococcus aureus* is dependent on its transpeptidation substrates. Mol. Microbiol*., 55***,** 799-807.

Pogliano, J., Pogliano, K., Weiss, D. S., Losick, R. and Beckwith, J. (1997). Inactivation of FtsI inhibits constriction of the FtsZ cytokinetic ring and delays the assembly of FtsZ rings at potential division sites. Proc Natl Acad Sci U S A*, 94***,** 559-64.

Roerdink, J. and Meijster, A. (2000). The Watershed Transform: Definitions, Algorithms and Parallelization Strategies. Fundamenta Informaticae*, 41***,** 187-228.

Schindelin, J., Arganda-Carreras, I., Frise, E., Kaynig, V., Longair, M., Pietzsch, T., Preibisch, S., Rueden, C., Saalfeld, S., Schmid, B.*, et al.* (2012). Fiji: an open-source platform for biological-image analysis. Nat Methods*, 9***,** 676-682.

Shaner, N. C., Lambert, G. G., Chammas, A., Ni, Y., Cranfill, P. J., Baird, M. A., Sell, B. R., Allen, J. R., Day, R. N., Israelsson, M.*, et al.* (2013). A bright monomeric green fluorescent protein derived from *Branchiostoma lanceolatum*. Nat Methods*, 10*, 407-9.

Son, S. H. and Lee, H. H. (2013). The N-terminal domain of EzrA binds to the C terminus of FtsZ to inhibit *Staphylococcus aureus* FtsZ polymerization. Biochem Biophys Res Commun*, 433*, 108-14.

Vagner, V., Dervyn, E. and Ehrlich, S. D. (1998). A vector for systematic gene inactivation in *Bacillus subtilis*. Microbiology*, 144 (Pt 11)*, 3097-104.

Veiga, H. and Pinho, M. G. (2009). Inactivation of the SauI type I restriction-modification system is not sufficient to generate *Staphylococcus aureus* strains capable of efficiently accepting foreign DNA. Appl. Environ. Microbiol.*, 75*, 3034-8.

Velasco, F. (1980). Thresholding using the ISODATA clustering algorithm. IEEE Transactions on Systems, Man and Cybernetics*, 10*, 771-774.

Whatmore, A. M. and Reed, R. H. (1990). Determination of turgor pressure in *Bacillus subtilis*: a possible role for K+ in turgor regulation. J Gen Microbiol*, 136*, 2521-6.

Xiao, J. and Goley, E. D. (2016). Redefining the roles of the FtsZ-ring in bacterial cytokinesis. Curr Opin Microbiol*, 34*, 90-96.

Yang, X., Lyu, Z., Miguel, A., McQuillen, R., Huang, K. C. and Xiao, J. (2017). GTPase activity-coupled treadmilling of the bacterial tubulin FtsZ organizes septal cell wall synthesis. Science*, 355*, 744-747.

CHAPTER IV

Peptidoglycan synthesis inhibition by oxacillin leads to modification of the *S. aureus* Z-ring ultrastructure

Chapter IV Summary

ABSTRACT 182
INTRODUCTION 183
EXPERIMENTAL PROCEDURES 186
Bacterial strains and growth conditions 186
Strain construction 189
S. aureus incubation with antibiotics 193
S. aureus sample preparation for microscopy 193
S. aureus imaging by Structured Illumination Microscopy (SIM) 194
Timelapse microscopy 194
Growth curves 195
Detection of PBPs with Bocillin-FL 196
Western blot analysis 196
RESULTS 198
Sub-inhibitory concentrations of oxacillin cause cell morphology defects in *S. aureus* MRSA strain COL 198
S. aureus cells invaginate during cell division in the presence of sub-MIC concentrations of oxacillin 202
Oxacillin-induced morphology changes alter Z-ring shape 204
Inhibition of PBP1 causes invagination of *S. aureus* cells 208
DISCUSSION 214
REFERENCES 217

Acknowledgements:
We thank E. Harry (University of Technology, Sydney) for the generous gift of the anti-FtsZ antibody and to T. Roemer (Merck) for kindly providing the DMPI compound.

Pereira AR contribution:
A. R. Pereira performed all experiments, except construction of COLPBP1TP and COLPBP3TP mutants (and their respective bocillin-FL assays), construction of pCNX-pbp2 and pCNX-pbp2TP plasmids and timelapses of COLPBP1TP and COLPBP1TPpCNXFtsZ$^{55\text{-}56}$-sGFP, performed by N.R. Reichmann. Strain COLΔPBP2 was constructed by P.R. Reed.

This chapter contains unpublished data.

ABSTRACT

Peptidoglycan (PG), the major component of the bacterial wall, protects cells from mechanical stress resulting from high intracellular turgor. During cell division, PG is remodeled by the combined activities of PG synthases that promote the inward growth of the division septum, and hydrolases, that break PG bonds. Contrary to *Escherichia coli*, *Staphylococcus aureus* synthesizes a septal plate at midcell without exterior invagination of the outer envelope layers. After the septum is completed, it is split and undergoes fast reshaping to form the curved new hemispheres of the two daughter cells. In this work we have observed that incubation with oxacillin at sub-minimum inhibitory concentrations (sub-MIC) abolishes the fast separation of *S. aureus*, giving rise to attached sister cells that show invagination at the exterior side of the closed septum. This phenotype is due to the inactivation of the transpeptidase domain of the Penicillin-Binding Protein PBP1. Interestingly, in these cells, where reshaping of the septum occurs very slowly, FtsZ localized as D-shaped structures instead of rings, in attached daughter cells. These FtsZ D-shaped structures can recruit downstream cell division proteins like MurJ and constrict while maintaining the D-shape. These results suggest that the external envelope defines the shape of the Z-ring in live *S. aureus* cells.

INTRODUCTION

Most bacteria are surrounded by a cell wall which exerts a fundamental role in cellular integrity and shape maintenance. The main component of the cell wall is peptidoglycan (PG), a net-like structure composed of strands of polymerized disaccharides of N-acetylglucosamine-N-acetylmuramic acid, crosslinked by peptide bonds. During bacterial growth, old PG bonds are broken by autolytic enzymes and new PG is synthesized and inserted into the cell wall net-like structure. Synthesis of new PG starts in the cytoplasm with the synthesis of PG precursors that are then attached to the lipid carrier bactoprenol and modified at the inner membrane to form lipid II - the precursor of PG. Lipid II is then flipped to the outer side of the membrane where it polymerizes through transglycosylation (synthesis of glycan chains) and transpeptidation (peptide crosslinking) reactions. These polymerization reactions are responsible for incorporating lipid II precursors into a macromolecular polymer. PG transglycosylation can be performed by several classes of proteins, namely penicillin-binding proteins (PBPs), monofunctional transglycosylases (Mgts) (Reed et al., 2011) or members of the sporulation elongation division and sporulation (SEDS) protein family (Meeske et al., 2016) while PG transpeptidation is catalyzed only by PBPs transpeptidase (TP) site. TP domains have three highly-conserved motifs, with conserved spacing in the primary protein structure including the SXXK motif that contains the catalytic serine (Goffin and Ghuysen, 1998). Some PBPs combine both transpeptidase and transglycosylase domains in the same protein (class A PBPs) while others possess only a transpeptidase catalytic site (class B PBPs). In *S. aureus*, from the four native PBPs (PBP1-4), only PBP2 is a class A PBP.

Because PG integrity is essential for bacterial survival, its synthesis pathway is a key target for different classes of antibiotics acting on different steps of the pathway. Beta-lactams act on the last stages of PG assembly by binding and acylating the TP catalytic site of PBPs, preventing the transpeptidation reaction and consequently inhibiting PG crosslinking. The mode of action of beta-lactams was thought to be the inhibition of PG synthesis and disturbance of the balance between PG synthesis and hydrolysis (Park and Strominger, 1957, Tomasz, 1979, Uehara et al., 2009). But surprisingly, *Streptococcus pneumoniae* mutants blocked for cell lysis still died in the presence of beta-lactams which suggested a more complex lysis-independent killing mechanism (Moreillon et al., 1990). Recently, Cho and colleagues showed that beta-lactams also induce a futile cycle of PG synthesis and degradation in *E. coli* which reinforces their lethal action (Cho et al., 2014).

The ability of methicillin resistant *S. aureus* (MRSA) strains to survive in the presence of beta-lactams derives mostly from acquisition of an extra PBP, PBP2a. This protein provides beta-lactam resistance since its unique TP catalytic site is less sensitive to acylation by the beta-lactam (Hartman and Tomasz, 1984, Reynolds and Brown, 1985). Therefore MRSA strains incubated with high concentrations of beta-lactams are able to perform the transpeptidation reaction through PBP2a enzyme and continue to grow. Although the MRSA mechanism of resistance relies on the acquisition of PBP2a, other native auxiliary proteins of *S. aureus* are necessary for full resistance to beta-lactams. Perhaps the best example of one of these auxiliary factors is PBP2. Upon inhibition of the PBP2 TP domain by oxacillin, it is thought that the transglycosylase domain of PBP2 cooperates with the TP domain of

PBP2a, leading to polymerization and crosslinking of PG (Pinho et al., 2001) albeit at lower levels than in the absence of antibiotics.

Given the relevance of the rate of PG synthesis for cell cycle progression, we wanted to study if this progression was affected by the presence of beta-lactams. In the absence of antibiotics, MRSA strain COL spends around half of its cell cycle without a septum (Phase 1) and the other half split between septum synthesis (Phase 2) and maturation (Phase 3) (Monteiro et al., 2015). After septum synthesis and maturation the cells rapidly pop (<2 msec) giving rise to the new daughter cells, again in Phase 1 (Monteiro et al., 2015, Zhou et al., 2015). Figure 1 from chapter III shows that although DMPI and oxacillin both inhibit PG synthesis, the effects of these antibiotics on *S. aureus* cell cycle progression was different. The MurJ inhibitor DMPI caused an accumulation of cells in Phase 1 (cells without a septum), while the transpeptidation inhibitor oxacillin caused a decrease in the number of cells in Phase 1 and an increase in the frequency of cells in Phase 2 (with an open septum) and Phase 3 (with a complete septum). Chapter III focused on the effects of DMPI and PC190723 incubation on the cell cycle. In this chapter we will address the effects of oxacillin on *S. aureus* cell division.

EXPERIMENTAL PROCEDURES

Bacterial strains and growth conditions

All the strains and plasmids used in this study are listed in Table IV.1. The sequences of the primers used are listed in Table IV.2. *S. aureus* strains were grown in tryptic soy broth (TSB, Difco) at 200 r.p.m with aeration at 37 °C or on tryptic soy agar (TSA, Difco) at 30 or 37°C. *E. coli* strains were grown in Luria–Bertani broth (Difco) with aeration, or Luria–Bertani agar (Difco) at 37 or 30°C. When necessary, antibiotics ampicillin (100 μg/ml), erythromycin (10 μg/ml), kanamycin (150 μg/ml) were added to the media. 5-bromo-4-chloro-3-indolyl β-D-galactopyranoside (X-gal, Apollo Scientific) was used at 100 μg/ml. Isopropyl β-D-1-thiogalactopyranoside (IPTG, Apollo Scientific) was used at 0.5 mM and cadmium chloride ($CdCl_2$, Sigma-Aldrich) at 0.1 μM.

Table IV.1 – Strains and plasmids used in this study.

Plasmids and strains	Relevant characteristics	Source or reference
Plasmids		
pMAD	*E. coli – S. aureus* shuttle vector with the *bgaB* gene encoding a ß-galactosidase and thermosensitive origin of replication for Gram-positive bacteria, Amp^r Ery^r	(Arnaud et al., 2004)
pCNX	Replicative vector containing the cadmium inducible P*cad* promoter; Amp^r Kan^r	(Monteiro et al., 2015)
pMADpbp1TP	pMAD-P_{spac}-*rbs- pbpAt940g* plasmid, to construct a PBP1S314A mutant; Amp^r Ery^r	(Reichmann, NR, unpublished)
pMADpbp3TP	pMAD-*pbpCt1174g_ c1175g_ t1176a_t1179c* plasmid to construct a PBP3S392G mutant; Amp^r Ery^r	(Reichmann, NR, unpublished)
pMADpbp4TP	pMAD-*pbpDt223g_ g222t* plasmid to construct a PBP4S75A mutant; Amp^r Ery^r	This study

pMAD-pbp2TPbig	pMAD-*recUtrunc-pbpBt1192g_c1193g_t1197c-down* where PBP2S398G was amplified from; Amp^r Ery^r	(Reichmann, NR, unpublished)
pCNX-pbp2	pCNX-*rbs-pbpB* plasmid, to ectopically express PBP2; Amp^r Kan^r	(Reichmann, NR, unpublished)
pCNX-pbp2TP	pCNX-*rbs-pbpBt1192g_c1193g_t1197c* to ectopically express PBP2S398G mutant; Amp^r Kan^r	(Reichmann, NR, unpublished)
S. aureus		
COL	MRSA strain	(Gill et al., 2005)
RN4220	MSSA strain. Mutagenized strain derived from NCTC8325-4 that accepts foreign DNA	R- Novick
COLPBP1TP	COL*pbpA*::*pbpAt940g* strain, expressing PBP1S314A TP mutant	(Reichmann, NR, unpublished)
COLPBP3TP	COL*pbpC*::*pbpCt1174g_ c1175g_ t1176a_t1179c* strain expressing PBP3S392G TP mutant	(Reichmann, NR, unpublished)
COLPBP4TP	COL*pbpD*::*pbpDt223g_ g222t* strain expressing PBP4S75A TP mutant	This study
COLΔPBP4	COL *pbpD* deletion mutant	(Memmi et al., 2008)
COLΔPBP2	COL *pbpB* deletion from codon N4 to codon G724	(Reed, PR, unpublished)
COLΔPBP2 pCNX-pbp2	COLΔPBP2 strain expressing PBP2 ectopically from pCNX plasmid; Kan^r	This study
COLΔPBP2 pCNX-pbp2TP	COLΔPBP2pCNX-*rbs-pbpBt1192g_c1193g_t1197c* strain, expressing PBP2S398G TP mutant; Kan^r	This study
ColFtsZ$^{55\text{-}56}$-sGFP	COL pCNX-ftsZ$^{55\text{-}56}$-sGFP, sandwich *ftsZ* fusion expressed from a replicative plasmid, under the control of P_{cad} inducible promoter; Kan^r	(Monteiro et al., 2018)
ColpSGEzrA-GFP	COLezrA::pSG5082-*ezrA-gfp*; Ery^r	(Monteiro et al., 2018)
ColJgZm	COL *murJ*::*murJ-sgfp*, Δ*spa*::P*spac-ftsZ-mcherry*	(Monteiro et al., 2018)
COLPBP1TP pCN-FtsZ$^{55\text{-}56}$-sGFP	COL*pbpA*::*pbpAt940g* strain (PBP1S314A TP mutant) expressing FtsZ$^{55\text{-}56}$-sGFP sandwich fusion from a replicative plasmid, under the control of the P_{cad} promoter; Kan^r	(Reichmann, NR, unpublished)

Table IV.2 – Primers used in this study. Underlined sequences correspond to restriction sites. Bold highlighting corresponds to *rbs* sequences.

Primer Name	Sequence (5'-3')
P1pbp1TP	GCTGAATTCTTCTACACAGCCCAGTCCAGAC
P2pbp1TP	CATTTTTTTTCCTCCTTATTTTTTCCCGGGAAAAGCTTAATTGTTATCC
P3pbp1TP	GAAAAAATA**AGGAGG**AAAAAAAATGGCGAAGCAAAAAATTAAAATT
P4pbp1TP	GCCGGATCCTTAGTCCGACTTATCCTTGTC
P5pbp1TP	TAAACGTGGTGATGATGTCC
P6pbp1TP	CTAACAGGATTTTCAACGC
P1pbp3TP	GCCGAATTCCACGTCTATGGATTGGGATAG
P2pbp3TP	CGCGGATCCTCCAACCGCAAATTGAGAAG
P3pbp3TP	CGCGGATCCGTAAAAGGTGGAACATTATTAG
P4pbp3TP	GCCGTCGACCTTGAGTGGACCAACCTCATC
P5pbp3TP	GGCGCATTTTGGAATGTAGTTAAC
P6pbp3TP	GTAGTTTCTGTCACCACATTC
P1pbp4TP	GATATCGGATCCGTAGTAATCGTATGGTTGTAA
P2pbp4TP	AATCTCCAGCTGCTATGACTAAATTAATG
P3pbp4TP	ATCTGTCAGCTGGATTCCACTTAGTATCGAT
P4pbp4TP	GAGCTCGAATTCTAGATACATGCATTTCTATCAT
P1pCNXpbp2	CAGGTCGACAAAAAATA**AGGAGG**AAAAAAAATGACGGAAAACAAAGG ATCTTCTC
P2pCNXpbp2	CGCATGGTACCTTAGTTGAATATACCTGTTAATCCACCGCTGTTTC
P1pMADpbp2TP	GCGCCCGGGCATTCAAATACGTTTTATC
P2pMADpbp2TP	CGCGGATCCACCAGTAGGGTGAGGATC
P3pMADpbp2TP	CGCGGATCCTTAAAACCTTTCTTAGCG
P4pMADpbp2TP	CGCGTCGACGAATTTTAAAGAAAGATATG

Strain construction

Pereira and colleagues showed that a mutation in the catalytic serine of PBP1TP domain was detrimental to cellular growth (Pereira et al., 2009). To avoid selection of suppressor mutants when constructing COLPBP1TP strain, the expression of a native PBP1 was ensured throughout the process. This was achieved by cloning the IPTG inducible promoter P_{spac} and a non-native *rbs* upstream of a full *pbpAt940g* mutated copy. This way, during the recombination process required for plasmid integration, expression of native *pbpA* was maintained. Following excision of the plasmid, the P_{spac} and the non-native *rbs* sequences would be removed, resulting in *pbpAt940g* under the control of native promoter and *rbs* (strain COLPBP1TP). In more detail, to construct COLPBP1TP strain two PCR fragments were amplified: one containing the P_{spac} promoter and an *rbs* sequence, amplified from pBCB13 plasmid using the pair of primers P1pbp1TP and P2pbp1TP and a second PCR fragment containing the full copy *pbpAt940g* mutated allele, amplified from pSKP1S314A (Pereira et al., 2009) using primers P3pbp1TP and P4pbp1TP. The *t940g* nucleotide change in *pbpA* results in a S314A mutation in PBP1TP domain and removes a Sau3AI restriction site, allowing easy screening of mutants. The two fragments were joined by overlap PCR using primers P1pbp1TP and P4pbp1TP. The resulting fragment was digested with EcoRI and BamHI, cloned in pMAD plasmid and transformed into *E. coli* DC10B competent cells creating pMADpbp1TP plasmid, which was confirmed by sequencing. Plasmid pMADpbp1TP was electroporated into competent RN4220 cells as described before (Kraemer and Iandolo, 1990) and subsequently transduced into COL using phage 80 α (Oshida and Tomasz, 1992). Integration and excision of pMADpbp1TP plasmid in COL was performed

as previously described (Arnaud et al., 2004) and in the presence of 0.1 mM of IPTG to ensure expression of native *pbpA*. During pMADpbp1TP excision through homologous recombination, P_{spac} and the non-native *rbs* were also excised, originating clones with either *pbpA* or *pbpAt940g* under the control of *pbpA* native promoter. To screen for COL clones where native *pbpA* was substituted for *pbpAt940g*, a PCR fragment encompassing nucleotide 940 of *pbpA* was amplified with primers P5pbp1TP and P6pbp1TP and digested with Sau3AI. Lack of Sau3AI digestion indicated the presence of mutated *pbpA*. Next-Generation DNA sequencing of the corresponding clone confirmed that *pbpAt940g* was the only introduced mutation. COL strain containing the S314A mutation in PBP1 was named COLPBP1TP. To express an FtsZ fluorescent derivative in this background we transduced pCN-FtsZ$^{55\text{-}56}$sGFP plasmid into COLPBP1TP strain, generating COLPBP1TPpCN-FtsZ$^{55\text{-}56}$-sGFP.

pCNX-pbp2 plasmid was constructed to ectopically express PBP2. Briefly, a PCR fragment encoding a non-native *rbs* and the full copy of *pbpB* was amplified using COL DNA as template and primers P1pCNXpbp2 and P2pCNXpbp2. The *rbs-pbpB* fragment was then cloned downstream of the cadmium inducible P_{cad} promoter in pCNX plasmid through digestion with SalI and KpnI, originating plasmid pCNX-pbp2. This plasmid was transformed into COLΔPBP2 mutant strain, originating COLΔPBP2pCNX-PBP2.

To construct plasmid pCNX-pbp2TP, a non-native *rbs* and a full copy of *pbpB* allele encoding for PBP2S398G (pbp2TP) were cloned in pCNX plasmid, downstream of the cadmium inducible P_{cad} promter. The pbp2TP sequence was amplified from pMAD-pbp2TPbig which was constructed as follows: two PCR fragments encompassing 1.7kb

upstream or downstream of nucleotide t1192 of *pbpB* were amplified using primers P1pMADpbp2TP/ P2pMADpbp2TP and P3pMADpbp2TP/ P4pMADpbp2TP, respectively. The two fragments were joined by overlap PCR using primers pairs P1pMADpbp2TP and P4pMADpbp2TP, digested with BglII and SmaI and cloned into pMAD, creating plasmid pMAD-pbp2TPbig. This plasmid contains two nucleotide exchanges (*t1192g* and *c1193g*) which mutate the catalytic serine from the TP domain to a glycine (S398G) and a silent mutation (*t1197c*) that introduces a BamHI restriction site to facilitate screening of clones. The pMAD-PBP2TPbig plasmid served as template to amplify the full *pbp2TP* allele using primers P1pCNXpbp2 and P2pCNXpbp2. The resulting PCR fragment was cloned downstream of the P_{cad} promoter of pCNX plasmid, after digesting with SalI and KpnI, resulting in plasmid pCNX-pbp2TP. To construct strain COLΔPBP2pCNX-PBP2TP, the pCNX-pbp2TP plasmid was transduced to COLΔPBP2.

To construct strain COLPBP3TP two regions of approximately 500 bp, upstream and downstream of *pbpC t1174* nucleotide, were amplified from COL DNA using the pairs of primers P1pbp3TP/P2pbp3TP and P3pbp3TP/P4pbp3TP. Primers P2pbp3TP and P3pbp3TP were used for site-directed mutagenesis of the *t1174g* and *c1175g* nucleotide in *pbpC* sequence, generating the S392G mutation of the catalytic serine of the PBP3 TP domain. These primers also introduced the *t1176a* and the *t1179c* silent mutations that create a BamHI restriction site to facilitate screening of *pbpCTP* clones. The two fragments were then digested with BamHI, joined by ligation and then amplified by PCR using primers P1pbp3TP and P4pbp3TP. The PCR product was digested with EcoRI and SalI, cloned into pMAD and used to transform *E. coli* DC10B competent

cells. Correct inserts were confirmed by sequencing and the final plasmid encoding the *pbpCTP* allele was named pMADpbp3TP. The plasmid was transduced to *S. aureus* strain COL, followed by plasmid integration and excision. Primers P5pbp3TP and P6pbp3TP were used to amplify a DNA fragment encompassing *pbpC t1174g* and *c1175g* nucleotides. Undigested PCR products of clones whose PCR products were digested by BamHI were sequenced to confirm the substitution of PBP3 by PBP3S392G, creating strain COLPBP3TP.

To construct strain COLPBP4TP two 600 bps regions, upstream and downstream of the *pbpD t223* nucleotide, were amplified using COL DNA as template and the pair of primers P1pbp4TP/P2pbp4TP and P3pbp4TP/P4pbp4TP respectively. Similarly to *pbpC*, primers P2pbp4TP and P3pbp4TP were used for site-directed mutagenesis of the *t223g* nucleotide generating the S75A mutation of the catalytic serine of the PBP4 TP domain. These primers also introduced the *g222t* nucleotide silent mutation that creates a PvuII restriction site to facilitate screening of the *pbpDTP* clones. The two fragments were digested with PvuII, joined by ligation and then amplified by PCR using primers P1pbp4TP and P4pbp4TP. The PCR fragment was then digested with EcoRI and BamHI, cloned into pMAD and used to transform *E. coli* DC10B competent cells. Correct inserts were confirmed by sequencing and the final plasmid encoding the *pbpDTP* allele was named pMADpbp4TP. Integration and excision of pMADpbp4TP plasmid was performed in strain COL. Primers P1pbp4TP and P4pbp4TP were used to amplify a DNA fragment encompassing *pbpD* nucleotide *t223g*. Undigested PCR products of clones whose PCR products were digested by PvuII were sequenced to confirm the substitution of PBP4 by PBP4S75A, creating strain COLPBP4TP.

S. aureus incubation with antibiotics

Overnight cultures were diluted 1/200 in fresh TSB and incubated at 37 °C with shaking. When cultures reached an OD_{600nm} of 0.2-0.3, they were incubated with either oxacillin (2; 4; 8 or 512 µg/ml, Sigma-Aldrich), D-cycloserine (62.5 µg/ml or 1 µg/ml, Apollo Scientific), DMPI (4 µg/ml or 0.063 µg/ml, gift from Merck), bacitracin (50 µg/ml or 0.79 µg/ml, Sigma-Aldrich), imipenem (1 µg/ml, Sigma-Aldrich), cefoxitin (8 µg/ml, Sigma-Aldrich), cephradine (4 µg/ml, Sigma-Aldrich) or cefotaxime (16 µg/ml, Apollo Scientific) for 1 hour at 37°C with aeration.

S. aureus sample preparation for microscopy

All microscopy experiments were performed using exponentially growing cultures (OD_{600nm} ~0.8). For experiments to visualize fluorescent protein derivatives, one milliliter of culture was pelleted by centrifugation, resuspended in PBS and two microliters were spotted on a thin layer of 1.2% agarose/PBS. When required, cells were labelled with fluorescent dyes. To visualize the cellular membrane, cultures were incubated with Nile red dye (Invitrogen) at a final concentration of 10 µg/ml at 37°C with shaking for 5 min. To label the cell wall we used the vancomycin-BODIPY-FL dye (Van-FL, Invitrogen), which binds to D-Ala-D-Ala in the PG. Van-FL was mixed in a 1:1 proportion with non-fluorescent vancomycin and the mix was used at a final concentration of 0.33 µg/ml to label cells for 5 min at 37°C with shaking. Double labelling of Van-FL and the fluorescent D-amino acid TAMRA-D-lysine (TDL) was performed by pelleting 1 ml of cell culture, resuspending in 200 µl of TSB and adding 0.33 µg/ml of Van-FL and 175 µM of TDL. Cells were incubated at 37°C with shaking for 5 min, washed once with 200 µl of PBS and spotted on a 1.2% agarose/PBS slide.

S. aureus imaging by Structured Illumination Microscopy (SIM)

Super-resolution SIM imaging was performed using an Elyra PS.1 microscope (Zeiss) with a Plan-Apochromat 63x/1.4 oil DIC M27 objective. Images were acquired using five phase shifts, either three or five grid rotations, with 34 µm grating period for the 561 nm laser (100 mW), 28 µm period for 488 nm laser (100 mW) and 23 µm period for 405 nm laser (50 mW). Images were captured using a Pco.edge 5.5 camera and reconstructed using ZEN software (black edition, 2012, version 8.1.0.484) based on a structured illumination algorithm, using synthetic, channel specific optical transfer functions and noise filter settings ranging from −6 to −8. When specified, a SIM Z-stack was performed by imaging the whole cell with a Z-step increment of 0.15 µm. Reconstruction of SIM images was performed using the Zen software and a point spread function (PSF) based on theoretical models. A maximum projection image of the 3D reconstruction is shown.

Timelapse microscopy

To follow cell division progression by SIM, an exponential growing culture of either COL or COLPBP1TP (OD_{600nm} ~0.8) was incubated with 10 µg/ml of Nile red for 5 min at 37°C with shaking, pelleted, resuspended in TSB supplemented with Nile red at 10 µg/ml and spotted on 1.2% agarose slides prepared in TSB:PBS (50:50). A time-lapse was then performed by acquiring SIM images every 5 min. A similar protocol was used to image cell division of COL in the presence of oxacillin: an early exponentially growing culture (OD_{600nm} ~0.4) was incubated with oxacillin at 8 µg/ml for 30 min at 37°C. After oxacillin incubation, one milliliter of the culture was labelled with 10 µg/ml of Nile

red for 5 min at 37°C with shaking, pelleted, resuspended in TSB supplemented with Nile red and oxacillin at the same concentration, and spotted on 1.2% agarose slides prepared in TSB:PBS (50:50) supplemented with oxacillin 8 µg/ml. A timelapse was then performed by acquiring SIM images every 5 min.

To image Z-ring constriction in the presence of oxacillin, a strain expressing a fluorescent FtsZ sandwich fusion (ColFtsZ$^{55\text{-}56}$-sGFP) was grown in the presence of 0.1 µM of $CdCl_2$. When the OD_{600nm} reached ~0.3 the culture was incubated with oxacillin at 8 µg/ml for 60 min at 37°C pelleted, resuspended in TSB supplemented with oxacillin (8 µg/ml) and $CdCl_2$ (0.1 µM), and spotted on 1.2% agarose slides prepared in TSB:PBS (50:50) supplemented with oxacillin 8 µg/ml and $CdCl_2$ 0.1 µM. A timelapse was then performed by acquiring SIM images every 3 min.

To image Z-ring constriction in the background of COLPBP1TP mutant, strain COLPBP1TPpCNXFtsZ$^{55\text{-}56}$-sGFP was grown in TSB supplemented with 0.1 µM of $CdCl_2$ at 37°C. Once the culture reached an OD_{600nm}~0.8, one milliliter was pelleted, resuspended in TSB supplemented with 0.1 µM of $CdCl_2$ and spotted on 1.2% agarose slides prepared in TSB:PBS (50:50) supplemented with $CdCl_2$ 0.1 µM. A timelapse was then performed by acquiring SIM images every 3 min.

Growth curves

An overnight culture of strain COL was diluted 1/200 in fresh TSB and grown at 37°C with aeration. When the culture reached an OD_{600nm} of 0.3 it was split and incubated either with no antibiotic (control) or with oxacillin at several concentrations (8; 32; 64; 128 or 512 µg/ml) and OD_{600nm} was recorded every 20 min.

Detection of PBPs with Bocillin-FL

S. aureus strains COL, COLPBP1TP, COLPBP3TP, COLΔPBP2, COLΔPBP4 and COLPBP4TP strains were grown overnight in TSB and strains COLΔPBP2pCNX-PBP2 and COLΔPBP2pCNX-PBP2TP were grown overnight in TSB supplemented with kanamycin 150 µg/ml. Cultures were then back-diluted 1/200 in fresh TSB and incubated at 37°C.When OD_{600nm} reached approximately 0.6, cells were harvested and broken with glass beads in a Fast Prep FP120 cell disrupter (Thermo Electron Corporation). Samples were centrifuged to remove unbroken cells and debris and total protein content of the clarified lysates was determined using the Bradford method and bovine serum albumin as a standard (Pierce BCA protein assay kit, Thermo-Fisher). Bocillin-FL (100 µM, Invitrogen) was then added to 100 µg of total protein and incubated at 30 °C for 10 min with shaking. The reaction was stopped by incubation with SDS-PAGE sample buffer (125 mM Tris-HCl, pH 6.8; 2 % SDS; 6 % (v/v) Glycerol; 2 mM DTT; 0.01 % (w/v) Bromophenol Blue) at 30 °C for 15 min. Protein samples were then separated in a 8% SDS-PAGE gel and the Bocillin-FL fluorescence was imaged using a FUJI Photo Film Imager FLA5100 using the 473 nm laser.

Western blot analysis

Total protein extracts of COL, COLΔPBP2, COLΔPBP2pCNX-PBP2 and COLΔPBP2pCNX-PBP2TP (see above) were boiled in SDS-PAGE sample buffer for 5 min and 40 µg were run in an 8 % SDS-PAGE gel. The gel was then transferred to a Hybond-P PVDF membrane (GE Healthcare) using a Semi-dry transfer cell (Biorad), at 10 V for 1 hour. The membrane was cut between 75kDa and the 55 kDa ladder markers to separate the regions containing PBP2 and FtsZ and then incubated with blocking

buffer (PBS; 5% milk; 0.5% Tween 20) for 1 h. The membrane region containing PBP2 (75kDa region) was incubated with a polyclonal anti-PBP2 antibody diluted 1/5000 in blocking buffer (Reed et al., 2011) and the membrane region corresponding to FtsZ (55kDa region) was incubated with an anti-FtsZ antibody diluted 1/5000 in blocking buffer for 16 h at 4 °C. Membranes were washed three times with PBS-T (PBS containing 0.5% Tween 20) and incubated with secondary antibodies (HRP anti-rabbit diluted 1/50,000 for PBP2 detection, GE Healthcare; HRP anti-sheep diluted 1/50,000 for FtsZ detection, Pierce). The detection was performed using an ECL Plus Western blotting detection system (Amersham) according to the manufacturer's guidelines.

RESULTS

Sub-inhibitory concentrations of oxacillin cause cell morphology defects in *S. aureus* MRSA strain COL

S. aureus morphology alterations as a consequence of exposure to beta-lactams have been studied mostly by electron microscopy and therefore using fixed samples (Lorian and Atkinson, 1975, Lorian and Atkinson, 1976). We decided to use the super resolution microscopy technique SIM to study in detail the effect on morphology of oxacillin at the minimum inhibitory concentration (MIC) and at sub-MIC levels on live *S. aureus* cells. For that purpose, MRSA strain COL was grown in the presence of 1xMIC of oxacillin (512 μg/ml) for 1 hour and imaged by SIM. We observed cells in Phase 3 with a clear invagination but no clear separation between the daughter cells (Figure 1, asterisk 1). This was surprising because the *S. aureus* cell envelope does not invaginate while the division septum is synthesized. Instead, after *S. aureus* cells finish septum synthesis, the two sister cells split extremely quickly, without any prior invagination (Figure 1, control). Additionally, some cells treated with oxacillin were tetrads (pairs of still attached sister cells already synthesizing a new septum (Figure 1, asterisk 2), similarly to what was published by Lorian and colleagues over four decades ago (Lorian and Atkinson, 1975, Lorian and Atkinson, 1976).

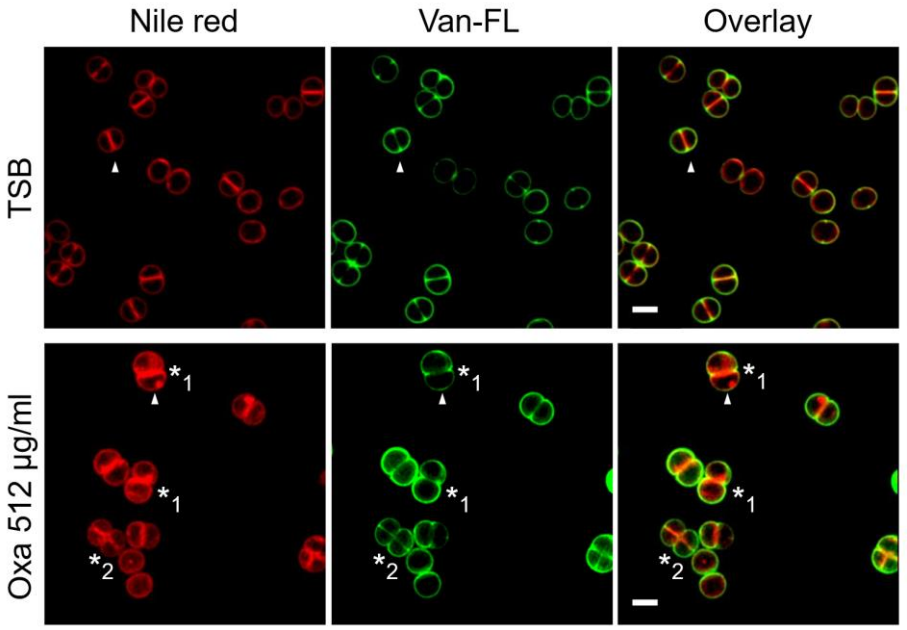

Figure 1: Inhibitory concentrations of oxacillin cause the appearance of invaginated *S. aureus* cells. MRSA strain COL was grown in the absence (TSB) or presence of 1xMIC of oxacillin (oxa 512 µg/ml) for 1 hour and incubated with the membrane dye Nile red and the cell wall dye Van-FL. Invaginated cells (asterisk 1) and tetrad cells (asterisk 2) were observed in the presence of oxacillin but not in its absence. Arrowheads correspond to cells with a closed membrane in Nile Red panel and open septum in Van-FL panel. Scale bar 1 µm.

We also observed the presence of invaginated cells in the presence of sub-MIC concentrations of oxacillin, even at the lowest oxacillin concentration tested (2 µg/ml).

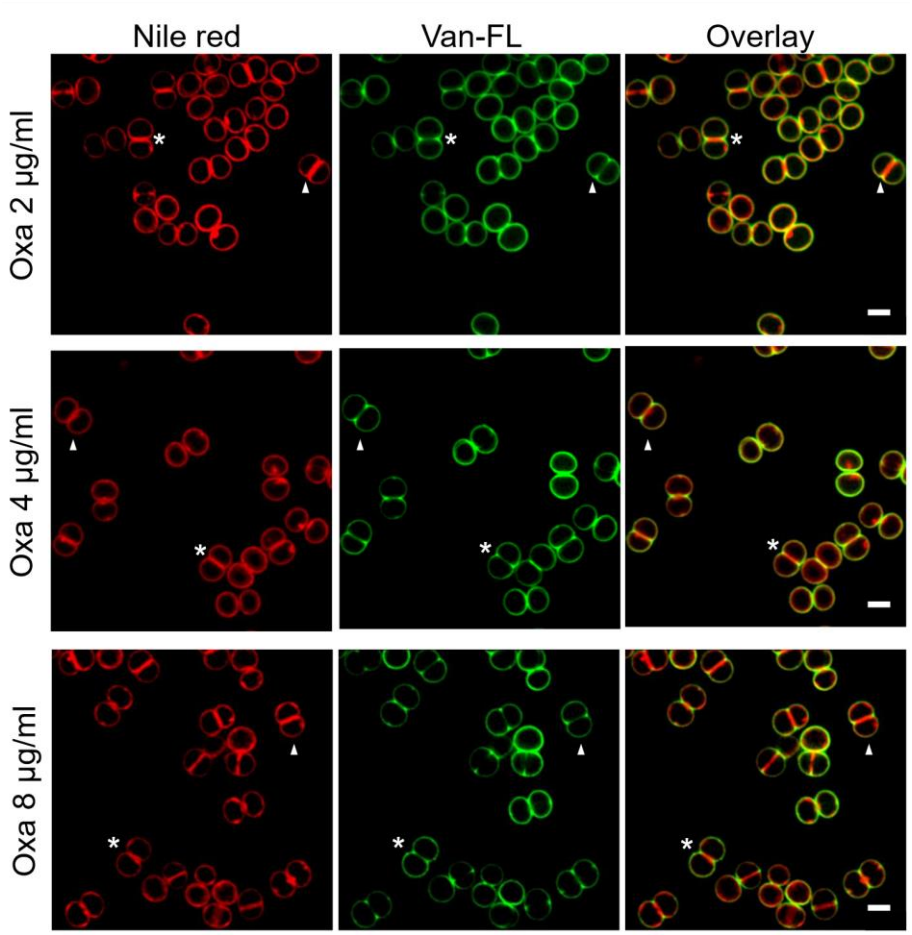

Figure 2: Sub-MIC concentrations of oxacillin cause the appearance of *S. aureus* invaginated cells. MRSA strain COL was grown in the presence of either 1/256 (oxa 2 µg/ml); 1/128 (oxa 4 µg/ml) or 1/64 (oxa 8 µg/ml) of the oxacillin MIC for 1 hour and incubated with the membrane dye Nile red and the cell wall dye Van-FL. The presence of invaginated cells (asterisks) was observed in all conditions. Arrowheads correspond to cells with a closed membrane in Nile Red panel and open septum in Van-FL panel. Scale bar 1 µm.

2D-SIM imaging of the cell wall, labelled with fluorescent vancomycin (Van-FL), and membrane, labelled with Nile red, showed cells with a closed membrane at the division site, separating the two daughter cells, but apparently an open septum, as determined by Van-FL

labelling (Figure 1 and 2, arrowheads). This was confirmed by imaging whole cells through a SIM Z-stack that was reconstructed in a 3D image (Figure 3, left panel). However, vancomycin is a large molecule that does not diffuse well into the septum (Pereira et al., 2007). Therefore the observed labelling pattern could derive from lack of accessibility of Van-FL to the central septal region. We therefore repeated the experiments but replaced VanFL with TDL, a fluorescent D-amino acid that is specifically incorporated in sites of active PG synthesis (Kuru et al., 2012). TDL labelling showed complete septa, even in cells for which Van-FL suggested the presence of an incomplete septum (Figure 3, right panel), confirming the limitations of the Van-FL dye in septal labelling.

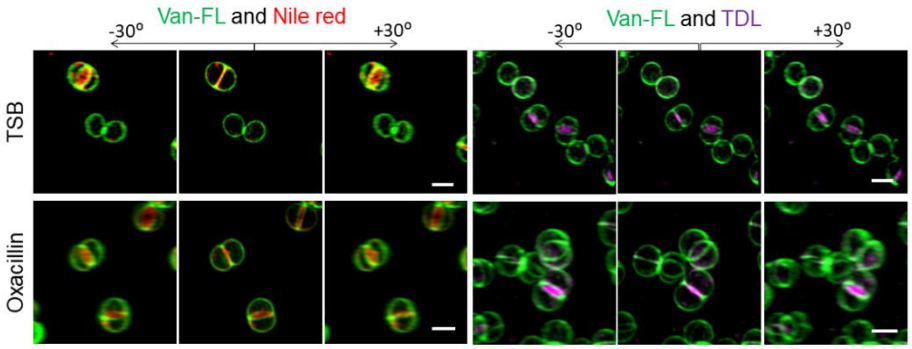

Figure 3: Van-FL dye does not completely stain the new septum of *S. aureus* MRSA strain COL. Imaging of *S. aureus* COL cells incubated with or without sub-MIC concentrations of oxacillin (4 µg/ml) for 1h and labelled with either (left) the cell wall dye Van-FL (green) and membrane dye Nile red (red) or (right) with the cell wall dyes Van-FL (green) and TDL (violet). A ±30° yy axis rotation is shown. While with Van-FL staining the septum in cells with a closed membrane appeared open, TDL (that labels active sites of PG incorporation) showed closed septa in equivalent cells. Scale bars 1 µm.

Because we consistently observed invaginated cells in the presence of 8 µg/ml of oxacillin (1/64x of the MIC, Figure 2), we chose this concentration for further experiments.

S. aureus cells invaginate during cell division in the presence of sub-MIC concentrations of oxacillin

To study morphogenesis of invaginated cells, we incubated COL with oxacillin at sub-MIC (8 μg/ml) for 30 min, labelled the cells with the membrane dye Nile red and transferred them onto an agarose pad containing oxacillin at the same concentration. We then followed cell cycle progression by timelapse SIM imaging. This experiment was also performed in the absence of oxacillin and, as previously shown (Monteiro et al., 2015), untreated COL cells with a complete septum (Phase 3) split with almost no prior invagination (Figure 4a, 60 to 65 min panels) originating two daughter cells, again in Phase 1. This transition from Phase 3 to Phase 1 cells occurs in less than 2 msec, in a "popping"-like motion (Zhou et al., 2015, Monteiro et al., 2015). In the presence of oxacillin, however, the fast popping and cell separation no longer occurred, and daughter cells started the next round of cell division before being fully separated from each other (Figure 4b). As there was no popping, there was no clear transition from a cell in Phase 3 to two cells in Phase 1 and the sister cells were still attached as an invaginated Phase 3 cell. Because in untreated COL cultures there is no cell cycle phase with these characteristics, we named the cell cycle phase corresponding to invaginated Phase 3 cells as Phase 4.

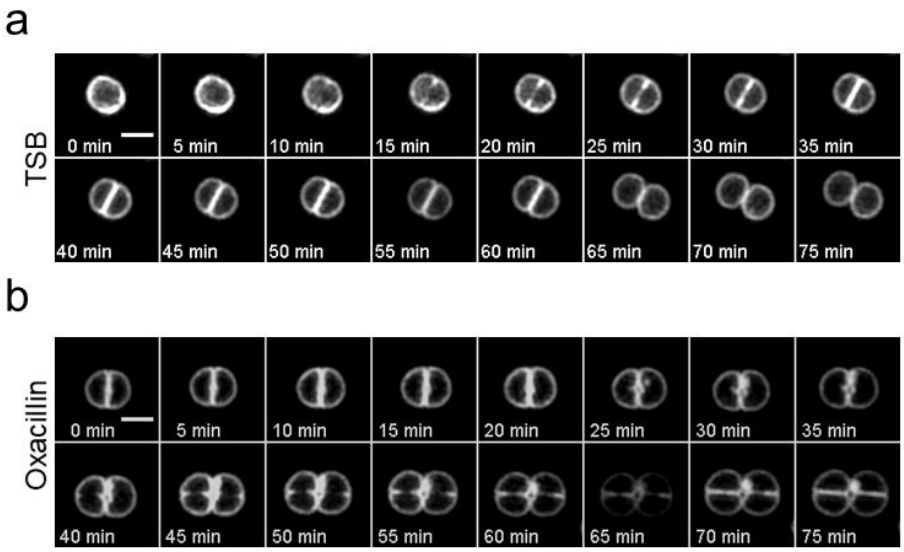

Figure 4: Oxacillin at sub-MIC impairs popping and increases duration of Phase 2. To observe cell cycle progression in COL cells treated with sub-MIC of oxacillin, an exponentially growing culture of COL was incubated with oxacillin 8 μg/ml for 30 min, labelled with Nile red and spotted on a TSB:PBS agarose pad containing oxacillin at the same concentration. A control was performed in the absence of oxacillin. SIM images were taken every 5 min in cells untreated **(a)** or treated with oxacillin 8 μg/ml **(b)**.

Interestingly, although in the presence of oxacillin at 8 μg/ml the cells seemed to take more time to reshape the septum, this did not impact cellular growth (Figure 5).

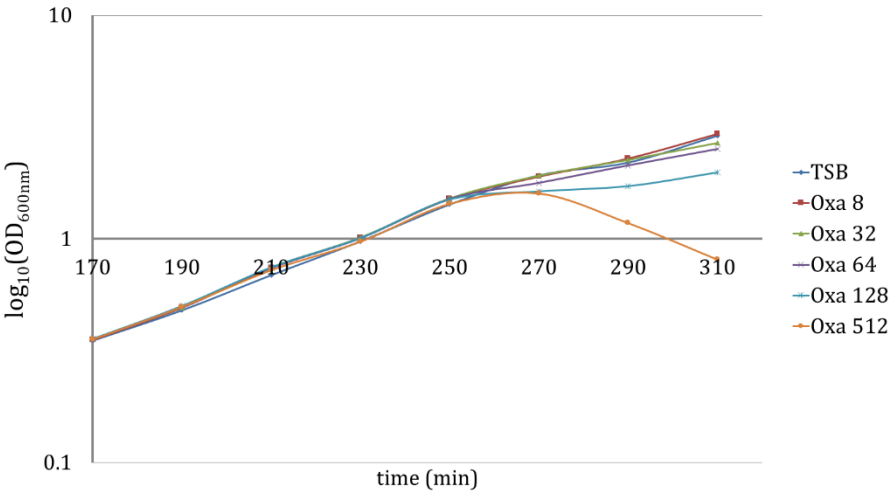

Figure 5: Growth curves in the presence of several concentrations of oxacillin. MRSA strain COL was grown at 37 °C to an OD_{600nm} of 0. 35 for 170 min, split in different aliquots and incubated with 1xMIC (512 µg/ml), 1/4xMIC (128 µg/ml), 1/8xMIC (64 µg/ml), 1/16xMIC (32 µg/ml) or 1/64xMIC (8 µg/ml) of oxacillin. OD_{600nm} measurements were performed every 20 min. Growth rate was not altered in the presence of 1/16xMIC (32 µg/ml) or 1/64xMIC (8 µg/ml) of oxacillin.

Oxacillin-induced morphology changes alter Z-ring shape

We next wondered how divisome proteins were localizing in Phase 4 cells where attached sister cells were initiating the next round of division. For this purpose, we imaged full $FtsZ^{55-56}$-sGFP rings by acquiring a SIM Z-stack in the presence or absence of sub-MIC levels of oxacillin (8 µg/ml). We observed that in the presence of oxacillin, FtsZ formed a D-shaped structure instead of a ring (Figure 6, right). These structures could also be observed in the absence of oxacillin, although at a lower frequency (Figure 6, left).

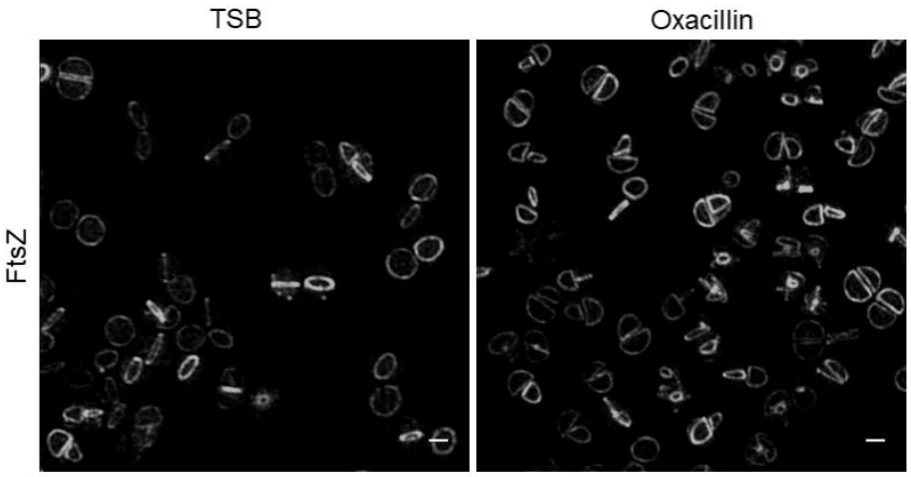

Figure 6: D-shaped FtsZ structures increase in frequency after incubation with oxacillin at sub-MIC. ColFtsZ$^{55\text{-}56}$-sGFP strain was grown for 1 hour with or without oxacillin (8 µg/ml). A SIM Z-stack was acquired and a fluorescence maximum projection is shown. While in the absence of inhibitors FtsZ$^{55\text{-}56}$-sGFP localized as a D-shape in 33% of the cells, this percentage increased to 77% in the presence of oxacillin (N>350). Scale bars 1 µm.

Because FtsZ is overexpressed in ColFtsZ$^{55\text{-}56}$-sGFP cells, the observed D shapes could be due to an excess of FtsZ, resulting in premature localization to the next plane of cell division. We therefore imaged EzrA-GFP as a proxy for FtsZ localization by acquiring a SIM Z-stack of COLpSGEzrA-GFP strain (Monteiro et al., 2018). EzrA-GFP was expressed from the native promoter in cells grown in the absence or presence of oxacillin sub-MIC (Figure 7). Similarly to FtsZ$^{55\text{-}56}$-sGFP structures, cell shape alteration caused by oxacillin increased the proportion of cells where EzrA-GFP localized as a D-shape instead of a ring (Figure 7).

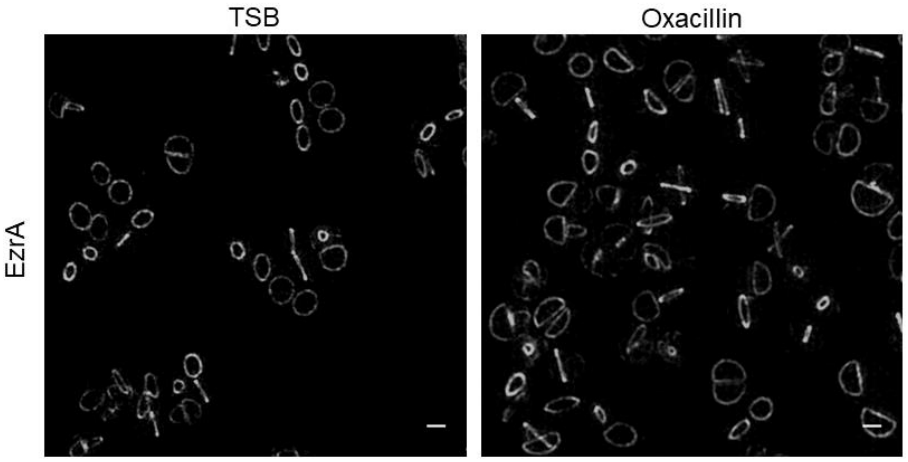

Figure 7: D-shaped EzrA-GFP structures increase after incubation with oxacillin sub-MIC. COLpSGEzrA-GFP strain was grown with or without oxacillin (8 μg/ml) for 1 hour and a SIM Z-stack was acquired. The fluorescence maximum projection is shown. In the absence of oxacillin (TSB) 24% of cells had EzrA-GFP localizing as a D-shaped structure, while in the presence of oxacillin this percentage increased to 60% (N>300). Scale bars 1 μm.

To determine if the D-shaped Z-rings were functional, i.e. capable of constricting and promoting division we performed timelapse imaging of FtsZ$^{55\text{-}56}$-sGFP in cultures incubated with sub-MIC of oxacillin for 30 min prior to SIM imaging on a TSB agarose pad containing oxacillin at the same concentration. These conditions recapitulated the localization of FtsZ$^{55\text{-}56}$-sGFP as a D-shaped structure instead of a ring (Figure 8). Interestingly, not only were D-shaped FtsZ structures able to constrict, but the D shape was maintained during the constriction process (Figure 8, asterisk).

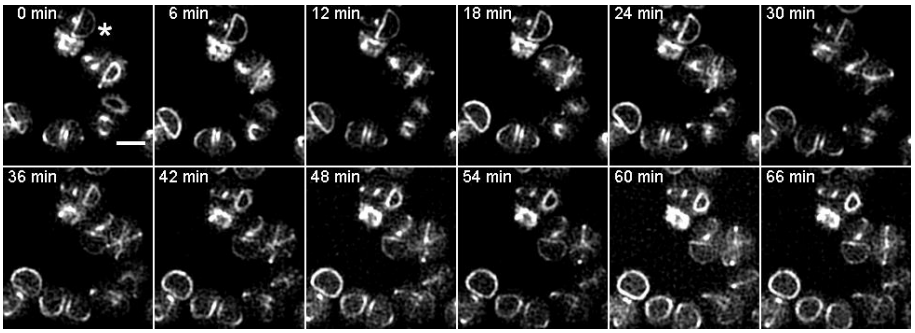

Figure 8: D-shaped Z structures undergo constriction. ColFtsZ$^{55\text{-}56}$-sGFP strain was grown for 30 min with oxacillin (8 µg/ml) and spotted on a TSB agarose pad containing oxacillin at the same concentration. Cadmium chloride was used at 0.1 µM during growth in TSB and on the agarose pad to induce expression of FtsZ$^{55\text{-}56}$-sGFP fluorescent fusion. Images were acquired by SIM every 3 min. Figure shows images taken every 6 min. The D-shaped structure marked with an asterisk constricted while maintaining the D-shape ultrastructure. Scale bar 1 µm.

We further tested functionality of D-shaped Z structures by the ability to recruit later divisome proteins. As previously shown, recruitment of the late divisome protein MurJ depends on the presence at midcell of the DivIB/DivIC/FtsL protein complex (Monteiro et al., 2018). Therefore, if the late divisome protein MurJ was recruited to a D-shaped divisome, this indicated that D-shaped FtsZ structures could recruit early and late divisome proteins. To test this, we imaged both FtsZ-mCherry and MurJ-sGFP in absence and presence of 8 µg/ml of oxacillin (Figure 9) and observed that while there are no D-shaped structures of MurJ in the absence of antibiotic, these structures arise in the presence of oxacillin indicating that a D-shaped divisome can recruit later cell cycle proteins.

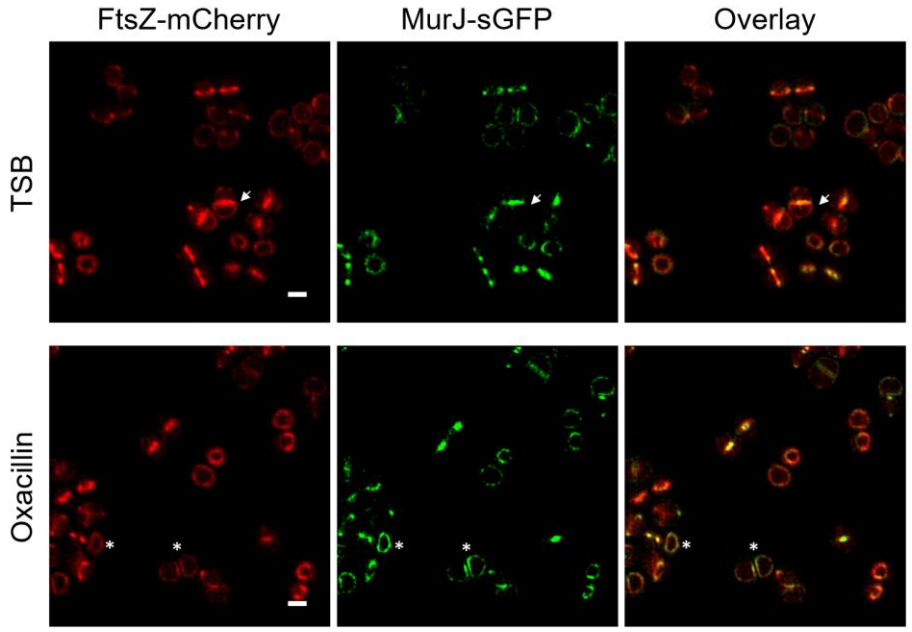

Figure 9: MurJ localizes as a D-shaped structure in the presence of sub-MIC oxacillin. Strain ColZmJg which expresses both FtsZ-mCherry and MurJ-sGFP, was incubated in the presence or absence of oxacillin (8 µg/ml) for 1 hour and spotted on an agarose pad. SIM imaging of FtsZ-mCherry and MurJ-sGFP shows that although some D-shaped FtsZ structures are present in TSB condition (top, arrow), MurJ can localize as a D-shape instead of a ring in the presence of oxacillin (bottom, asterisks). Scale bars 1 µm.

Inhibition of PBP1 causes invagination of *S. aureus* cells

To determine if oxacillin was leading to invaginated cells due to the inhibition of a specific PBP TP or due to a general consequence of cell wall synthesis inhibition, we incubated, for one hour, the MRSA strain COL with various cell wall targeting antibiotics: D-cycloserine, that inhibits D-alanine formation and D-ala-D-ala ligation; bacitracin, that inhibits bactoprenol recycling, DMPI, that inhibits MurJ activity and also with beta-lactam antibiotics with higher affinity to a specific PBP (see table IV.3) namely imipenem, cephradine, cefoxitin, cefotaxime and oxacillin. While all beta-lactam antibiotics tested led to the appearance of

Phase 4 cells, the other cell wall synthesis inhibitors D-cycloserine, bacitracin and DMPI did not.

Table IV.3 – Effect of cell wall synthesis inhibition on *S. aureus* morphology

Antibiotic (target)	Concentration	Phase 4?
D-cycloserine (Ddl)	1/64X MIC or 1xMIC	No
DMPI (MurJ)	1/64X MIC or 1xMIC	No
Bacitracin (UppS)	1/64X MIC or 1xMIC	No
Oxacillin (PBP1,2,3,4)	1/64X MIC or 1xMIC	**Yes**
Imipenem (PBP1)	1/64X MIC	**Yes**
Cefotaxime (PBP1,2)	1/64X MIC	**Yes**
Cephradine (PBP3)	1/64X MIC	**Yes**
Cefoxitin (PBP4)	1/64X MIC	**Yes**

Although there is some specificity of the tested beta-lactams for a particular PBP TP site, it is difficult to determine concentrations that *in vivo* reflect this specificity (Georgopapadakou et al., 1982, Chambers and Sachdeva, 1990, Beise et al., 1988). Nevertheless, we quantified the cell cycle phase frequency in cells incubated with different beta-lactams and saw a higher frequency of Phase 4 cells in the presence of oxacillin (which targets PBP1-4) and imipenem (which targets preferentially PBP1TP domain), suggesting that inhibition of PBP1TP could be key for the emergence of invaginated cells (Figure 10).

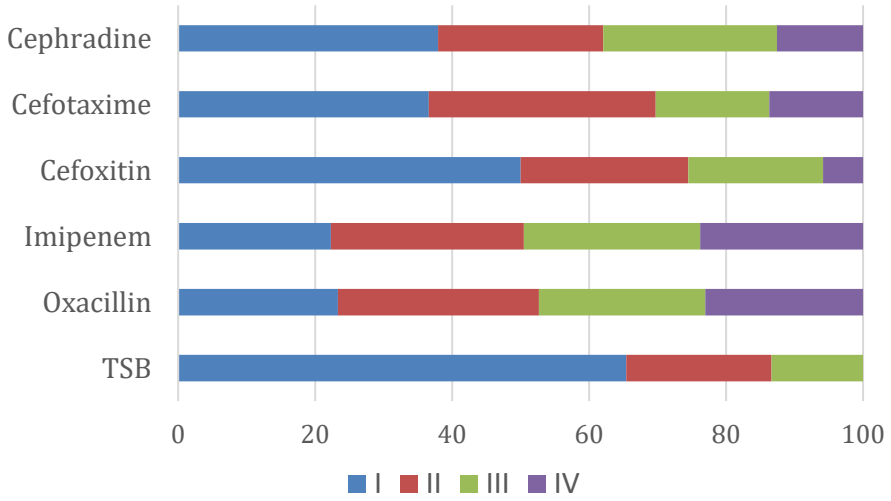

Figure 10: Effect of imipenem on cell cycle progression mimics that of oxacillin. The cell cycle phase distribution was measured in MRSA strain COL incubated with a 1/64xMIC of various beta-lactam antibiotics for 1h, followed by SIM imaging of membrane (stained with Nile red) and cell wall (stained with Van-FL). With the exception of oxacillin, these beta-lactams target more specifically PBP1 (imipenem); PBP2 (cefotaxime); PBP3 (cephradine) or PBP4 (cefoxitin). Blue bars correspond to cells without a septum (Phase 1); red bars cells with an open septum (Phase 2); green bars cells with a closed septum (Phase 3) and violet bars invaginated Phase 3 cells (Phase 4).

To confirm the data obtained with different beta-lactams we mutated the catalytic serine of the conserved SXXK TP domain of PBP1-4 and investigated which mutation led to the appearance of invaginated cells. We did not construct a PBP2a mutant because the phenotype of invaginated cells arises when using 1/64x of the MIC of oxacillin, a concentration which presumably inhibits all PBPs except PBP2a. We therefore constructed *S. aureus* COL mutant strains encoding either a mutated PBP1S314A (COLPBP1TP strain), PBP3S392G (COLPBP3TP) or PBP4S75A (COLPBP4TP) proteins. After several attempts we could not construct a strain expressing PBP2TP as the sole source of PBP2 in the

cell (data not shown). Instead, we expressed either the wildtype PBP2 protein or the TP mutant PBP2S398G protein from the replicative plasmid pCNX in the background of COLΔPBP2 (Reed, P. R., and Pinho, M. G., unpublished) (strain COLΔPBP2pCNX-PBP2 or COLΔPBP2pCNX-PBP2TP respectively). Inactivation of the TP catalytic site of the four TP mutants was confirmed by labelling whole protein extracts of these cultures with a fluorescent derivative of penicillin (bocillin-FL), which is a substrate analogue and therefore labels PBPs with an intact TP active site (Figure 11).

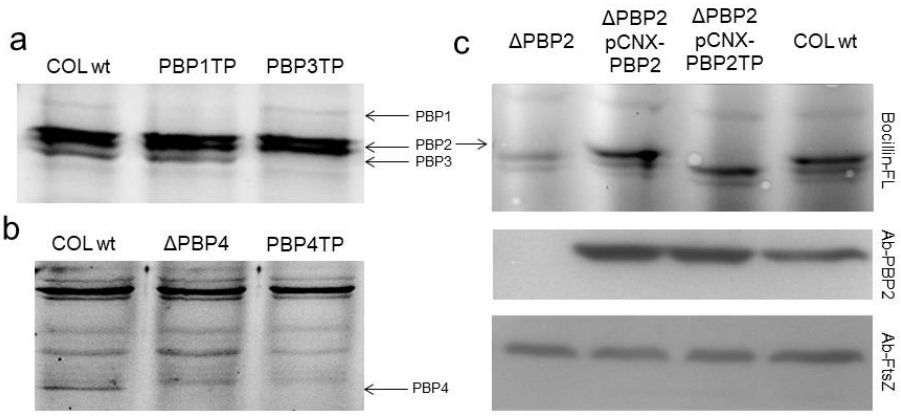

Figure 11: Bocillin-binding assays show TP domain inactivation of PBP1TP; PBP2TP; PBP3TP and PBP4TP mutants. (a) Whole protein extracts of COL wt; COLPBP1TP; and COLPBP3TP; **(b)** COL wt; COLΔPBP4 and COLPBP4TP and (c) COLΔPBP2; COLΔPBP2pCNX-PBP2; COLΔPBP2pCNX-PBP2TP and COL were incubated with bocillin-FL and separated by SDS-PAGE. The absence of a fluorescent band with the corresponding size for each PBP indicates inactivation of the TP domain. For the PBP2 samples **(c)** a Western blot against PBP2 (Ab-PBP2) with FtsZ used as a loading control (Ab-FtsZ) was performed, confirming PBP2 protein production from pCNX plasmid.

We then observed the cell morphology of PBPTP mutants by SIM (Figure 12). In agreement with Pereira and colleagues (Pereira et al., 2009) , COLPBP1TP had invaginated cells, recapitulating the phenotype

observed in the presence of sub-MIC oxacillin. In contrast, mutations of the TP domains from PBP2, PBP3 and PBP4 did not result in invaginated cells, demonstrating that this phenotype is due to the specific lack of transpeptidation activity of PBP1.

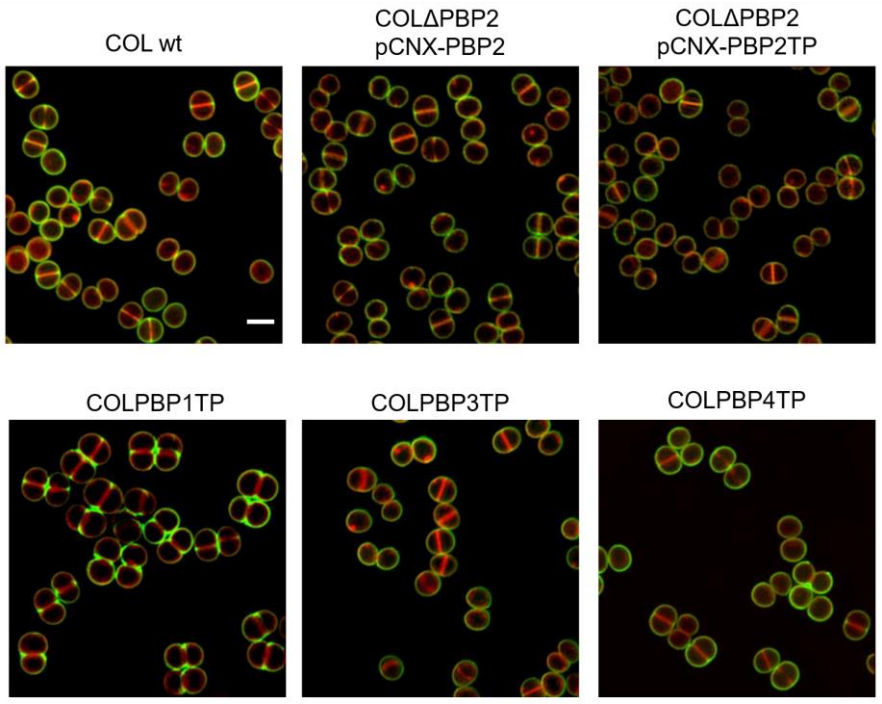

Figure 12: PBP1TP inactivation leads to invaginated cells. COL; COLΔPBP2pCNX-pbp2; COLΔPBP2pCNX-pbp2TP; COLPBP1TP; COLPBP3TP and COLPBP4TP cells were stained with the cell wall dye Van-FL (green) and the membrane dye Nile red (red) and imaged by SIM. Invaginated cells were present only in the PBP1TP mutant. Scale bar 1 μm.

Similarly to what was observed with sub-MIC oxacillin, timelapse microscopy of COLPBP1TP strain showed that this mutation impaired fast sister cell separation during transition from Phase 3 to Phase 1, leading to slow invagination (Figure 13).

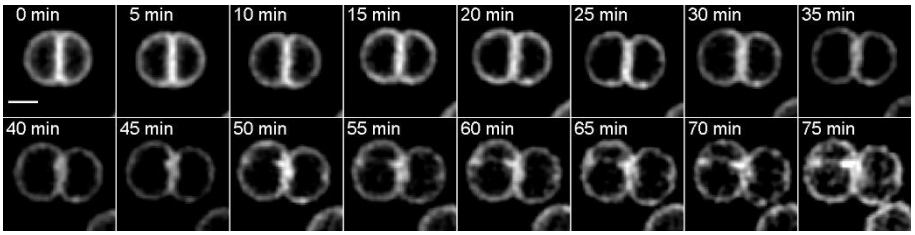

Figure 13: Inactivation of *S. aureus* PBP1TP domain impaired fast septum popping during cell division. Dividing cells of COLPBP1TP were labelled with membrane dye Nile red and imaged by SIM every 5 min. Timelapse images show daughter cells that are unable to separate quickly, originating an invaginated cell (Phase 4). Scale bar 1 μm.

Furthermore, we followed FtsZ$^{55\text{-}56}$-sGFP constriction in cells with an inactive PBP1TP and observed FtsZ localizing as D-shaped structures that were able to constrict, mimicking the FtsZ ultrastructure variation observed with oxacillin (Figure 14).

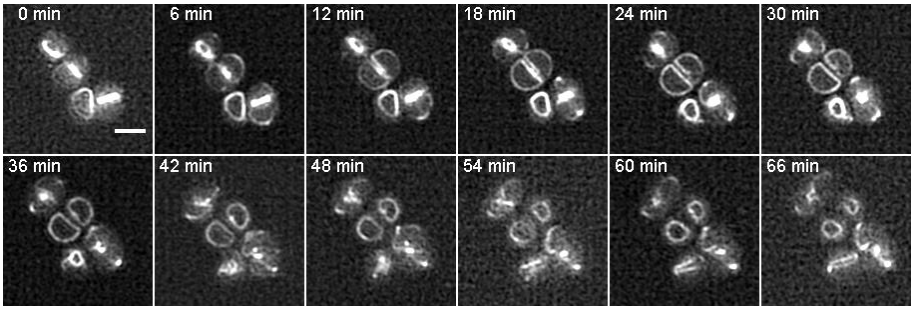

Figure 14: PBP1TP inactivation led to D-shaped FtsZ structures that can constrict. COLPBP1TPpCNX-FtsZ$^{55\text{-}56}$-sGFP strain was grown in TSB plus $CdCl_2$ (0.1 μM) and dividing cells were spotted on a pad containing TSB supplemented with $CdCl_2$ (0.1 μM). Snapshots were taken every 3 min by SIM. Figure shows snapshots taken every 6 min. The shape alteration originated by PBP1TP inactivation led to the formation of D-shaped FtsZ structures which constricted over time without changing their shape. Scale bar 1 μm.

DISCUSSION

Initial studies of the effect of oxacillin on *S. aureus* cell division were performed over 40 years ago, when clustered cells with thick septa, unable to separate, were observed by electron microscopy (EM) (Lorian and Atkinson, 1976). Although at first these results seem to be counterintuitive, thickening of the septum could derive from cells making PG via transglycosylation alone, which could result in unstructured loose PG (Cushnie et al., 2016). Clusters of cells could result from beta-lactam-induced alterations of the cell wall composition which would inhibit autolysins activity (Cushnie et al., 2016). We have now observed by SIM the fate of live MRSA cells after incubation with oxacillin. Sub-MIC concentrations of oxacillin were sufficient to induce a deregulation between PG synthesis and autolysis, observed by the presence of invaginated cells. Cells incubated with oxacillin could complete septum synthesis (Phase 3), but were unable to split quickly, and instead slowly invaginated. Unlike *E. coli* cells that invaginate while synthesizing the septum, the observed oxacillin-induced invagination of *S. aureus* cells only occurred after septum closure (Phase 3) and we did not observe Phase 2 invaginated cells (invaginated with an open septum). Both autolysin activity and turgor pressure seem to be important in reshaping *S. aureus* septum to a hemisphere (Monteiro et al., 2015). However, *S. aureus* autolysin mutants like *sle1* still show fast daughter cell separation. Our data might suggest that modifications of PG composition caused by oxacillin prevent rapid separation. Alternatively, a deregulation between synthesis and autolysis could lead to problems during cell splitting.

In chapter III we showed that if we inhibit the same process (PG synthesis) with two different inhibitors (PG transpeptidation inhibitor

oxacillin versus MurJ inhibitor DMPI), cells are arrested at different phases of the cell cycle. In this chapter we performed experiments with antibiotics that block the cytoplasmic and membrane stages of PG synthesis (D-cycloserine and bacitracin, respectively). Similarly to addition of DMPI, these antibiotics did not result in morphology alterations resulting in invaginated cells. This indicates that defects in sister cell separation are not a result of general inhibition of PG synthesis. Specific mutation of each *S. aureus* PBPTP catalytic site showed that PBP1TP inactivation was sufficient to cause invaginated cells, favoring the hypothesis that PBP1TP alone is linked to fast daughter cell separation.

In the absence of antibiotics, *S. aureus* COL cells spend around a fourth of the cell cycle with a closed septum (Phase 3) that later reshapes into the hemispheres of the daughter cells. In the presence of sub-MIC oxacillin (8 μg/ml), the septum takes more time to reshape, increasing the proportion of D-shaped, attached, daughter cells in the population. Although in these conditions septum reshaping was slower, this did not cause a growth defect, indicating that cell division (and presumably Z-ring assembly) progressed normally. Interestingly, in these conditions, FtsZ and EzrA formed D-shaped structures that recapitulated the shape of the cell, curved at the older cell wall and flat at the new. SIM imaging of FtsZ and EzrA in the absence of antibiotics showed the presence of D-shaped Z structures, although at lower frequencies. Because D-shaped FtsZ was also observed in the absence of inhibitors, it is unlikely that PBP1TP inactivation on its own modifies FtsZ directly. Instead, we suggest that cellular geometry, defined by PG, imposes the Z-ring shape. Although D-shaped FtsZ structures exist in wild-type cells, these

structures do not constrict in that shape because when the flat septum reshapes to a hemisphere, FtsZ accompanies this shape shift before starting constriction (see chapter III, Figure 6). In contrast, in cells incubated with oxacillin, the D-shaped FtsZ structures started constriction while still in a D shape. Although it has been shown that pure FtsZ filaments, tethered to membranes, tend to adopt ring structures (Erickson et al., 1996, Loose and Mitchison, 2014, Szwedziak et al., 2014), our data suggests that in live *S. aureus* cells, any inherent curvature that the FtsZ filaments might have is not sufficient to counteract the cellular shape imposed by the PG geometry. It is remarkable that D-shaped FtsZ filaments formed in the presence of oxacillin/PBP1TP inhibition maintain the D-shape during cytokinesis since the angle at the point where the flat septum intersects the peripheral wall is very different from that in a ring, where curvature is homogeneous. It will be interesting to model how FtsZ filaments can properly assemble and perhaps bend the membrane when attached to surfaces with different curvatures.

REFERENCES

Arnaud, M., Chastanet, A. and Debarbouille, M. (2004). New vector for efficient allelic replacement in naturally nontransformable, low-GC-content, gram-positive bacteria. Appl. Environ. Microbiol*., 70*, 6887-6891.

Beise, F., Labischinski, H. and Giesbrecht, P. (1988). Selective inhibition of penicillin-binding proteins and its effects on growth and architecture of *Staphylococcus aureus*. FEMS Microbiology Letters*, 55*, 195-202.

Chambers, H. F. and Sachdeva, M. (1990). Binding of β-Lactam Antibiotics to Penicillin-Binding Proteins in Methicillin-Resistant *Staphylococcus aureus*. The Journal of Infectious Diseases*, 161*, 1170-1176.

Cho, H., Uehara, T. and Bernhardt, T. G. (2014). Beta-lactam antibiotics induce a lethal malfunctioning of the bacterial cell wall synthesis machinery. Cell*, 159*, 1300-11.

Cushnie, T. P., O'Driscoll, N. H. and Lamb, A. J. (2016). Morphological and ultrastructural changes in bacterial cells as an indicator of antibacterial mechanism of action. Cell Mol Life Sci*, 73*, 4471-4492.

Erickson, H. P., Taylor, D. W., Taylor, K. A. and Bramhill, D. (1996). Bacterial cell division protein FtsZ assembles into protofilament sheets and minirings, structural homologs of tubulin polymers. Proc Natl Acad Sci U S A*, 93*, 519-23.

Georgopapadakou, N. H., Smith, S. A. and Bonner, D. P. (1982). Penicillin-binding proteins in a *Staphylococcus aureus* strain resistant to specific beta-lactam antibiotics. Antimicrob Agents Chemother*, 22*, 172-5.

Gill, S. R., Fouts, D. E., Archer, G. L., Mongodin, E. F., Deboy, R. T., Ravel, J., Paulsen, I. T., Kolonay, J. F., Brinkac, L., Beanan, M.*, et al.* (2005). Insights on evolution of virulence and resistance from the complete genome analysis of an early methicillin-resistant *Staphylococcus aureus* strain and a biofilm-producing methicillin-resistant *Staphylococcus epidermidis* strain. J. Bacteriol*., 187*, 2426-2438.

Goffin, C. and Ghuysen, J. M. (1998). Multimodular penicillin-binding proteins: an enigmatic family of orthologs and paralogs. Microbiol Mol Biol Rev*, 62*, 1079-93.

Hartman, B. J. and Tomasz, A. (1984). Low-affinity penicillin-binding protein associated with beta-lactam resistance in *Staphylococcus aureus*. J Bacteriol*, 158*, 513-6.

Kraemer, G. R. and Iandolo, J. J. (1990). High-frequency transformation of *Staphylococcus aureus* by electroporation. Current Microbiology*, 21*, 373-376.

Kuru, E., Hughes, H. V., Brown, P. J., Hall, E., Tekkam, S., Cava, F., de Pedro, M. A., Brun, Y. V. and VanNieuwenhze, M. S. (2012). *In situ* probing of newly synthesized peptidoglycan in live bacteria with fluorescent D-amino acids. Angew. Chem. Int. Ed. Engl., *51*, 12519-23.

Loose, M. and Mitchison, T. J. (2014). The bacterial cell division proteins FtsA and FtsZ self-organize into dynamic cytoskeletal patterns. Nat Cell Biol, *16*, 38-46.

Lorian, V. and Atkinson, B. (1975). Abnormal forms of bacteria produced by antibiotics. Am J Clin Pathol, *64*, 678-88.

Lorian, V. and Atkinson, B. (1976). Effects of subinhibitory concentrations of antibiotics on cross walls of cocci. Antimicrob Agents Chemother, *9*, 1043-55.

Meeske, A. J., Riley, E. P., Robins, W. P., Uehara, T., Mekalanos, J. J., Kahne, D., Walker, S., Kruse, A. C., Bernhardt, T. G. and Rudner, D. Z. (2016). SEDS proteins are a widespread family of bacterial cell wall polymerases. Nature, 634–638.

Memmi, G., Filipe, S. R., Pinho, M. G., Fu, Z. and Cheung, A. (2008). *Staphylococcus aureus* PBP4 is essential for beta-lactam resistance in community-acquired methicillin-resistant strains. Antimicrob Agents Chemother, *52*, 3955-66.

Monteiro, J. M., Fernandes, P. B., Vaz, F., Pereira, A. R., Tavares, A. C., Ferreira, M. T., Pereira, P. M., Veiga, H., Kuru, E., VanNieuwenhze, M. S., *et al.* (2015). Cell shape dynamics during the staphylococcal cell cycle. Nat Commun, *6*, 8055.

Monteiro, J. M., Pereira, A. R., Reichmann, N. T., Saraiva, B. M., Fernandes, P. B., Veiga, H., Tavares, A. C., Santos, M., Ferreira, M. T., Macario, V., *et al.* (2018). Peptidoglycan synthesis drives an FtsZ-treadmilling-independent step of cytokinesis. Nature, *554*, 528-532.

Moreillon, P., Markiewicz, Z., Nachman, S. and Tomasz, A. (1990). Two bactericidal targets for penicillin in pneumococci: autolysis-dependent and autolysis-independent killing mechanisms. Antimicrob Agents Chemother, *34*, 33-9.

Oshida, T. and Tomasz, A. (1992). Isolation and characterization of a Tn*551*-autolysis mutant of *Staphylococcus aureus*. J Bacteriol, *174*, 4952-4959.

Park, J. T. and Strominger, J. L. (1957). Mode of action of penicillin. Science, *125*, 99-101.

Pereira, P. M., Filipe, S. R., Tomasz, A. and Pinho, M. G. (2007). Fluorescence ratio imaging microscopy shows decreased access of vancomycin to cell wall synthetic sites in vancomycin-resistant *Staphylococcus aureus*. Antimicrob Agents Chemother, *51*, 3627-33.

Pereira, S. F., Henriques, A. O., Pinho, M. G., de Lencastre, H. and Tomasz, A. (2009). Evidence for a dual role of PBP1 in the cell division and cell separation of *Staphylococcus aureus*. Mol Microbiol*, 72*, 895-904.

Pinho, M. G., de Lencastre, H. and Tomasz, A. (2001). An acquired and a native penicillin-binding protein cooperate in building the cell wall of drug-resistant staphylococci. Proc Natl Acad Sci U S A*, 98*, 10886-91.

Reed, P., Veiga, H., Jorge, A. M., Terrak, M. and Pinho, M. G. (2011). Monofunctional transglycosylases are not essential for *Staphylococcus aureus* cell wall synthesis. J. Bacteriol*., 193*, 2549-56.

Reynolds, P. E. and Brown, D. F. (1985). Penicillin-binding proteins of beta-lactam-resistant strains of *Staphylococcus aureus*. Effect of growth conditions. FEBS Lett*, 192*, 28-32.

Szwedziak, P., Wang, Q., Bharat, T. A., Tsim, M. and Lowe, J. (2014). Architecture of the ring formed by the tubulin homologue FtsZ in bacterial cell division. Elife*, 3*, e04601.

Tomasz, A. (1979). The mechanism of the irreversible antimicrobial effects of penicillins: how the beta-lactam antibiotics kill and lyse bacteria. Annu Rev Microbiol*, 33*, 113-37.

Uehara, T., Dinh, T. and Bernhardt, T. G. (2009). LytM-domain factors are required for daughter cell separation and rapid ampicillin-induced lysis in *Escherichia coli*. J Bacteriol*, 191*, 5094-107.

Zhou, X., Halladin, D. K., Rojas, E. R., Koslover, E. F., Lee, T. K., Huang, K. C. and Theriot, J. A. (2015). Bacterial division. Mechanical crack propagation drives millisecond daughter cell separation in *Staphylococcus aureus*. Science*, 348*, 574-8.

CHAPTER V

Conclusions and future perspectives

Over the past years, novel microscopy super resolution techniques, coupled with new probes that mark places of PG synthesis, enabled exciting observations on the way different bacteria divide. Our knowledge about regulation of bacterial cell division has expanded due to the level of detail with which we can now observe bacterial proliferation. For me this is the most exciting time to ask questions on how small organisms, like *Staphylococcus aureus*, modify their shape, perform cell division, and adapt their growth to the presence of antibiotics.

Who came first, rods or cocci? An evolutionary perspective on bacterial shape

It is interesting to wonder what was the shape of the first walled bacterial cell. Because a spherical cell possessing just one PG synthesis machinery is simpler, it is intuitive to imagine that this would be the primitive morphology and that rod-shaped bacteria would result from cocci acquiring an extra machinery for cell elongation. However, evolutionary analysis of how bacterial shapes are distributed in the tree of life, shows that the deepest tree branches are composed of rod cells, with cocci bacteria dispersed across different branches (Siefert and Fox, 1998). Additionally, although there are several reports on gene deletions that convert rods to cocci (Henriques et al., 1998, Jones et al., 2001, Aldea et al., 1988), the reverse shape transition of cocci-to-rod was never observed. Similarly, during evolution, several cases of rod-to-cocci transitions occurred while spherical shapes have never been observed to revert to rod shape, indicating that cocci morphology might be an evolutionary dead-end (Siefert and Fox, 1998). As the genes that coordinate elongation (like MreB) are usually absent in cocci bacteria

(Pinho et al., 2013), one can speculate that the first bacteria were rods which later gave rise to cocci by losing MreB and other proteins involved in elongation. Some previous attempts have been made to show whether a spherical bacterium like *S. aureus* could transition into a rod-shaped cell by introducing cytoskeletal elements involved in elongation. But neither expression of *Bacillus subtilis* MreB (Yepes et al., 2014) or Mbl (Pinho, M.G., unpublished results) results in elongated *S. aureus* cells. This is probably because movement of MreB patches requires PG synthesis (Garner et al., 2011, Domínguez-Escobar et al., 2011, Teeffelen et al., 2011), and perhaps MreB may not interact with *S. aureus* PG synthesis machinery in a way that would be able to promote its movement. In this thesis we report the first observation on how the cocci *S. aureus* can produce elongated cells by shifting the path of PG deposition from concentric rings at the septum to a one-turn helix path, through modification of FtsZ localization. However, the resulting shape alteration was not homogeneous in the entire population, indicating that it does not correspond to a robust elongation mechanism. The observation that *S. aureus* cells can elongate by introducing PG in more than one place in the peripheral wall suggests that, introduction of a minimal elongation machinery in cocci (perhaps MreB/RodA/PBP2), which would incorporate PG along the cell axis, could perhaps convert spherical cells into rods in a robust way.

An evolutive shape switch from rod to cocci has been shown in *Neisseria meningitidis* and *Moraxella catarrhalis*, during adaptation to the nasopharynx, the same niche occupied by *S. aureus* (Veyrier et al., 2015, Edwards et al., 2012). Interestingly, the FtsZ^{G193D} mutant was previously shown to have attenuated virulence in a murine model (Tan et al., 2012). Our observation that FtsZ^{G193D} mutant cells exhibit an elongated

morphology, is therefore in agreement with the suggested hypothesis that a spherical shape may constitute a selective advantage for pathogens that colonize the nasopharynx, possibly due to the decrease in the cell surface area exposed to the immune system (Veyrier et al., 2015).

Plasticity of FtsZ filament arrangement in live *S. aureus* cells: arcs, helices and "Ds"

In vitro, membrane-tethered FtsZ filaments tend to assemble as ring-like structures (Osawa and Erickson, 2013, Szwedziak et al., 2014, Loose and Mitchison, 2014). However, *in vitro* data has also shown that FtsZ filaments have some degree of plasticity, as they can organize in helical structures (Arumugam et al., 2012) or in filaments with different degrees of bending (Erickson and Osawa, 2017). In live cells, FtsZ filaments usually assemble as rings (Rowlett and Margolin, 2015). In this work we observed that FtsZ filaments from *S. aureus* cells have a high degree of structural plasticity and can assemble in different structures that still promote cytokinesis. In chapter II we saw that mutations in FtsZ caused filaments to assemble in arcs and helices. Importantly, the arc structures of FtsZ can promote asymmetric constriction. This indicates that a non-continuous ring can still promote cellular division in the place where the filament is located, suggesting that FtsZ filaments do not need to be organized as a continuous ribbon-like structure that condenses to promote constriction. This is in line with previous observations in *C. crescentus* and other species which can perform constriction with incomplete rings of FtsZ (Yao et al., 2017).

Strikingly, in chapter IV, we observed that when *S. aureus* cells adopt a D-shape, the FtsZ filament ultrastructure instead of localizing as a ring, mimics the cell shape. This suggests that PG mechanical constrain

of cellular shape determines FtsZ filament structure. To confirm this hypothesis, in the future, we could produce spheroplasts of D-shaped cells, by removing the PG shape constraint, and observe whether FtsZ D-shapes go back to ring structures.

FtsZ filaments of several species have been observed to polymerize as straight, curved and highly curved filaments, indicating that there is flexibility for these filaments to adopt different curvature conformations *in vitro* (Erickson and Osawa, 2017). Importantly, FtsZ filament bending has been suggested as a possible mechanism for membrane deformation that can lead to constriction initiation. If bending of FtsZ filaments was the sole source of constrictive force generation, the filaments would need to be mechanically rigid (Erickson and Osawa, 2017). However, some observations suggest that the filaments of FtsZ may be too flexible to generate constrictive force (Arumugam et al., 2012). Although no live cell microscopy technique allows visualization of individual FtsZ polymers, FtsZ filaments assembled as a D-shaped ultrastructure seem to organize in two conformations that do not exist in a ring: (i) at the flat region of the D-shaped structure FtsZ filaments seem to have no curvature, although a curvature smaller than the SIM resolution limit could be present (<150 nm) and (ii) at the intersection of the flat septum with the cell periphery, the FtsZ filaments might adopt a bent conformation to accommodate the shape at the vertex of the D. Together, these observations suggest that FtsZ filaments co-exist in the same cell with enough bending plasticity to accompany cellular shape, indicating that FtsZ filaments do not form rigid structures. Importantly, FtsZ filaments organized in non-ring conformations were still able to recruit downstream cell division proteins and promote constriction,

suggesting that FtsZ filament bending might not influence cellular constriction.

FtsZ treadmilling and PG synthesis drive *S. aureus* cytokinesis

Although great advances in understanding FtsZ and PG synthesis contribution to cytokinesis have been made in the past few years, it is still unclear how the division machinery generates the necessary force to constrict the cell. In this work we showed that *S. aureus* Z-ring constriction is biphasic, as it starts with a period of slow/no constriction, followed by a period of fast constriction. Importantly, the turning point from slow to fast constriction coincides with the recruitment of the protein that targets PG synthesis to midcell (MurJ) (Monteiro et al., 2018). After this point *S. aureus* constriction no longer requires FtsZ treadmilling and is presumably powered by septal PG synthesis. Our observations suggest that FtsZ treadmilling is dispensable for cells undergoing division to finish it. But it is possible that FtsZ filaments exert a role of force generation during the initial stages of cell division. Our observations are consistent with a model where FtsZ filaments, moving through treadmilling, could generate a small force that slightly pinches the cell membrane causing a small deformation (Li et al., 2007), bellow the resolution limit of SIM. This would require a small force of a few pN, instead of a continuous force to counteract turgor pressure (~300 nN in Gram-positive species) (Xiao and Goley, 2016) which correlates well with models estimating the maximum force generated by FtsZ filaments (Coltharp and Xiao, 2017, Lan et al., 2009, Allard and Cytrynbaum, 2009, Osawa and Erickson, 2018). This slight membrane deformation through FtsZ pulling could be important to generate a small pocket between the

membrane and the old PG to directionally accommodate new PG subunits at the septum. Once PG synthesis enzymes had enough space to inwardly insert new PG molecules, treadmilling would no longer be necessary and cytokinesis could proceed until completion, driven by the insertion of new PG material. One way to test this would be to image FtsZ localization before the start of PG synthesis (prior to MurJ recruitment) with higher resolution techniques like CLEM, similarly to what was performed for FtsZ and FtsN in *E. coli* (Daley et al., 2016). Another role for treadmilling in early steps of cytokinesis could be to distribute PG synthesis enzymes homogeneously around the division plane so that new PG is inserted throughout the entire septum perimeter (Yang et al., 2017, Bisson-Filho et al., 2017). Consistent with this idea, in *S. aureus* cells incubated with the treadmilling inhibitor PC190723, 15% of Z-rings constricted defectively. However, it remains to be determined whether FtsZ treadmilling in *S. aureus* also leads to PG synthesis proteins moving directionally, like in *E. coli* and *B. subtilis* (Yang et al., 2017, Bisson-Filho et al., 2017). Further experiments that block the movement of PG synthesis proteins without disrupting FtsZ treadmilling could clarify the role of each process in constriction initiation.

Overall, we characterized the biphasic Z-ring constriction during the *S. aureus* cell cycle and showed that constriction is dependent on FtsZ treadmilling only during the early stages of cell division. We have also observed that FtsZ filaments can adopt different ultrastructures, such as arcs, helices and "Ds" that are still capable of recruiting downstream divisome proteins and lead to PG insertion and constriction. Additionally, we showed that alterations in FtsZ ultrastructure that lead to PG incorporation away from midcell (at the peripheral wall) lead to *S. aureus*

elongation. This work has confirmed *S. aureus* as an excellent bacterial model to answer questions about PG synthesis and cell division.

REFERENCES

Aldea, M., Hernandez-Chico, C., de la Campa, A. G., Kushner, S. R. and Vicente, M. (1988). Identification, cloning, and expression of *bolA*, an *ftsZ*-dependent morphogene of *Escherichia coli*. J Bacteriol*, 170***,** 5169-76.

Allard, J. F. and Cytrynbaum, E. N. (2009). Force generation by a dynamic Z-ring in *Escherichia coli* cell division. Proc Natl Acad Sci U S A*, 106***,** 145-50.

Arumugam, S., Chwastek, G., Fischer-Friedrich, E., Ehrig, C., Monch, I. and Schwille, P. (2012). Surface topology engineering of membranes for the mechanical investigation of the tubulin homologue FtsZ. Angew Chem Int Ed Engl*, 51***,** 11858-62.

Bisson-Filho, A. W., Hsu, Y. P., Squyres, G. R., Kuru, E., Wu, F., Jukes, C., Sun, Y., Dekker, C., Holden, S., VanNieuwenhze, M. S.*, et al.* (2017). Treadmilling by FtsZ filaments drives peptidoglycan synthesis and bacterial cell division. Science*, 355***,** 739-743.

Coltharp, C. and Xiao, J. (2017). Beyond force generation: Why is a dynamic ring of FtsZ polymers essential for bacterial cytokinesis? Bioessays*, 39***,** 1-11.

Daley, D. O., Skoglund, U. and Soderstrom, B. (2016). FtsZ does not initiate membrane constriction at the onset of division. Sci Rep*, 6***,** 33138.

Domínguez-Escobar, J., Chastanet, A., Crevenna, A. H., Fromion, V., Wedlich-Söldner, R. and Carballido-López, R. (2011). Processive movement of MreB-associated cell wall biosynthetic complexes in bacteria. Science*, 333***,** 225-228.

Edwards, A. M., Massey, R. C. and Clarke, S. R. (2012). Molecular mechanisms of *Staphylococcus aureus* nasopharyngeal colonization. Mol Oral Microbiol*, 27***,** 1-10.

Erickson, H. P. and Osawa, M. (2017). FtsZ Constriction Force - Curved Protofilaments Bending Membranes. Subcell Biochem*, 84***,** 139-160.

Garner, E. C., Bernard, R., Wang, W., Zhuang, X., Rudner, D. Z. and Mitchison, T. (2011). Coupled, circumferential motions of the cell wall synthesis machinery and MreB filaments in *B. subtilis*. Science*, 333***,** 222-225.

Henriques, A. O., Glaser, P., Piggot, P. J. and Moran, C. P., Jr. (1998). Control of cell shape and elongation by the *rodA* gene in *Bacillus subtilis*. Mol Microbiol*, 28***,** 235-47.

Jones, L. J., Carballido-Lopez, R. and Errington, J. (2001). Control of cell shape in bacteria: helical, actin-like filaments in *Bacillus subtilis*. Cell*, 104***,** 913-22.

Lan, G., Daniels, B. R., Dobrowsky, T. M., Wirtz, D. and Sun, S. X. (2009). Condensation of FtsZ filaments can drive bacterial cell division. Proc Natl Acad Sci U S A*, 106*, 121-6.

Li, Z., Trimble, M. J., Brun, Y. V. and Jensen, G. J. (2007). The structure of FtsZ filaments in vivo suggests a force-generating role in cell division. EMBO J*, 26*, 4694-4708.

Loose, M. and Mitchison, T. J. (2014). The bacterial cell division proteins FtsA and FtsZ self-organize into dynamic cytoskeletal patterns. Nat Cell Biol*, 16*, 38-46.

Monteiro, J. M., Pereira, A. R., Reichmann, N. T., Saraiva, B. M., Fernandes, P. B., Veiga, H., Tavares, A. C., Santos, M., Ferreira, M. T., Macario, V.*, et al.* (2018). Peptidoglycan synthesis drives an FtsZ-treadmilling-independent step of cytokinesis. Nature*, 554*, 528-532.

Osawa, M. and Erickson, H. P. (2013). Liposome division by a simple bacterial division machinery. Proc Natl Acad Sci U S A*, 110*, 11000-4.

Osawa, M. and Erickson, H. P. (2018). Turgor Pressure and Possible Constriction Mechanisms in Bacterial Division. Front Microbiol*, 9*, 111.

Pinho, M. G., Kjos, M. and Veening, J.-W. (2013). How to get (a)round: mechanisms controlling growth and division of coccoid bacteria. Nat. Rev. Microbiol.*, 11*, 601-614.

Rowlett, V. W. and Margolin, W. (2015). The bacterial divisome: ready for its close-up. Philos Trans R Soc Lond B Biol Sci*, 370*.

Siefert, J. L. and Fox, G. E. (1998). Phylogenetic mapping of bacterial morphology. Microbiology*, 144 (Pt 10)*, 2803-8.

Szwedziak, P., Wang, Q., Bharat, T. A., Tsim, M. and Lowe, J. (2014). Architecture of the ring formed by the tubulin homologue FtsZ in bacterial cell division. Elife*, 3*, e04601.

Tan, C. M., Therien, A. G., Lu, J., Lee, S. H., Caron, A., Gill, C. J., Lebeau-Jacob, C., Benton-Perdomo, L., Monteiro, J. M., Pereira, P. M.*, et al.* (2012). Restoring methicillin-resistant *Staphylococcus aureus* susceptibility to beta-lactam antibiotics. Sci. Transl. Med.*, 4*, 126-135.

Teeffelen, S. v., Wang, S., Furchtgott, L., Huang, K. C., Wingreen, N. S., Shaevitz, J. W. and Gitai, Z. (2011). The bacterial actin MreB rotates and rotation depends on cell-wall assembly. Proc. Natl. Acad. Sci. U S A*, 108*, 15822-7.

Veyrier, F. J., Biais, N., Morales, P., Belkacem, N., Guilhen, C., Ranjeva, S., Sismeiro, O., Pehau-Arnaudet, G., Rocha, E. P., Werts, C.*, et al.* (2015). Common Cell Shape Evolution of Two Nasopharyngeal Pathogens. PLoS Genet*, 11*, e1005338.

Xiao, J. and Goley, E. D. (2016). Redefining the roles of the FtsZ-ring in bacterial cytokinesis. Curr Opin Microbiol*, 34***,** 90-96.

Yang, X., Lyu, Z., Miguel, A., McQuillen, R., Huang, K. C. and Xiao, J. (2017). GTPase activity-coupled treadmilling of the bacterial tubulin FtsZ organizes septal cell wall synthesis. Science*, 355***,** 744-747.

Yao, Q., Jewett, A. I., Chang, Y. W., Oikonomou, C. M., Beeby, M., Iancu, C. V., Briegel, A., Ghosal, D. and Jensen, G. J. (2017). Short FtsZ filaments can drive asymmetric cell envelope constriction at the onset of bacterial cytokinesis. Embo j*, 36***,** 1577-1589.

Yepes, A., Koch, G., Waldvogel, A., Garcia-Betancur, J. C. and Lopez, D. (2014). Reconstruction of *mreB* expression in *Staphylococcus aureus* via a collection of new integrative plasmids. Appl Environ Microbiol*, 80***,** 3868-78.